Influence of nozzle type and configuration and surface roughness on heat transfer during metal quenching with water

Dissertation
Zur Erlangung des akademischen Grades

Doktoringenieur
(Dr.-Ing.)

Vorgelegt von

M.Sc. Yuan Fang

Geb. am 22.05.1990

In Anhui, China

Genehmigt durch die
Der Fakultät für Verfahrens- und Systemtechnik
Der Otto-von-Guericke-Universität Magdeburg

Gutachter:
Prof. Dr.-Ing. Eckehard Specht
Institut für Strömungstechnik und Thermodynamik (ISUT)
Otto-von-Guericke-Universität Magdeburg

Prof. Dr.-Ing. Udo Fritsching
Institut für Werkstofftechnik (IWT)
Universität Bremen

Prof. Dr.-Ing. Jürgen Rüdiger Böhmer
Institut für Technik
Universität Hildesheim

Eingereicht am: 07.Mai.2019

Promotionskolloquium am: 19. Nov.2019

Preface

This dissertation is submitted to Otto von Guericke University, Magdeburg for the degree of Doctor of Philosophy. The research described herein was conducted under the supervision of Prof. Dr.-Ing. Eckehard Specht from February 2015 to August 2019. To the best of my knowledge, this work is original except where suitable references are made to previous works. Neither this, nor any substantially similar dissertation has been submitted for any degree, diploma, or qualification at any other university or institution.

Yuan Fang
Magdeburg, 07.05.2019

Abstract

Controlling of cooling rate during metal manufacturing is critical, since an improper cooling leads to severe defect formation and thereafter reduce the productivity. In order to optimize the cooling behavior, analysis of heat transfer during metal quenching with liquid sprays and jets are of great importance and hence presented in this research.

Experiments are conducted in laboratory to study the effect of process variables on the cooling performance. The metal samples of different types are heated up to a required initial temperature prior to being quenched. The rear surface of the metal plate is coated manually with high temperature thermal sprays in order to achieve a high and stable emissivity, which is crucial in application of infrared thermography. The parameters on boiling curves such as rewetting, DNB temperatures, and maximum heat flux are then evaluated based on the measured temperature histories.

Before performing parametric studies of the heat transfer during metal cooling, a systematic determination of surface emissivity for two kinds of thermal coating are carried out. The two thermal coatings, named after their manufacturers, are “Senotherm” and “Ulfalux”, respectively. Their performances at high initial temperatures are crucial to the measurement accuracy.

In chapter 3, single nozzles such as full cone, flat spray and full jet nozzles are investigated. Furthermore, inline and staggered nozzle fields consisted of full jet nozzles are also supplemented to the experimental plans. All the used nozzles are produced by Lechler®. The used full cone nozzle has a cone angle of 60°. The average spray flux is 7.6 kg/(m²s) at a volume flow rate of 1.2 l/min and a plate-to-nozzle spacing of 50 mm. In experiments with full cone nozzle, the effect of sample thickness is thoroughly studied, since it is not well quantified in previous researches. It has been found out that rewetting and DNB temperatures, maximum heat flux increase with the metal sample thickness. The spray angle of the studied flat spray nozzle is 60°. As for flat spray nozzle, variables such as nozzle inclination angle and liquid volume flow rate are investigated to determine their influences on the cooling behavior. At last, the experiments with full jet nozzle are systematically carried out. The effect of variables such as initial temperature, jet velocity, metal thickness, metal type and nozzle diameter are studied and presented. Furthermore, experiments with inline and staggered nozzle fields consisted of full jet nozzles are carried out. Nevertheless, it has been found that there is no significant difference on cooling performance between these two nozzle fields.

Chapter 4 deals with the effect of surface roughness on cooling behavior under several cooling strategies. In order to study the effect of surface roughness on quenching behavior, metal samples with different levels of roughness are used. The investigated metal alloys are categorized into two groups: aluminum and copper alloy.

The investigated aluminum alloys are AA 5083 and AA 6082, while CuCrZr and CuSn4 for copper alloys. Their surface conditions are measured with a stylus profilometer to depict the characteristic values such as arithmetic mean roughness R_a, maximum roughness depth R_{max} etc. It has been observed that spray impingement is mostly affected by the surface roughness, while its influence during cooling with liquid jet and mold is marginal.

Keywords: Metal Quenching, Liquid Spray and Jet Impingement, Heat Transfer Analysis, Boiling Curves, Wetting Front Propagation, Surface Roughness

Zusammenfassung

Die Steuerung der Kühlrate während der Kühlung von Metallen ist bedeutsam, da eine unsachgemäße Kühlung zu einer starken Defektbildung im Gefüge führen kann, die sich auf die Produktivität des Prozesses auswirkt. Um das Kühlverhalten zu optimieren, ist die Analyse der Wärmeübertragung beim Quenchen von Metallen mit Sprays und Strahlen von großer Bedeutung und wird daher in dieser Dissertation untersucht.

Experimente werden im Labor durchgeführt, um den Einfluss von Prozessvariablen auf die Kühlleistung zu untersuchen. Die Metallproben verschiedener Art werden vor der Abkühlung auf eine Anfangstemperatur erhitzt. Die Rückseite der Metallplatte wird manuell mit einer Hochtemperatur-Thermo-beschichtung lackiert, um einen hohen und stabilen Emissionsgrad zu erreichen, da dieser für die Anwendung der Infrarot-Thermografie von entscheidender Bedeutung ist. Die Parameter wie Benetzungs-, DNB-Temperatur und maximale Wärmestromdichte werden aus den gemessenen Temperaturprofilen abgeleitet.

Bevor parametrische Untersuchungen zur Wärmeübertragung bei der Metallkühlung durchgeführt werden, wird eine systematische Bestimmung des Emissionsgrades für zwei thermische Beschichtungen durchgeführt. Die beiden nach ihren Herstellern benannten Beschichtungen sind "Senotherm" und "Ulfalux". Die Messgenauigkeit der Temperatur wird entscheidend durch die Beschichtung bestimmt.

Zunächst wird die Kühlung mit einzelnen Düsen untersucht. Im Mittelpunkt stehen Vollkegel-, Flachstrahl- und Vollstrahldüsen. Alle verwendeten Düsen kommen von der Firma Lechler®. Die verwendete Vollkegeldüse hat einen Sprühwinkel von 60°. Die durchschnittliche Wasserbeaufschlagungsdichte beträgt 7,6 kg/(m²s) bei einem Volumenstrom von 1,2 l/min und einem Abstand von Metallpatte zur Düse von 50 mm. In den Experimenten mit der Vollkegeldüse wird der Effekt der Probendicke gründlich untersucht, da er in früheren Untersuchungen nicht gut quantifiziert wurde. Es stellt sich heraus, dass sich die Benetzungs- und DNB-Temperatur bzw. den maximalen Wärmestromdichte mit der Metallprobendicke erhöht.

Der Sprühwinkel der untersuchten Flachstrahldüse beträgt 60°. Der Düsenneigungswinkel und der Flüssigkeitsvolumenstrom werden variiert, um den Einfluss auf das Kühlverhalten zu bestimmen. Schließlich werden die Versuche mit einer Vollstrahldüse systematisch weitergeführt. Die Auswirkungen von Variablen wie Anfangstemperatur, Metalldicke, Metallart und Düsendurchmesser werden dargestellt. Fluchtend und versetzt angeordnete Düsenfelder, die aus Vollstrahldüsen bestehen, ergänzen den Versuchsplan. Es hat sich jedoch herausgestellt, dass zwischen diesen beiden Düsenfeldern keine signifikanten Unterschiede in der Kühlleistung bestehen.

Um den Einfluss der Oberflächenrauheit auf das Abkühlverhalten zu untersuchen, werden Metallproben mit unterschiedlichen Rauheiten verwendet. Ein Teil der Metallproben wird direkt aus dem Barren entnommen, die von Nichteisenmetallherstellern hergestellt werden. Die untersuchten Metalllegierungen werden in zwei Gruppen eingeteilt: Aluminium- und Kupferlegierungen. Die untersuchten Aluminiumlegierungen sind AA 5083 und AA 6082, während CuCrZr und CuSn4 für Kupferlegierungen verwendet werden. Ihre Oberflächenzustände werden mit einem Stylus-Profilometer gemessen, um die charakteristischen Werte wie den arithmetischen Mittenrauwert R_a, die maximale Rautiefe R_{max} usw. darzustellen. Es wurde beobachtet, dass bei Einsatz von Spraydüsen die Abkühlung sehr stark von der Oberflächenrauheit beeinflusst wird, während bei Vollstrahldüsen und Kokillenstrahlen der Einfluss der Oberflächenrauheit gering ist.

Schlüsselwörter: Metallabkühlung, Vollkegel-, Vollstrahl- und Flachstrahldüsen, Thermoanalyse, Siedekurven, Benetzungsfrontausbreitung, Oberflächenrauheit

Contents

1. Introduction

1.1 Overview and motivation

Quenching or rapid cooling refers to the process which frequently occur during hardening and continuous casting of metal. In these processes, the temperature can reach 500 °C or higher. Hence, boiling is inevitable to occur at such high surface temperature. Therefore, in order to control the boiling process and the products' quality, it is necessary to understand the characteristics of different cooling techniques. The following methods are widely used in different applications due to their unique features. Impinging liquid jets are used where intense cooling rate should be achieved, while spray cooling is used where a moderate but uniform cooling is required, e.g. in the secondary cooling of continuous cooling of steel. If the being cooled object is dimensionally wide, then a series of liquid jets or sprays should be applied to achieve a fast but also relatively uniform cooling, e.g. in a run-out-table. Cooling with an array of liquid jets from a mold is preferably used in direct chill (DC) casting process of non-ferrous metals such as aluminum and its alloys, copper, etc. In the secondary cooling of DC casting, a liquid curtain is formed and flows downwards due to gravity on the solidified surface. This research work consists of three quenching methods:

1. A single nozzle, e.g. full jet, flat fan and full cone nozzle,
2. A nozzle field consisting of single full jet nozzles,
3. A mold with stationary and moving hot plates.

For any aforementioned quenching method, the basic mechanism of heat transfer is similar but complicated; which involves boiling and therefore requires a thorough understanding. When a low-temperature liquid contacts a hot surface, all the modes of boiling (a two-phase heat transfer process), besides single-phase forced convection, are simultaneously presented. At first, a vapor layer is formed which cuts off the direct contact between liquid and solid. This regime is named as film boiling, characterized by a very low efficiency of heat transfer; with the surface continuously being cooled, the vapor layer does sustain until the so-called Leidenfrost point is reached. The hot surface is now partially contacted with the liquid, which is designated as transition boiling. A larger amount of generated vapor accompanying an abrupt increase in heat flux can then be observed. Subsequently, boiling continues as the surfaces temperature keeps decreasing until the maximum heat flux is reached. At this point, the surface temperature is called DNB temperature, which is an abbreviation for '**D**eparture from **N**ucleate **B**oiling'. An intensive bubble formation can be observed when the surface temperature is lower than the DNB temperature. This regime is termed as nucleate boiling, which features a dramatic decrease in heat flux with a small reduction of surface temperature. When the saturation temperature of the coolant is

reached, two-phase boiling ceases, followed by a forced convection. The historical researches and investigations on boiling phenomena will be detailed in the following sections.

From the description of the transient boiling above, it is obvious that rapid cooling occurs once the surface of the metal cools down to the rewetting temperature, T_{Rew}. Terms such as rewetting, sputtering, Leidenfrost and minimum film boiling temperature have been used interchangeably in the literature [1]. Leidenfrost effect is a phenomenon when a liquid is brought into contact with a surface whose temperature is much higher than the liquid's saturation temperature. It is seen that the liquid is levitated above a vapor film. A threshold value exists for this phenomenon to happen, below which the evaporation rate is insufficient to maintain the stable vapor film. This threshold is historically and classically referred to as the *Leidenfrost Temperature*. In this research work, the rewetting temperature is used because of its straightforward meaning. Moreover, the method to determine the rewetting temperature proposed by J. Filipovic et al. [2] is adopted. Some rewetting temperatures reported in the literature are compiled in **Table 1.1**. It can be seen that the rewetting temperature varies significantly based on different conditions, which demonstrates the necessity of a thorough experimental investigation to build up an in-house database for further practice.

Taking DC casting of aluminum process as an example, the improper cooling is responsible for either undesirable micro-/macro-segregation or unwanted residual stress and distortion. This can be avoided or minimized with many ways, such as regulation of jet impingement velocity, addition of salt or salt mixtures into the cooling water and the process-tailored casting velocity instead of a constant one, etc. Hence, operation parameters whose combination has impact on the final product's quality have to be defined and organized. For example, how are the rewetting and DNB temperature influenced by different cooling methods? What is the effect of material type and thickness on the cooling rate? How to quantify the effect of surface roughness or structure on the cooling behavior? What is the outcome with altering the casting velocity? All such questions need and can only be answered by experimental investigations. Extensive experimental researches and studies have been conducted in the past, trying to describe and explain the two-phase quenching process. Meanwhile, plenty of empirical correlations as well as analytical solutions were proposed to predict the rewetting and DNB temperature and maximum heat flux in order to construct the boiling curve. However, to the best knowledge of the author, there are only few published researches which cover the effect of individual experimental parameters for various cooling methods. Moreover, the proposed models and correlations cannot be extended to another application, which motivates the author to complete the current in-house database.

Table 1.1: List of experimental studies on rewetting temperature, T_{Rew}, during quenching with flowing liquid (arranged chronologically)

Author(s)	Material	Initial temperature [°C]	Cooling process	Coolant feature	Rewetting temperature [°C]
Hall et al. [3, 4] (2001)	Copper	650-800	Circular liquid jet	Water, 25 °C, 2 - 4 m/s	150-450
Liu & Wang[5] (2001)	AISI 316	1000	Circular liquid jet	Water, 55 -95 °C,1 - 3 m/s	300 -1000
Liu et al.[6](2002)	Carbon steel, AISI 316	900	Circular liquid jet	Water, 13-30 °C,5.6 -6.5 m/s	900
Zhang[7] (2005)	Carbon steel	850	Circular liquid jet	Water, 40°C, 2.3 m/s	450 - 850
Gradeck et al. [8](2006)	Nickel	~600	Planer liquid jet	Water, 85°C, 1.2 m/s	580
Wendelstorf et al. [9] (2007)	Nickel	200 - 1100	Spray	Water, 18°C, 3 - 30 kg/(m²s)	300 - 400
Abdalrahman et al.[10] (2014)	AA6082	560	Spray	DI Water + salt; Probe water from industry ,20°C,--	240 - 275 240 - 350
Wang et al.[11] (2016)	AISI 304L	200 – 900	Circular liquid jet	Water,10 – 40 °C, 1.99 – 3.98 m/s	200 – 850
Sarkar et al. [12] (2018)	AISI 304	~1050	3x3 array of circular jets	DI water + additives, --, 0.189 – 1.89 m/s	900

The measurement of surface temperature is the basis for estimation of surface heat flux. Many approaches can be applied to measure the transient temperature history. Commonly used thermocouples are reported in many literatures [3-5, 9, 11]. They are put into the drilled holes beneath the quenching surface at a depth from 1 – 3 mm. However, the precision of the location is questionable. Additionally, the improper implant of thermocouples will also incur disturbances in the temperature field inside the metal sample. Some other researchers used non-contact techniques such as infrared thermography to record the temperature history [10, 13]. It is known that performing quenching experiments at very high temperature is difficult because of technological problems. The shortage of appropriate sensors and materials as well as corrosion at high temperature, etc. should be taken into consideration. The largest

difficulty, according to the author, is the direct measurement of the surface temperature on the quenching side. That is why the word ‘estimation’ is used when surface heat flux needs to be determined. All these difficulties lead to an inescapable result; current industrial designs, applications and productions are generally based on empirical relations originated from experience or rule of thumb.

The inverse heat conduction solution approach is used to obtain surface heat flux and temperature distribution with the temperature values measured inside the solid. Normally, if the boundary and initial conditions as well as the thermo physical properties are specified, the generalized heat conduction equation is solved to determine the interior temperature distribution for a given domain. This is classically called ‘direct problem’[14]. But if one or more boundary conditions are unknown; instead the temperature values measured at some interior regions are known, then the estimation of the unknown boundary condition(s) needs to be considered. This kind of problem belongs to one category of so called ‘inverse problem’[14]. Mathematically, inverse problem is classified as ill-posed problem, whose solution is so sensitive with the errors contained in the input measurements. The disadvantages of thermocouple described in last paragraph make the measuring results much more vulnerable to the experimental errors. Based on this, infrared thermography seems more promising to provide a better accuracy.

With all above description, it is clearly seen that a better solution to improve the understanding of various quenching techniques is essential. This situation has led to intense discussion and cooperation in the past and will encourage more and more efforts in the future. Meanwhile, this will be the basis framework of the current research.

1.2 Fundamentals of quenching

As described in section 1.1, quenching of hot surfaces is a very complex phenomenon which involves two-phase boiling. The main heat transfer mechanism is thus dominated by the phase-change process. During the whole cooling procedure, a plenty of vapor bubbles are rapidly formed, grown and departed from the surface. Several reasons are proposed by Schweizer [15] for the enhancement of heat transfer during boiling compared with that in single-phase forced convection:

- A thin liquid micro-layer is formed at the bubble foot, which improves heat transfer rate greatly.
- The motion of the vapor bubbles contributes to the enhancement of the single phase convection by agitating the liquid near the surface.
- The thermal resistance is lowered due to the removal of the thermal boundary layer at each bubble cycle.

The boiling curve is a representation for how the heat flux varies against the surface temperature. First constructed by Nukiyama (1934) in an experiment of pool boiling with water, thus boiling curve is also referred to as Nukiyama’s curve. A typical

pool boiling curve is depicted in **Figure 1.1**. The four distinct regimes in the Nukiyama curve obtained during quenching are described as:

1. Film boiling: during the quenching process, it appears when the surface temperature is higher than rewetting temperature at certain experimental conditions. It features a stable vapor layer that forms between the liquid and the heated surface. The vapor escapes into the liquid above once it is generated at the liquid-vapor interface. Hence, conduction through the vapor layer is the dominant heat transfer mechanism during the film boiling regime. The region ends when the surface temperature approaches the Leidenfrost point or the minimum heat flux point or in current thesis rewetting point.
2. Transition boiling: This regime is characterized by a fluctuation between nucleate and film boiling. The intermittent contact between the liquid and the heated surface enhances the heat transfer which can be observed in Figure 1.1. The heat flux increases while the surface temperature decreases. At the end of this regime, the heat flux reaches its maximum value, which is named as maximum heat flux (MHF).

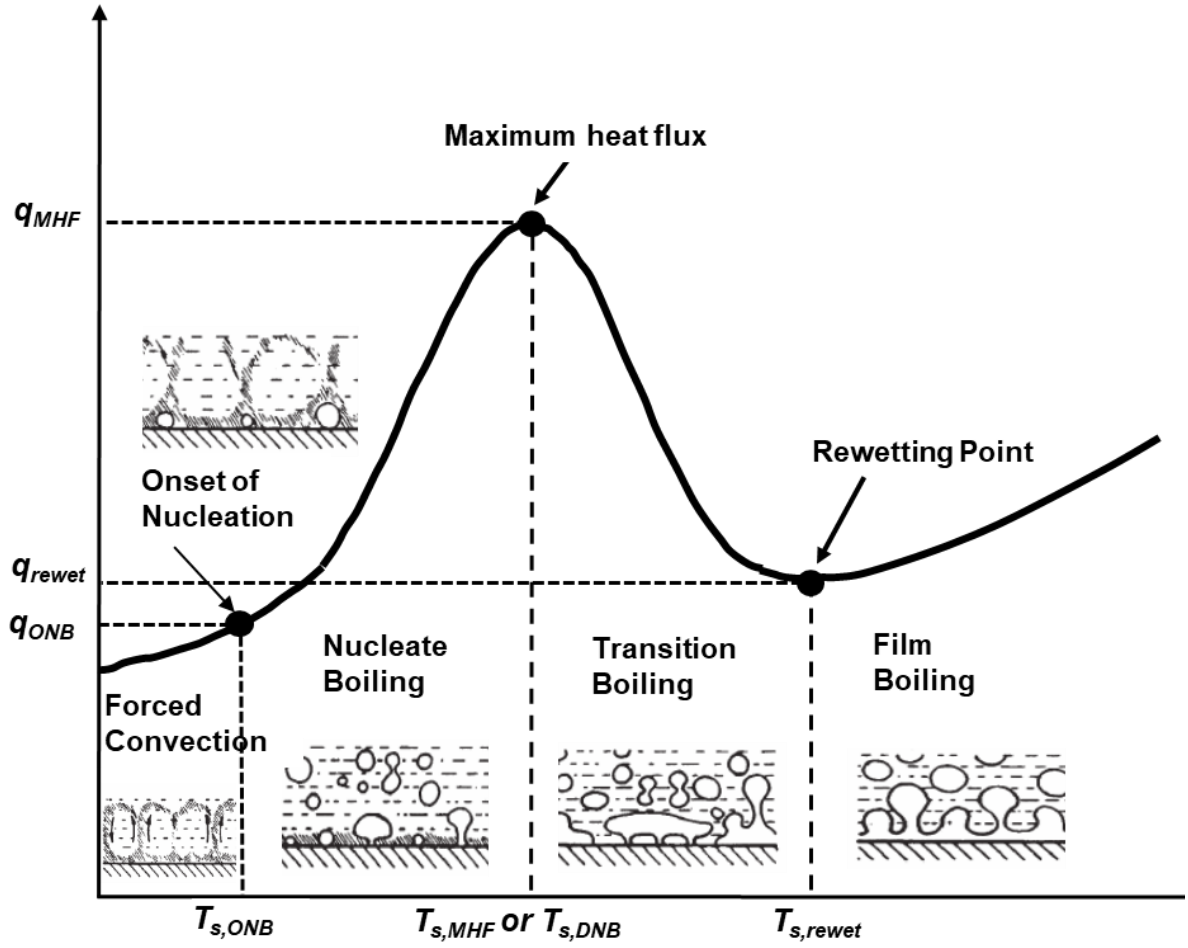

Figure 1.1: A typical boiling curve with distinct boiling regimes. The schematics of bubble dynamics for various boiling regimes are adapted from[16].

3. Nucleate boiling: In this regime, the bubbles extensively nucleate, grow and depart from the heated wall. The end of this boiling zone is characterized by the onset of nucleate boiling (ONB).
4. Single phase convection: when the surface superheat is low, any possibly generated vapor bubble is immediately condensed in the subcooled liquid surrounding it.

Pool boiling is a boiling process under natural convection conditions, however in jet impingement quenching process, liquid is forced to flow over the heated surface. The effect of hydrodynamics of the jet is quite significant on the overall heat transfer. Therefore in Figure 1.1, the terminology used in pool boiling is tailored to describe the forced convection boiling in a more accurate way. For example, the critical heat flux is more common to be used in pool boiling, while maximum heat flux is preferred in jet impingement quenching. The detailed literature review for these regimes are presented in section 1.4.

1.3 Casting process and problems definition

Casting is a manufacturing process which has been used for thousand years. It is a process in which the molten liquid is solidified in a mold with specific shapes and dimensions. In metallurgy, the common used methods for semi-finished products are continuous casting for steel and direct chill (DC) casting for non-ferrous metals and their alloys, such as aluminum and copper. In the conventional continuous casting of steel, the molten liquid is directed into the mold and freezes a thin solid shell against the water-cooled mold surfaces. In contrast to the continuous casting (CC) of steel, the DC casting is only semi-continuous; the billet or ingot is withdrawn vertically to a shorter length (~ 10 m) until the process should be stopped. Besides, in the conventional continuous casting of steel, the strand out of the mold is normally strategically bent to follow a curved path and then straightened flat prior to torch cutoff; however, for materials with higher thermal conductivity with much lower melting point, e.g. aluminum, faster internal heat extraction results in a shorter liquid pool in the casting process [17].

Although there are many differences between casting processes for aluminum and steel, there are also similarities when heat transfer is taken into consideration. The main purpose is the heat extraction from the molten and solidifying metal. The heat transfer phenomena occurring on the strand surface is schematically shown in **Figure 1.2**. A complex interplay of various heat transfer mechanisms is involved in both casting processes, which includes heat extraction by convection at mold (termed as primary cooling) and heat transfer directly to the cooling water below the mold (termed as secondary cooling). It is not difficult to find out that the difference in liquid pool depth for both processes is significant.

Water cooling is not only responsible for the heat removal rate, but also inducing thermal stresses and strains owing to thermal contraction of the metal. The high

temperature gradient across the solid shell during the rapid cooling can generate thermal strains as the shell expands and contracts [17]. It is also reported by Sengupta et al. [17] that, 80% of the total heat content is extracted by the chill water in secondary cooling during the steady-state operation of DC casting. Hence, improper heat extraction rate especially in secondary cooling will result in severe quality issues.

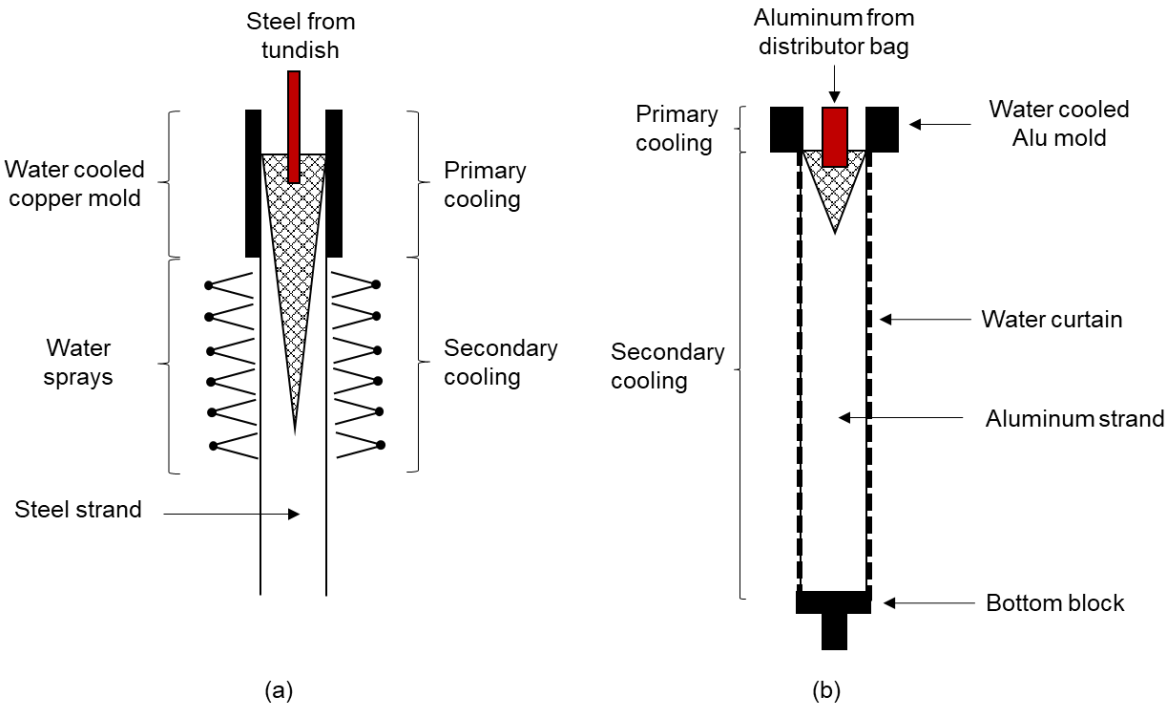

Figure 1.2: Schematics of the cooling processes, for (a) continuous casting of steel and (b) DC casting of aluminum. (They are adapted from [17, 18] and modified to the purpose of current thesis.)

Brimacombe and Sorimachi [19] have summarized the causes of cracking problems in continuous casting of steel. Excessive spray in secondary cooling brings about rapid cooling and enlarges the tensile strains at the slab surface, which leads to opening of small cracks formed in the mold. In contrary, insufficient spray cooling in the secondary cooling region will make the slab to bulge out if the slab surface becomes too hot. All this could result in severe defects such as triple point cracks, midface cracks, midway cracks, centerline cracks and center aggregation, as shown in **Figure 1.3**. Meanwhile, secondary cooling which leads to strong temperature fluctuations also aggravate these cracks.

In the DC casting, it was reported that [20], a high casting velocity tends to cause hot tears, while the cold cracks are prone to occur when the casting velocity is smaller. Meanwhile, hot tears could also form due to frictional forces between the mold and ingot surface. Additionally, thermal stresses generated in secondary cooling also leads to macro deformation of the ingot base or so-called butt curl especially during the start-up phase. Typical material failures encountered in industrial manufacturing are shown in **Figure 1.4**.

Therefore, a thorough understanding on the factors which could significantly affect the cooling rate in the secondary cooling zone is essential. However, due to the difference between continuous casting and DC casting, the cooling process with single nozzle, with nozzle field and with mold should be separately studied and analyzed.

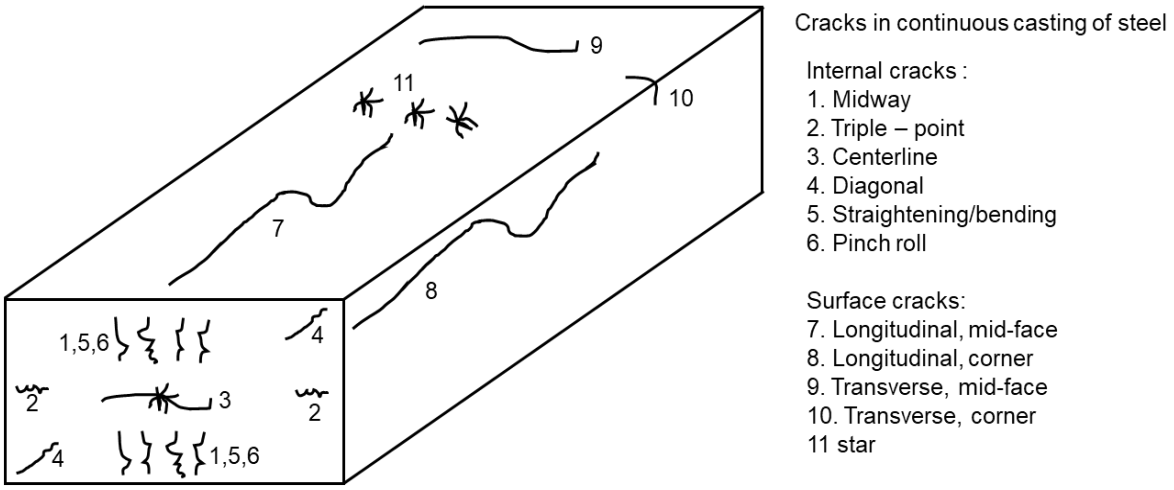

Figure 1.3: Schematic of crack defects in continuous casting of steel. This figure is adapted from [19] and reconstructed.

(a) (b) (c)

Figure 1.4: A typical (a) quarter point crack and (b, c) J cracks taken from industry.

1.4 Literature review – State of art

1.4.1 Quenching mechanism

A hot surface can be visually divided into three regions, when it is quenched by a cold liquid as the surface temperature is higher than rewetting temperature. This is shown in **Figure 1.5**. The wetted and dry region is separated by a visually gray ring with a small thickness. The ring is denoted as wetting front, which is most important to be investigated in the whole quenching test. It is well known in the thermal community that within the wetting front, different boiling mechanisms can occur.

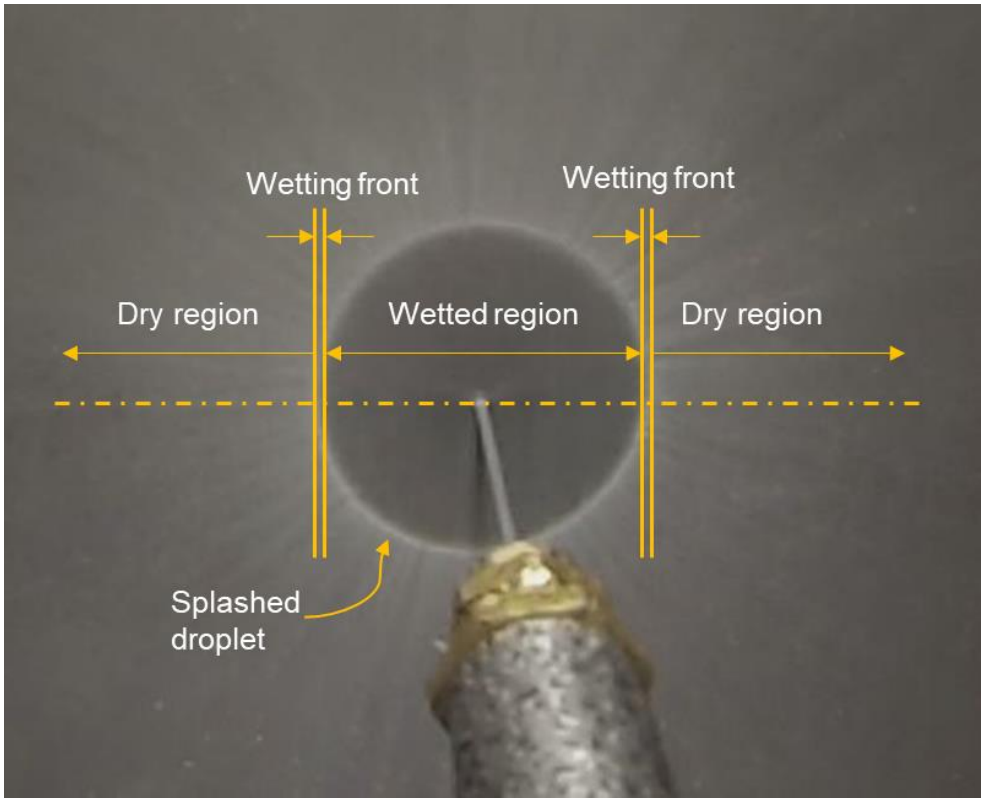

Figure 1.5: Snapshot showing the wetted and dry region at a certain time during a jet impinging an aluminum alloy surface

At a certain time the hot surface experiences four distinct heat transfer regimes which have been shown in **Figure *1.1***. Review on respective regime is presented as follows:

(a) Film boiling regime

A thin layer of vapor exists between the hot surface and incoming liquid when the surface temperature is higher than rewetting temperature. The heat is dominantly transferred by conduction and radiation through the vapor layer which results in a poor cooling rate. The lowest temperature in this regime is termed as rewetting temperature or Leidenfrost temperature [10, 21]. This temperature is affected by several parameters and experimentally studied. Meanwhile, a number of investigations have also reported various correlations to predict the rewetting temperature. Baumeister and Simon [22] have given a semi-empirical correlation to define the rewetting temperature for liquid metals, cryogens, hydrocarbons and water. The expression is given in **Eq. 1.1:**

$$T_{rew} = T_L + \frac{\frac{27}{32} T_{crit} \left\{ 1 - exp\left(-0.52 \left[\frac{10^4 (\rho_s / A)^{4/3}}{\sigma_{Lg}} \right]^{1/3} \right) \right\} - T_L}{exp(\,0.00175\eta) erfc(0.042\sqrt{\eta})} \qquad \text{Eq. 1.1}$$

Bernardin and Mudawar [23] have performed sessile drop evaporation experiments with acetone, benzene, FC-72, and water on heated aluminum surfaces which were either polished, particle blasted, or rough sanded, to study the influence of fluid

properties, surface roughness, and surface contamination on the Leidenfrost point (LFP). The experimental results were then used to assess existing models; however, the discrepancy between the experimental LFP values and those predicted by the models suggested that an accurate and robust theoretical model is not available. Hence, a house database is necessary to be built up to cover the domestic experimental conditions.

(b) Transition boiling regime

The intermittent contact between the surface and liquid manifests that transition boiling is dominant, which is accompanied by a significant increase in heat flux as well as an abrupt decrease in the surface temperature. The regime ends when the heat flux reaches a maximum value which is known as burn-out temperature, or critical temperature or DNB temperature. The term of DNB temperature will be used through this work.

Klinzing et al.[24] reported correlations to define the heat flux in this regime for spray cooling, which is shown in **Eq. 1.2**:

$$\dot{q} = \dot{q}_{CHF} - \frac{\dot{q}_{CHF} - \dot{q}_{MIN}}{(\Delta T_{CHF} - \Delta T_{MIN})^3}[\Delta T_{CHF}^3 - 3\Delta T_{CHF}^2 \Delta T_{MIN} + 6\Delta T_{CHF}\Delta T_{MIN}\Delta T - 3(\Delta T_{MIN} + \Delta T_{CHF})\Delta T^2 + 2\Delta T^3] \quad \text{Eq. 1.2}$$

The critical heat flux in **Eq. 1.2** is given by Mudawar and Valentine [25] as in **Eq. 1.3**.

$$\frac{\dot{q}_{CHF}}{\rho_g h_{Lg} \dot{Q}} = 122.4[1 + 0.0118(\frac{\rho_L}{\rho_g})^{1/4}(\frac{\rho_L c_{p,L} \Delta T_{sub}}{\rho_g h_{Lg}})](\frac{\sigma}{\rho_L \dot{Q}^2 d_{32}})^{0.198} \quad \text{Eq. 1.3}$$

(c) Nucleate boiling regime

The nucleate boiling occurs when the surface temperature lies between the saturated temperature of the liquid and DNB temperature. In this regime, water is in direct contact with the hot surface where the intensive bubble generation leads to an extensive bubble coalescence. Therefore, the created strong thermal barrier induce a significant reduction in heat flux until the surface drops to the liquid saturated temperature. A correlation is reported by Mudawar and Valentine[25] as in **Eq. 1.4**.

$$\dot{q} = 1.87 \times 10^{-5}(\Delta T)^{5.55} \quad \text{Eq. 1.4}$$

(d) Single phase convection

Heat transfer in this regime is very low compared with the other three boiling regimes, since there is no boiling involved in this regime.

Based on the discussion above, it is obvious that, a higher rewetting temperature means an earlier initiation of the rewetting which will shorten the whole quenching process; as the heat flux in transition and nucleate boiling is quantitatively much higher than that in the film boiling regime. Hence a better understanding, furthermore controlling of the rewetting phenomenon is essential when quenching is discussed. This can be more clearly seen in a temperature history during a quenching trial as shown in **Figure 1.6**. It can be seen, the temperature is at first decreased at a very low rate due to the low heat transfer rate in film boiling. As the liquid-hot surface contact proceeds through the transition and nucleate boiling, a significant temperature drop is inevitable due to an intense heat extraction rate. In the single-phase convection, the cooling effect is weakened since there is no boiling involved.

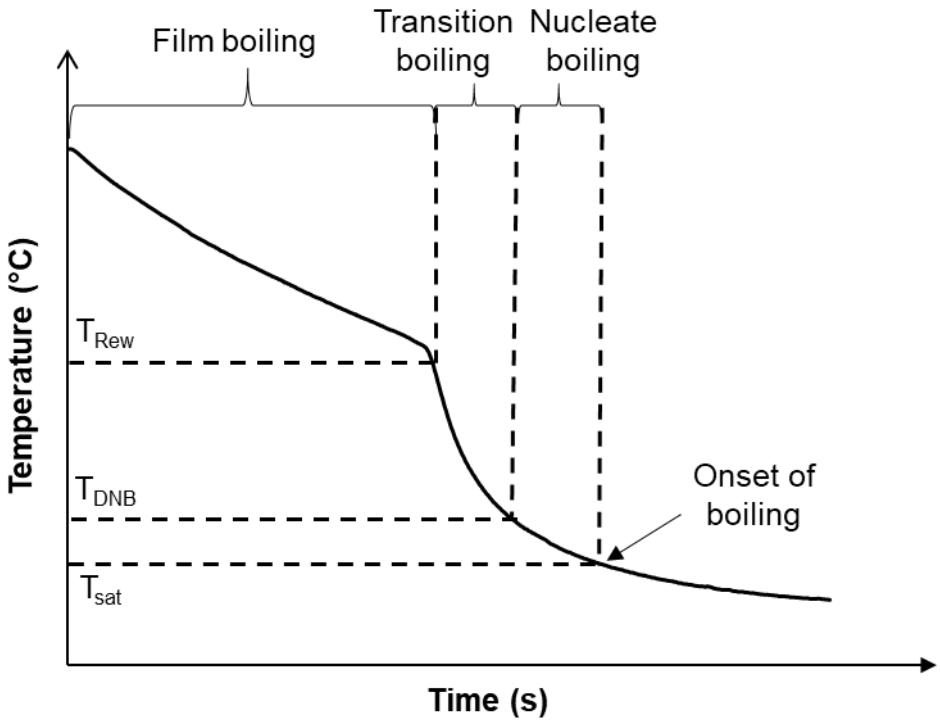

Figure 1.6: Schematics of a temperature history divided into four boiling regimes

1.4.2 Jet impingement quenching

Jet impingement quenching is normally classified as a flow boiling process. A flow boiling differs significantly from the pool boiling due to the forced convection effect of the liquid flow. Due to the high heat transfer rate of the liquid jet, its application potential is significant. Such applications include heat treatment in metallurgy such as extrusion and forging, heat removal under consideration of safety such as in nuclear reactor.

Impingement jets can be classified as either free-surface or submerged. Submerged jets discharge into a space containing the same liquid at reset, while free-surface jets exude into an ambient gas before striking on the target surface (Noted the surface can be either totally dry or already accumulated with a liquid pool (plunging)).

These categories are depicted in **Figure 1.7**. In this research work, free surface circular liquid jets are most often to be used.

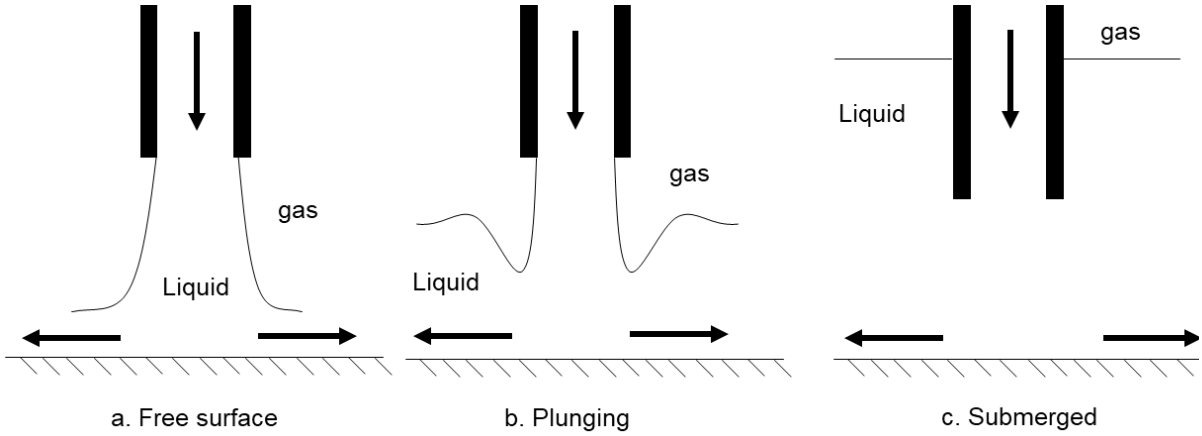

Figure 1.7: Categories of impingement liquid jets

The heat transfer mechanism involved in a liquid jet was already extensively studied by different authors and groups. Preliminary work was published mainly in Japanese research journals during 1970's and 1980's [26-28]. Although these work have given insight into the jet impingement phenomenon, the proposed correlations and heat transfer predictions have their limitation due to the inadequate measurement methods. Many studies since then on jet impingement quenching have been conducted in order to improve the understanding of thermo-physical mechanism occurred in the high-temperature quenching process. Factors including but not limited to Reynolds number (Re) or jet velocity, coolant temperature, nozzle-surface spacing were experimentally and numerically investigated and discussed.

Influence of jet velocity

The jet velocity is normally defined as the liquid velocity at the nozzle orifice. The terms such as water flow rate, Reynolds number can be also read in the open literatures. These terms are interrelated which means that jet velocity can be deduced from a given water flow rate or Reynolds number.

Karwa and Stephan [29] found out an increase of wetting front velocity as jet velocity increases which is shown in **Figure *1.8***. It can be also seen that the wetting front velocity is reducing as the wetting front is radially growing.

Wang et al.[11] reported that the rewetting temperature was not susceptible to the jet velocity as shown in **Figure 1.9**, which is in congruence with results obtained by Lee and Shen [30]. The both articles suggested that the rewetting temperature was almost independent of $v_j \Delta T_{sub}$.

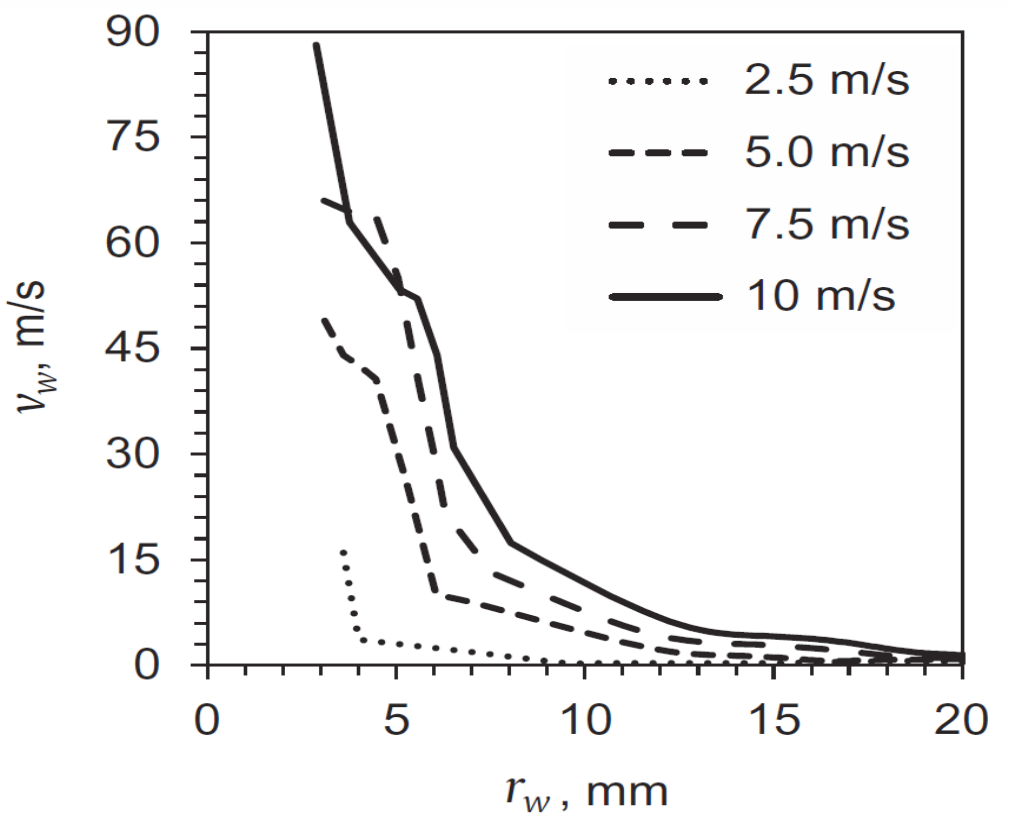

Figure 1.8: Effect of jet velocity on wetting front velocity (adapted from [29])

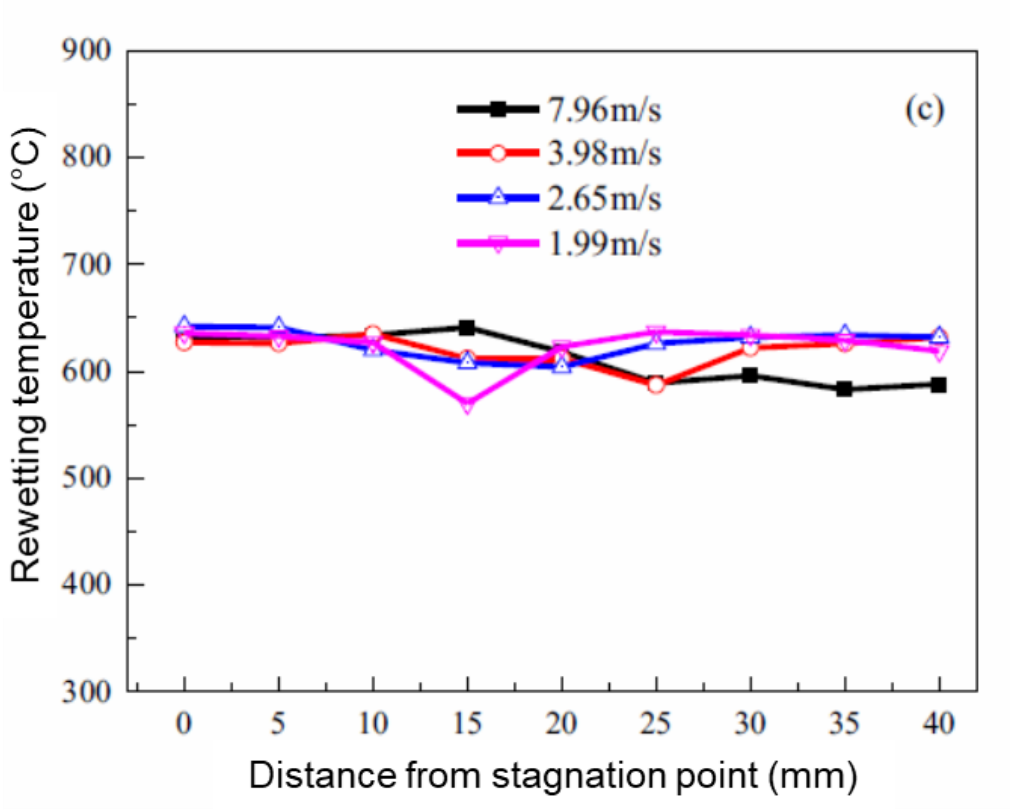

Figure 1.9: Effect of jet velocity on rewetting temperature (adapted from [11])

Influence of liquid temperature or subcooling

The liquid temperature was also extensively studied in the whole quenching process. It was reported in [31] that the boiling curve in fully developed nucleate boiling regime was independent of jet subcooling.

Mozumder et al. [32] have reported maximum heat flux as a function of jet subcooling during quenching a hot cylinder with different experimental conditions as depicted in **Figure 1.10**. It was shown that a higher maximum heat flux can be achieved with a higher liquid subcooling.

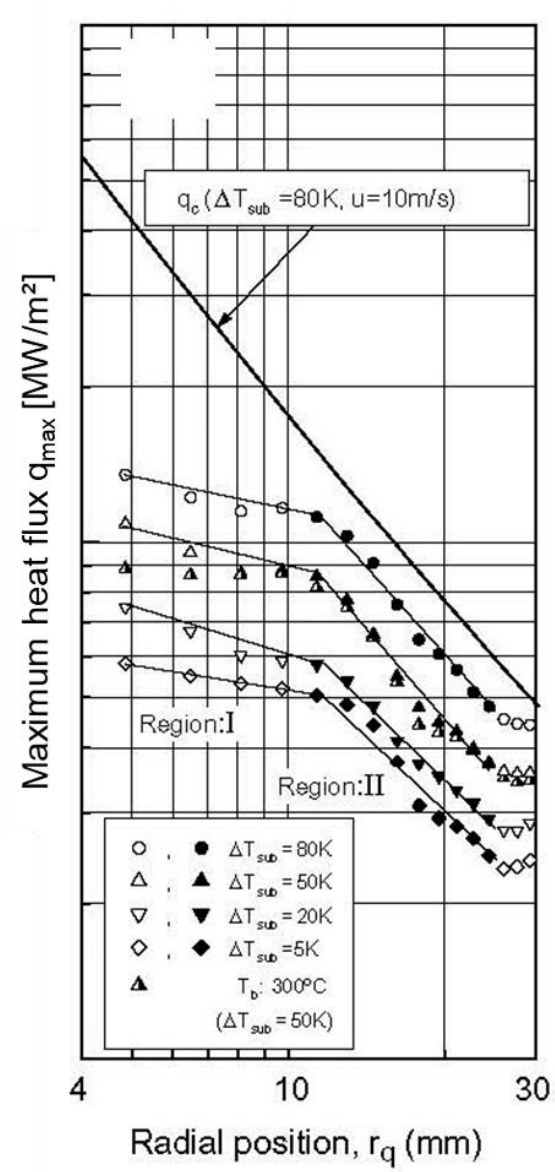

Figure 1.10: Effect of subcooling on maximum heat flux over radial position (adapted from [32])

Influence of additives in the coolant

Besides the subcooling and jet velocity, another possible variable related to the coolant is the additives in the used liquid. Singh et al. [33] performed jet impingement

experiments with TiO_2 based nanofluid. It is found out that heat transfer is enhanced using nanofluid compared to water, as shown in **Figure 1.11**.

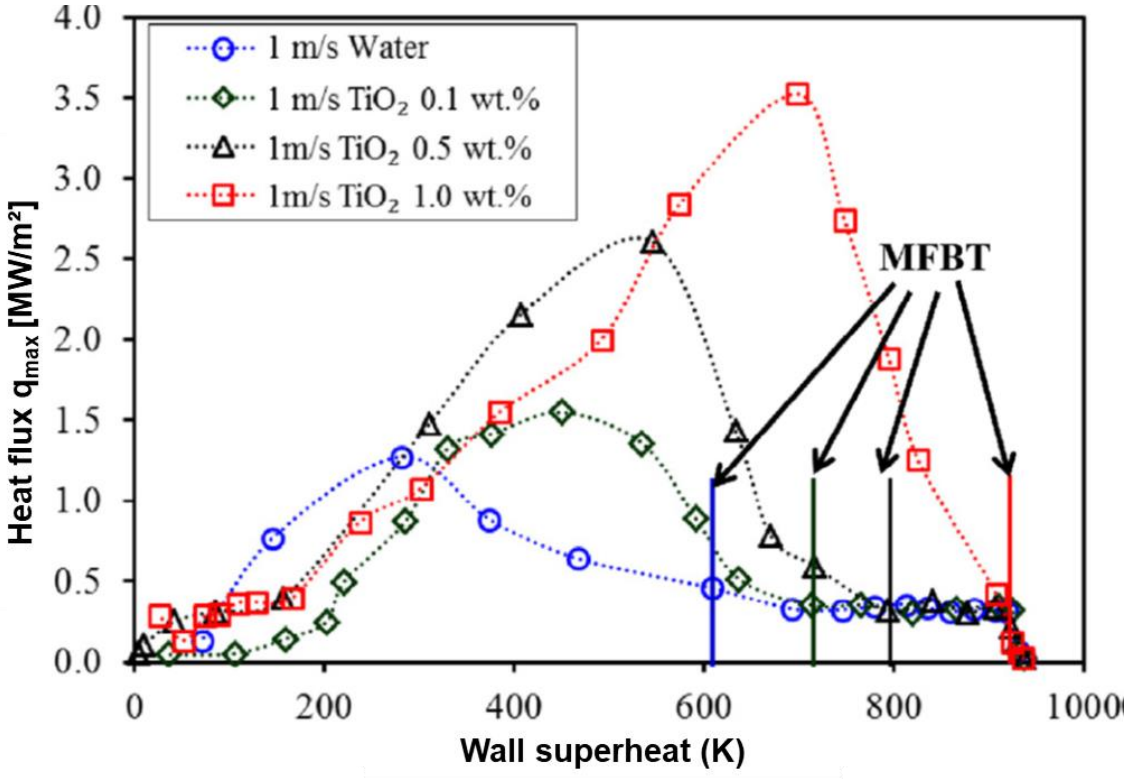

Figure 1.11: Effect of TiO_2 concentration on boiling curve (adapted from[33])

Influence of surface material

Mozumder et al. [32] also investigated effect of material on the quenching performance by using copper, brass and block. The initial temperature and jet velocity were remained as 400°C and 10 m/s respectively. As shown in **Figure 1.12**, the maximum heat flux is a strong function of metal type. It was concluded that material with a higher thermal conductivity results in a higher maximum heat flux.

Hammad et al. [34] performed similar experiments and justified that the difference of thermal conductivity contributes to the deviation of maximum heat flux as depicted in **Figure 1.13**.

Influence of initial surface temperature

Wang et al.[11] conducted experiments to test the influence of initial temperature on the whole quenching performance with a liquid jet impinging on the AISI 304L steel. They found out that the rewetting temperature is severely affected by the initial temperature. A higher surface temperature leads to a higher rewetting temperature as shown in **Figure 1.14**.

However, as shown in **Figure 1.13** reported by Hammad et al.[34], the effect of initial surface temperature on the maximum heat flux is not that significant.

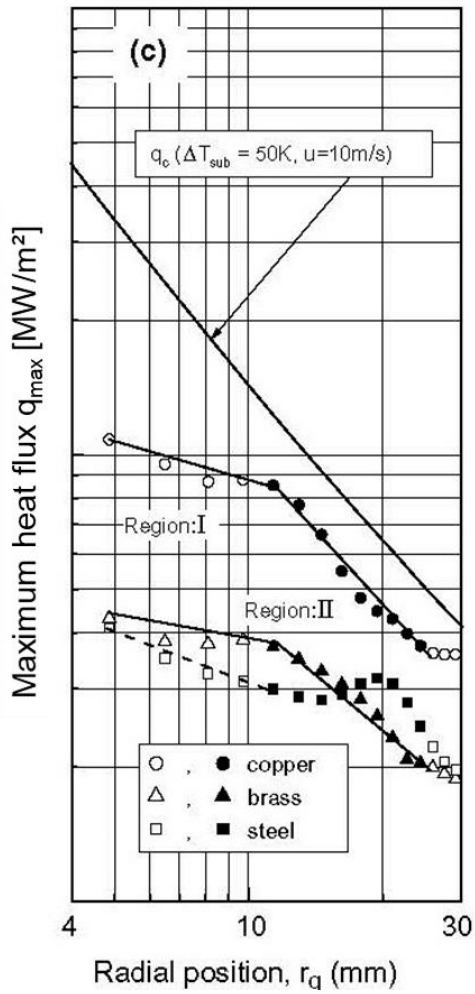

Figure 1.12: Maximum heat flux over radial position for three metal types (adapted from [32])

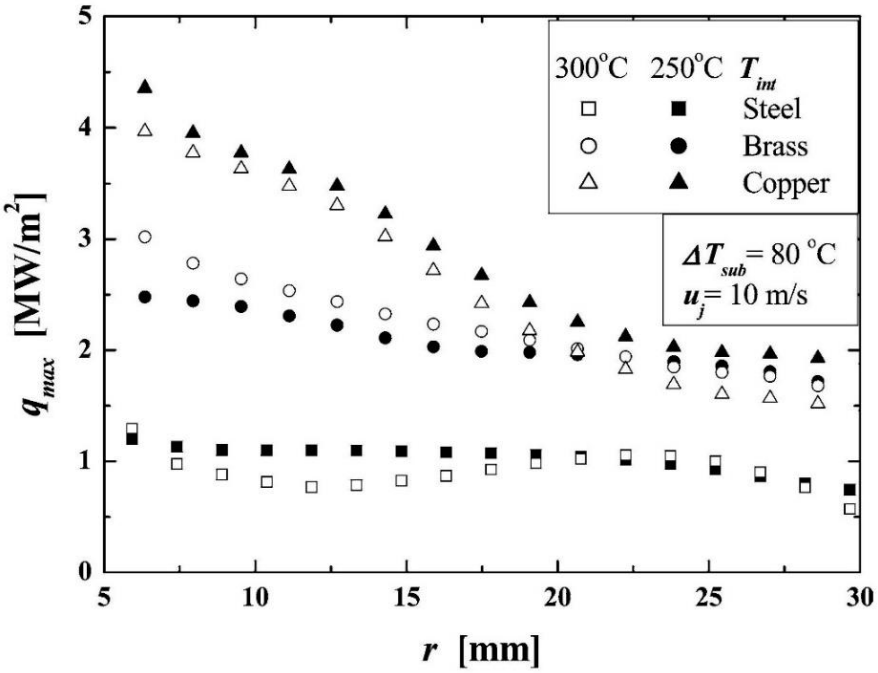

Figure 1.13: Effect of material and initial temperature on the maximum heat flux(adapted from[34])

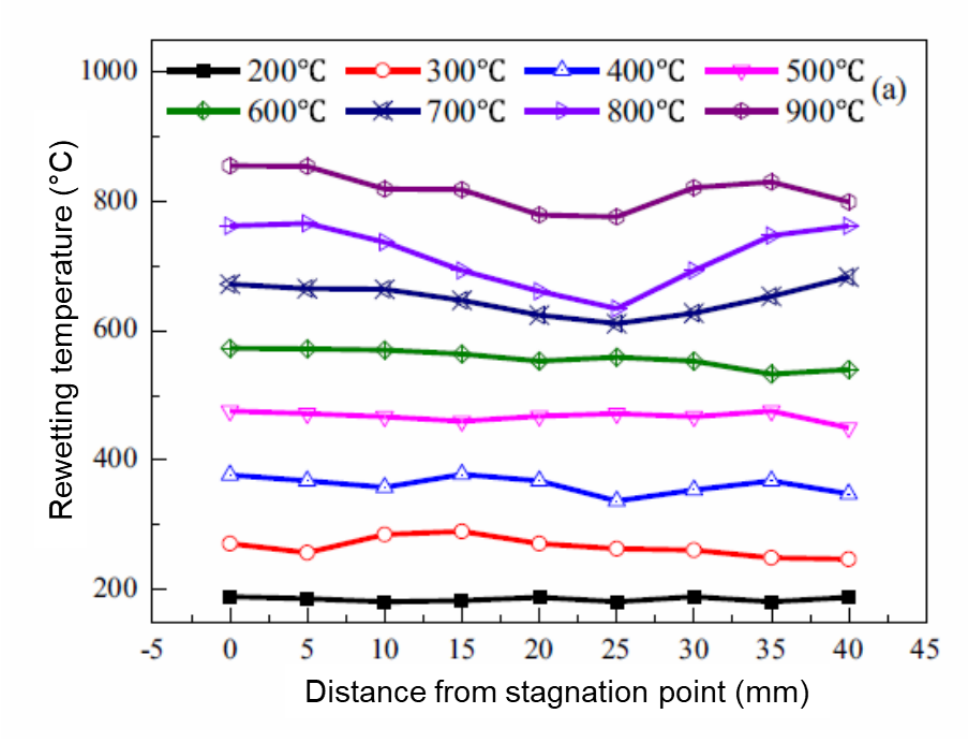

Figure 1.14: Effect of initial surface temperature on rewetting temperature (adapted from[11])

Influence of surface condition

It is well known that the ingot surface is not smooth during the industrial production. Hence it worth investigating the influence of the surface condition on the cooling performance when a liquid jet is applied. Qiu and Liu [35] have performed experiments to study the effect of surface condition on jet impingement heat transfer. The copper surface was coated with titanium dioxide (TiO_2) which had significantly reduced the solid-liquid contact angle to nearly zero degree and made the surface superhydrophilic. It was reported that, the critical heat flux on the superhydrophilic surface is about 30% higher than that on conventional copper surface because of the decreasing contact angle.

Influence of multiple jets

To the best knowledge of the author, the effect of multiple liquid jets on boiling was firstly investigated by Monde et al. [36]. Two or four saturated water jets were used to impinge onto a circular heater surface. A character length (maximum distance from the jet center to the edge of the jet controlled area) was defined to distinguish the different configurations. Later on, Monde and Inoue [37] re-examined the data and suggested that the correlation which was developed for single jet is applicable for multiple jets with acceptable accuracy.

Recently, Sarkar et al. [12] investigated the efficiency of a jet array during cooling a hot steel plate with surface temperature above 900 °C. It was reported that, the

cooling rate is enhanced by 60 % in case of a jet array compared to a single jet at the same water flow rate and impingement height.

Influence of sample thickness

Similarly with the initial surface temperature, the plate thickness is another indication of how much energy can be stored in the plate.

Agrawal et al. [38] recently published the results for investigating the surface thickness on rewetting phenomenon, which is demonstrated in **Figure 1.15**. It has been observed that at a certain Reynolds number, with the increase in surface thickness, the wetting front velocity reduces.

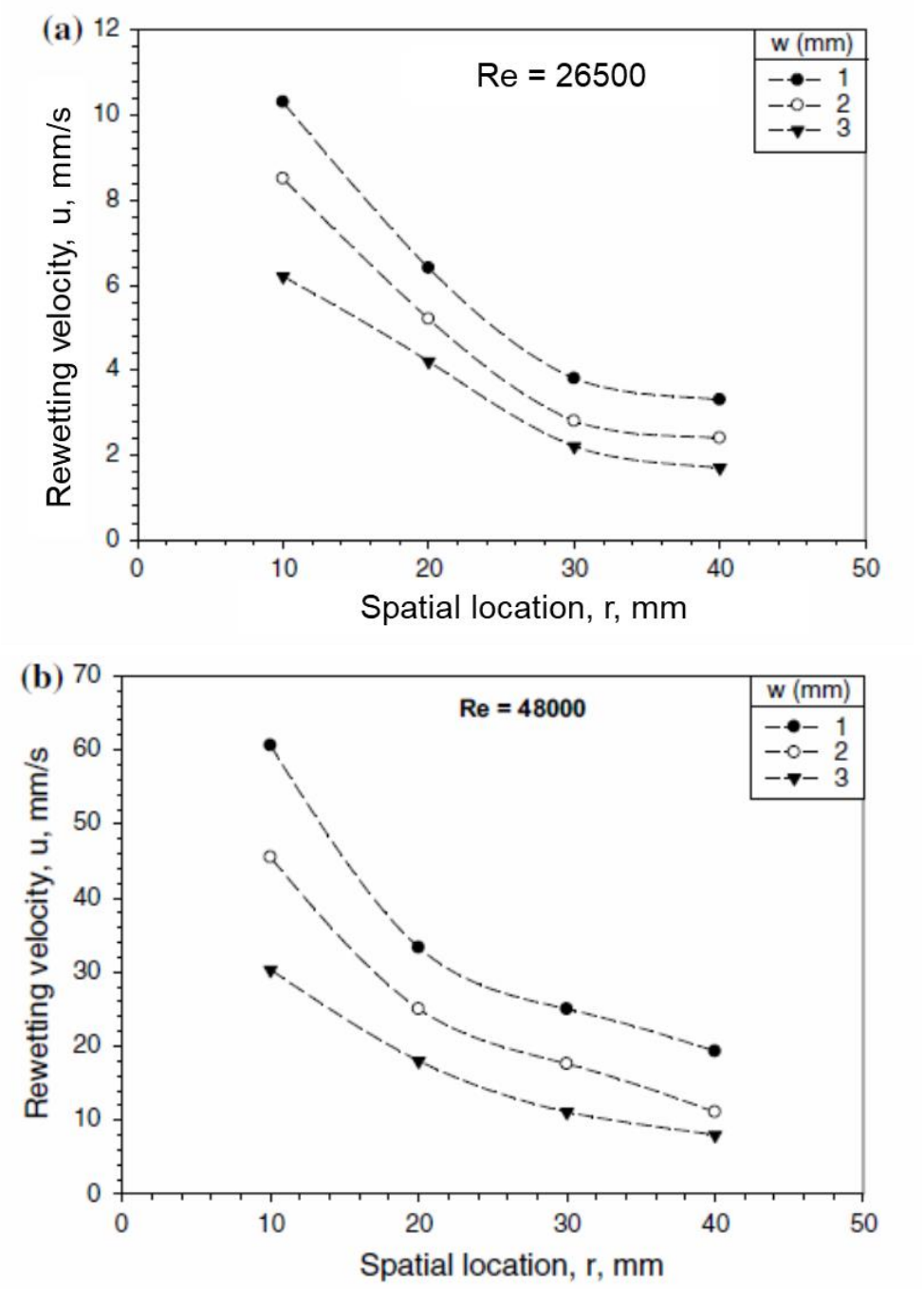

Figure 1.15: Effect of surface thickness on rewetting velocity (adapted from [38])

1.4.3 Mold cooling

The concept of using a mold during direct chill (DC) casting has been developed for a long time in industrial production. It was first invented in 1936-1938 almost simultaneously in Germany (W. Roth, VAW) and the USA (W.T. Ennor, ALCOA) [39]. DC casting is primarily used for producing non-ferrous metal and its alloys such as aluminum, cooper etc. The molten metal from the melting furnace is poured into the mold which is initially enclosed by a bottom block. The cooling due to the direct contact with the cold wall of the mold is termed as primary cooling. When the metal strand emerges from the mold, the cooling water impinges directly on the solidified surface, which is named as secondary cooling. **Figure 1.16** is the schematic representation of DC casting process with main process parameters being underlined.

A poor understanding of the heat transfer process during the DC casting process will inevitably arouse the undesirable defects, including hot tears, cold cracks, bleed-outs, and, in extreme cases, break-outs. Because of that, the cooling boundary conditions are measured preferably with experiments. The objective of the measurements is to obtain the boiling curves which can thereafter be used in the numerical simulations.

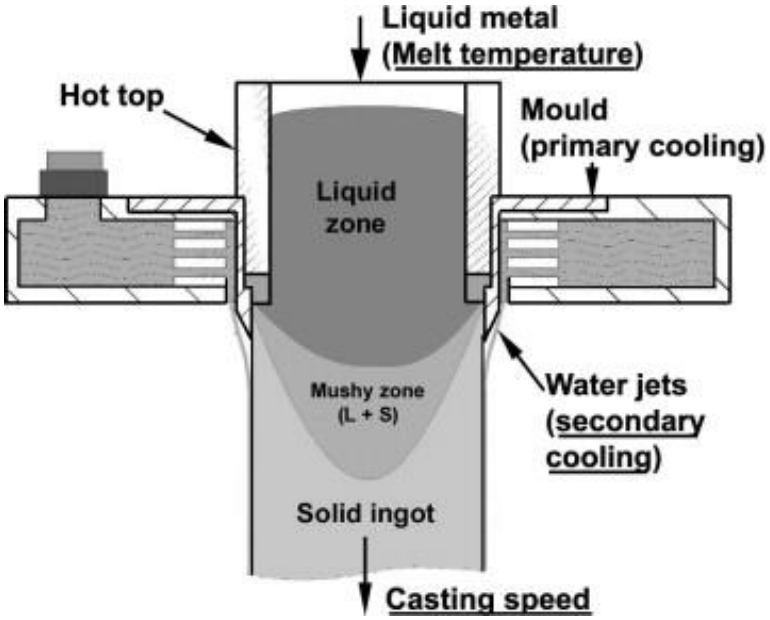

Figure 1.16: Schematic representation of DC casting (adapted from [39])

Weckman and Niessen[40] were the first to quantify the water spray heat transfer in a thermal model for DC casting in 1980s. Their work were further extended by Watanabe and Hayashi,[41] who had distinguished the magnitude difference of heat transfer in the impingement zone and in the free-falling zone. Grandfield et al. [20], Langlais et al. [42] and Hamilton [43] have performed extensive experiments to study the influence of water properties (temperature, flow rate, and quality) on heat extraction during secondary cooling. The results from these studies demonstrated an insignificant relationship between water flow rate and heat flux under high water flow rate conditions

Investigation results from different authors have been summarized by Wells et al. [44] as shown in **Table 1.2**. It is found that, although estimated maximum heat flux from most researchers have the same order (i.e. MW/m²), the temperature at the MHF and the boiling curve in film and transition boiling vary greatly.

Table 1.2: Maximum heat flux from different authors.

Researchers	DNB temperature (°C)	Maximum heat flux (MW/m²)	Metal sample	Method
Weckman[40]	-	1	AA 6063	Industrial trial
Bakken[45]	130-150	5	AA 6063	Industrial trial
Wiskel[46]	180	2.5-3.0	AA 5182	Industrial and laboratory trial
Watanabe[41]	150	1.0-3.0	AA 5052	Industrial trial
Tarapore[47]	-	3	AA 2024	Industrial trial
Kraushaar[48]	200-250	3-8	Al	Industrial trial
Grandfield[20]	~150	6	Al	Laboratory trial
Maenner[49]	~130	4.4-6.6	AA 5052	Industrial and laboratory trial

Effect of impingement and free-falling zone

Generally, the sample surface during secondary cooling can be divided into two regimes based on the experienced heat transfer: the impingement zone, where the water directly strikes onto the surface, and a free-falling zone, where the water flows down the sample surface. Wells et al. [44] performed the calculation based on the partition. It was reported that the boiling curve for impingement region is higher over the entire temperature range, which is shown in **Figure 1.17**. It can be seen that maximum heat flux in impingement zone is about 20% higher than that in the free-falling zone.

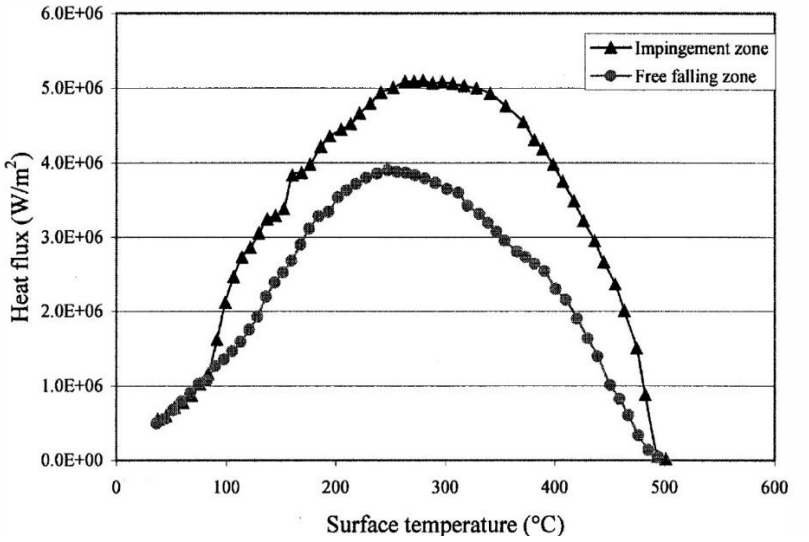

Figure 1.17: Boiling curves for impingement and free-falling zones (from [44])

Influence of jet velocity

Determination of the velocity of individual jet during quenching with mold is not an easy task. More often, it is calculated based on the water flow rate and the orifice dimension.

Nallathambi and Specht [50] did experiments to investigate the influence of coolant velocity by using a mold with 10 orifices. The rectangular nickel plate with initial temperature of 600 °C was cooled at the front side, while the temperature at rear side is recorded with an infrared camera. The measured temperature was solved with inverse method proposed by Ling et al. [51] to estimate the heat flux on quenching side. They found out that the increase in jet velocity will not increase the heat extraction from the hot surface.

Wells et al. [44] performed stationary test with five different flow rates: 0.25, 0.32, 0.38, 0.43 and 0.47 L/s. Their results indicated a slight increase in heat transfer with increasing flow rate, especially in the transition and nucleate boiling regimes as shown in **Figure 1.18**.

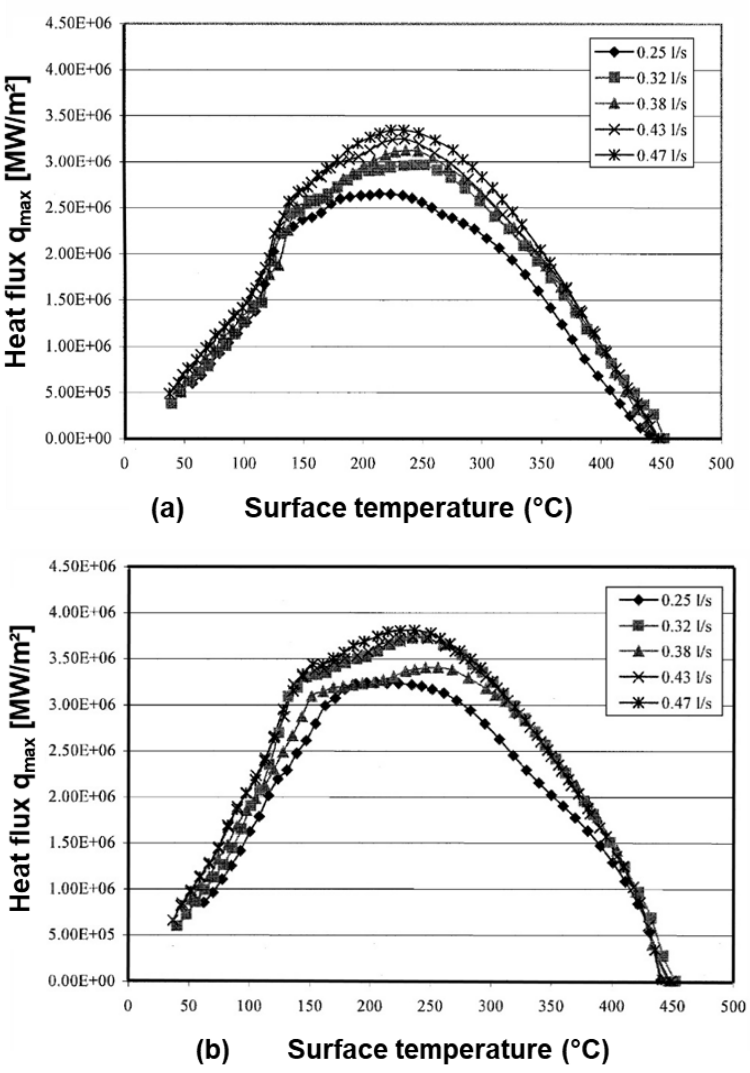

Figure 1.18: Effect of water flow rate on boiling curves (as-cast surface AA 5182) for: (a) impingement zone; (b) free-falling zone. (adapted from [44])

Influence of metal type

The casting recipe in industrial application is mainly dependent on the mechanical and thermo physical properties of the cast metal.

According to the investigation by Wells et al. [44], the discrepancy in boiling curves is attributed to the difference of thermal conductivity. They found out that, the effect of the alloy is most pronounced when surface temperature approaches to DNB temperature for both impingement and free-falling zone, as shown in **Figure 1.19**.

Both Alam [52] and Abdalrahman [53] presented results regarding the influence of metal type with mold. The used metal are AA 2024, Inconel and Nickel. They both found out that, a higher thermal penetration coefficient $(k \cdot \rho \cdot c_p)^{-1/2}$ leads to a faster wetting front propagation which is shown in **Figure 1.20**.

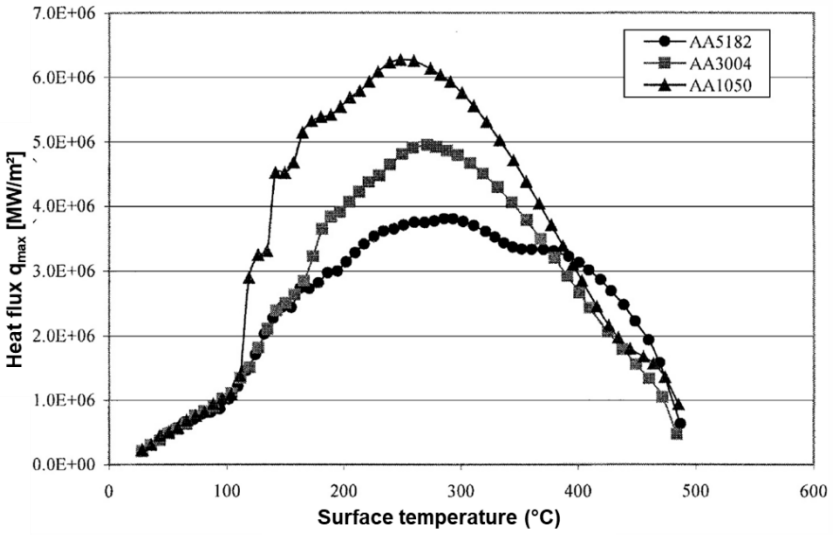

Figure 1.19: Effect of alloy on boiling curve in impingement zone (adapted from [44])

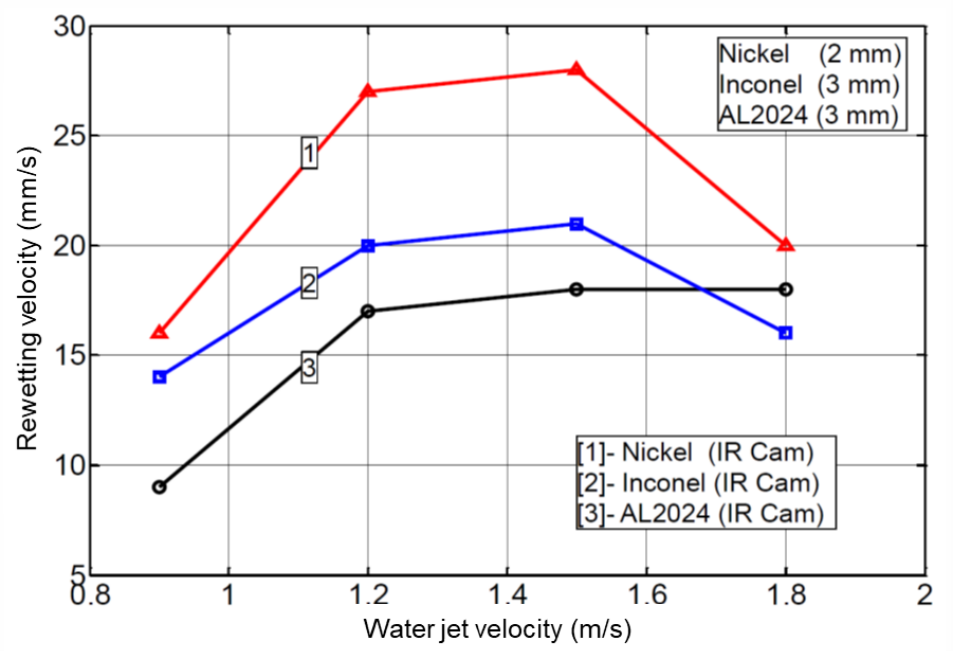

Figure 1.20: Effect of metal type on wetting front velocity (adapted from [53])

Influence of initial temperature

Thermal conductivity demonstrates the ability of a material to transfer thermal energy within the solid content; the initial temperature, however, demonstrates the total amount of thermal energy that is available to be transferred.

Abdalrahman reported the influence of initial temperature on rewetting temperature by using a mold quenching on a nickel sheet with 2 mm thickness. The jet velocity is calculated as 1.2 m/s. The sheet was heated up to 400, 500, 600, 700 °C for investigating the effect of initial temperature. As shown in **Figure 1.21**, a higher rewetting temperature is observed with a higher initial temperature.

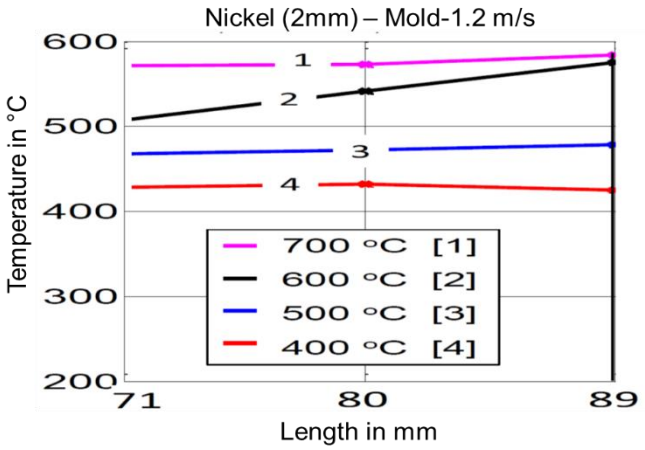

Figure 1.21: Effect of initial temperature on rewetting temperature (adapted from [53])

Similarly, Wells et al. conducted quenching tests on an as-cast surface AA 5182 with initial temperature of 300 °C, 350 °C, 400 °C, 450 °C, and 500 °C. Their results showed that the initial temperature has a significant impact on heat transfer in both the impingement and free-falling zones. This effect is most profound in the transition and nucleate boiling regimes, which is shown in **Figure 1.22**.

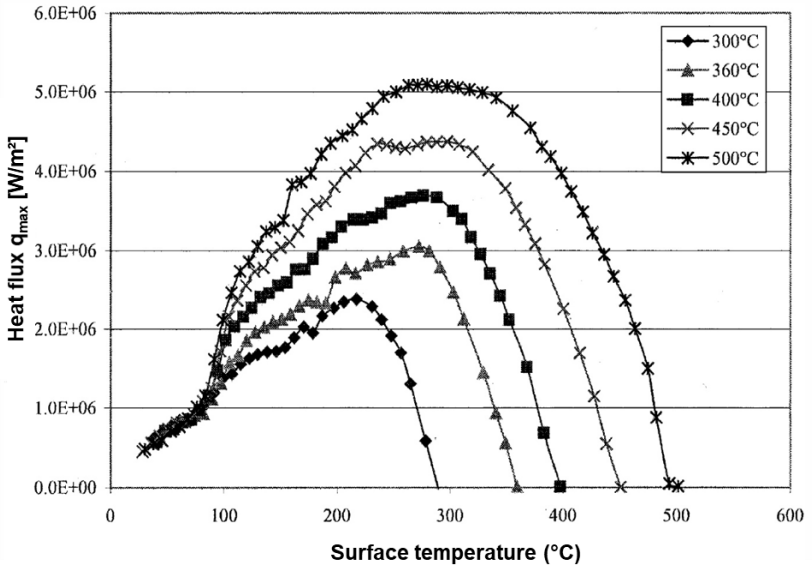

Figure 1.22: Effect of initial temperature on boiling curve for the impingement zone (adapted from [44])

Influence of casting speed

It is well known that casting parameters play an important role in the occurrence of casting defects. Suyitno et al. [54] performed experiments to study the effects of casting speed and alloy composition on structure formation and hot tearing. It was manifest that the grain structure is strongly influenced by the casting speed and alloy composition. Meanwhile, the hot tearing is mostly susceptible to occur at high casting speeds (180 -200 mm/min). Zhang et al. [55] also investigated the influence of casting parameters on microstructure of an AA 7050 billet during DC casting. They found that, increasing casting speed produces a higher cooling rate in the solidification range, which refines the grain structure.

To get boiling curves as boundary condition in inverse models, Caron and Wells [56] carried out experiments with both stationary and moving plate. The advanced cooling front or pre-cooling for both cases was thoroughly discussed. The displacement system they used can move the sample at casting speeds at 10 to 20 mm/s. The effect of the casting speed on the boiling curve is shown in **Figure 1.23**. At an initial temperature less than rewetting temperature, the boiling curves are similar. It can be seen that the curves for a moving sample start at a lower temperature than the curve for a stationary sample (v_c = 0 mm/s). This is mainly explained by the advanced cooling front due to the axial heat conduction from warm area into the impingement region.

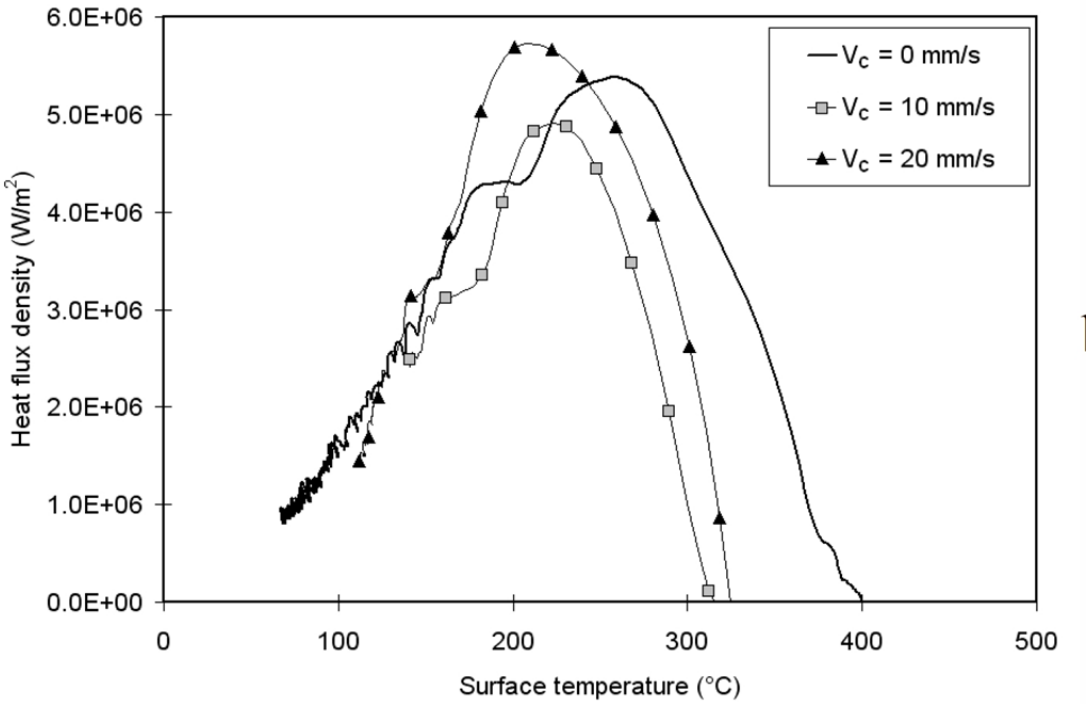

Figure 1.23: Effect of casting speed on boiling curve (adapted from [56])

1.5 State of metal quenching at OvGU

At the Otto von Guericke University Magdeburg, since 2011, practical experience has been gained on the influential variables during cooling processes with different

nozzle configurations and mold. Initially, smaller nickel samples were examined. Over time, larger metal samples with different thicknesses and material were considered.

Alam [52] studied mainly spray and mold during quenching with nickel and AA 6082: In his study, two types of spray have been employed, i.e. pneumatic spray (liquid with air) and hydraulic spray (Only liquid). It has been found out that, the spray flux or spray flux is the most essential parameter which can alter the heat transfer rate in both type of sprays. Meanwhile, the different salts have been added into the deionized water to investigate the influence of salinity on heat transfer with both spray nozzles. It was observed that addition of salts increases the heat transfer in film, transition and nucleate boiling. Moreover, the mold is also used to quench the hot plate. Similarly, two types of molds were utilized: one with eight orifices with each having diameter 4.78 mm; the other with seven orifices with each 2.5 mm. It was observed that the increase in water jet velocity will not enhance the heat extraction from the hot surface.

Abdalrahman [53] continued the investigation of the influence of salinity with hydraulic spray nozzle. He found out that the maximum heat flux, DNB temperature, and the rewetting temperature increase approximately linearly with the salt concentration. Meanwhile, samples with mean rough values of 0.2, 1.7 and 7.7 µm were utilized to investigate the influence of surface roughness on the cooling behavior. It was found that a higher roughness decreased the cooling rate. He also reported that there is an optimum jet velocity during quenching hot surface with a mold. This optimum value lies in the range of 1.2 to 1.5 m/s under his experimental conditions.

Sabariman [21] proposed a theoretical model to predict the heat flux in film boiling region while a spray nozzle is applied. The influence of size and velocity of the droplet, spray flux, surface temperature, water temperature, and the salinity level can be included in this model. The comparison between the model and experimental results from both domestic trials and open literatures was made, which proves the model to be able to capture the influence of those factors in the film boiling when a spray nozzle is applied. Quenching with mold was also investigated, following the previous work. He divided the experiments into two categories: stationary case, where both mold and hot surface were fixed; moving case, where the mold moved upwards with the plate fixed. In his experiments, he has chosen the optimum range which was proposed by Abdalrahman [53]. The jet velocity for the stationary case was selected as 1.2 to 1.5 m/s and was kept constant as 1.2 m/s for the moving case. However, in his calculations, he did not distinguish the difference between impingement and free-falling zone.

It can be seen that, most of the previous studies at the University Magdeburg are mainly focused on spray and mold. Although there are already a lot of publications for the jet impingement cooling, it is still essential to study the phenomenon domestically and build up the own database of jet impingement. By the way, the difference between impingement and free falling zone should also be made.

1.6 Closure

As stated earlier, the jet impingement boiling process is complex and more efforts need to be given for a better understanding of the boiling heat transfer. Due to limitation of the opening publications in this field, much more experimental research is necessary, especially under conditions which are similar to that in aforementioned industrial applications.

The objective of this work is to study heat transfer during quenching non-ferrous metals with experimental conditions which are comparable to that encountered in industry. The experimental results of cooling with liquid jet and mold are quantitatively presented. Experimental variables which can dramatically alter the cooling behavior are thoroughly addressed. Their influence on rewetting & DNB temperature, maximum heat flux, and wetting front propagation are presented.

A good comprehension of cooling mechanism during the secondary cooling regime is essential since defects occur mostly due to the improper cooling recipe. Hence, the factors, which influence the boiling characteristics, must be identified and described quantitatively. They can be employed as boundary conditions in mathematical simulations which can further understand the casting process. To study the boiling characteristics under different conditions, quenching facility is improved; Parameters which are explored in this work are listed in **Table 1.3**.

The results of this experimental work will be the quantitative values under different experimental conditions which will give detailed information regarding the jet impingement and mold cooling. The following content will be contributed by this work:

1. A domestic data base of the boiling heat transfer with liquid jet impingement and mold in the quenching process is developed,
2. The experimental variables during the quenching process is quantitatively characterized to describe the influence on rewetting & DNB temperature, maximum heat flux, wetting front propagation etc.
3. An outlook for future research regarding the quenching process is established.

Table 1.3: Experimental matrix of this work

Cooling methods / Variables	***Spray***	***Full jet***	***Flat fan***	***Mold***
Volume flow rate	Spray flux [21]	Jet velocity	Volume flow rate	Jet velocity
Liquid temperature T_L	Sabariman [21]	x	-	x
Water quality	Sabariman [21]	x	-	x
Inclination angle	-	-	x	x
Material	Sabariman [21]	x	x	x
Surface roughness	x	x	-	x
Thickness s	x	x	-	x
Initial temperature T_0	Sabariman [21]	x	x	x
Casting speed v_c	-	-	-	x

Investigated variables		**Nozzle Field**
Coolant-related	Volume flow rate	x
	Liquid temperature T_L	-
	Salinity (Water quality)	-
	Inclination angle	-
Sample-related	Material	x
	Surface roughness	-
	Thickness s	-
	Initial temperature T_0	x

2. Experimental and Analysis Methodology

2.1 Experimental facility

The experimental setup is schematically shown in **Figure 2.1**. All essential apparatus and components are included in this illustration. An essential part of this facility is the sliding rail which allows the metal sample to be heated up in an electrical furnace with a desired initial temperature. The metal plate is mounted with two supporting rods to the sliding rail. Additionally, the rods are connected with two plastic sliders that are embedded in the rail. This will ensure the movement of the plate to be as smooth as possible. After heating, the metal sheet is brought into the cooling chamber. The heat loss, especially at a high test temperature, is kept as low as possible during the movement of the sample. The nozzle pressure is built up with a gear pump. Alternatively, a centrifugal pump can be used which is mainly used for larger volume flow rates. Both pumps convey the cooling medium from a water tank to the nozzle or mold. The liquid pressure at the nozzle outlet is regulated by changing the number of revolutions of the pump. The liquid from the nozzle is initially reflected by a deflector between the nozzle and the hot sample which prevents the water jet from touching the heated metal sample. The installed unit works with the principle of a guillotine and is operated by a rigid rope.

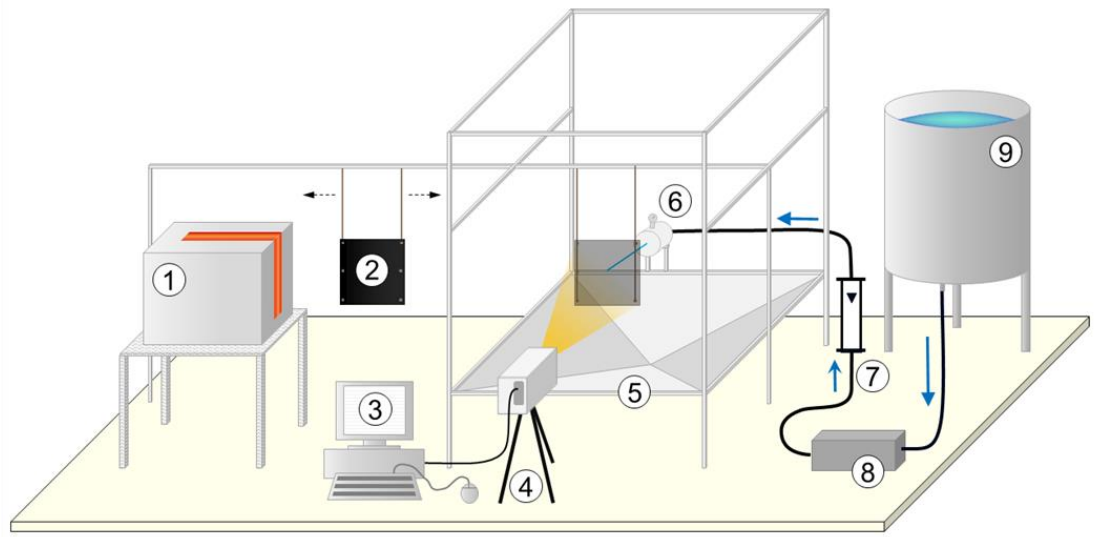

1. Furnace, 2. Metal Sample, 3. PC, 4. Infrared camera, 5. Cooling chambe,
6. Nozzle with pressure gauge, 7. Flowmeter, 8. Pump system, 9. Water tank with heating function

Figure 2.1: Schematic of experimental setup

The data acquisition system consists of an infrared (IR) camera connected to a computer. The software "ThermaCAM Researcher 2001" records the transmitted data and saves them. The installation of the cooling chamber prevents the uncontrolled spreading of the liquid droplet which might deteriorate the thermal image quality. In

addition, the resulting vapor during the quenching process is held in the chamber and thus does not reach the receiving area of the camera lens. Furthermore, the nozzle including manometer can be easily replaced. The nozzle spacing to the metal sample being tested is also easily adjustable.

2.2 Infrared thermography

When temperature measurement is discussed, the most often mentioned technique is to use a thermocouple. A thermocouple is a device which produces a temperature-dependent voltage as a result of the thermoelectric effect, and this voltage signal can be interpreted to measure the temperature. However, several issues aroused by implementing a thermocouple limit their applications, they are as follows:

1. Attaching a thermocouple at a specific position with a requirement of firm contact is normally not possible; this will sometimes break the examined sample.
2. If the fine measurement is required, especially when a high spatial resolution is needed; this preludes using the thermocouples since every thermocouple has a specific size.
3. Thermocouples are often used in high-temperature applications. In this case, the practical life is limited by thermocouple aging, which will definitely deteriorate the measurement accuracy.

All objects above absolute zero temperature (0 K) emit infrared radiation. Hence, an alternative for temperature measurement is to use the infrared thermography which detects the emitted radiation power from the measured surface. With this technique, the temperature can be measured at higher frequency and various positions in real time.

Infrared thermography has been brought into scientific community for long time. Infrared thermography has been brought into scientific community for long time. Specht and coworkers [10, 21, 53, 57, 58] have used IR thermography for analyzing heat transfer with different cooling methods during metal quenching. Labergue et al. [13, 59] used an infrared camera to measure the temperature during cooling of a hot surface using sprays and jets. Freund et al. [60] calculated the local heat transfer coefficient based on the measured temperature with infrared camera.

In this work, infrared camera ‘ThemaCAM SC 3000’, produced by FLIR systems Inc., was used, which is shown in **Figure 2.2**. This camera provides the ability to measure temperature with different quality by varying the measuring frequencies and temperature ranges. Four temperature ranges (-20 to 80 °C, 10 to 150 °C, 100 to 500 °C and 350 to 1500 °C) can be selected with four options of the desired frequency (50, 150, 250 and 750 Hz). Noting that, when a higher frequency is chosen, the size of the thermal image will be smaller. For example, when 50 Hz is selected, the full resolution of this infrared camera (320 × 240 pixel) can be reached; while for 150 Hz,

the maximum resolution is reduced to 80 × 320 pixels. For the purpose of accuracy and suitability, all the measurements in this work have been carried out with a frequency of 50 Hz, with which 50 thermal photos can be taken in one second.

Figure 2.2: Infrared camera from FLIR Systems

'ThemaCAM researcher 2001' is the software with which the detected infrared signal by infrared camera can be presented as thermal images. If the recorded process is transient, the output is a thermal video. The temperature history can then be obtained by proper analysis of the video. **Figure 2.3** shows the parameters which will influence the accuracy if they are not suitably adjusted. In order to achieve a high surface emissivity, the measured side of the sample is sprayed with a high temperature graphite coating. This will ensure a higher accuracy of the temperature measurement.

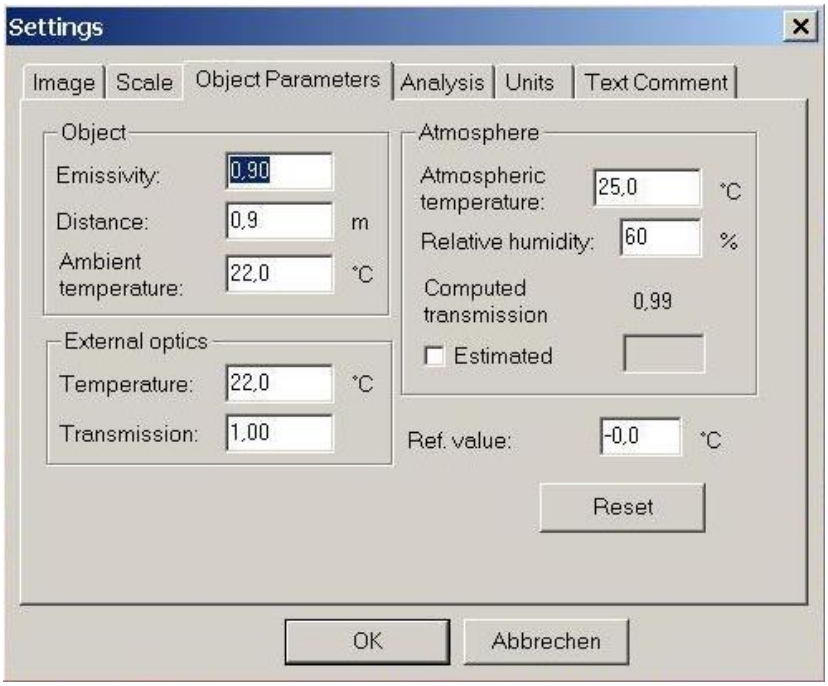

Figure 2.3: Parameter setting of the infrared camera

2.3 Shutter

In the experiments, water strikes onto the surface of a metal sample as a spray, full or flat spray which requires a pressure that is set with a pump. It is essential that the pressure remains constant throughout the cooling process. This is solved by an incorporation of a shutter plate which is shown in **Figure 2.4**.The shutter plate is proved to be the ideal solution in several test runs.

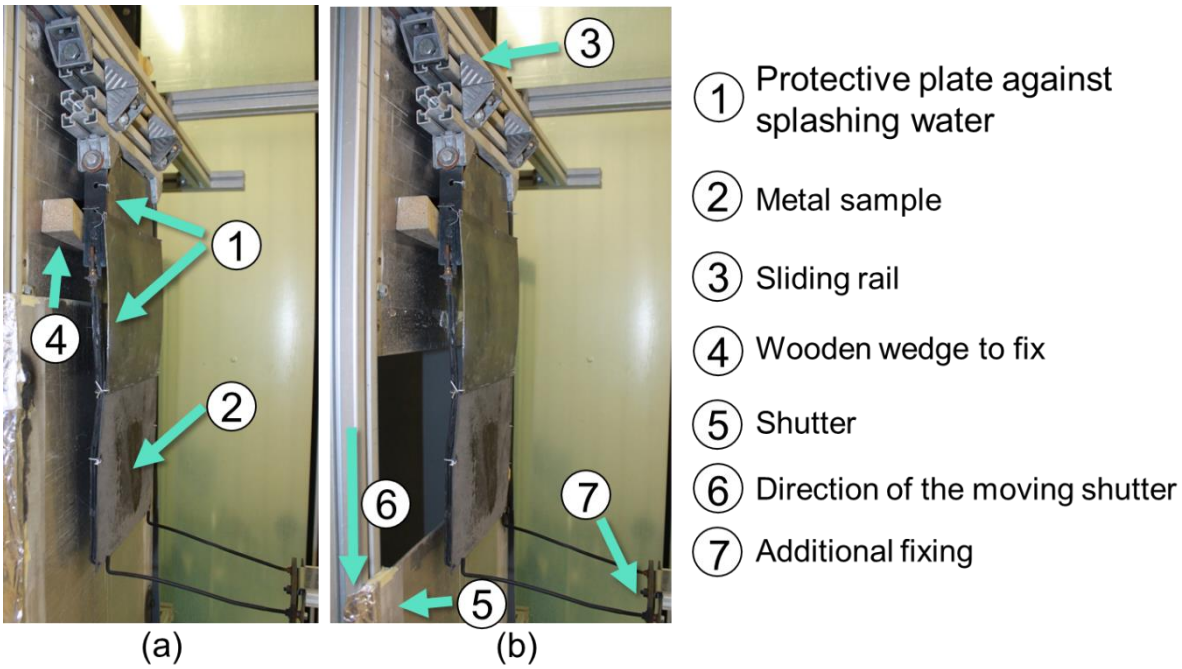

Figure 2.4: Shutter and positioning of the sample plate

At the beginning of each experiment, the shutter is pulled up with a rigid rope and anchored in that position as shown in **Figure 2.4 (a)**. Enough time has been given to achieve the stable nozzle pressure, when the water jet initially strikes the shutter. Only when the rope is released, the shutter moves vertically downwards due to the gravity, as shown in **Figure 2.4 (b)**. Afterwards, the water jet hits the previously placed metal sample with a constant pressure. Due to this installation, the beginning of the cooling process can be better controlled.

2.4 Furnace

A very important part of the setup is the furnace. Here, the metal samples are heated with a heat intensity of around 1 kW. The heating is done by ten heating coils that are embedded in the ceramic fiber boards. Additionally, the oven has an outer covering made with 5 cm thick calcium silicate plates. The two sorts of boards are used because they are very stable and easy to be machined. At the same time, they are environmentally friendly and can be disposed without additional consideration. By installing these two insulating layers, the heat loss through the furnace wall is very low due to the low thermal conductivity of both layers. The largest heat loss occurs at the

entrance and the top opening. The top opening of the furnace is kept very narrow and intended for the supporting rods. This allows the metal sample, which is fixed by two rods to be pulled in or out directly into the oven. The positioning of the metal sample in the electric furnace is shown in **Figure 2.5**.

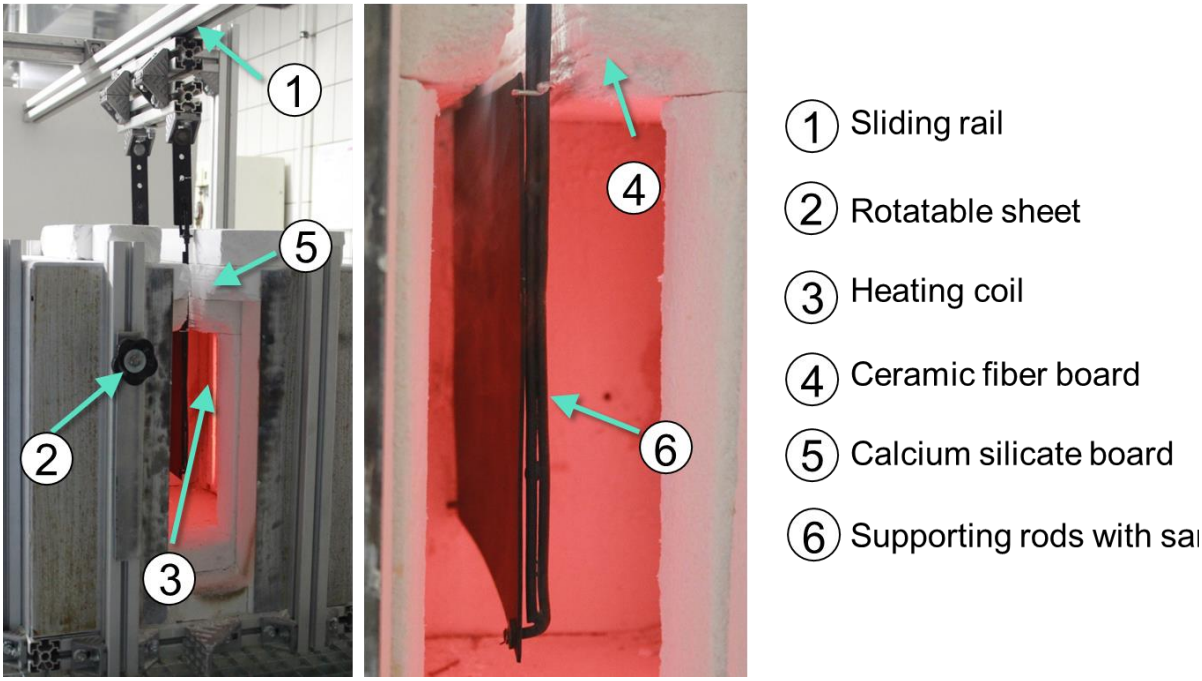

Figure 2.5: Metal sample inside the electrical furnace

The length of the supporting rods is adjusted so that the top edge of the fastened plate does not touch and damage the insulation boards. There is also a temperature sensor which measures the air temperature in the electric furnace. A digital display is mounted for the visual inspection of the inside temperature. It takes about 2.5 hours for a heating process to 900 °C.

2.5 Investigated Nozzles

In this work, different nozzles and two nozzle fields are investigated. All tested nozzles are produced by the manufacturer "Lechler". These are axial full cone, flat spray and full jet nozzles. The nozzle field is a home-made and consists of nine (inline) or ten (staggered) full jet nozzles.

A schematic representation of the tested nozzles is shown in **Figure 2.6**. The typical liquid spray and jet formed by the different nozzles are demonstrated. In the full-jet nozzle, the impinging jet of water flows radially outward. The flat spray nozzles have an initially rectangular footprint which propagates on both sides with similar volume flow. Full cone or spray nozzles theoretically produce a uniform circular area. The nozzle field studied in this work composed of the same full jet nozzles.

Figure *2.7* depicts the initial spray diameter on metal surface. The spray angle and nozzle spacing are very important due to their direct influence on the footprint area.

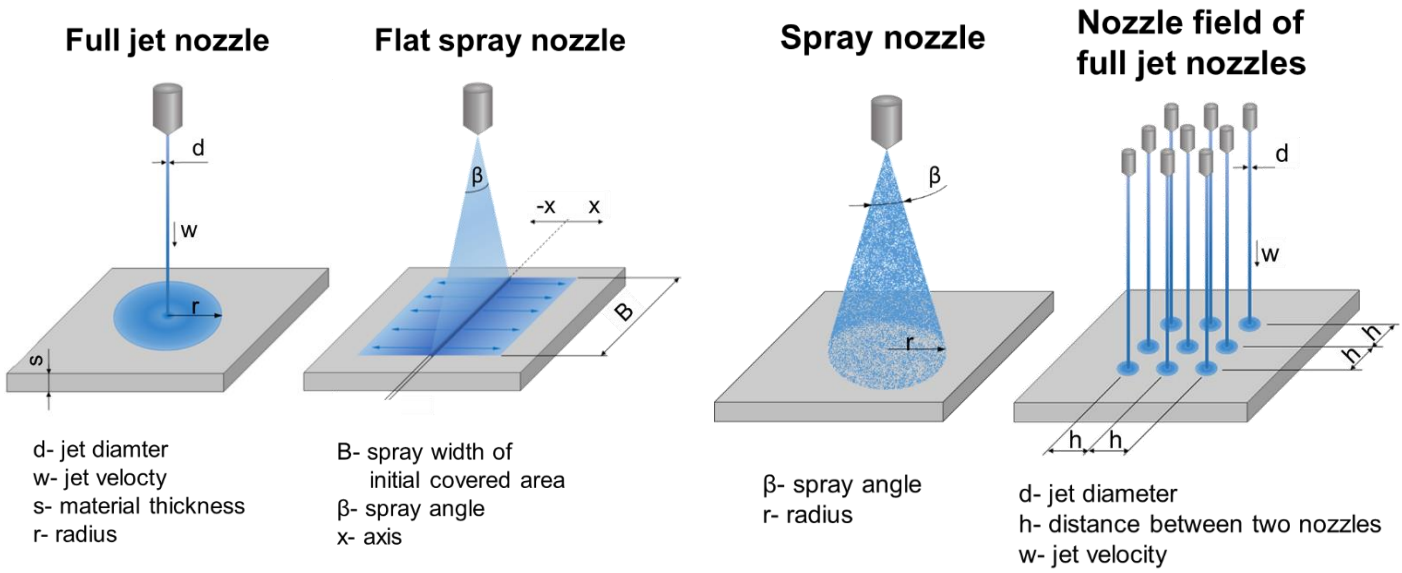

Figure 2.6: Schematics of the investigated nozzles

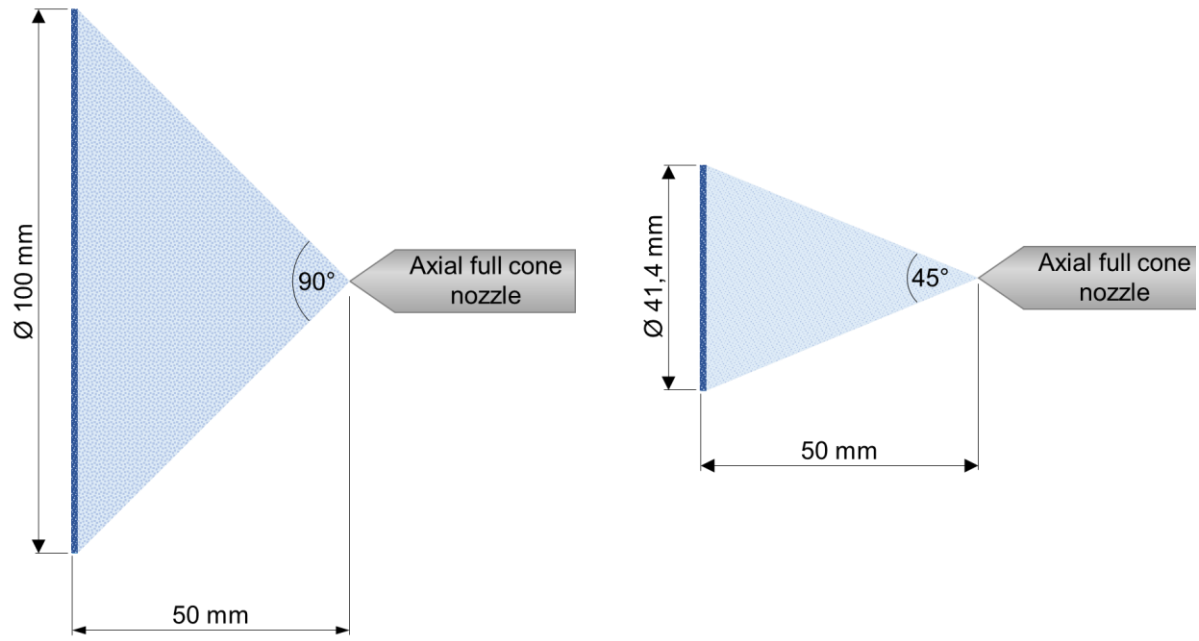

Figure 2.7: Initial spray footprint on the sample surface with different spray angels

Table 2.1 lists the used nozzles in this work and the serial number is based on when they are bought (Noting that they might be not produced by Lechler in the future).

Table 2.1: An overview of the investigated nozzles

Nozzle type	Nozzle designation according to Lechler	Features
Full jet nozzle	544.360	Stainless steel, d = 1.05 mm
	544.400	Stainless steel, d = 1.3 mm
Spray nozzle	460.404	Spray angle β = 60 °
Flat spray nozzle	632.674	Flat spray angle β = 60 °

The inline (a) and staggered (b) arrangements are schematically shown **Figure 2.8**. In this work, the selected nozzle is full jet nozzle with diameter 1.05 mm. The distance between the nozzles are held constant. However, the nozzle-to-nozzle spacing and nozzle type can be accommodated in various tests.

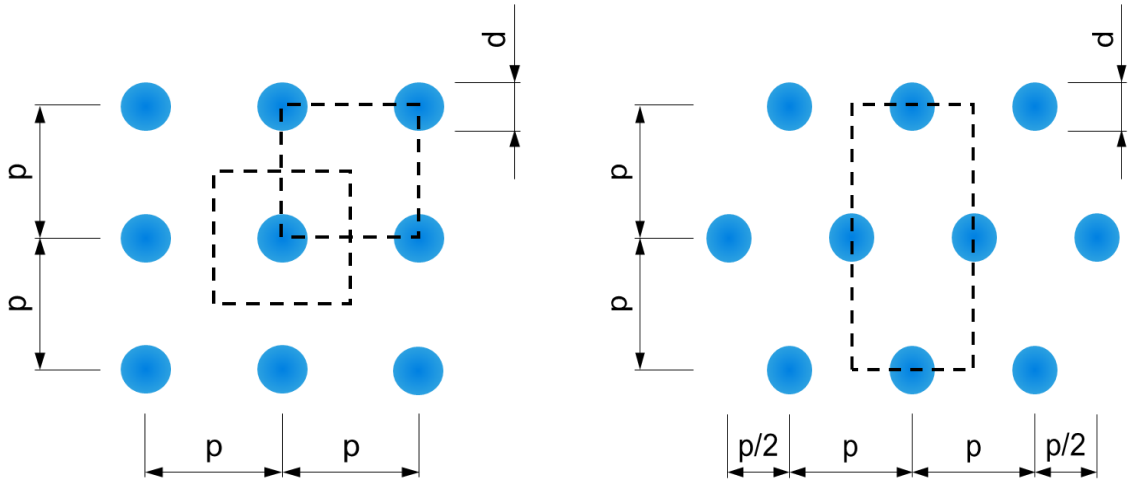

(a) Inline (b) Staggered

Figure 2.8: Schematics of inline and staggered configuration (h= 35 mm, d= 1.05 mm, h/d= 33)

2.6 Mold

A miniature of the mold in industrial application has been finished according to domestic requirements, as shown in **Figure 2.9**. This is used to mimic the cooling process which occurs during the secondary cooling zone in the DC casting process.

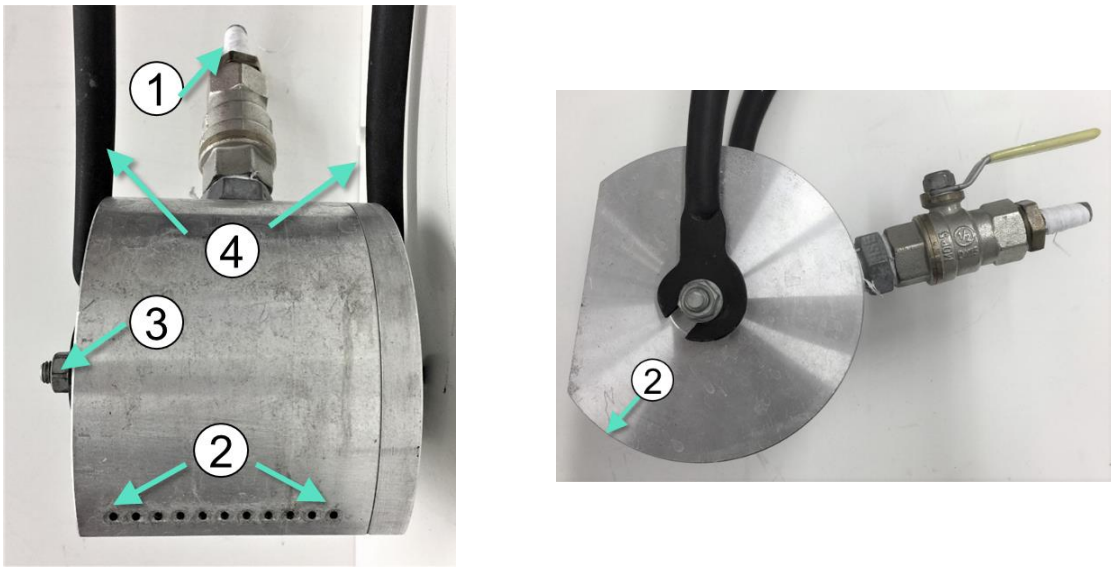

Figure 2.9: Photo of the mold used in this work ((a) front view; (b) side view): 1.water supply, 2. Orifices, 3. Adjustable screw for angle variation, 4. Supporting rods

The mold has totally 11 orifices, each with 2 mm in diameter. The distance between the centers of orifices is 6 mm. A water curtain will be formed and then flow vertically on the surface due to gravity. In all experiments with static and moving plate,

the distance between the orifice and plate is set constant as 8 mm, which enables the smooth variation of the mold-to-plate angle. This cooling method is operated under moving and static modes, as depicted in **Figure 2.10**. In the static instance, the mold is so fixed that water jets from the mold can directly impinge on the top area of the hot surface; in the moving instance, the plate is mounted onto a truss which is connected to the DC motor. The motor can then move the plate from top to bottom with a preset casting velocity.

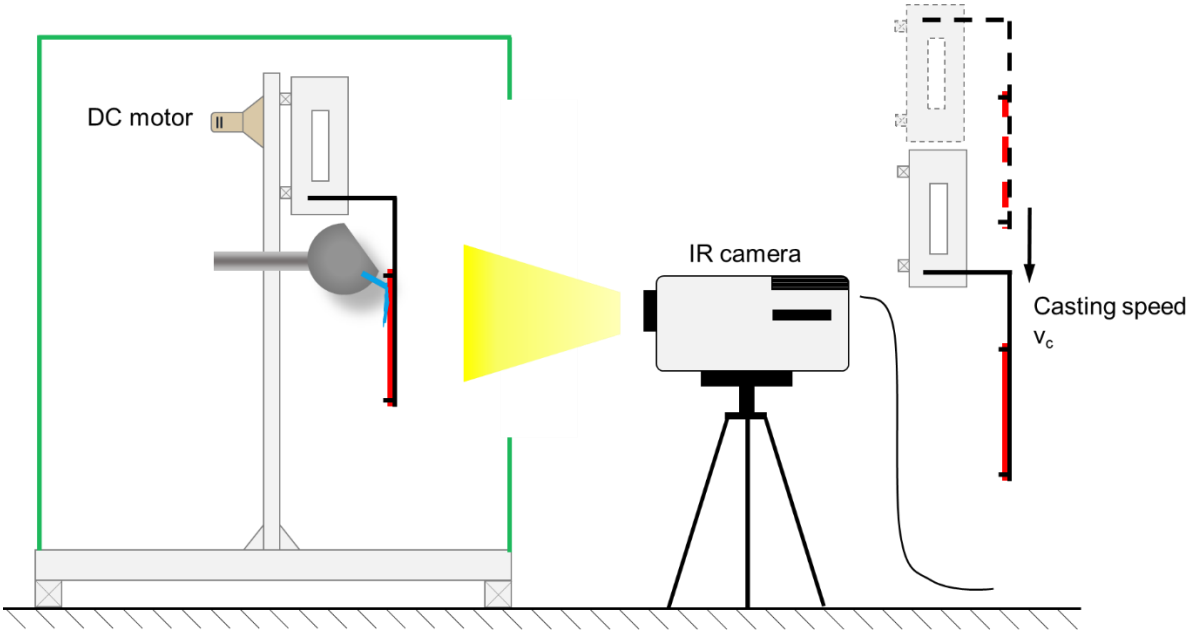

Figure 2.10: Schematics of static and moving mechanism

The movement of the motor is controlled by a set controller (IT 116 Flash), as shown in **Figure 2.11**. It is a one axis-controller which enables the linear or rotary motion with a two phase-stepper motor. 128 micro steps for one-full step is established for this controller, which makes a very smooth motion not impossible. At last, the communication between IT116 and PC is realized via a serial interface (RS232).

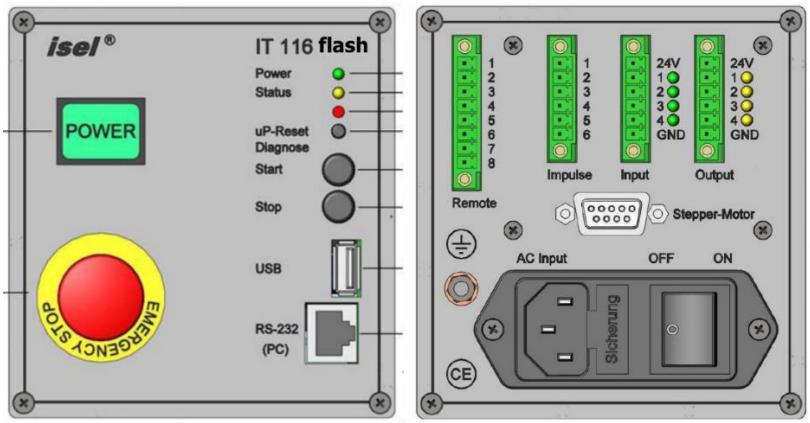

Figure 2.11: Schematics of the front(left) and back(right) side of the IT 116 Flash (This is adapted from the user manual)

2.7 Metal samples

In this work, commercially pure nickel, nicrofer, aluminum alloys, cooper alloys were used. The metals are machined into different shapes according to the used cooling method. For example, a rectangular plate is used to fit the overall size of a nozzle field. The back side of the metal sample is painted black with a commercial thermo-painting to get a high and stable emissivity. The quenching side is machined as requested, i.e., polished, original industrial surface, or artificial structure.

Figure 3.7 shows the two investigated surfaces: one with artificial cubic pin structure, the other with original industrial surface. For conciseness, not all the samples will be shown. It is worth mentioning that, the size of the metal sample is maintained same when differences between nozzle field and a single nozzle are compared.

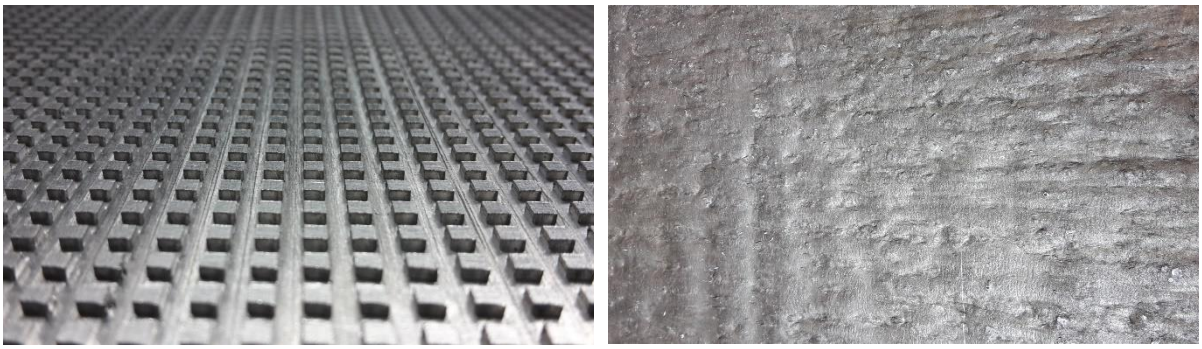

(a) AA 6082 with cubic pin fins (b) AA 5083 from industry

Figure 2.12: surface structure of investigated metal samples

2.8 Implementation of experiments

It is necessary to clarify how the experiments in this research were conducted, because experimental results should also be possible produced in another testing facility. Generally, there are two main steps which should be followed: preparation and execution.

2.8.1 Preparation

The metal samples in different thickness and shape are used several times in the course of the experiments. At the beginning of each measurement, the sheets are straightened with the aid of a straightening machine followed by a careful treatment of the metal surface with an angle grinder. After cleaning, a thermal coating in matt black is applied to the metal surface. Here it is possible to choose between the Ulfalux and the Senotherm coating. The measured emissivity and its influence on measured temperature profiles can be found in **Section 2.12**. After a drying phase of twelve hours, the metal plates are heated for about three minutes at 300 ° C and then cooled in the air. This is to ensure a stable thermal coating during the quenching process.

All experiments are carried out in the laboratory. For this purpose, the electrical furnace is used to heat up the metal plate. It takes about 2 hours to reach 900 °C. The desired temperature is then given, which is slightly higher than the required initial temperature. For instance, to achieve a desired initial temperature of 500 °C, 520 °C is accordingly adjusted. This temperature difference is essential to compensate the heat loss during the sample movement from the furnace to the cooling chamber. While the furnace is heated up to the preset temperature, the metal sample to be tested is fixed to the thin supporting rods made of stainless steel. Wires are used for attachment and should prevent the release of the sheet during the cooling process. In addition, a cross brace is installed above the metal sample, which significantly minimizes the deformation of the metal sample and provides better infrared images. In addition, a protective layer was mounted above the metal sample as shown in **Figure 2.4**, which prevents splashing water from reaching the front measuring window. Subsequently, the pump system is prepared when the water tank is filled and specific volume flow rate is selected.

The Infrared camera position is adjusted to capture the appropriate thermal image of the metal sample. The camera is connected to the lab computer through ‘ThemaCAM Researcher 2001’, where essential parameters such as object emissivity, the ambient temperature are defined. Furthermore, the camera focus is manually regulated in order to achieve thermal images with higher accuracy. Additionally, image directory should be created to save the measurement data.

2.8.2 Execution

The metal sample could be moved into the cooling chamber as the set temperature is reached. Simultaneously, the pump is initialized until the required nozzle pressure is attained. A wooden wedge is used to fix the metal sample additionally. The software displayed the current surface temperature of the sheet. Shortly before reaching the initial temperature, the infrared recording is started with releasing the shutter.

Due to the limitation of the infrared camera, two recordings must be performed to obtain the whole temperature curve, when the required initial temperature is greater than 500 °C. These two recordings are attained by conducting experiments under two temperature regimes: 100 – 500 °C (low regime) and 350 °C – 1500 °C (high regime). The cooling process with the high regimes is firstly recorded. The initial temperature at some specific position can thus be read from the thermal recording. A new measurement is then performed at low regime. For this purpose, the metal sample is first heated up to the previously measured initial temperature which can be determined by using an infrared thermometer from "Voltcraft". This method is necessary because the infrared camera cannot display temperatures over 500 °C correctly at the lower temperature regime. A same initial temperature is absolutely required to combine these two measurements.

Each measurement is followed by a detailed analysis to acquire necessary parameters to quantify the boiling curves. The analysis is detailed in **Section 2.11**.

2.9 Repeatability of the experiments

In the experimental work, the accuracy and precision of the measured temperature is primarily guaranteed by the infrared camera. With specific numerical methods, the temperature gradient or cooling rate can be determined. The overall accuracy of the measured temperature is around 3 % which is illustrated by repeated temperature measurements under the same experimental conditions as shown in **Figure 2.13**. Hence, all the experiments which are included in this work have been repeated at least twice in order to avoid the experimental error.

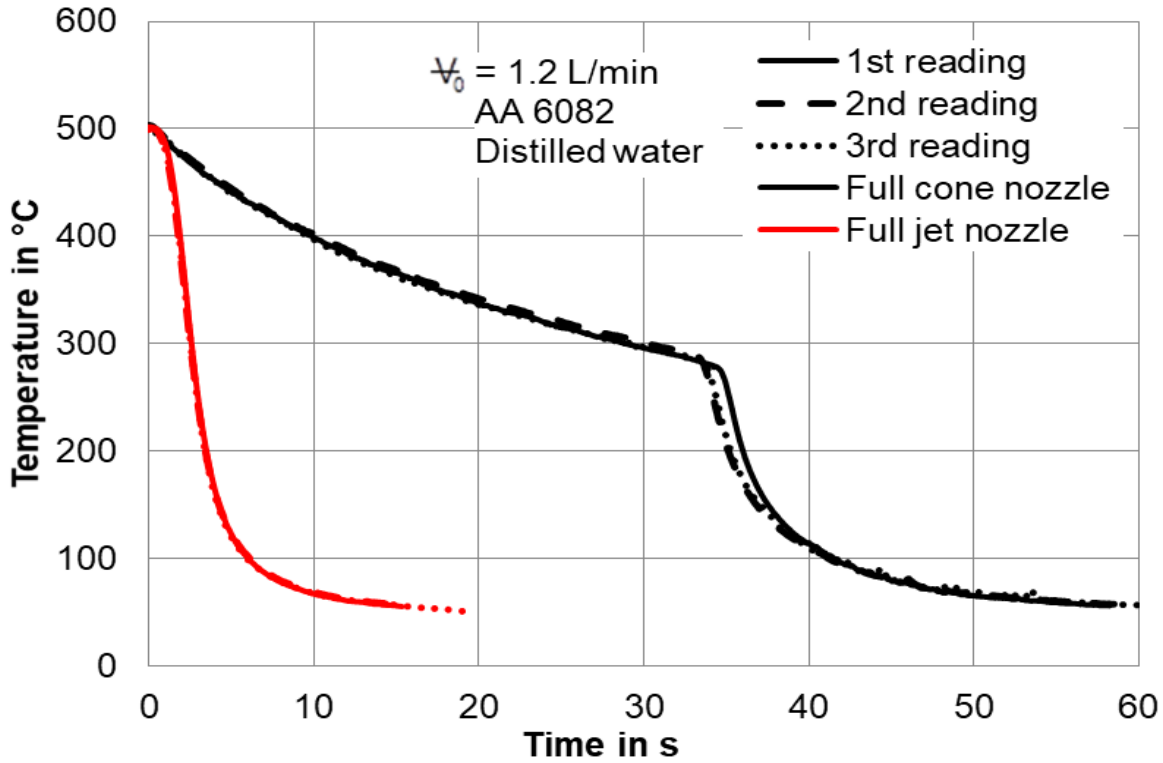

Figure 2.13: Repeatability of selected experiments at r(adius) = 19 mm

2.10 Experimental plan

As addressed in Table 1.3, the experiments under specific conditions of interest for different cooling methods are detailed as below.

2.10.1 Single nozzle

(a) Full cone nozzle with spray angle of 60 °

1. Influence of thickness *s*

Table 2.2: Experiments of different thickness with full cone nozzle

	s = 3 mm	s = 5 mm	s = 10 mm
AA 6082	×	×	×

2. Influence of surface roughness

Table 2.3: Experiments of surface roughness with full cone nozzle: (a) artificial surface; (b) industrial surface of AA 5083 and CuSn4

	R_a = 0.3 µm	Cubic pin fins
AA 6082	×	×

(a)

	R_a = 0.7 µm	R_a = 46.2 µm (from industry)
Material: AA 5083	×	×
	R_a = 4 µm	R_a = 14.7 µm (from industry)
Material: CuSn4	×	×

(b)

(b) Full jet nozzle

1. Influence of nozzle outlet pressure

Table 2.4: Experiments of jet velocity with full jet nozzle

	p = 1 bar	p = 5 bar	p = 9 bar
Nickel, 2 mm	×	×	×

2. Influence of thickness

Table 2.5: Experiments of sample thickness with full jet nozzle (orifice = 1.3 mm)

	s = 2 mm	s = 3 mm	s = 4 mm
Nicrofer	×	×	×

3. Influence of metal type

Table 2.6: Experiments of different metal samples with full jet nozzle

	Nickel	Nicrofer	Copper B14
T_0 = 500 & 850 °C	×	×	×

4. Influence of surface roughness

Table 2.7: Experiments of surface roughness with full jet nozzle: (a) artificial surface; (b) industrial surface.

	R_a = 0.3 µm	Cubic pin fins
AA 6082	×	×

(a)

	R_a = 4 µm	R_a = 14.7 µm (from industry)
CuSn4	×	×

(b)

(c) Flat spray nozzle

1. Influence of inclination angle

Table 2.8: Experiments of inclination angle with flat spray nozzle

	α = 25°	α = 45°	α = 65°	α = 90°
Nickel	×	×	×	×

2. Influence of nozzle outlet pressure

Table 2.9: Experiments of nozzle outlet pressure with flat spray nozzle

	p = 1 bar	p = 5 bar	p = 9 bar
Nickel	×	×	×

2.10.2 Nozzle field consist of full jet nozzles (orifice = 1.05 mm)

1. Influence of jet velocity

Table 2.10: Experiments of jet velocity with nozzle fields

	v_j = 9.5 m/s	v_j = 15.9 m/s	v_j = 20.4 m/s
Nickel	×	×	×

2. Influence of initial temperature

Table 2.11: Experiments of initial temperature with nozzle fields

	T_0 = 500 °C	T_0 = 700 °C	T_0 = 850 °C
Nickel	×	×	×

3. Influence of nozzle configuration

Table 2.12: Experiments of nozzle configuration with nozzle fields

	Inline	Staggered	Singular
Nickel	×	×	×

2.10.3 Mold

1. Influence of surface roughness

Table 2.13: Experiments of surface roughness for various metal alloys with a mold

	Smooth (R_a = 3 µm)	Rough (R_a = 43 µm)
CuCrZr	×	×
	Smooth (R_a = 4 µm)	Rough (R_a = 15 µm)
CuSn4	×	×
	Smooth(R_a = 1 µm)	Rough (R_a = 46 µm)
AA 5083	×	×
	Smooth (R_a = 0.3 µm)	Rough (cubic pin fins)
AA 6082	×	×

2.11 Methodology of Analysis

In order to calculate heat transfer coefficients or heat flux, the energy balance under transient condition should be applied which bases on the first law of thermodynamics.

2.11.1 One dimensional method for single nozzle and nozzle field

In this research work, major results for single nozzle and nozzle field are deduced by one-dimensional analysis, in which the temperature difference along the thickness direction is assumed negligible. However, the larger heat flux in the regime of nucleate and transition boiling makes this assumption untenable, since a large temperature difference between the quenching and measuring side could be expected. Hence, a method to determine the temperature history on quenching surface based on the measured values should be further developed and validated. This method is normally named as ‘‘Inverse Heat Conduction Problem (IHCP)’’. The ill-posed nature of the inverse analysis demands sophisticated mathematical formulation and numerical analysis. Considering this, a calculation and comparison has been made to quantify the disparity between the one-dimensional model and two-dimensional inverse method. Sabariman [21] has compared the temperature difference along with time by using an inverse method which is developed by Nallathambi and Specht [50]. It is reported that the maximum temperature difference between quenched and measured surface is around 15 °C, which is depicted as in **Figure 2.14**. It can be found out that in the film boiling regime where low heat flux is observed, the temperature difference is small compared with that in nucleate and transition regime. This indicates that the results for nucleate and transition boiling based on one-dimensional analysis are inherently prone to contain higher errors.

Despite that, one-dimensional analysis has its own advantages. For example, it is easier to be programmed and needs less numerical manipulations. And in order to minimize the errors caused by the one-dimensional analysis, plates with small thickness are preferred. The used plates for experiments with single nozzle or nozzle field in this work has the maximum thickness of 4 mm. To make it clear, the one dimensional energy balance for cylindrical coordinate will be depicted in detail.

As shown in **Figure 2.15**, the energy balance can be written as:

$$Q_{condution,in} - Q_{condution,out} - Q_j - Q_{convection} - Q_{radiation} = \frac{dH}{dt} \qquad \text{Eq. 2.1}$$

Heat loss due to $Q_{convection}$ and $Q_{radiation}$ are neglected due to their small magnitude compared with the energy extracted by the liquid jet Q_j. Therefore, Eq. *2.1* is simplified as follows:

$$Q_{condution,in} - Q_{condution,out} - Q_j = \frac{\partial H}{\partial t} \qquad \text{Eq. 2.2}$$

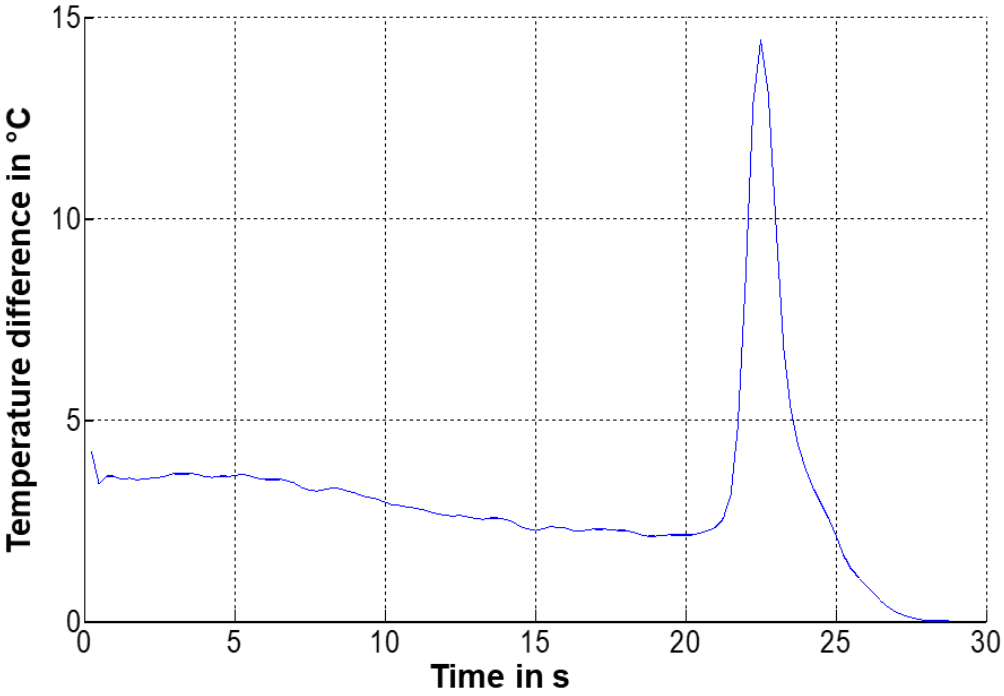

Figure 2.14: Temperature difference across the thickness during quenching a 2 mm aluminum alloy (adapted from [21])

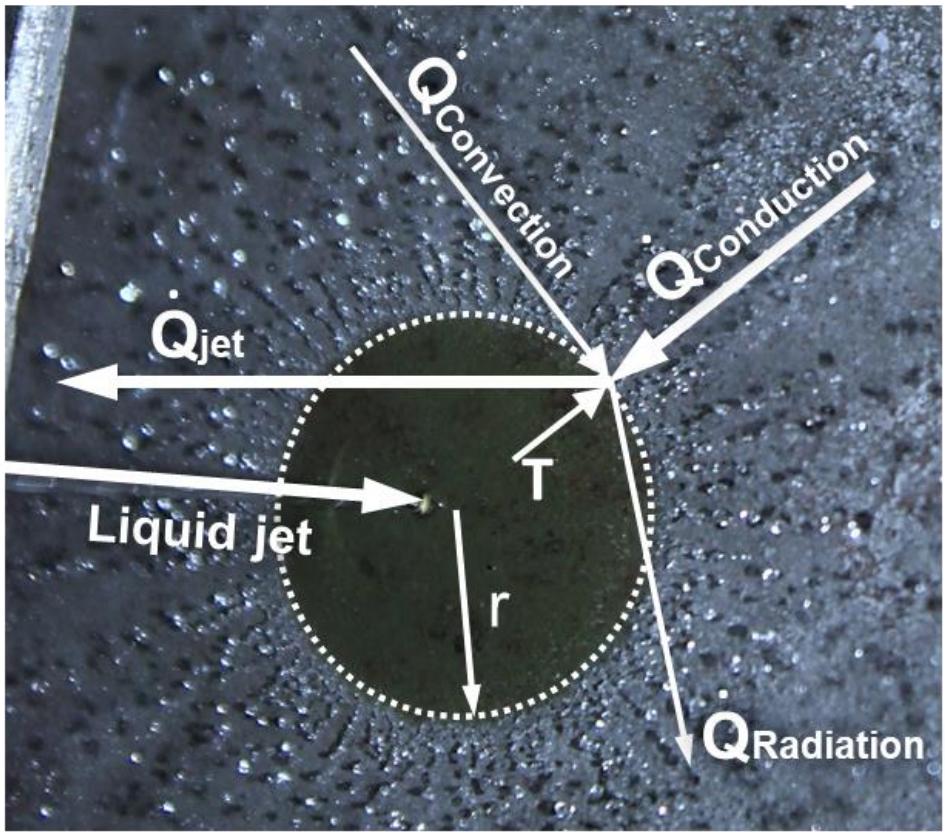

Figure 2.15: Heat transfer analysis during quenching with liquid jet

Heat flow goes into the control volume due to axial conduction is defined as:

$$Q_{condution,in} = A_r q_r = (2\pi rs) q_r \quad \text{Eq. 2.3}$$

Where heat flux in radial direction is determined based on Fourier's law in one-dimensional case: $q_r = -k\frac{\partial T}{\partial r}$.

Along with Taylor series expansion which is depicted as:

$$f(x+dx) = f(x) + f'(x)\frac{dx}{1!} + f''(x)\frac{(dx)^2}{2!} + f'''(x)\frac{(dx)^3}{3!} + \cdots\cdots \quad \text{Eq. 2.4}$$

The heat flow goes out of the control volume can be deduced only when the terms except the first two at right hand side are truncated in Eq. 2.4. Hence, $Q_{conduction,out}$ can be expressed as:

$$Q_{condution,out} = (2\pi rs) q_{r+dr} = (2\pi rs)\left(q_r + \frac{\partial (q_r)}{\partial r} dr\right) \quad \text{Eq. 2.5}$$

Heat flow due to liquid jet cooling can be regarded as a convection heat transfer which has an uncomplicated expression as follows:

$$Q_j = A_j q_j = (2\pi r dr) q_j \quad \text{Eq. 2.6}$$

where q_j is the heat flux contributed by the impinging liquid jet and can be calculated as $q_j = h_j(T_s - T_L)$.

The enthalpy change within the control volume is depicted as:

$$\frac{\partial H_e}{\partial t} = \rho c_p (2\pi r dr s)\frac{\partial T}{\partial t} \quad \text{Eq. 2.7}$$

Summarizing the equations from Eq. 2.1 to Eq. 2.7, it yields:

$$h_j(T_s - T_L) = q_j = ks\left(\frac{1}{r}\frac{\partial T}{\partial r} + \frac{\partial^2 T}{\partial r^2}\right) - \rho c_p s\frac{\partial T}{\partial t} \quad \text{Eq. 2.8}$$

This analysis model can be applied when the wetting front moves radially towards circumferential region which means it can be used when a spray or a full jet nozzle is applied.

Similarly, if the wetting front is straight such as in application of a flat spray nozzle, a modification of the formulation of heat flux should be made according to the Cartesian coordinate. The concrete deduction will be omitted since it is quite similar to that of the circular wetting front and the final equation is given as:

$$h_j(T_s - T_L) = q_j = ks\frac{\partial^2 T}{\partial x^2} - \rho c_p s\frac{\partial T}{\partial t} \quad \text{Eq. 2.9}$$

Where the x-coordinate is the direction of straight moving front.

2.11.2 Eulerian Solution of Boiling Curve for Impinging Water Jet from a Mold on Moving Hot Metal Plate

As mentioned in Section 2.6, a house made mold is also investigated in this research work. Since the plate is moving, the analysis method above is not so

appropriate to describe heat transfer mechanism. An Eulerian steady state method is formulated by Kulkarni and Specht [61] in which pre-cooling, transition and nucleate boiling are well described.

The difference between Lagrangian and Eulerian coordinate will be discussed prior to the mathematical formulation, since it might provoke confusions if it is not clearly clarified. **Figure 2.16** Shows the position of metal plate at three different time points. The cooling starts with the impingement of the mold jets on the bottom edge of the metal plate. This time point is set as the starting time t = 0. As time elapses, the metal plate moves downwards without varying the spatial position of the impingement point of the mold jets which is determined in Eulerian coordinate as z = 0. This coordinate is oriented in the direction of the movement of the strand.

To get another graphical representation of the temperature field, Lagrangian coordinate x is introduced and the spatial point x = 0 is set at the bottom edge of the moving plate and its positive direction is defined against the plate movement.

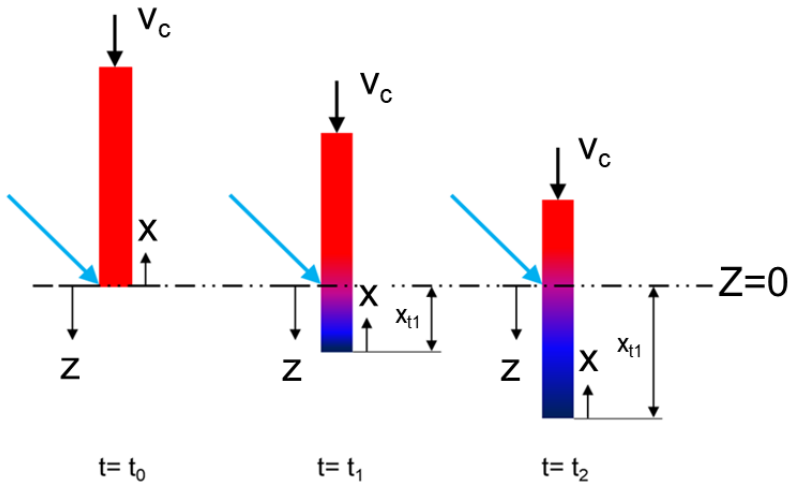

Figure 2.16: Explanation of Lagrangian and Eulerian coordinates

Considering the moving velocity v_c, the following relationship between the Eulerian coordinate z and Lagrangian coordinate x results in:

$$z = x_{t_n} - x = v_c \times t_n - x \qquad \text{Eq. 2.10}$$

With this equation, the temperature field based on Eulerian coordinate T= f(z) can be derived from T = f(x) for a certain time t_n. The Lagrangian representation T = f(x) demonstrates an easily understandable temperature field on the plate at different time points.

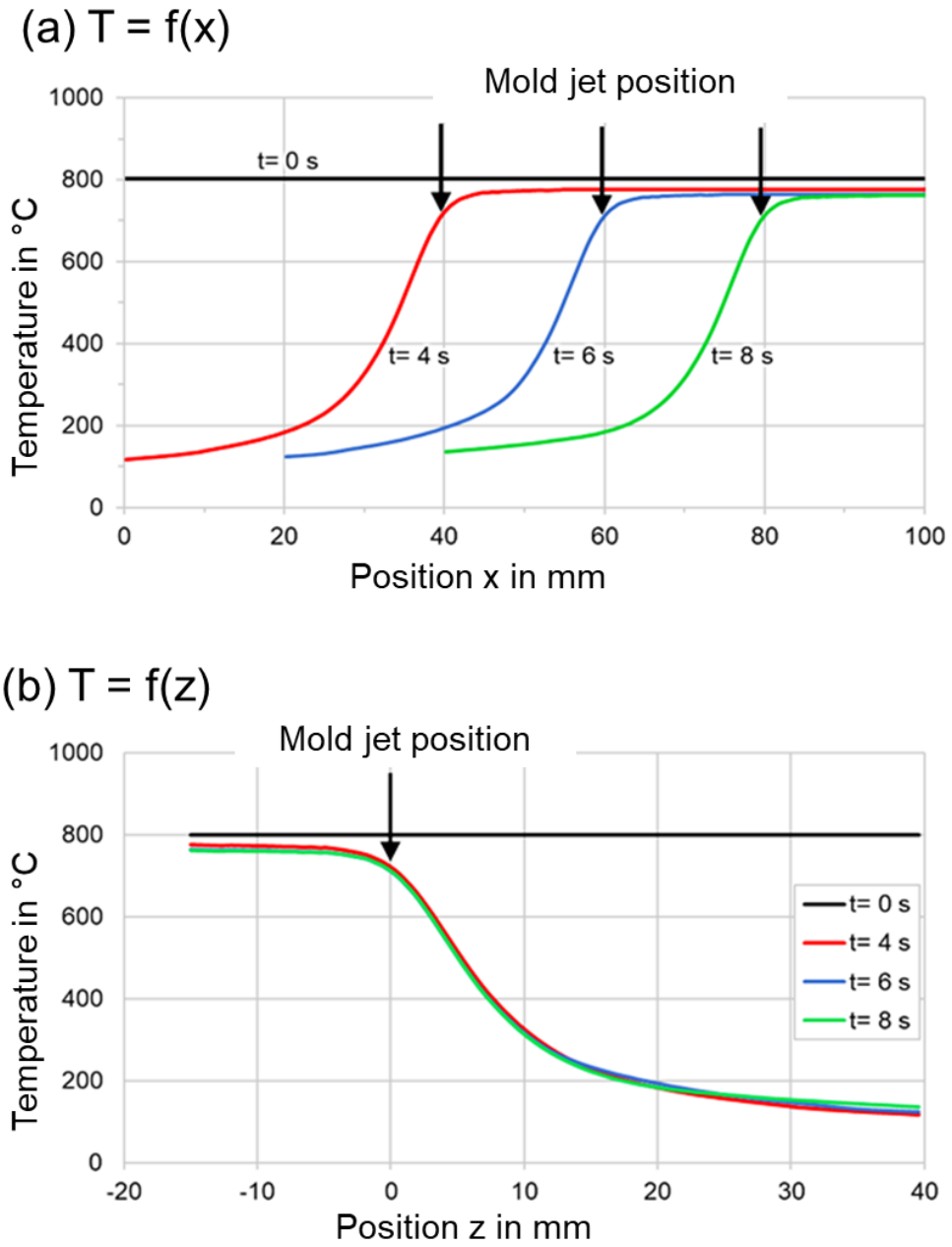

Figure 2.17: Lagrangian and Eulerian representations of temperature distribution at three different time points.

If, however, the surface temperature is shown as a function of z, then higher temperatures are obtained in the negative range of z. The advantage of this representation is that the impingement point of the mold jets can be immediately identified. In the negative range of the z values, the temperature variation can be detected before liquid cooling starts and the temperature gradients are a consequence of the heat conduction in the axial direction. In the positive range of the z values, the temperature gradients are the result of cooling by the mold jets. Another advantage is that the quasi-stationary state of the temperature in the central region of the metal plate can be particularly highlighted.

This is evidenced by the fact that the temperature curves are almost identical at different time points, which is observed in the experiments and shown in **Figure 2.17**. Both figures are the temperature representation during the cooling of a nickel plate with initial temperature of 800 °C. The top figure (a) shows the temperature as a function of the Lagrangian coordinate x fixed to the plate at the cooling times of 4, 6 and 8 seconds. For a better understanding, the position of the mold jets on the metal sample is also displayed for respective times. And the temperature curves at the respective times are visually very similar. If these temperature curves are mirrored and superimposed at the position of the mold jets according to the Eulerian coordinate where z = 0 means the impingement point of the mold jets , the bottom figure (b) is obtained. The temperature curves for the cooling times 4, 6 and 8 seconds are almost congruent. This means that after a certain start-up time, a quasi-stationary temperature field develops on the moving metal sample. Only the temperature curves at the beginning and at the end of the cooling process will differ from the curves shown here. The advantage is that in the quasi-stationary range the cooling process can be approximated quite well by a single curve, thereby facilitating the process programming.

The mathematical formulation of quasi-steady state was described in detail by Agrawal and Sahu [62] and the conduction equation can be written as:

$$k\frac{\partial^2 T}{\partial z^2} - \frac{q_j}{s} = \rho c_p v_c \frac{\partial T}{\partial z} \qquad \text{Eq. 2.11}$$

Where v_c is the casting velocity or plate moving velocity.

The determined heat flux q_j will be further used as a boundary condition in the two-dimensional domain. Considering the quasi-steady state, the two-dimensional conduction equation to be solved is given as:

$$\rho c_p v_c \frac{\partial T}{\partial z} = k\left(\frac{\partial^2 T}{\partial z^2} + \frac{\partial^2 T}{\partial y^2}\right) \qquad \text{Eq. 2.12}$$

This equation is solved with a 2D-Finite Difference Model using central difference discretization and by adding ghost points along the boundaries with Neumann boundary condition [61].

The boundary conditions are depicted as follows:

Quenching side: $\frac{\partial T}{\partial y} = -\frac{q}{k}$

Measuring side $\frac{\partial T}{\partial y} = 0$

Bottom: $\frac{\partial T}{\partial z} = 0$

Top: $T = T_0$

2.11.3 Data processing with ThemaCAM Researcher

The temperature recorded by the infrared camera will be further processed with the software ‘‘ThermaCAM Researcher 2001’’. For both circular and rectangular

wetting front, the measuring points (also named as ‘spot’) should be at first placed onto the thermal images as shown in **Figure 2.18**.

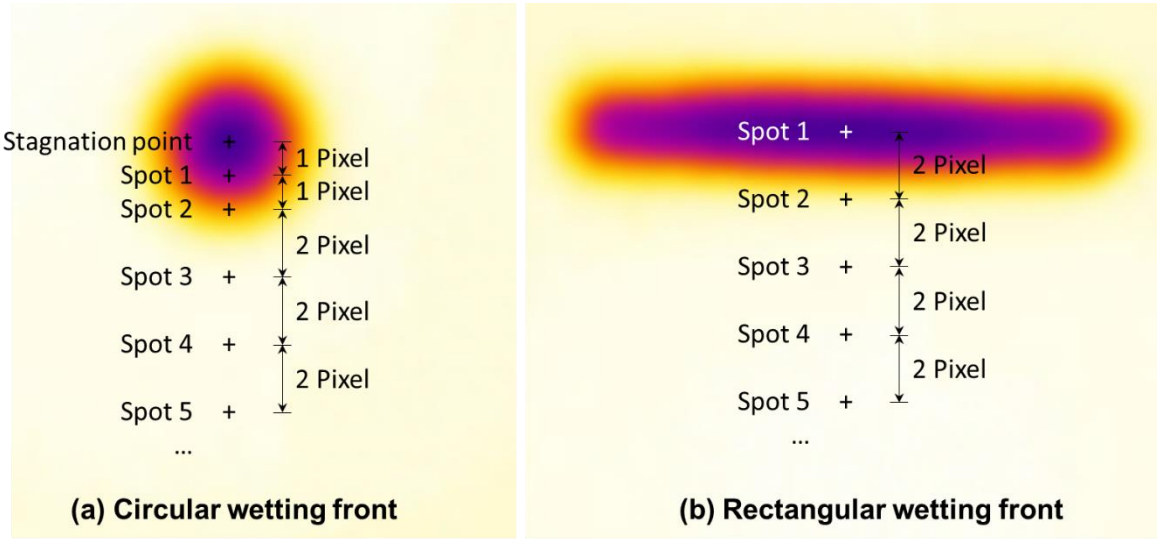

Figure 2.18: Thermal images with placed spots for (a)circular (e.g. spray, full jet nozzle) and (b) rectangular (e.g. mold, flat spray nozzle) wetting front

As each spot scans the temperature with time for specific spatial point, placing sufficient points on the thermal images will ensure a complete spatial and temporal recovery of the temperature field. The temperature field is generally presented in a matrix in which column stands for time and row for position of the placed spots.

2.11.4 Temperature curve smoothing and fitting

Smoothing the cooling curves or temperature profiles is very important in current measurements which will minimize disturbances caused by splashing droplet in the measuring window and so on.

Figure 2.19 shows the smoothing of four selected cooling curves with the "locally weighted scatter plot smooth (lowess)" function of a span of 5%. The smaller outliers within the curves are subsequently corrected without having a major impact on the readings, since the errors caused by their fluctuation will be intensified during the temperature differentiation.

An analytical expression of temperature curves can be done by curve fitting. Review of two methods i.e. Boltzmann function and cubic spline fitting are shown in **Figure 2.20**. From these two figures, cubic spline method is visually much better than Boltzmann function. Hence, cubic spline function is applied in this work, as it can offer a better approximation of the temperature curves for the whole cooling process.

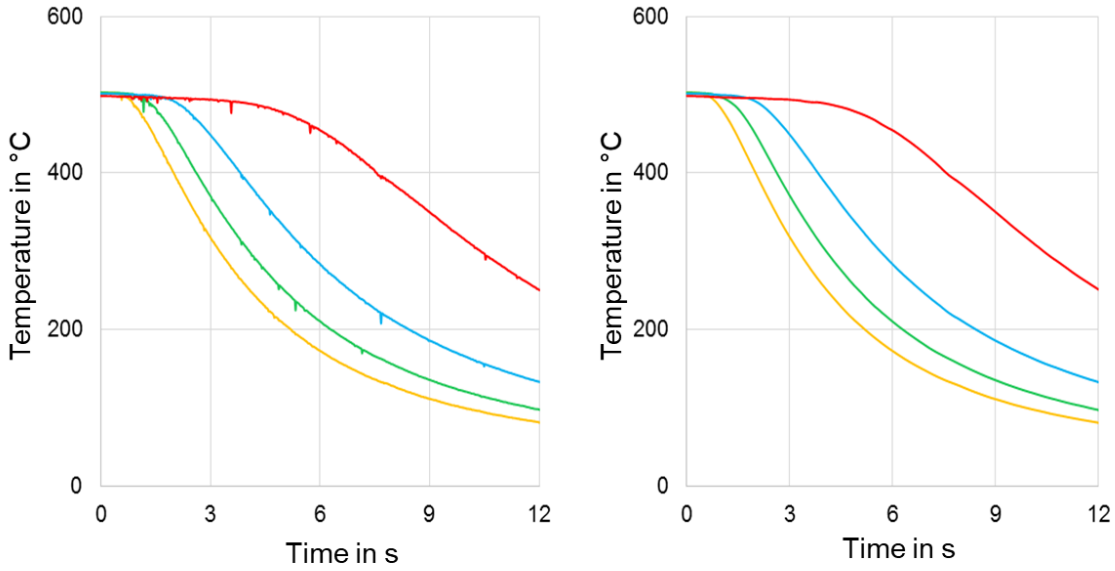

(a) Raw data (b) Smoothed data

Figure 2.19: Smoothing of temperature curves with "locally weighted scatter plot smooth (lowess)" function programmed in MatLab

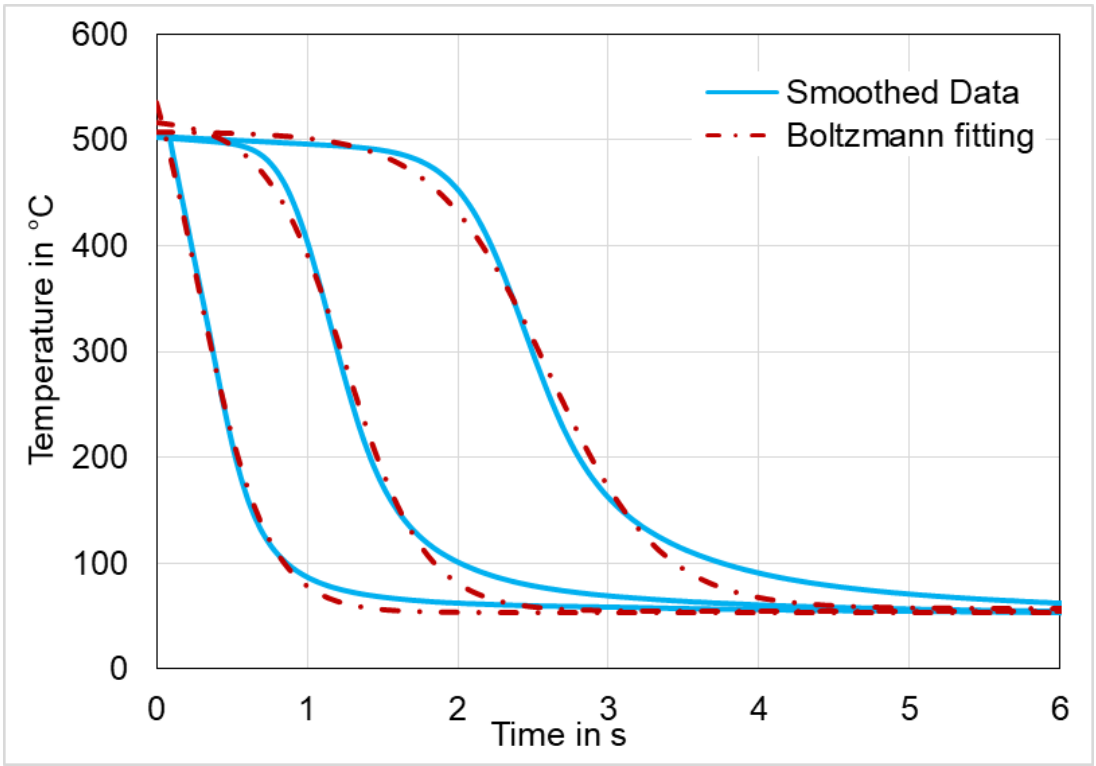

(a)

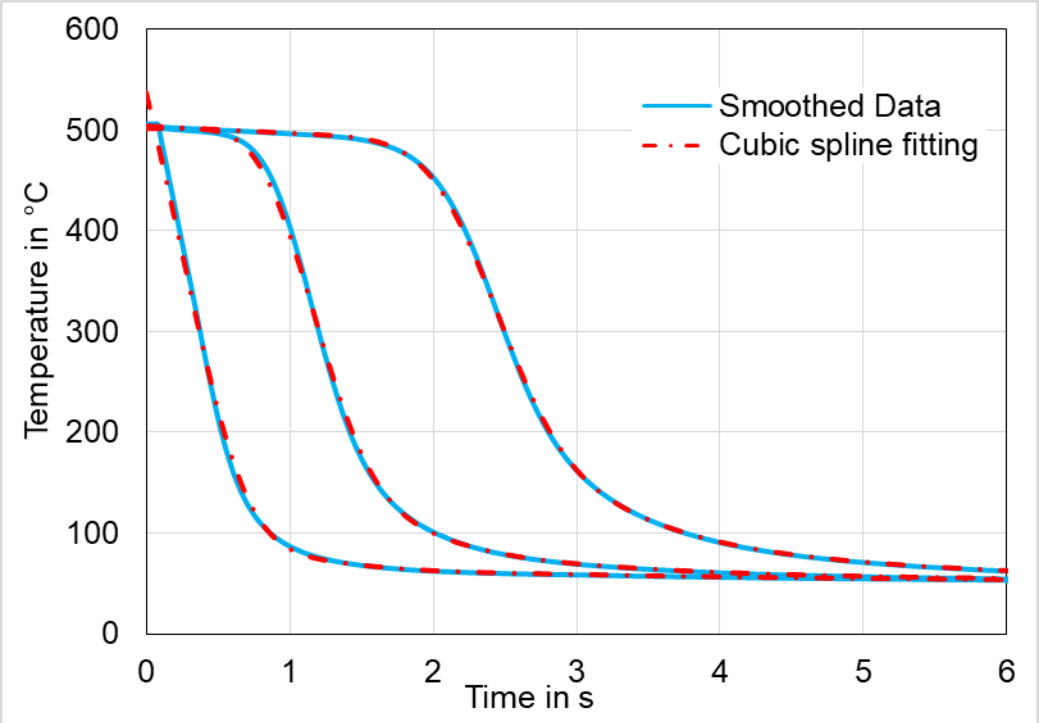

(b)

Figure 2.20: Comparison between smoothed original data with (a) Boltzmann function fitting, (b) Cubic spline fitting

2.11.5 Determination of Rewetting and DNB temperature

As mentioned in section 1.2, rewetting and DNB temperatures are essential to build up the boiling curves. If they can be determined conveniently, the reconstruction of the boiling curves is not a tough task. Filipovic et al. [2] proposed that, the minimum of the second derivate of temperature could be used to position the leading edge of the wetting front. And this method will be adopted in this work as shown in **Figure 2.21**. The temperature curves experience a sharp decrease when the wetting front arrives followed by a constant temperature. The solid red curves represent the temperature histories for r_1 and r_2; the dotted black is the respective second derivatives, on which the global minimum is employed to indicate whether the wetting front arrives or not. As can be seen, T_1 and T_2 are the rewetting temperatures for these two radii, respectively. In order to evaluate wetting front velocity, the elapsing time for the rewetting front to travel from one radius to the next and the distance between them should be recorded. Hence, the time t_1 and t_2 are listed together with their radii to be further differentiated to get the wetting front velocity. And Video recordings on the quenching side are supplemented to validate this mathematical method as shown in **Figure 2.22**. It is clearly seen that the mathematically determined wetting front deviates slightly from the measured video recording and the difference is only about 5 %. Therefore, to avoid tedious analysis of video frames, the mathematical determination of wetting front and its corresponding temperatures are utilized in the whole research.

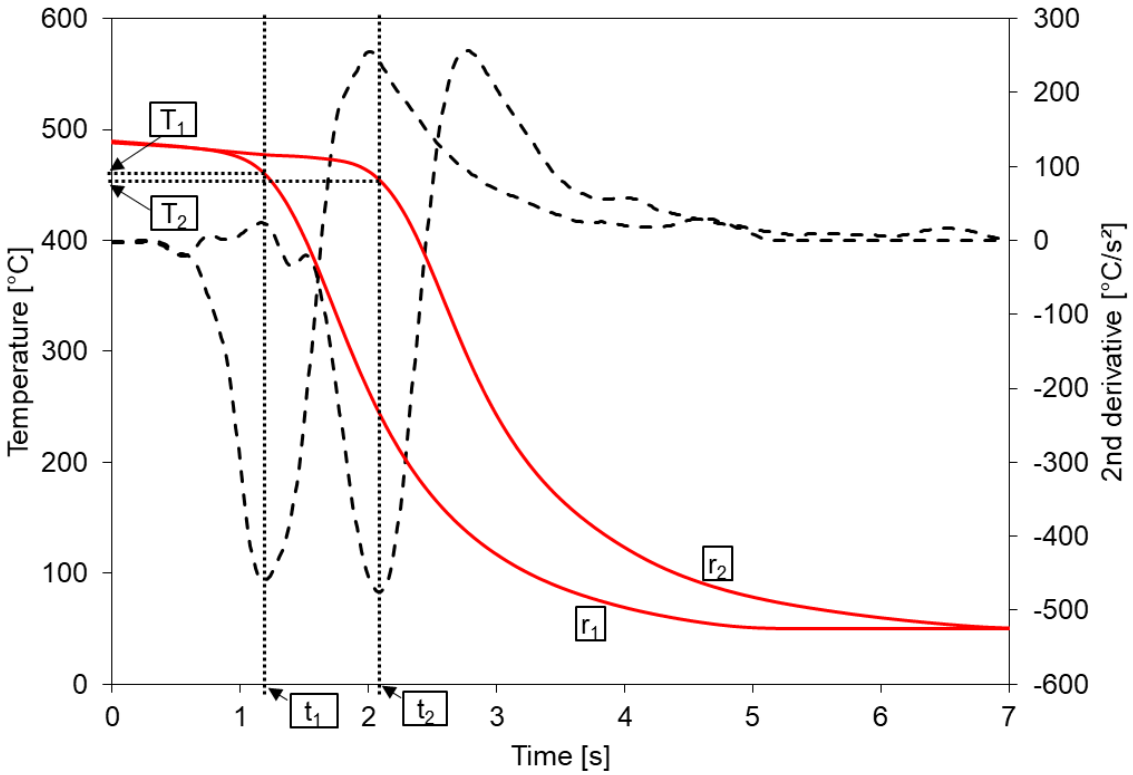

Figure 2.21: Determination of rewetting temperature and its position

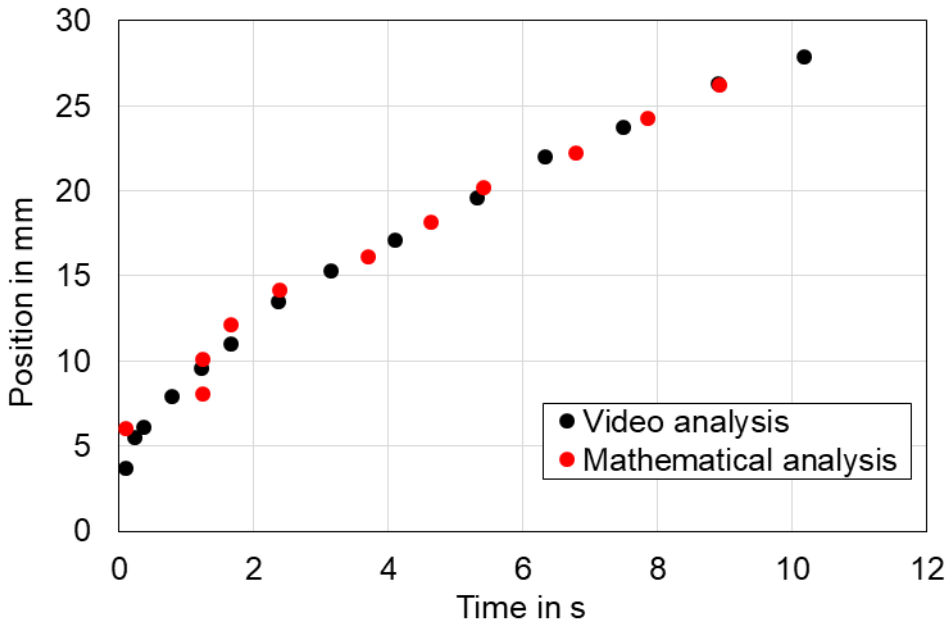

Figure 2.22: Comparison between mathematical and experimental determination of wetting front

In addition, another very important parameter to construct the boiling curve is called DNB temperature which corresponds the maximum heat flux. **Figure 2.23** shows how maximum heat flux and DNB temperature are determined in this research work.

The same approach will be then conducted for every measuring point to get a full knowledge of the rewetting and DNB temperatures over the distance as well as the propagation of wetting front and maximum heat flux.

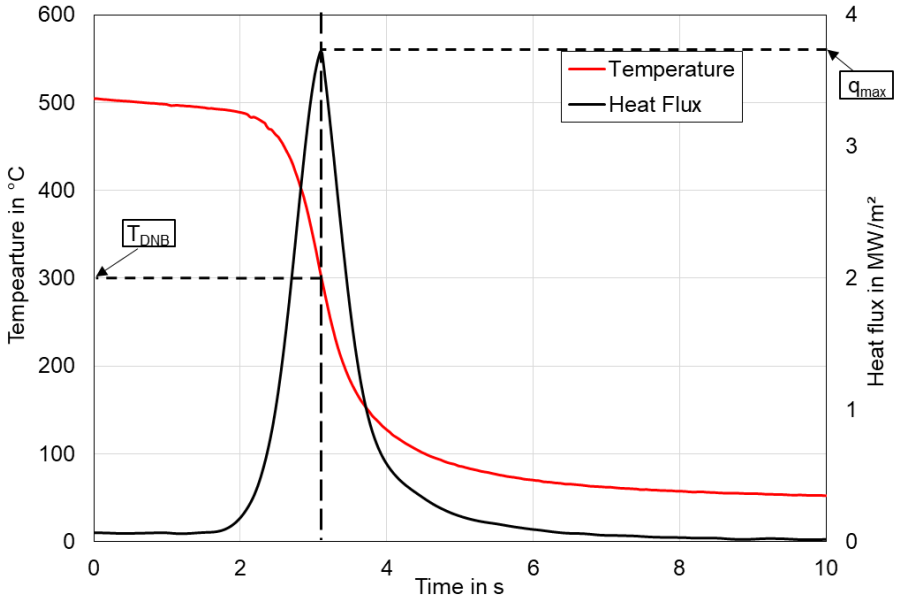

Figure 2.23: Determination of DNB temperature as well as the maximum heat flux for a certain radius

2.12 Determination and influence of surface emissivity

In general, surface emissivity ε is defined as the ratio of thermal radiation of a real object to the radiation of a black body at the same temperature. The black body is an idealized concept, which adsorbs entire incident electromagnetic radiation, regardless of frequency or incident angle. The emissivity of such a body is defined as 1.

For the conducted experimental works with infrared thermography, it is necessary to know and determine the surface emissivity of the two applied thermal coatings as shown in **Figure 2.24**.

Figure 2.24: Used thermal coatings: Senotherm (left, up to 500 °C); Ulfalux (right, up to 1200 °C)

A correct determination of the corresponding surface emissivity allows a more accurate measured surface temperature by means of a thermal imaging camera. An incorrectly adjusted emissivity would strongly affect the measurements and even distort them.

The aim of the investigations is to graphically depict the emissivity as a function of the surface temperature of the material sample. In addition, it should be determined whether a fixed value for the emissivity during the cooling process can be defined. A cooling was considered starting from T_0 = 850 °C. At a temperature smaller than 100 °C, the measurements are terminated because these temperature ranges are not of interest in this research work. The ambient temperature at the time of the experiments was T_{amb}= 22 ° C.

To determine the emissivity, two nickel plates (230x250 mm) with a thickness of 1 mm were clamped together as shown in **Figure 2.25**. The outer surface of the two sheets was coated with the thermal spray to be investigated. A type K thermocouple was firmly clamped at the center between the two plates which facilitates the accurate determination of the thermocouple position in the infrared image system. The thermocouple was then connected with a data logger, which sent the measured temperatures to a measuring computer. In addition, the infrared camera described in **section 2.2** with a distance of 1 m recorded the temperature history on the coated surface. In order to achieve a complete emissivity distribution, two measurements at different initial temperatures were conducted.

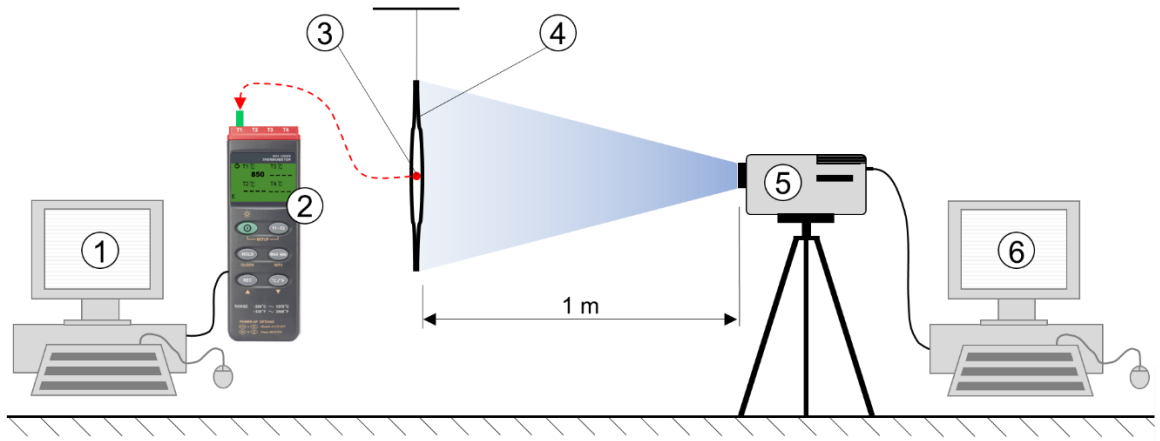

Figure 2.25: Schematic experimental setup for determination of surface emissivity

At the beginning, the plate assembly was heated to 900 °C and then removed from the oven. After correct positioning of the sheets with respect to the infrared camera, the data logger and the camera software "ThermaCAM Researcher" were started simultaneously. The measured data were then compared to determine the surface emissivity. Furthermore, the respective emissivity was determined with the help of the software "ThermaCAM Researcher". The program used a preset emissivity during the

measurement and compared the measured values with those from the data logger to calculate a new emissivity.

2.12.1 Emissivity of ‘‘Senotherm’’ thermal coating

For this experiment, the Senotherm oven spray was used. Initially, an emissivity of ε = 0.9 was specified in the infrared camera software, which will be corrected if necessary later on. **Table 2.14** lists the measured temperatures with data logger and infrared camera for the lower and upper measuring ranges as well as the associated emissivity.

Table 2.14: Emissivity of ‘‘Senotherm’’ thermal coating

Low range (100 - 500 °C)				**High range (350 - 1500 °C)**			
Time [s]	**Temperature [°C]**		**Emissivity ε [-]**	**Time [s]**	**Temperature [°C]**		**Emissivity ε [-]**
	DL	**IR-Camera**			**DL**	**IR-Camera**	
0	498.9	501.7	0.91	0	768,6	794,4	0,95
30	400.7	395.1	0.88	4	729,8	754,6	0,95
60	339.8	332.5	0.87	8	696,2	698,7	0,91
90	293.3	287.9	0.87	12	639,5	660,9	0,95
120	260.1	252.1	0.85	16	613,2	628,1	0,94
150	231.7	223.2	0.84	20	589,9	598,8	0,92
180	206.0	199.5	0.85	24	569,6	572,7	0,91
210	186.7	179.7	0.84	28	532,8	549,3	0,95
240	168.3	163.0	0.85	32	517,3	527,9	0,93
270	154.2	148.8	0.84	36	501,8	508,5	0,92
300	141.1	136.4	0.85	40	488,3	490,7	0,91
330	129.6	125.6	0.85	44	462,1	474,3	0,94
360	119.6	116.1	0.85	48	450,4	459,3	0,93
390	111.2	107.8	0.85	52	439,7	445,3	0,92
420	103.3	100.4	0.86	56	430,0	432,2	0,91
Average ε [-]			**0.86**	**Average ε [-]**			**0.93**
DL = Data logger, IR-Camera = Infrared camera							

A graphical illustration of the emissivity can be found in **Figure 2.26**. It is noticeable that the emissivity at the lower range decreases slightly with the decreasing temperature. With a cooling from 501.7 °C to 100.4 °C, the emissivity drops by 0.05. By contrast, the emissivity at the high measuring range fluctuates around the mean value 0.93. The deviation of emissivity between the high and low ranges is mainly contributed by the physical property of the thermal coating. According to the user manual, the ‘‘Senotherm’’ coating will be not consistent when it is applied at the temperature higher than 500 °C.

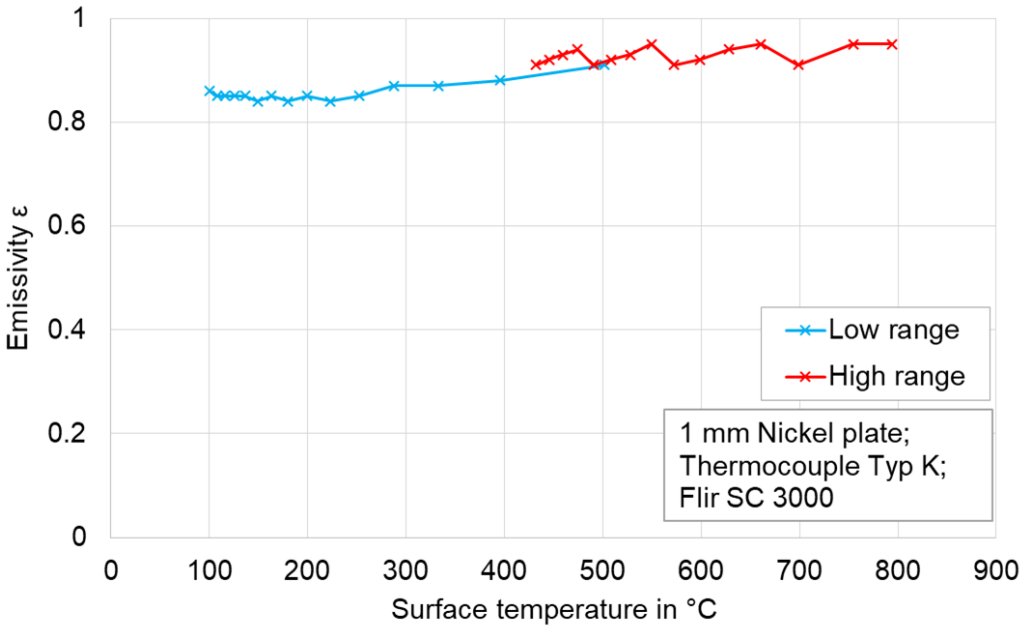

Figure 2.26: Emissivity of thermal coating ‘‘Senotherm’’ against surface temperature

In this research work, ‘‘Senotherm’’ is preferred for the experiments with 500 °C as initial temperature and an average emissivity of 0.86 is therefore accepted.

2.12.2 Emissivity of ‘‘Ulfalux’’ thermal coating

In order to investigate the effect of a higher initial temperature (> 500 °C) on the cooling process, a thermal coating that can withstand higher temperature is needed. In this section, a thermal coating produced by the company ‘‘Ulfalux Lackfabrik GmbH’’ is selected and its emissivity is experimentally obtained. For conciseness, this thermal coating will be simply named as ‘‘Ulfalux’’.

Similar to the experiment conducted for ‘‘Senotherm’’, the emissivity is preselected as 0.9 during the cooling process which will be later corrected if necessary. The measured temperatures and determined emissivity are shown in **Table 2.15**. A better illustration is given in **Figure 2.27**. It can be noticed that in the high temperature range, the fluctuation is relatively stronger than that in the low temperature range for this specific infrared camera. The average emissivities for low and high ranges are 0.84 and 0.86 respectively. The relative difference is 2.3% which means ‘‘Ulfalux’’ thermal coating provides a much stable measurement result even when the temperature reaches a high level.

In the temperature range of 430-500 °C, the emissivities for both measuring ranges deviate by ± 0.05. The slight differences are expected. Since the average emissivities for both measuring ranges are similar, a constant emissivity will be selected as 0.85 for the whole cooling process. This value will be used for subsequent experimental work with ‘‘Ulfalux’’ thermal coating.

Table 2.15: Emissivity of ‘‘Ulfalux’’ thermal coating

Low range (100 - 500 °C)				High range (350 - 1500 °C)			
Time [s]	Temperature [°C]		Emissivity ε [-]	Time [s]	Temperature [°C]		Emissivity ε [-]
	DL	IR-Camera			DL	IR-Camera	
0	501.8	483.2	0.84	0	831.0	808.1	0.86
30	400.7	385.3	0.84	4	787.6	754.3	0.84
60	339.8	327.1	0.84	8	748.7	708.9	0.83
90	293.3	283.6	0.85	12	681.5	669.9	0.88
120	260.1	249.1	0.83	16	652.2	636.0	0.86
150	231.7	221.1	0.83	20	625.9	606.0	0.85
180	206.0	198.0	0.84	24	602.6	579.4	0.84
210	186.8	178.7	0.83	28	560.8	555.4	0.88
240	168.6	162.6	0.84	32	542.4	533.7	0.88
270	154.5	148.6	0.84	36	526.0	514.1	0.87
300	142.2	136.5	0.84	40	509.5	496.0	0.86
330	130.2	126.0	0.85	44	481.5	479.2	0.89
360	120.8	116.7	0.85	48	468.8	464.1	0.88
390	112.5	108.5	0.84	52	456.2	449.8	0.88
420	104.2	101.2	0.86	56	444.6	436.7	0.87
Average ε [-]			**0.84**	**Average ε [-]**			**0.86**
DL = Data logger, IR-Camera = Infrared camera							

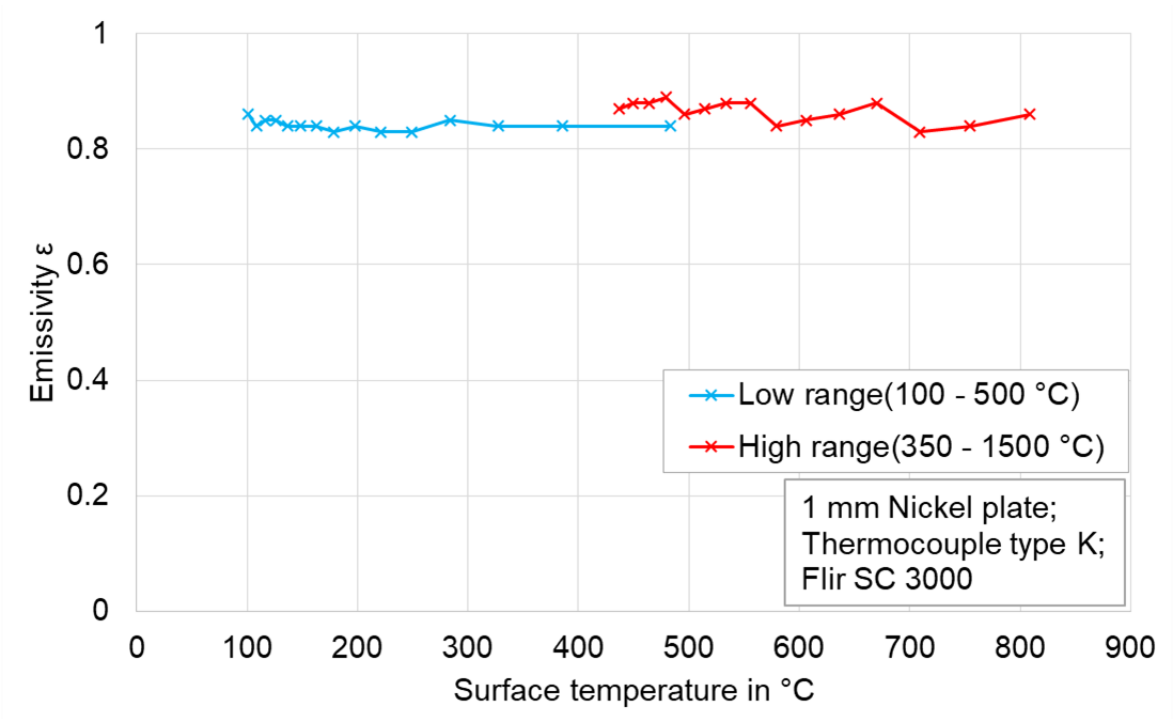

Figure 2.27: Emissivity of thermal coating ‘‘Ulfalux’’ against surface temperature

2.12.3 Comparison of both thermal coatings under cooling experiments of water

In this section the performance of aforementioned thermal coatings will be compared during quenching experiments under two initial temperatures: 500 °C and 850 °C. At T_0 = 500 °C, aluminum alloy AA 6082 with a thickness of 2 mm will be used; while Nickel plate with 2 mm will be utilized at T_0 = 850 °C.

Water with a temperature of 20 °C is pumped through a full jet nozzle from Lechler at a pressure of p = 5 bar. The nozzle with the serial number 544.360 has an orifice diameter of d = 1.05 mm and has a volume flow of $\dot{V} = 1\ l/min$ for the aforementioned pressure. The cooling curves and the rewetting and DNB temperature are evaluated and compared.

Figure 2.28 shows the influence of thermal coatings on the recorded temperature curves at different radius.

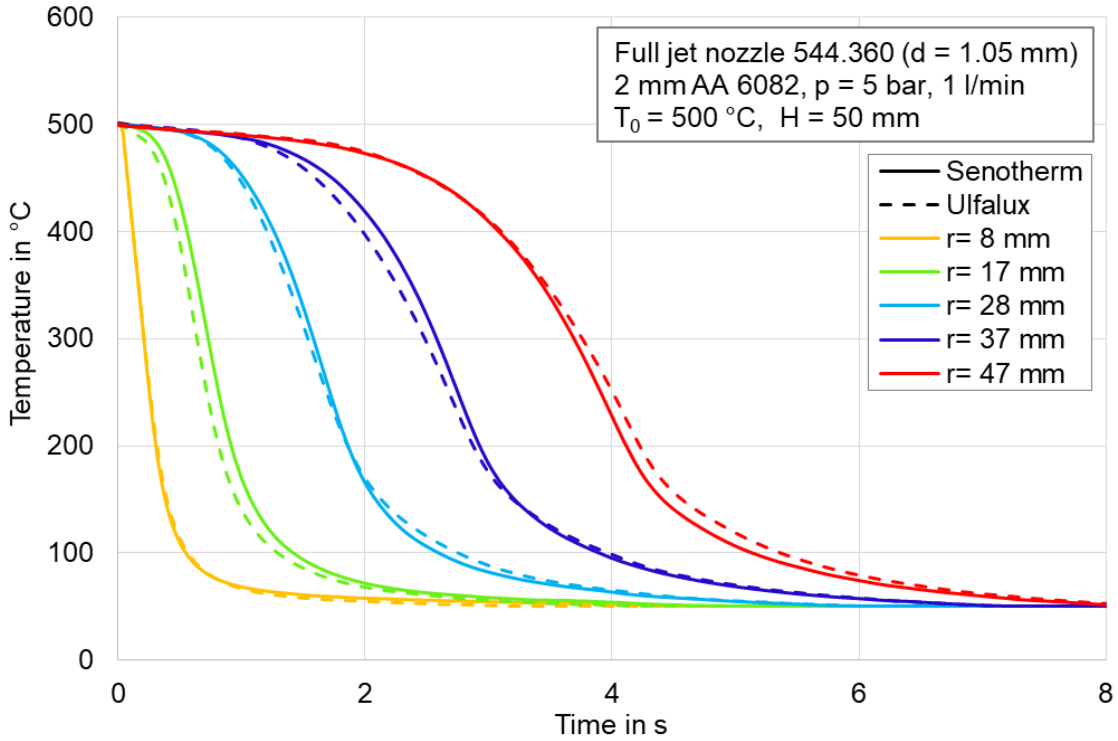

Figure 2.28: Comparison of Temperature curves for “Senotherm” and “Ulfalux” on AA 6082

At the radius r = 8 mm which is close to the stagnation region, temperature curves for both coatings are very similar. However, differences between the thermal coatings can be observed at other radii. For example, at radius r = 47 mm, slight difference in the transition boiling is followed by a temperature difference of 24 °C in the nucleate boiling. This difference might be caused by the unpredictable plate deformation. In addition, the thermal coatings are applied manually and therefore uneven on the metal surface. Although a visual inspection of the thermal coating is performed before each measurement, but this is considered as inaccurate.

Figure 2.29 compares the rewetting and DNB temperatures for the “Ulfalux” and “Senotherm” coatings. Both temperatures are plotted as a function of the radius.

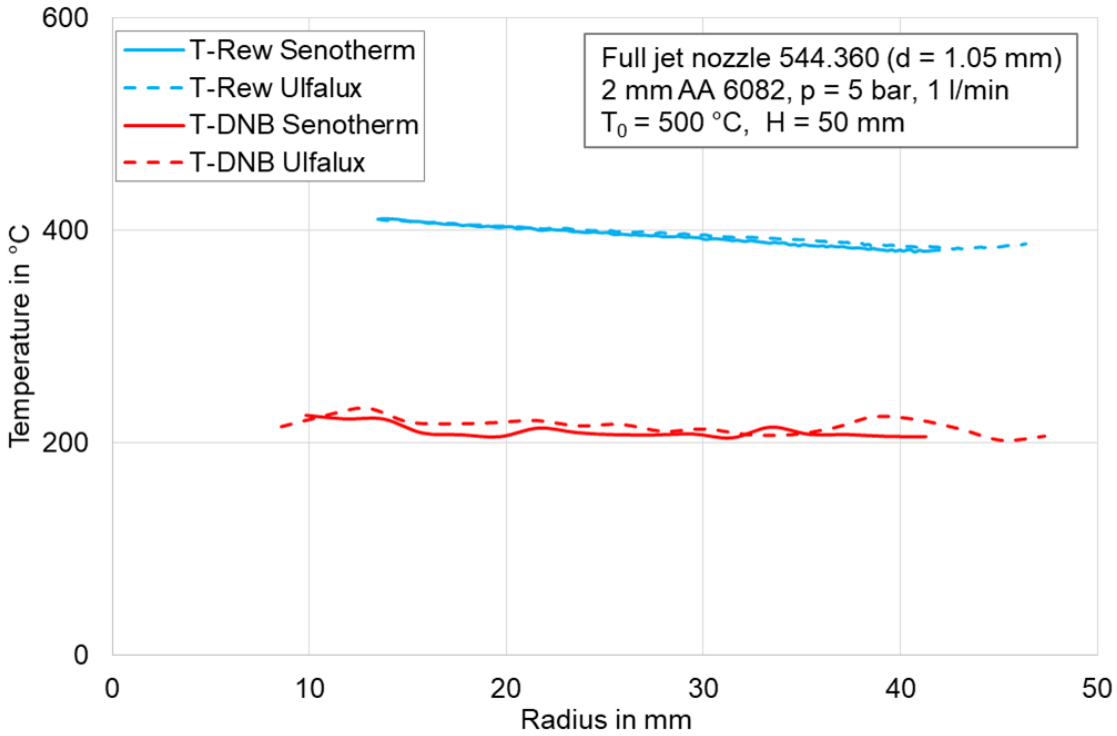

Figure 2.29: Comparison of rewetting and DNB temperatures for “Senotherm” and “Ulfalux” on AA 6082

It shows that in terms of rewetting temperature, the difference between the two thermal coatings can be neglected. For both thermal coatings, the average rewetting temperature is 395 ° C, which is 100 °C smaller than initial temperature T_0 = 500 °C. Slight fluctuations can be observed when DNB temperatures are considered. For example, at the radius r = 20 mm a deviation of ΔT = 13 °C between the two thermal coatings can be observed.

Finally, it can be stated that there is no significant difference between the two thermal coatings during quenching tests with aluminum sheets at T_0 = 500 °C. The slight deviation in the cooling curves as well as in the rewetting and DNB temperatures can be attributed to the deformation of the individual aluminum sheets. This has to be taken into account since other experiments have also been carried out with the aluminum alloy. It could also be assumed that slight fluctuations can occur for the comparison of repeated measurements.

The comparison with nickel plate at T_0 = 850 °C is illustrated in **Figure 2.30**. For the sake of clarity, temperatures at five selected radii are considered and compared. It can be noticed that at radii r = 15 mm and r = 25 mm the temperature curves are almost identical for both coatings. However, this situation does not apply to the other radii. For instance, differences can be found at the radius 9 mm near the stagnation region. After one second, the nickel plate with “Senotherm” coating has a surface temperature 301 °C which is 89 °C higher than “Ulfalux” coating. By contrary, the temperature

obtained for “Ulfalux” thermal coating is overall higher than “Senotherm” at the radius 29 mm.

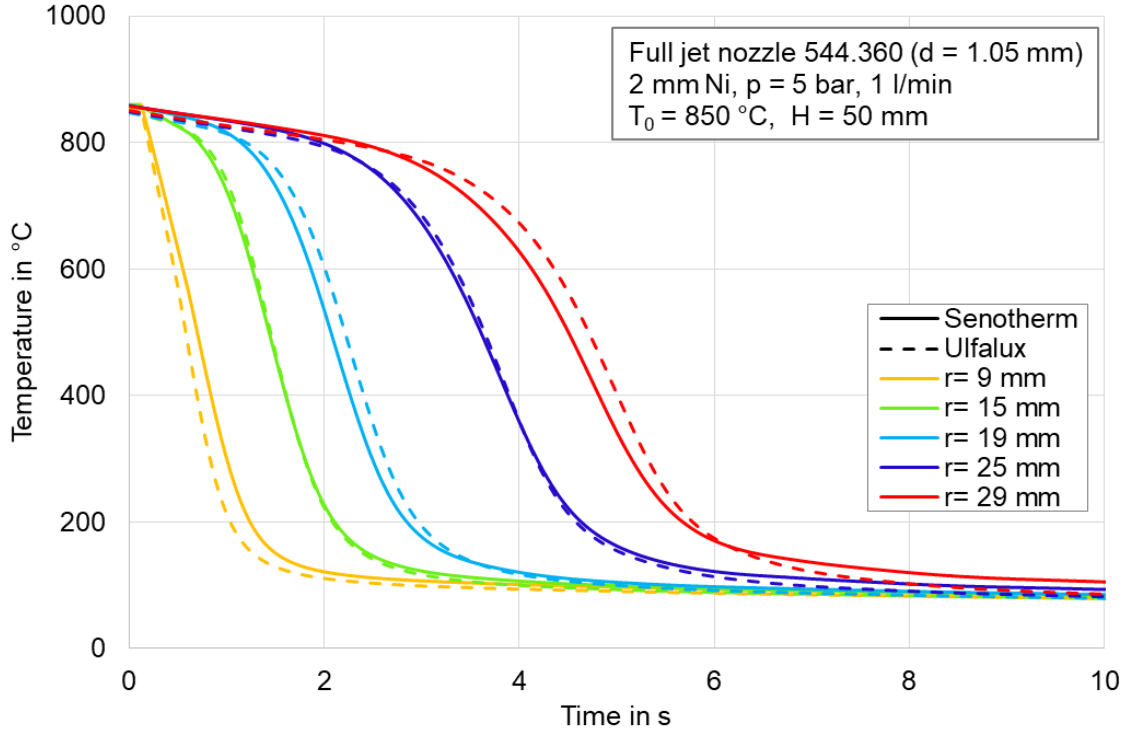

Figure 2.30: Comparison of Temperature curves for “Senotherm” and “Ulfalux” on Nickel

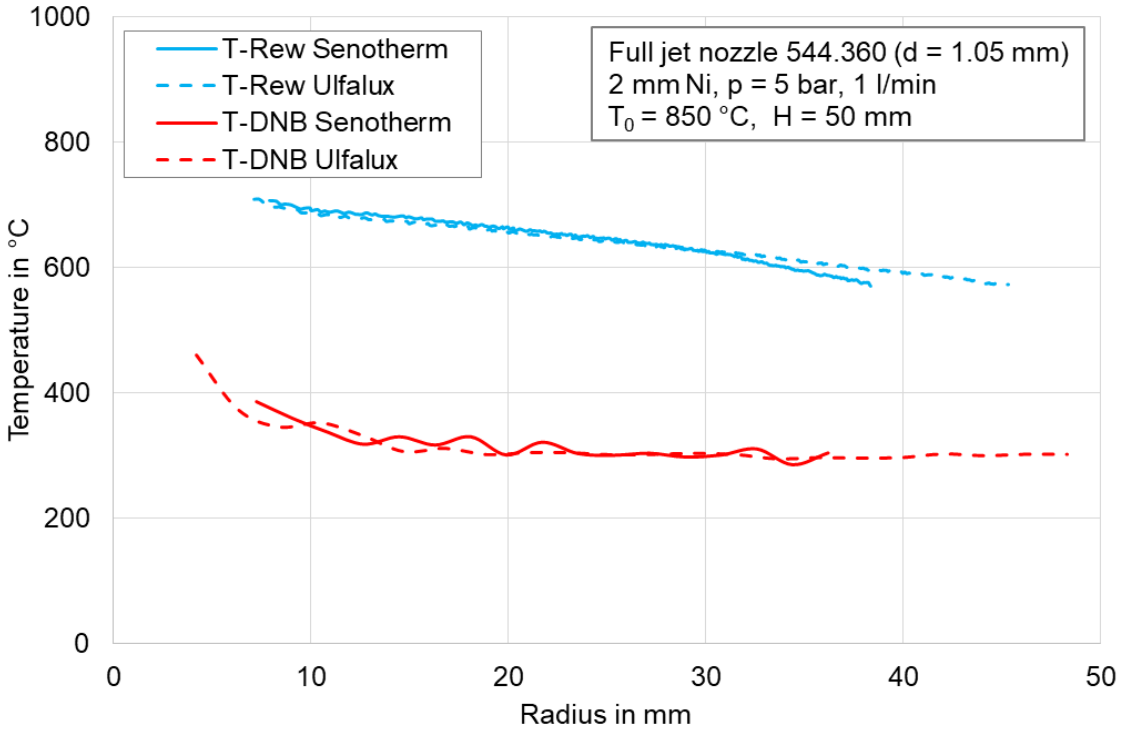

Figure 2.31: Comparison of rewetting and DNB temperatures for “Senotherm” and “Ulfalux” on Nickel

Similarly, the illustration of rewetting and DNB temperatures in **Figure 2.31** shows that the rewetting temperatures are similar for the two coatings. Only in the downstream measuring range r ≥31 mm, the rewetting temperature for the “Senotherm” decreases faster. This difference can be attributed to the different coatings, again a slight deformation is not negligible. Due to the temperature drop in the downstream measuring range, the average rewetting temperature of the “Senotherm” coating is 638 °C, 10 °C higher than that of the Ulfalux coating. The DNB temperatures fluctuates, which is caused during the determination of the heat flux. A comparison of the two thermal coatings shows no major differences.

For nickel sheets, similar to aluminum sheets, no significant differences in rewetting and DNB temperatures between the two thermal coatings are noticed. The deviation of temperature curves is caused mainly by the suitability of thermal coatings, since the maximum operation temperature of “Senotherm” is 600 °C as discussed in section 0. Another cause of the slight fluctuations is the deformation of the nickel sheet. This deformation can only be minimized and always occurs in the cooling processes in the laboratory as well as in industrial applications.

A short summary will shed light on the selection of thermal coating in the application of infrared thermography. An accurate determination of surface emissivity is the major factor which will either enhance or deteriorate the measurement. A higher surface emissivity is always wanted in order to reduce the reflection which occurs frequently on low emissivity surface. Hence, a thin layer of thermal coating that can provide a correct and high-temperature-stable emissivity is very promising. In this research work, it has studied the performance of two thermal coatings which are not economically expensive. And “Senotherm” will be used in the case where initial temperature is lower than 500 °C, while “Ulfalux” for temperature lower than 1200 °C.

3. Heat Transfer Analysis of Metal Quenching with Single Nozzles

3.1 Overview

This chapter is comprised with the results for single nozzles which are in form of full cone, full jet, flat spray. And more parameters need to be considered when a nozzle field is applied, such as the nozzle arrangement, nozzle-to-nozzle spacing etc. A comprehensive results of temperature distribution and resulting heat flux for single nozzles and nozzle field are presented. The focus of this chapter is given to influential parameters for the full jet nozzle and the nozzle field that consists of several full jet nozzles. Finally, the experimental conditions which alter the rewetting and DNB temperatures as well as maximum and minimum heat fluxes are well quantified to shed light on the optimization of industrial practices.

3.2 Investigation of full cone and flat spray nozzles

3.2.1 Introduction

Spray cooling has been widely utilized in many applications, from low temperature regime such as in electronics to high temperature regime such as in metallurgical applications. In general, two types of sprays are usually used in industrial applications: two-fluid sprays and one-fluid sprays. The most used fluid is water in case of one-fluid spray nozzles; on the other hand, the air is commonly supplemented as the second fluid in a two-fluid spray system. In this work, only one-fluid spray nozzles will be investigated, since performance of a two-fluid or air-assisted spray nozzle is difficult to be predicted[63].

One fluid spray nozzle can be also named as pressure spray nozzle which is suggested by Liang and Mudawar [63]. The momentum of liquid emanated from a spray nozzle break up liquid into fine droplets which then impinge on the hot surface individually. The advantage of spray cooling can be summarized as follows:

1. The breakup of liquid enlarges the surface area to volume ratio and induces relatively uniform spatial distribution of the liquid as well, which contribute to a uniform heat removal.
2. The liquid separation from the heated surface is depressed during the strong boiling. The momentum of individual droplets can compensate the opposing vapor momentum perpendicular to the surface and permit liquid to penetrate through the vapor layer created by bubble nucleation. This factor is very beneficial to generate high heat flux cooling as described by Yang et al. [64].

The imperfections of spray cooling include high pressure drop and increasing probability of nozzle clogging due to its small size of fluid passage.

One-fluid spray nozzles can be categorized into three major types according to the distribution manner of droplets on the surface: full cone, flat spray and hollow cone. Full cone spray nozzles cover the entire impact area with liquid droplets. Flat spray nozzles produce a narrow rectangular to oval shaped impact area. Most droplets are concentrated in the periphery region of the impact are when a hollow cone nozzle is applied. In this research only the first two types of spray nozzles are investigated, namely, full cone and flat spray nozzle.

3.2.2 Investigation of a full cone nozzle

At Otto von Guericke University Magdeburg, full cone nozzle has been intensely studied in last decade. Practical experience of parametric influence has been gained. However, the influence of sample thickness and surface roughness are not yet investigated and therefore studied and discussed in this research. And the influence of surface roughness will be detailed in Chapter 4. Among the parameters it is found that the influence of spray flux (in literature: volumetric flux) is the most significant in spray cooling. It is confirmed by its dominant influence on heat transfer compared to other hydrodynamic parameters [25] [52].

As mentioned, the effect of sample thickness with full cone nozzle on heat transfer will be discussed in the following section. This is a factor which is not well characterized in the open literatures and publications. Mozumder et al. [32] have also pointed out that the size of the test piece will influence the heat transfer in terms of maximum heat flux.

The temperature profiles for three thicknesses (3, 5, 10 mm) are presented in **Figure 3.1**. The cooling tests have been performed at volume flow rate of 1.2 l/min and water temperature at 18 °C. The used full cone nozzle is produced by Lechler® which has a bore diameter of 1.5 mm and a spray angle of 60°. The distance between the plate and the nozzle is held constant as 50 mm, which indicates the radius of a theoretical spray footprint on the metal surface is approximately 29 mm .It is clearly seen that, at the beginning of the cooling process, the temperature of the plate is quite uniform which indicates a proper and an effective thermal soaking inside the electrical furnace. Taking the temperature profiles for thickness of 10 mm as an example, the cooling time from 500 °C to saturation temperature of water 100 °C can be divided into two portions: from start to 17.5 s, the temperature decreases gradually from 500 °C to around 300 °C; afterwards, a rapid temperature drop can be observed from 17.5 s to 21 s as the temperature gradient is larger in this regime. This can be attributed to the collapse of the vapor layer that is paramount in the film boiling region when the spray strikes on the surface. It can also be said that the overall cooling efficiency is dominated by the film boiling period as depicted by the time ratio 17.5/3.5 = 5.

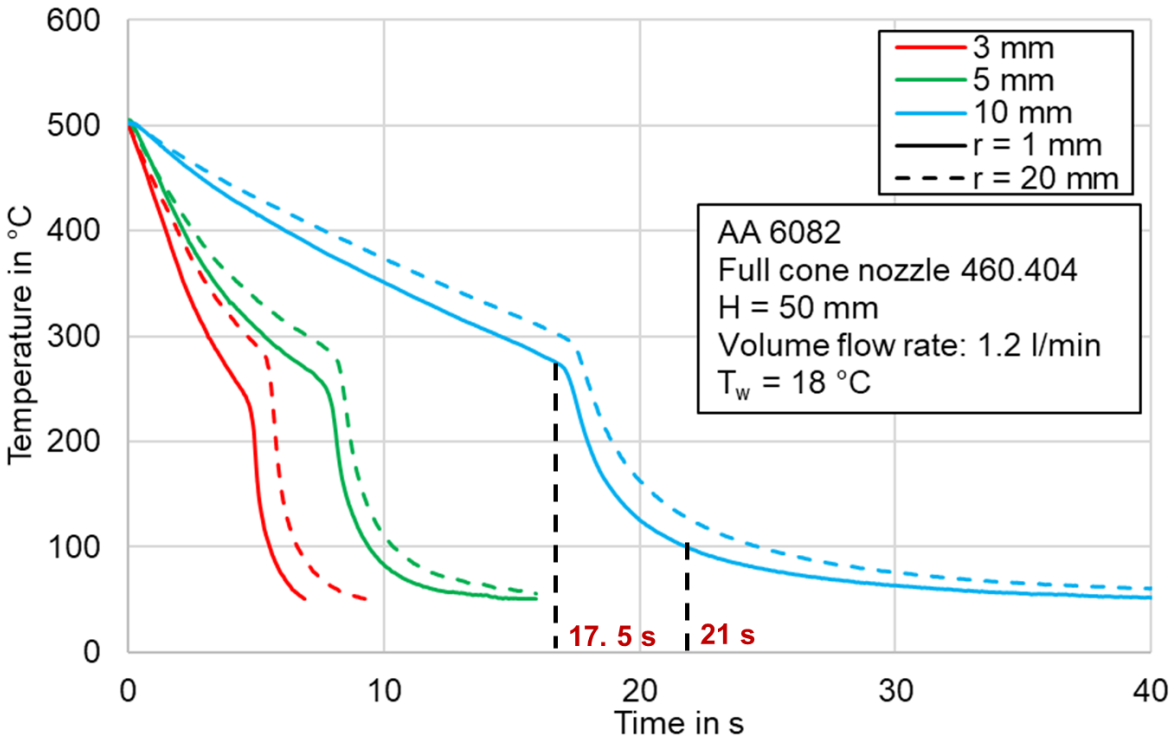

Figure 3.1: Comparison of temperature profiles for different thickness at two radii

The difference of temperature variations between 3 mm and 5 mm is not significant as compared with that between 5 mm and 10 mm. This is mainly due to the fact that a thicker plate has much more stored energy to be extracted under the same cooling strategy, which can also be demonstrated by the boiling curves as shown in **Figure 3.2**. The overall heat flux for 10 mm is larger than that for 3 mm and 5 mm. The maximum heat flux increases with increase in the thickness from 3 mm to 10 mm, the highest value of 2.36 MW/m² is observed with a thickness of 10 mm. It is also important to understand how the maximum heat flux develops on the heated surface during the cooling test, because the highest heat transfer rate and the maximum temperature gradients appear accompanying it. **Figure 3.3** illustrates how the maximum heat flux changes with radius as well as the thickness. The maximum heat flux remains almost constant at the radius smaller than 20 mm and then decrease with the radius. This is in accordance with the spray flux distribution of the used spray nozzle as shown in **Figure 3.4**. A slight increase of spray flux from 0 to 20 mm agrees quite well with that of maximum heat flux for 3 and 5 mm. This once again proves the spray flux as the most influencing variable in applications of full cone nozzle. The maximum heat flux is smaller for the thickness of 10 mm compared with that of 5 mm when the radius is larger than 15 mm. This is mainly due to the fact that the longer film boiling period in case of 10 mm thickness leads to a lower bulk solid temperature compared with 5 mm, which further reduce the extracted heat flux.

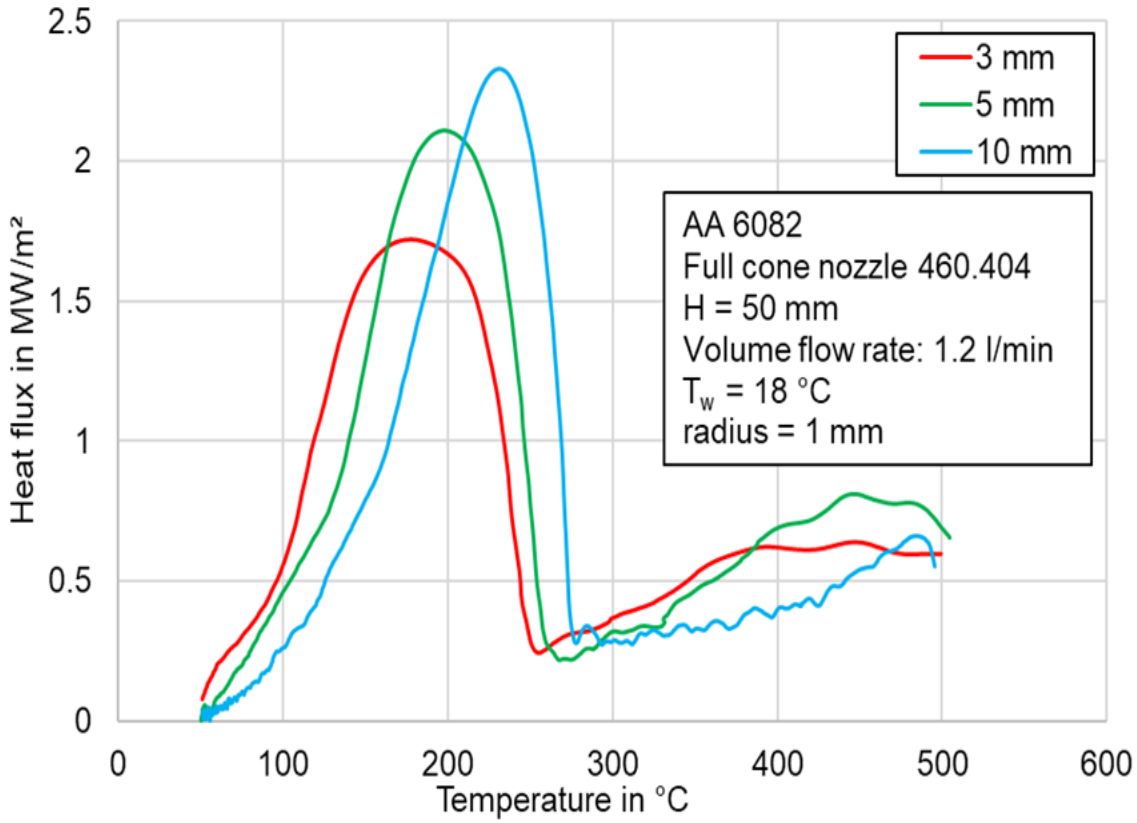

Figure 3.2: Comparison of heat flux for three thicknesses at radius = 1 mm

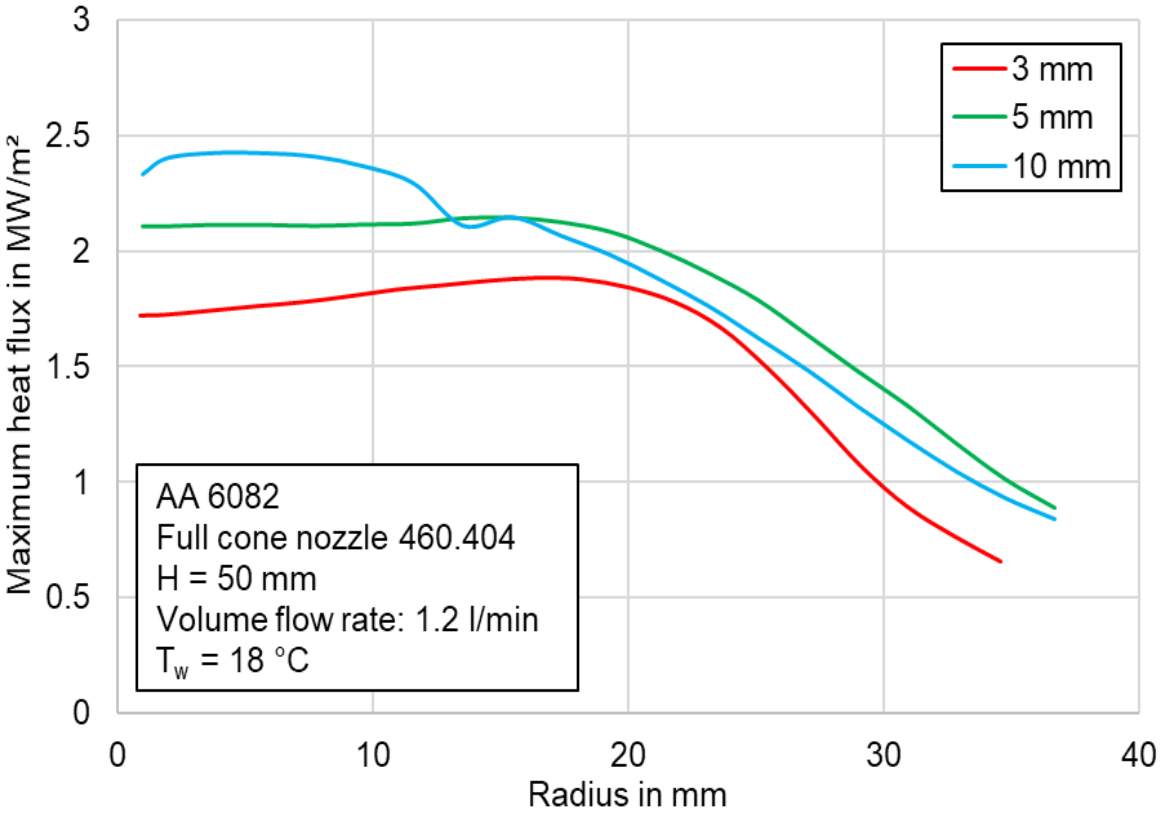

Figure 3.3: Effect of thickness on maximum heat flux

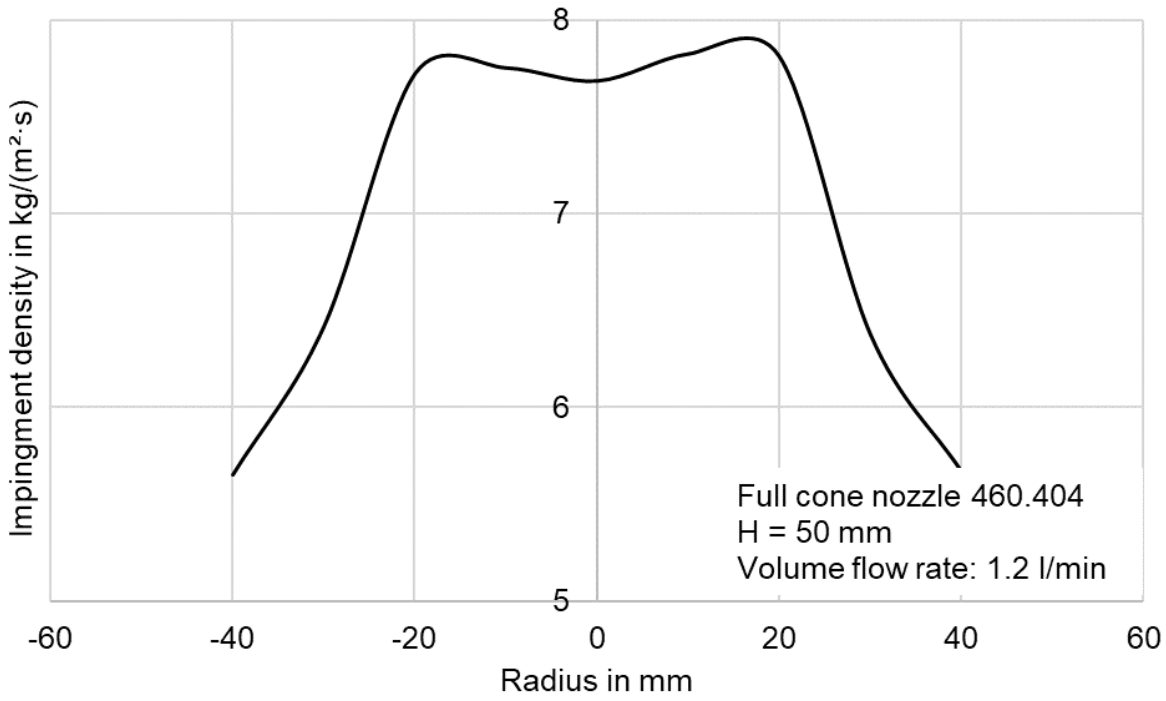

Figure 3.4: Spray flux distribution with the used full cone nozzle

The corresponding rewetting and DNB temperatures for three thickness are depicted in **Figure 3.5**. Similar tendency can also be observed: from center to around 20 mm, both rewetting and DNB temperatures increase slightly which indicate a relatively uniform distribution of water droplets. An increase of rewetting and DNB temperatures are well characterized by the decreasing spray flux at radius larger than 20 mm for all three thicknesses.

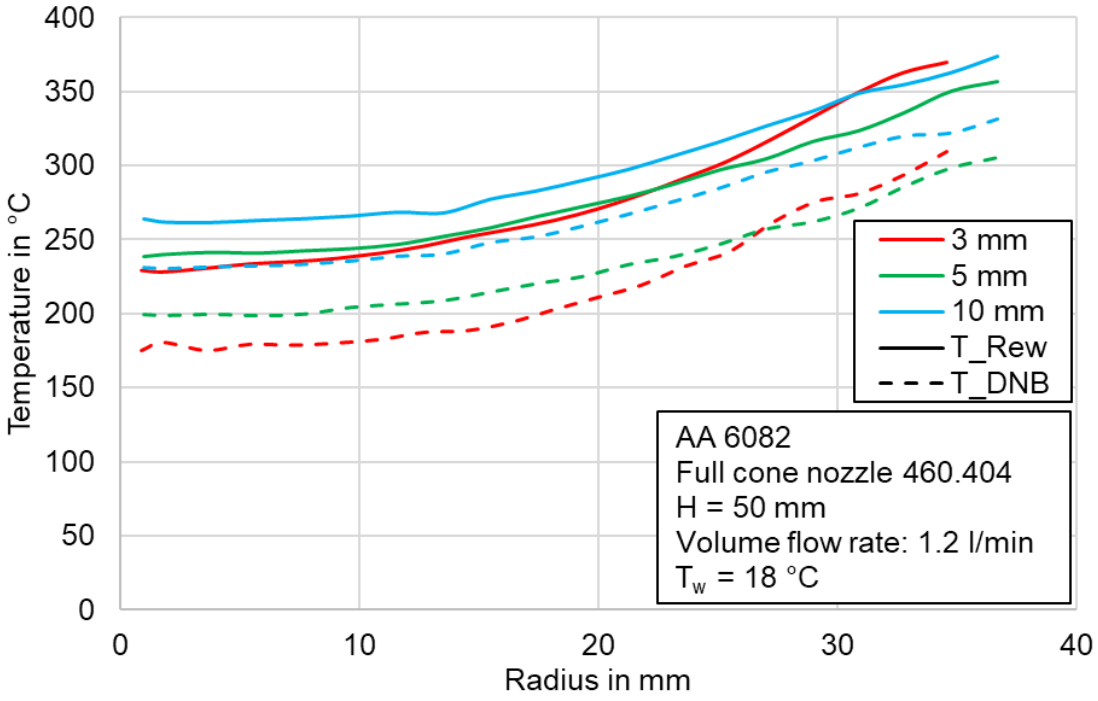

Figure 3.5: Effect of thickness on rewetting and DNB temperatures

3.2.3 Investigation of a flat spray nozzle

3.2.3.1 Introduction

Flat spray nozzle is characterized by a concentrated spray in an oval or a rectangular shape when it impacts on the metal surface. Few open publications are dealt with flat spray nozzle. Vorster et al. [65] conducted experiments with a flat spray nozzle with a spray angle of 60°. The spatial and time-resolved measurements are used to investigate the influence of spray cooling mechanisms such as bubble formation and the flow field development. Ramstorfer et al. [66] has performed experimental investigations with an air-assisted flat spray nozzle. It was concluded that the distribution of heat transfer coefficient was in good agreement with that of spray flux.

In this research, the investigated flat spray nozzle (serial number 632.674) produced by Lechler® has a spray angle of 60°. At pressure of 1, 5 and 9 bar, the respective volume flow rates are 3.4, 7.5 and 10 l/min. The nozzle was deliberately chosen to achieve a larger initial covering length B when the flat spray strikes on the metal plate. The length B = 58 mm specified in the following diagrams of this chapter refers to a horizontal nozzle spacing of 50 mm and an inclination angle of 90°. Here it is necessary to distinguish the inclination angle and spray angle as shown in **Figure 3.6**. The spray angle describes how the spray expands when it emanates from the nozzle orifice. However, the inclination angle determines the axial nozzle inclination towards the metal surface. As the inclination angle decreases from 90°, the path from the nozzle orifice to the hot surface increases; an increase in the initial impacting length B can then be expected which will exceed 58 mm compared with that at an inclination angle of 90°.

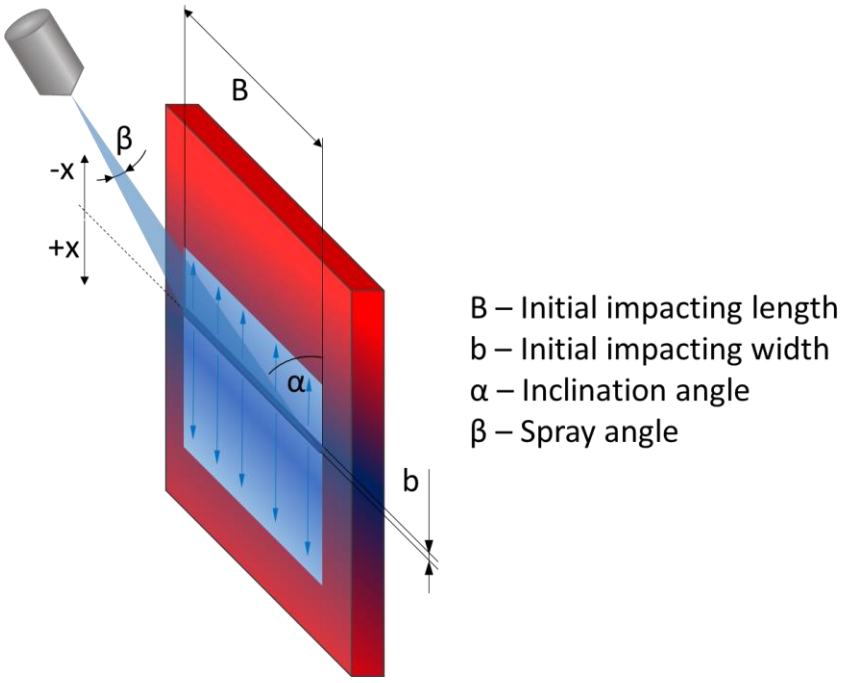

Figure 3.6: Clarification of inclination (α) and spray (β) angle

3.2.3.2 Effect of inclination angle on heat transfer

The inclination has been mainly investigated for a full cone nozzle. Visaria and Mudawar [67] have developed a model which successfully predict the effects of spray inclination on maximum heat flux. It was shown that both the spray impact area and the volumetric flux decreases with increasing inclination angle away from normal. Fu et al. [68] has conducted experiments by varying the spray inclination angle from 0° to 60°. It was reported that the average cooling rate and heat flux reach the maximum when the inclination angle is 30°.

Figure 3.7 shows the influence of the inclination angle α on the wetting front velocity. While at an inclination angle of 90 °, the liquid flows uniformly in both directions (+ x) and (-x) as shown in Figure 3.14. With the reduction of the inclination angle, the flow rate in positive x direction is increasing, which will inevitably leads to an acceleration in the wetting front propagation, which agrees well with the findings of Visaria and Mudawar[67]. The evaluation of the experimental results in the following figures always refers to the positive direction (+ x).

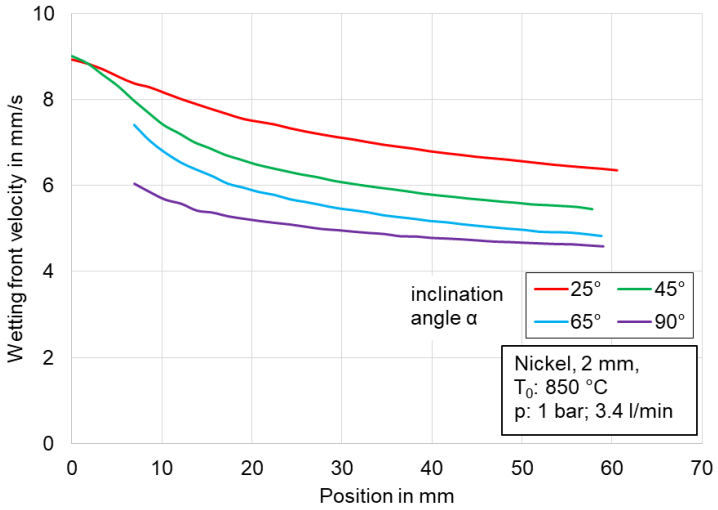

Figure 3.7: Effect of inclination angle on the wetting front velocity

The rewetting and DNB temperatures for an aluminum alloy 6082 is shown in **Figure 3.8**. The rewetting temperatures for spray angles from 45° to 90° possess the same decreasing tendency with increasing position. Only the values for an inclination angle of 25° show a very large deviation to a position of approx. 20 mm. This can be attributed to the spray momentum in the positive direction. At an angle of 25°, the initial impact of the flat spray on the hot surface is no longer so rigorous that it will break the vapor layer immediately; hence a longer film boiling is expected which reduces the rewetting temperature at the initial impacting area. It can also be noted that the DNB temperatures are almost independent of inclination angle which fluctuates around 200 °C.

Figure 3.9 shows the rewetting temperature as a function of the inclination angle for a nickel plate at an initial temperature of 850 °C. The previous findings that the rewetting temperature increases with the initial temperature are reflected again. The

values are for the angle 65° and 90° are expected; however, the rewetting temperature for 45° also depicts a large reduction at the initial impact area besides the results for 25°. Again, this can be explained by the mild impact of the flat spray at 25° and at 45°. And also combined with Figure 3.16, it leads to a conclusion that a higher initial temperature promotes the film boiling. Both figures show the same qualitative tendency for different materials and thus confirm that a flat spray nozzle with an inclination angle smaller than 25° (at T_0= 500 °C) or 45° (at T_0= 850 °C) lowers the rewetting temperature significantly. The decrease of the rewetting temperature is accompanied by a reduction of the heat flux near the initial impact area, as shown in **Figure 3.10**.

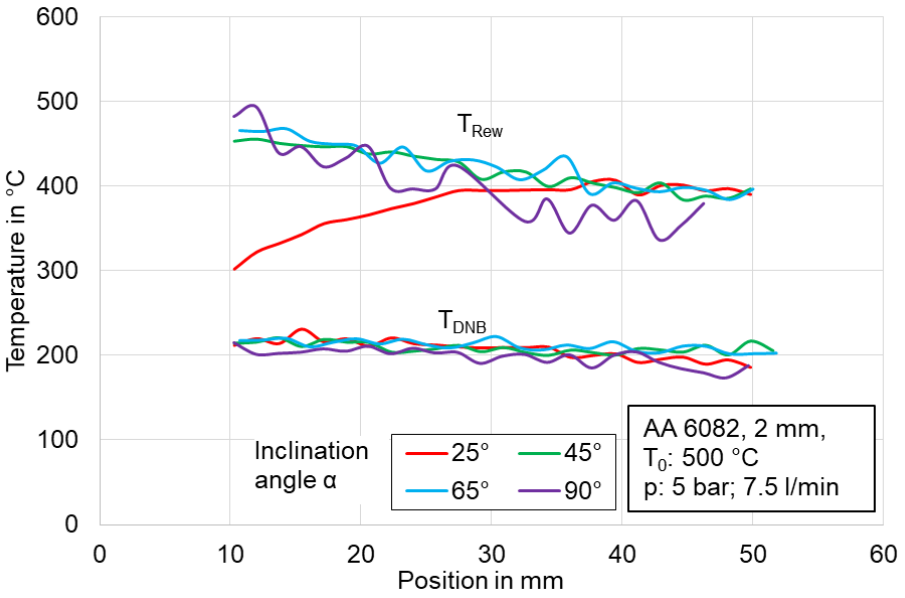

Figure 3.8: Effect of inclination angle on rewetting and DNB temperatures for AA 6082

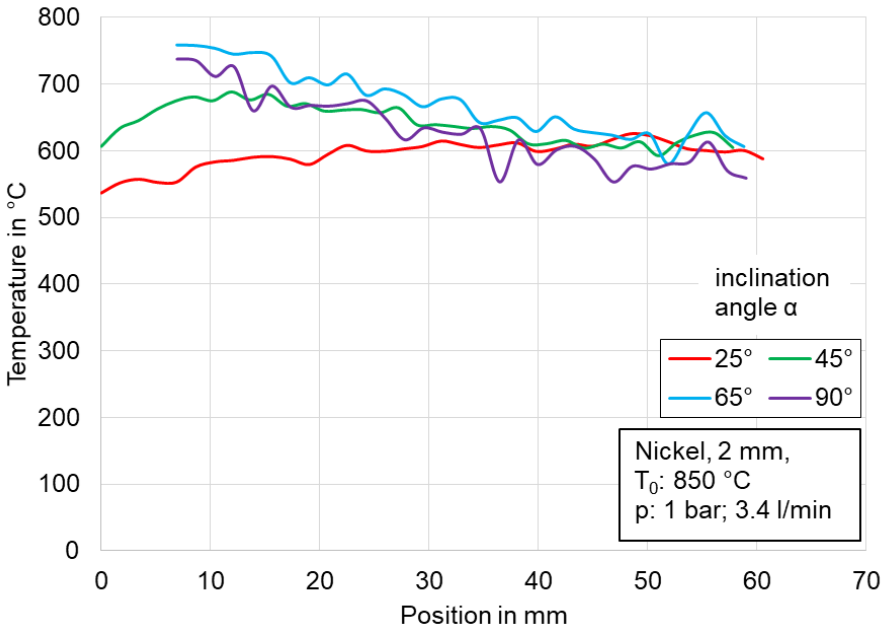

Figure 3.9: Effect of inclination angle on rewetting temperature for nickel

Several statements can be derived from Figure 3.10. At an inclination angle of 25°, an approximately constant heat flux over the whole measurement range reached. The heat flux generated in the near range of initial impact area at inclination angles of 45° to 90° are very large and then hyperbolically fall off with the increasing position until a constant value is reached. The high heat flux for angles from 45° to 90° from the vicinity of the impact area to about 10 mm is the direct effect of the striking flat spray. However, after 30 mm, the behaviors are totally reversed, since the influence of the volume flow rate dominates. The liquid flow in the positive direction (+x) is greater at 25° and induces a greater heat flux there than at 90°. This is related to the fact that at 90° the liquid flows almost equally in two opposite directions on the metal surface.

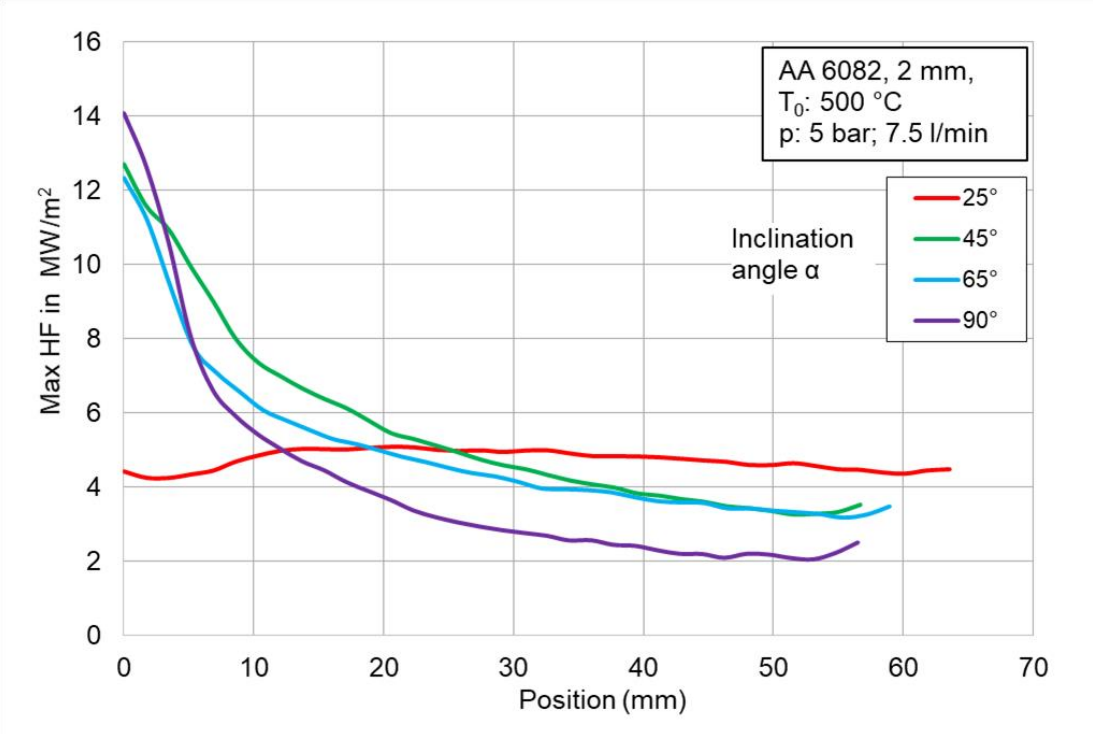

Figure 3.10: Effect of inclination angle on maximum heat flux with a flat spray nozzle

3.2.3.3 Effect of nozzle outlet pressure on heat transfer

The nozzle outlet pressure determines the volume flow rate of the emanating flat spray which describes the potential cooling ability of the fluid. The nozzle outlet pressure will be simplified as pressure in the following chapters, if no additional information is given. As mentioned, in this research, the selected pressures are 1, 5 and 9 bar respectively, the corresponding volume flow rates are 3.4, 7.5 and 10 l/min.

Figure 3.11 describes the temperature histories for three positions under 1, 5 and 9 bar. The Initial temperature was set 750 °C and inclination angle was selected as 45°. It can be seen that for all three pressures, the temperature gradient is the largest at the theoretical impact line which is denoted as x = 0 mm. The temperature difference between 5 and 9 bar can be neglected until the distance reaches 10 mm. The discrepancy between 1 and 9 bar enlarges when the wetting front moves further referring to the curves at 0 and 20 mm. It is attributed to the liquid flow on the hot

surface. At higher pressure, the emanating flat spray with higher momentum makes the wetting front moves much faster, which can further be proved by the wetting front velocity as shown in **Figure 3.12**.

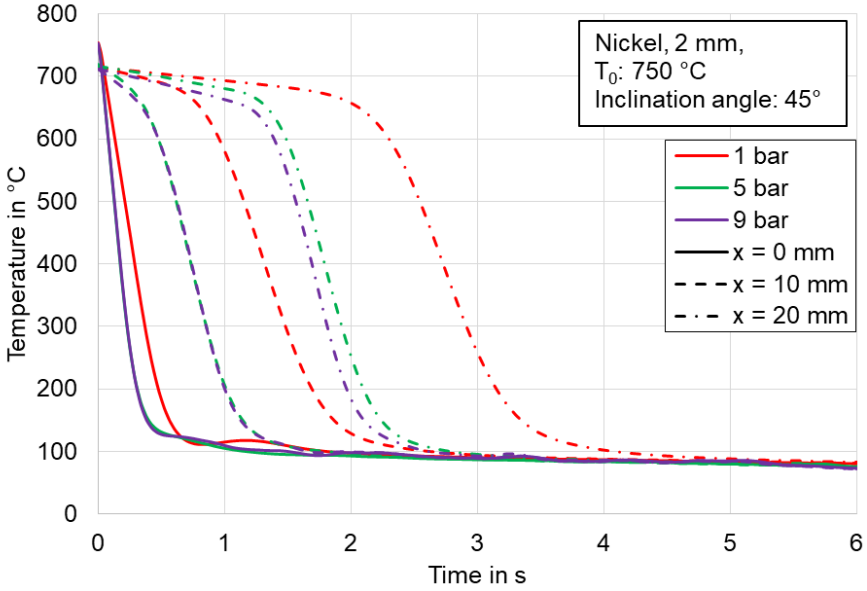

Figure 3.11: Temperature curves at 1, 5 and 9 bar with a flat spray nozzle

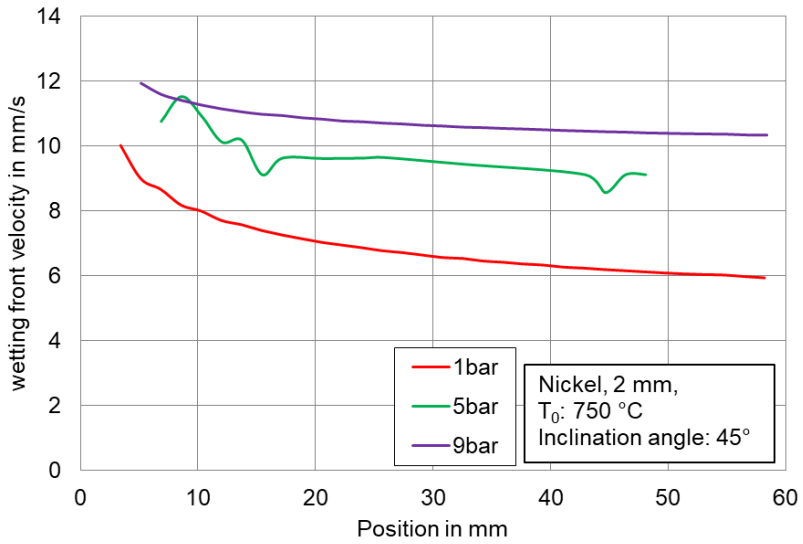

Figure 3.12: Wetting front velocity at 1, 5 and 9 bar with a flat spray nozzle

The comparison of rewetting and DNB temperatures at three pressures are then presented in **Figure 3.13**. It is surprisingly noticed that both rewetting and DNB temperatures are almost independent of the pressure. The rewetting temperature decreases slightly with the wetting front propagation; while DNB temperature remains constant at 300 °C. This phenomenon will be further encountered when a full jet nozzle is studied. The rewetting temperature is defined when rewetting, e.g. direct contact between cooling medium and hot surface, occurs. It is the surface temperature rather than the liquid temperature. During the propagation of the wetting front, the rewetting occurs only under specific conditions. At different liquid pressure, the phenomenon

occurred at wetting front should be similar, although higher pressure promotes faster wetting front. This might be the reason for the slight alteration of rewetting and DNB temperatures when liquid pressure is changing.

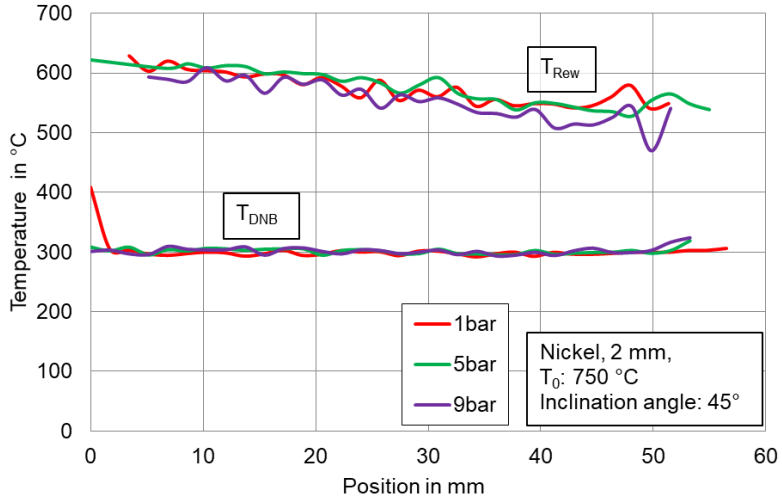

Figure 3.13: Effect of pressure on rewetting and DNB temperature for nickel

The heat flux at two locations on the surface will be compared at different pressures as illustrated in **Figure 3.14**. The cooling efficiency can be drastically improved by increasing the pressure from 1 bar to 5 bar; while the increasing from 5 bar to 9 bar can be regarded as negligible, which agrees well with the temperature measurements in Figure 3.19. Several interesting phenomena can be observed in the curves. At the theoretical impact line x = 0 mm, the heat flux remains almost constant, namely 11.5 MW/m² for 1 bar, 17.5 MW/m² for 5 bar and 18 MW/m² for 9 bar when the surface temperature is higher than 300 °C. This indicates that a high yet stable heat flux can be achieved at the impact region with flat spray nozzle at a specific inclination angle. By contrary, typical boiling curves can be observed at the downstream location x = 20 mm.

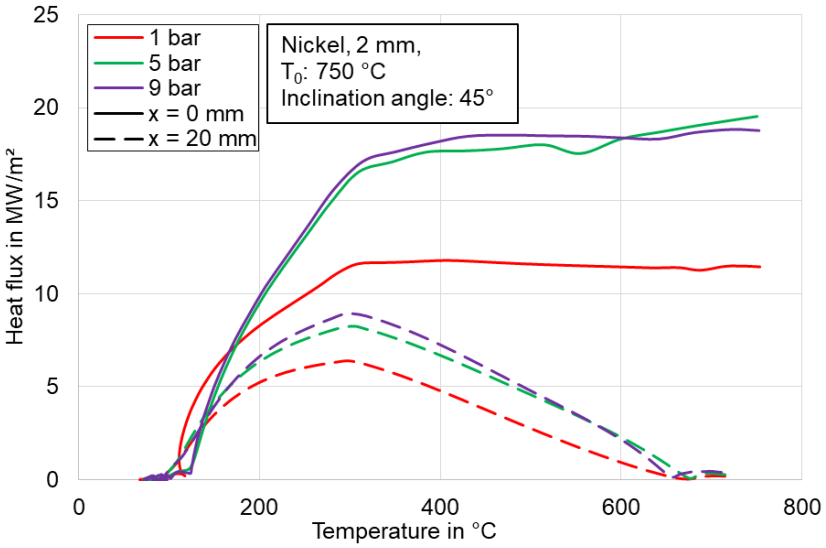

Figure 3.14: Effect of pressure on boiling curve with a flat spray nozzle

3.3 Investigation of nozzle field comprised of full jet nozzles

3.3.1 Introduction

In this section, the experimental investigation regarding inline and staggered nozzle field will be discussed. Both arrangements consist of full jet nozzles which have the same bore diameter of 1.05 mm. The detailed arrangements can be found in Figure 2.8. The investigated parameters include jet velocity, plate initial temperature, nozzle arrangement as well as metal type.

It is necessary to discuss the parameters which have paramount effects when a singular full jet is utilized to cool a hot surface prior to discussion of nozzle fields. There are several review papers available regarding on liquid jet cooling. Qiu et al. [31] reviewed the developments of jet impingement cooling but mainly focused on nucleate boiling region. Molana and Banooni [69] reviewed the abilities, limitations and features of the liquid impingement. They have summarized available correlations for Nusselt number. And the effect of multiple liquid jets have also been emphasized.

The variables which have effects on heat transfer during liquid jet impingement can be mainly categorized into two groups: jet parameters such as jet velocity, jet diameter, subcooling (jet temperature) etc. and surface parameters such as surface conditions, initial temperature, thickness, etc.. Jet array introduces more variables such as jet-to-jet spacing (or jet pitch p), numbers of jets etc. The effects of aforementioned variables on rewetting and DNB temperatures as well as maximum heat flux are essential to build up overall boiling curves, since the resulting boiling curves are the key input for the thermal as well as mechanical simulations.

3.3.2 Investigation of singular full jet nozzle

3.3.2.1 Introduction

As mentioned, it is quite important to study the influential parameters with a single liquid jet impingement prior to discussion of nozzle fields. For conciseness, several not all parameters will be selected and discussed in this section.

First of all, snapshots of the quenching with a full jet nozzle is shown in **Figure 3.15**. The wetting front moves radially towards circumferential areas; while the water is deflected away from the hot surface as droplets. The deflection at the wetting front takes place due to the forces exerted by the generated vapor in this region. According to the visual observation, the size of the water droplets becomes coarser and the velocity becomes smaller during the propagation of wetting front which is marked by the red dotted ellipse. This can be attributed to two reasons:

- The liquid film velocity in the wetting region reduces as the wetting front propagates; as a result, the splashing liquid droplets have lower initial momentum.
- The liquid temperature also increases as wetting front travels radially outwards which limit its ability to condense the generated vapor bubbles in the wetting

front region; hence, an higher resistance force caused by increasing generated vapor is expected.

Due to the high temperature involved in the present experimental studies, the liquid film hydrodynamics in wetting region cannot be directly measured; besides, the splashing droplet velocity and size are not quantitatively determined.

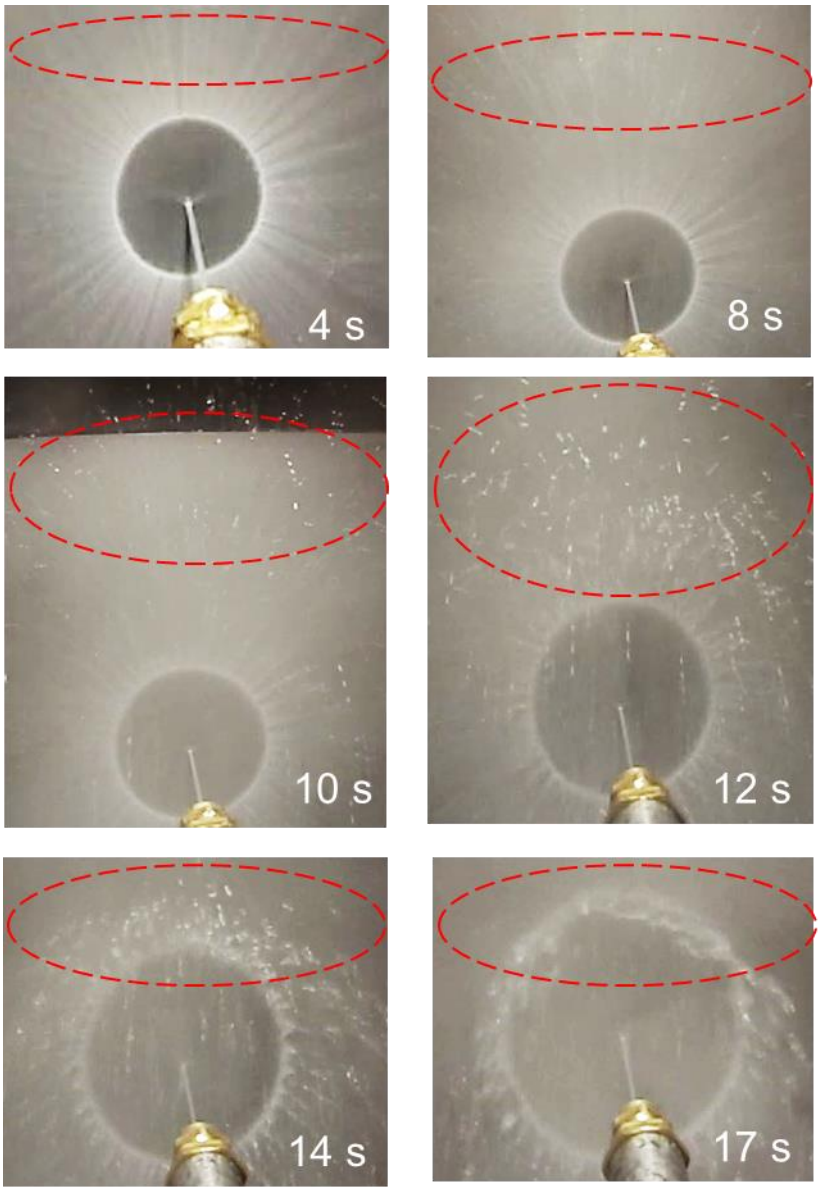

Figure 3.15: Snapshots during quenching a hot surface with a full jet nozzle

3.3.2.2 Effect of outlet pressure (jet velocity) on heat transfer

Depending on the nozzle diameter, the nozzle pressure always corresponds to a specific jet velocity. Based on the measurements of the volume flow rates, jet velocities are calculated for the tested nozzles which has been listed in **Table 3.1**. For calculation of Reynolds number, the kinematic viscosity of water is taken as 1.004×10^{-6} m²/s at 20 °C, since the most experiments were carried out with water at this temperature.

The temperature histories under three pressures are shown in **Figure 3.16**. The initial temperature was 850°C, the used full jet nozzle has a bore diameter of 1.05 mm. It can be clearly seen that, the temperature histories for stagnation region (r = 0 mm) is totally different from that at downstream or wall jet regions (e.g. r = 10 and 20 mm), which is attributed by the jet momentum development on the hot surface. At stagnation region, the impinging liquid jet has the largest momentum which can easily and immediately remove the potential generated vapor layer between the hot surface and liquid jet. This hydrodynamic momentum fades away as the wetting front moves toward circumferential area which turns heat transfer into wall jet cooling. Hence, the temperature gradient decreases dramatically.

The effect of pressure once again shows large influence when 1 bar and 5 bar are compared; while the deviation of 5 and 9 bar is negligible. These findings are in congruent with that for flat spray nozzle as illustrated in **Section 3.2.3.3**.

Table 3.1: Relations between pressure and jet velocity for used nozzles

Full jet nozzle	Pressure p in bar	Jet velocity in m/s	Reynolds number
Lechler 544.320 d=0.8 mm	1	11	8.765×10^3
	5	22	1.75×10^4
	9	30	2.39×10^3
Lechler 544.360 d=1.05 mm	1	10	1.05×10^4
	5	19	1.99×10^4
	9	26	2.72×10^4
Lechler 544.400 d=1.3 mm	1	11	1.42×10^4
	5	21	2.72×10^4
	9	28	3.62×10^4

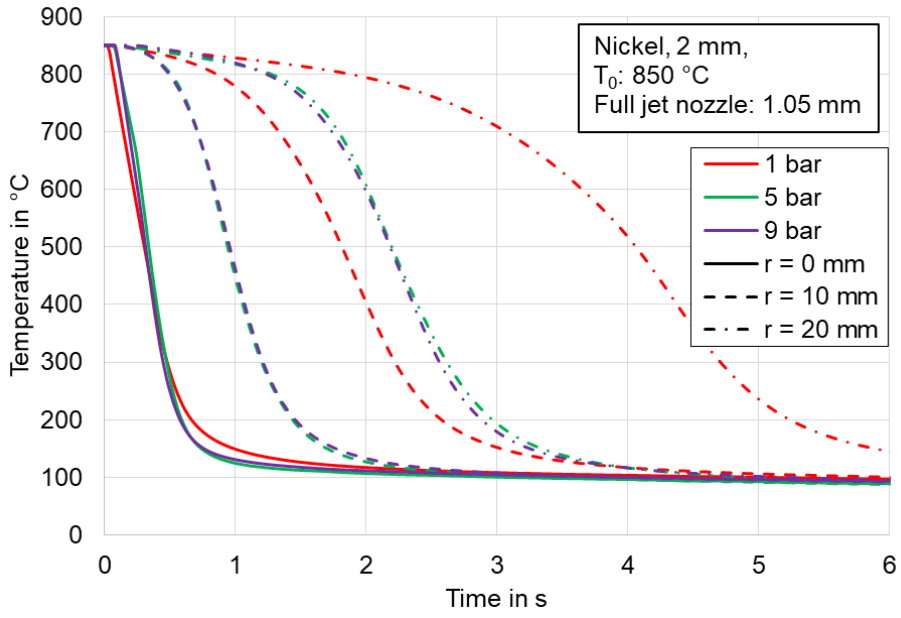

Figure 3.16: Effect of pressure on temperature histories for a full jet nozzle

The maximum heat flux distribution along the wetting front propagation further prove this argument as depicted in **Figure 3.17**. At the stagnation region, the maximum heat flux under three pressures are quite similar with a value around 25 MW/m². The local maximum heat flux decreases as the wetting front propagates radially towards the downstream location. During the movement of wetting front, the deviations between 1, 5 and 9 bar incrementally increase. A larger pressure benefits a faster wetting front movement which leads to an earlier liquid contact at a certain radius on the hot surface. The faster wetting front movement promotes a better overall cooling effect. These facts will inevitably increase the heat flux as shown in Figure 3.17.

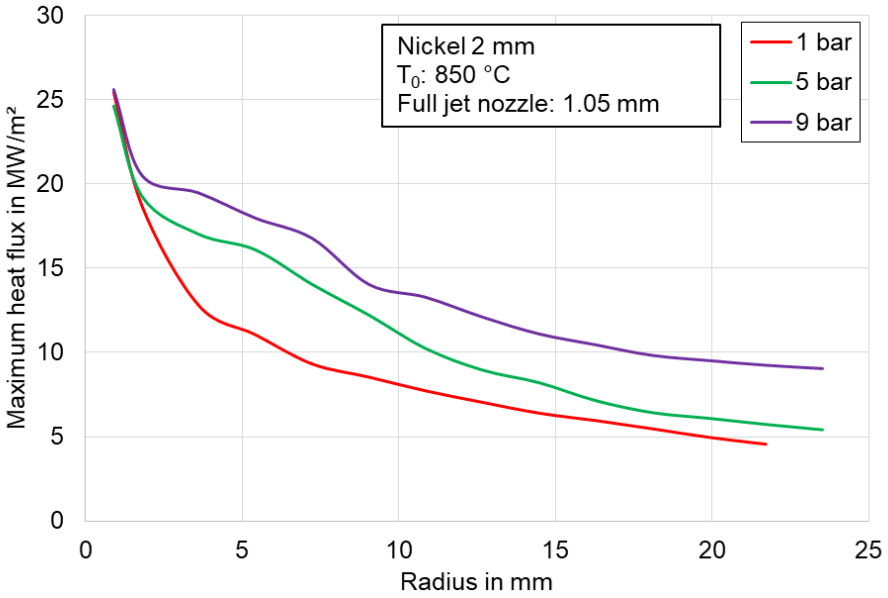

Figure 3.17: Effect of pressure on maximum heat flux for a full jet nozzle

However, rewetting and DNB temperatures are nearly independent of the pressure. Three sub-plots for rewetting temperatures under three initial temperatures (500 °C, 700 °C and 850 °C) are depicted in **Figure 3.18**, respectively. It is clear that no rewetting temperatures can be found in the vicinity of the stagnation point up to approx. 5 mm, which indicates an immediate wetting of the surface occurs in this area. The rewetting temperatures are determined for a 2 mm thick nickel sheet. The influence of initial temperature, nozzle diameter and nozzle pressure have been clearly demonstrated. The jet velocity at specific pressure for full jet nozzle with specific diameter can be found in Table 3.1. It is noticeable that with increasing radius away from the stagnation region, the rewetting temperature drops slightly. This reduction increases with the increasing initial temperature of the plate, as a higher initial temperature benefits an overall cooling performance by decreasing the bulk solid temperature as the wetting front movement is slower. This is further evidenced by the smallest rewetting temperatures at lowest pressure (1 bar) for smallest nozzle diameter (0.8 mm). At a certain initial temperature, a lower pressure and a smaller nozzle diameter can only provide minimum volume flow rate which will reduce the wetting front velocity. As mentioned, this will then promote the cooling at the downstream location

due to thermal conduction from those areas into wetted regions. The rewetting temperatures for a nozzle diameter of 1.05 mm were also determined. For clarity, these are not shown here but are included in **Figure 3.19**. They arrange themselves between the values of the nozzle with d = 0.8 mm and d = 1.3 mm. A distinct conclusion can be made is that the main influence on the rewetting temperature is the plate initial temperature at the beginning of cooling. So in general, **Table 3.2** collects the rewetting temperatures for 2 mm nickel plates at a wide range of jet velocities.

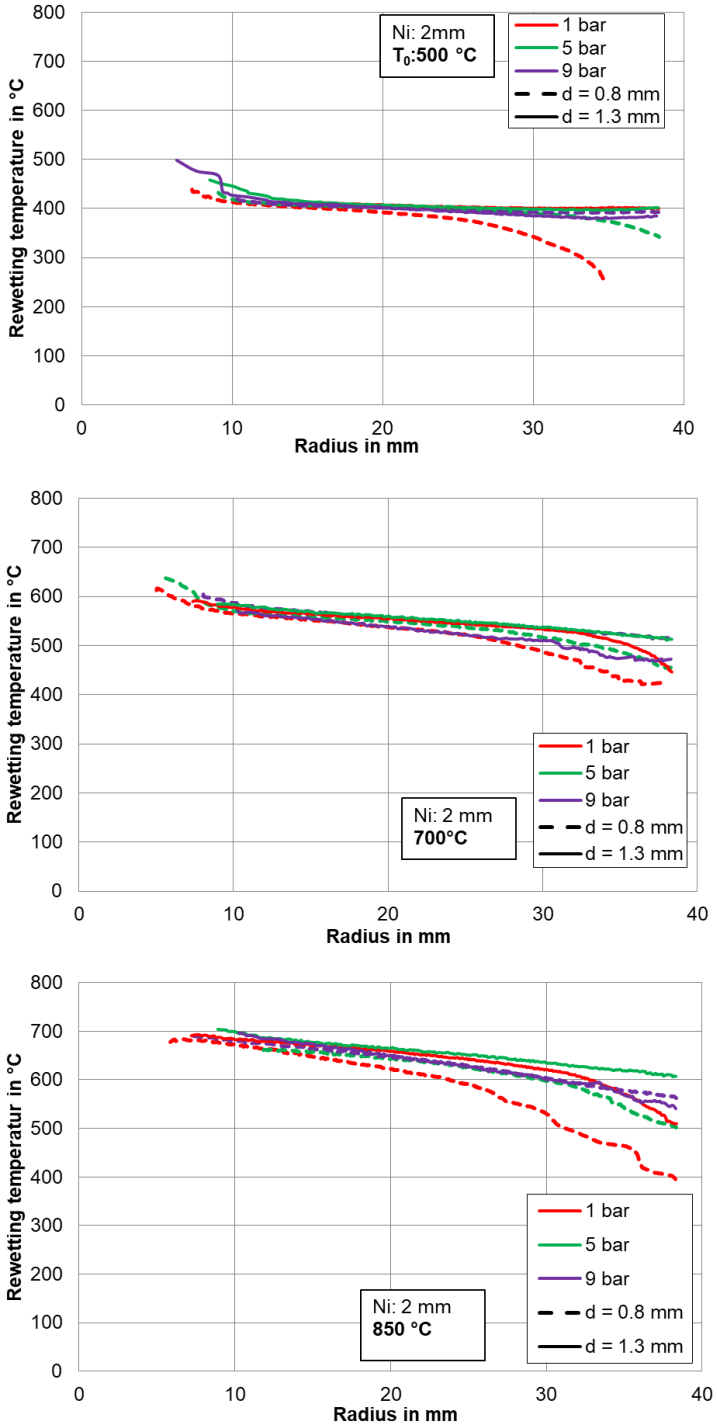

Figure 3.18: Effect of pressure on rewetting temperatures for full jet nozzles under initial temperatures of 500°C (top), 700 °C (mid), 850 °C(bottom)

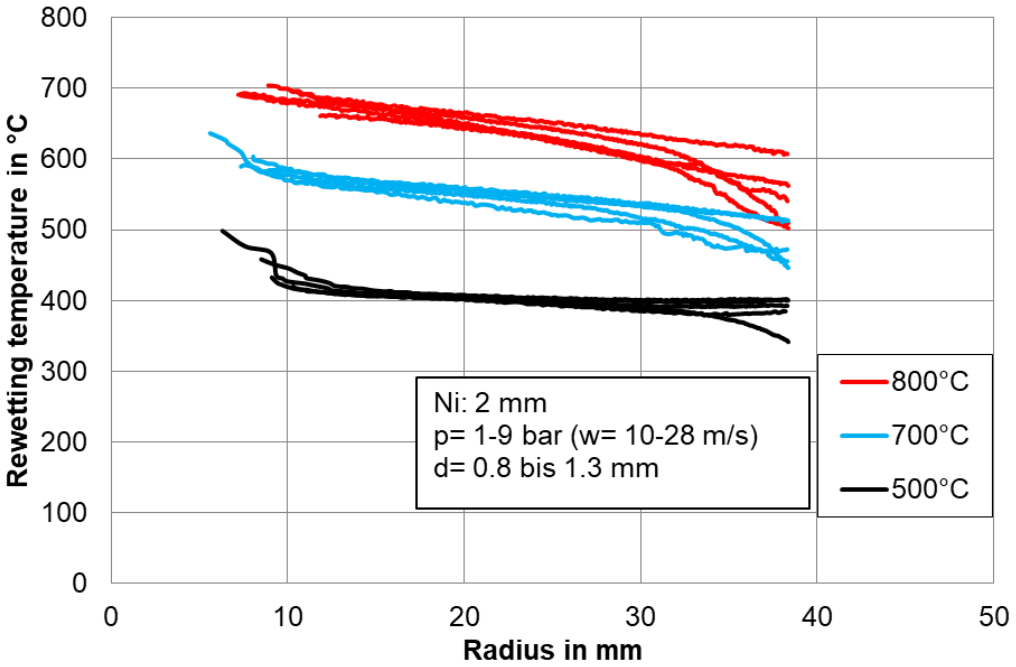

Figure 3.19: A summary of rewetting temperatures over a wide range of jet velocity under 500, 700 and 850 °C

Table 3.2: A collection of rewetting temperatures for 2 mm nickel plate in a wide range of jet velocity

Initial temperature in °C	Rewetting temperature in °C
500	400
700	580 - 500
850	680-580
Valid for radius from 10mm to 35 mm	

Similarly, **Figure 3.20** depicts the DNB temperatures under 500°C, 700°C and 850°C for a 2 mm thick nickel plate. Compared to the rewetting temperatures, it is noticeable that the DNB temperatures fluctuates by about 100 °C for a certain initial temperature, which is caused by the uncertainty during numerical calculation of heat flux. The DNB temperatures are about 100 to 350 °C below the rewetting temperatures according to the initial temperatures. They characterize the boiling mechanism from transition to nucleate boiling. At initial temperature of 500 °C, the DNB values lies between 200 and 300 °C; at 850 °C between 300 and 400 °C. It can be concluded that a dramatically increasing of DNB temperature cannot be achieved by increasing initial temperature, which can be better clarified from the summary as shown in **Figure 3.21**. It is obvious that the influence of initial temperature on DNB values is much more significant than nozzle outlet pressure.

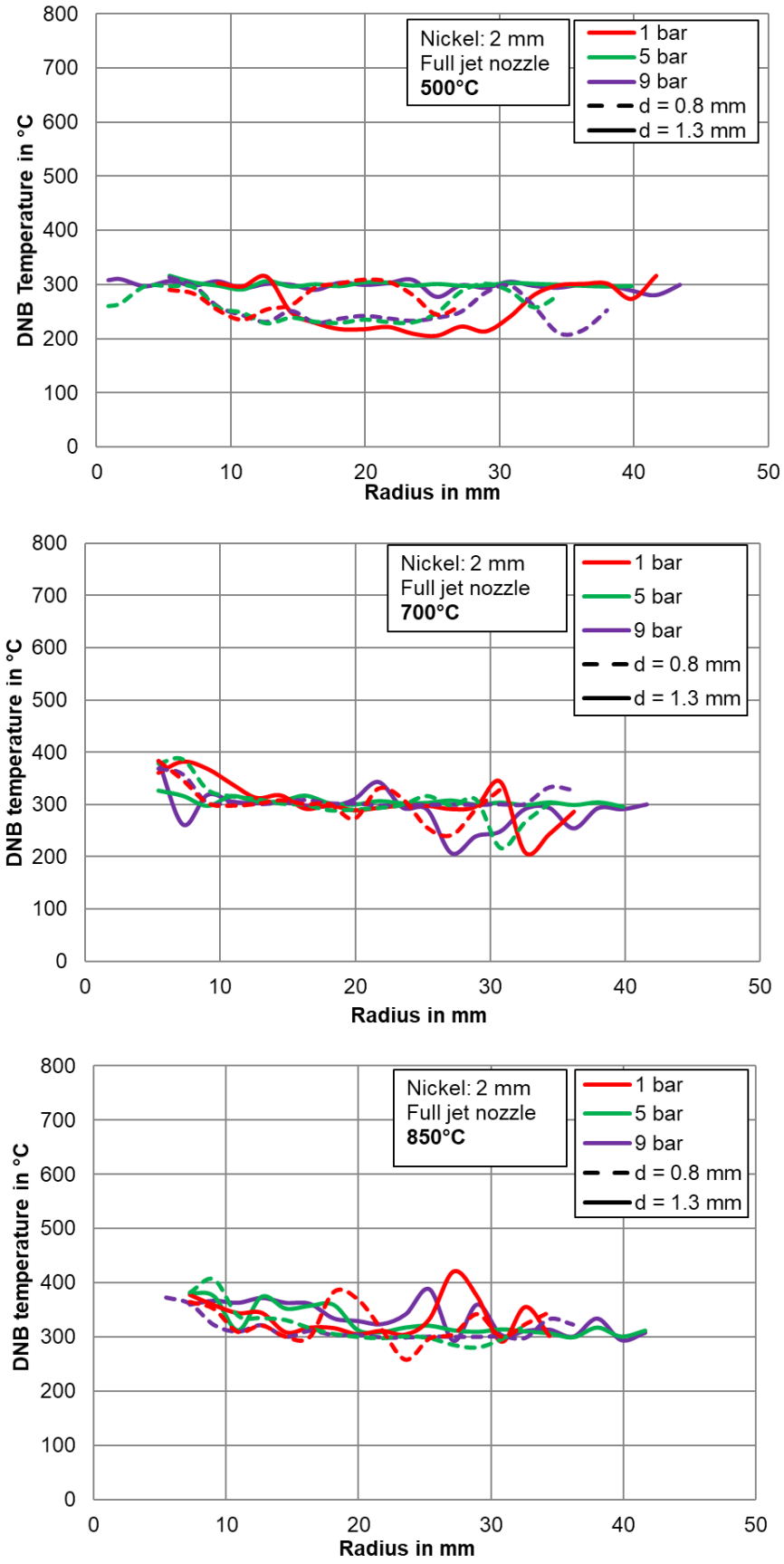

Figure 3.20: Effect of pressure on DNB temperatures for full jet nozzles under initial temperatures of 500°C (top), 700 °C (mid), 850 °C(bottom)

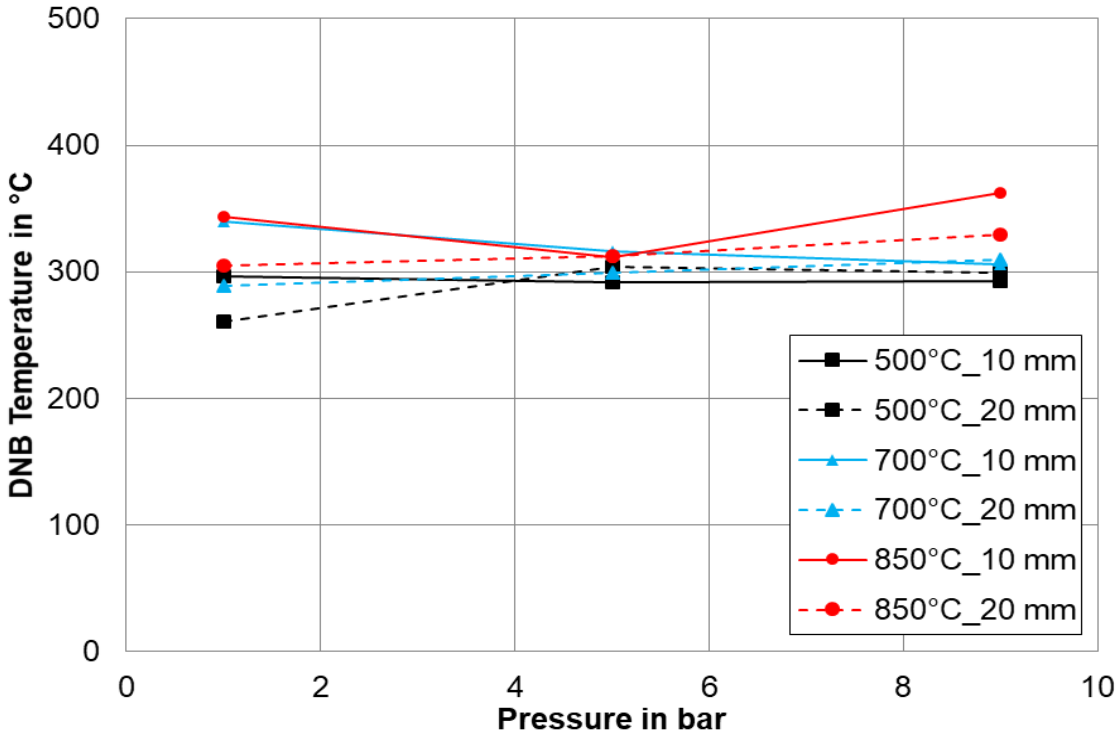

Figure 3.21: DNB temperature with respect to pressure at two radii: 10 mm and 20 mm under 500, 700, 850 °C

3.3.2.3 Effect of sample thickness

Similar to the investigation for a spray nozzle, the sample thickness is also studied with a single full jet nozzle. It has been reported that wetting front velocity decreases as the sample becomes thicker [38]. Similar tendency can also be observed in current research. **Figure 3.22** illustrates the wetting front velocity dependency on the sample thickness. It has been observed that the wetting front reduces with the increasing metal sample thickness. The metal sample was heated up to 850 °C before the cooling started. Hence, a thicker plate can store higher initial energy. Panda and Prasad [70] have performed computational and experimental investigations with a shower head of impinging liquid jets. They concluded that the temperature gradient is larger for thicker plate than thinner plate. Hence, the rewetting state for a 2 mm plate can be attained earlier than a 4 mm plate which makes the liquid temperature rise more for plate with 4 mm thickness. All these factors will impede the wetting front movement from stagnation point to the downstream locations as well as heat transfer. The maximum heat flux evolution can be found in **Figure 3.23**. It can be clearly seen that the maximum heat flux for 1 mm thick plate near the stagnation region is 9 MW/^{2}; while 6.2 and 5.9 MW/m^2 for 3 and 4 mm, respectively.

Although numerous work has been published, a generalized correlation for both heat flux and wetting front velocity seems not possible to be available in those literatures. Moreover, the proposed correlations are merely based on individual experimental conditions. Hence, a comparison between different correlations is not an

easy task to conclude an exact quantitative criteria for the cooling of impingement jet. However, the present experimental results are in line with observations reported by other researchers under various experimental parameters. Karwa et al. [71] has investigated the influence of jet velocity on wetting front propagation. They used a horizontal flat stainless steel plate with thickness of 20 mm. The initial temperature is remained as 900 °C. They reported that the wetting front velocity as 1 and 3 mm/s at 24 mm downstream location respectively with jet velocity of 2.85 and 6.4 m/s. Meanwhile, the wetting front velocity at 24 mm spatial location is 3.2 mm/s with surface of 4 mm thickness for jet velocity of 25.6 m/s or Re = 25,500 in present study. Based on experimental results, Agrawal et al. [38] proposed a correlation, in which jet velocity or jet Reynolds number is the dominant factor on dimensionless wetting front velocity, Peclet number. Their results are depicted in **Figure 3.24** along with our experimental results with Re = 25,500, thickness = 3 and 4 mm for different spatial locations.

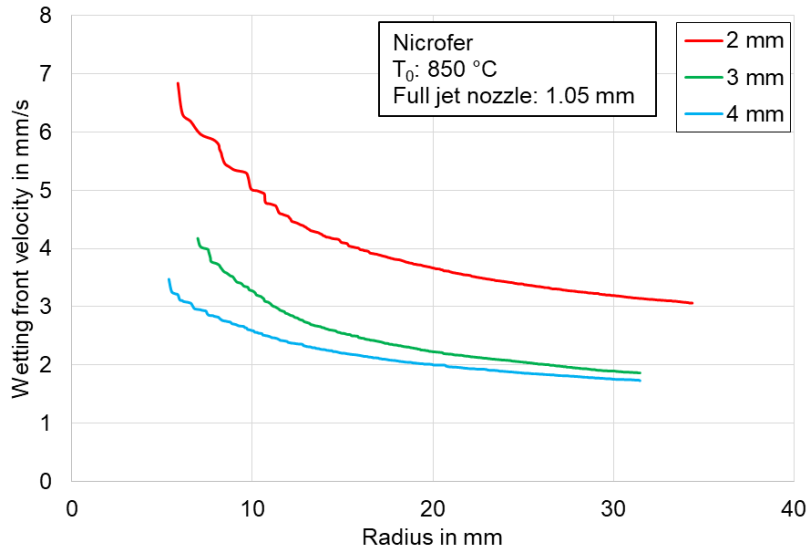

Figure 3.22: Effect of sample thickness on wetting front velocity

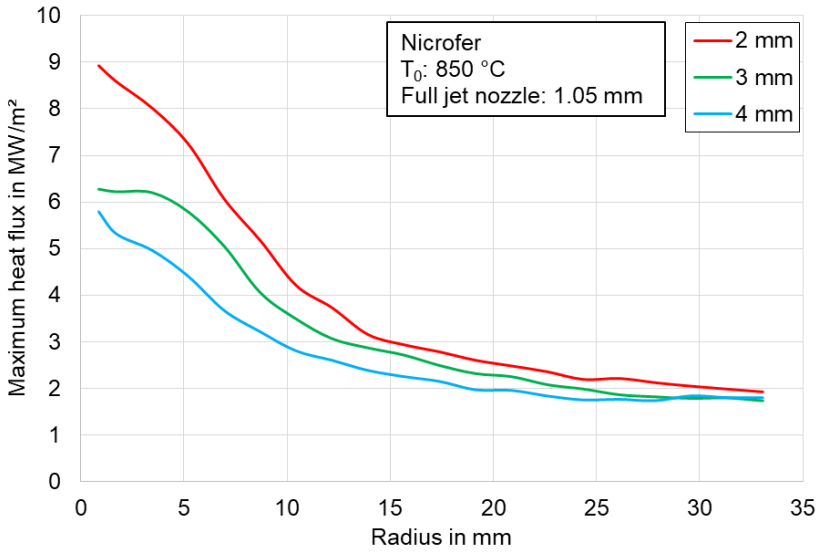

Figure 3.23: Effect of sample thickness on maximum heat flux

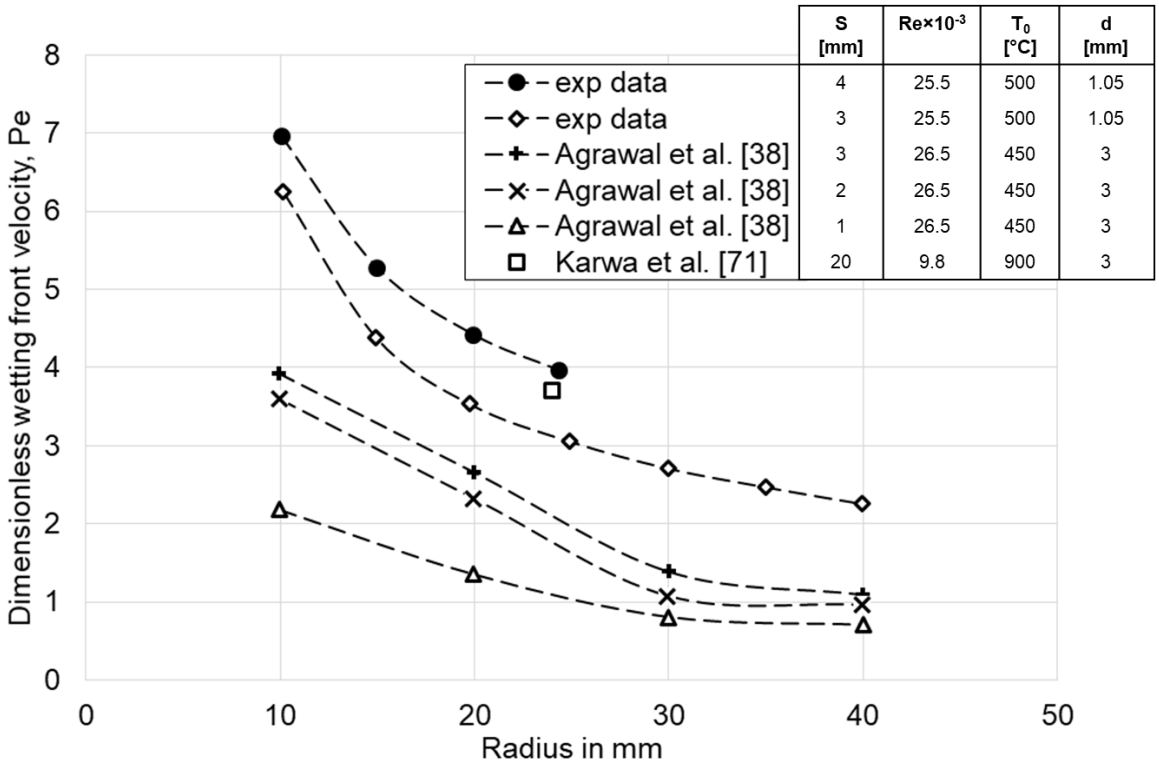

Figure 3.24: Comparison of dimensionless wetting front velocity between in-house and publication results

3.3.2.4 Effect of metal type

In this section, the effect of different kinds of metal with a full jet nozzle is studied. The nomenclature and thermo-physical properties of the investigated metal types are concluded in **Table 3.3** and **Table 3.4** respectively.

Table 3.3: Nomenclature of the used materials

Name in text and figures	Detailed representation of the metals
Nickel	LC-Nickel 99.2 – alloy 201 (UNS*: N02201)
Nicrofer	Nicrofer 6020 hMo – alloy 625 (UNS: N06625)
Copper B14	Copper Alloy CuSn4 – Wieland-Werke AG (UNS: C51100)
***UNS: Unified Numbering System (USA)**	

Table 3.4: Thermo-physical properties of the used materials

Material	**Copper B14**		**Nicrofer**		**Nickel**	
Temperature [°C]	300	500	300	500	300	500
Density [kg/m3]	8850		8400		8900	
Thermal conductivity [W/m/K]	145	161	14.4	17.3	60	58.5
Specific capacity [J/kg/K]	394	400	480	525	570	525
Heat penetration coefficient [W*s ^{0,5}/m^2/K]	22500	23900	7600	8700	17450	16500

Nickel is the most used metal in current research. The dependency of the rewetting and DNB temperatures and heat flux on technical parameters such as nozzle outlet pressure was investigated. The rewetting temperatures of copper B14, and nicrofer are compared with those of nickel as shown in **Figure 3.25**. The experiments were conducted at a nozzle pressure of 5 bar and an initial temperature of 500 and 850 °C. The thickness of the metals are the same as 4 mm. It is clearly seen that metal type has a great influence on the cooling performance at 500 °C. This deviation is much larger when the initial temperature rises to 850 °C. Taking a radius 15 mm as an example, the rewetting temperature for nickel is 430 °C while for nicrofer 30 °C higher at the initial temperature of T_0 = 500 °C; the rewetting temperature for nickel is 610 °C while for nicrofer almost 100 °C higher at T_0 = 850 °C. This is mainly attributed to the difference of the thermal conductivity, since density and specific heat capacity vary not significantly for the three materials. The higher thermal conductivity of cooper B14 can transfer heat within the material body faster than that of nicrofer which has a very low thermal conductivity. The thermal conductivity of nickel is between these two materials; hence the order (nicrofer-nickel-copper) is obvious in Figure 3.25. The same tendency can also be found in DNB temperatures as well as wetting front velocity, depicted in **Figure 3.26** and **Figure 3.27**, respectively. The three figures make it clear that a smaller thermal conductivity is responsible for the poorer heat conduction from dry region towards the wetted region, which results in a higher temperature at wetting front.

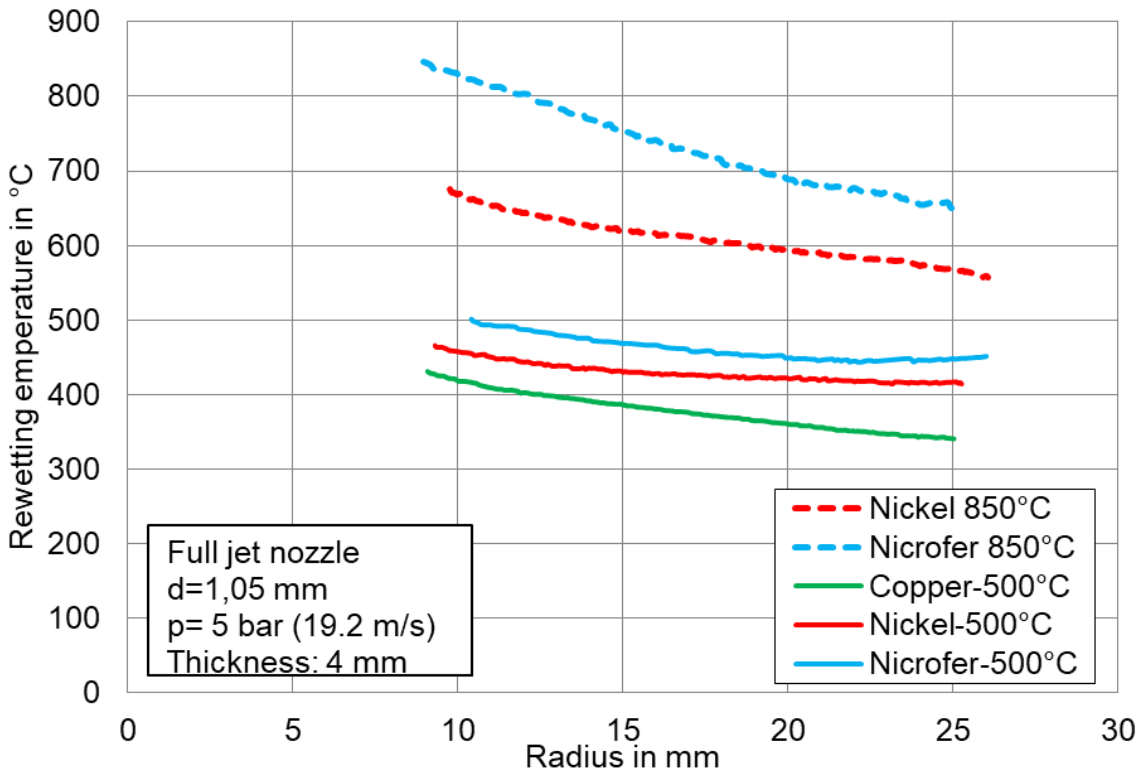

Figure 3.25: Effect of materials on rewetting temperatures with full jet nozzle

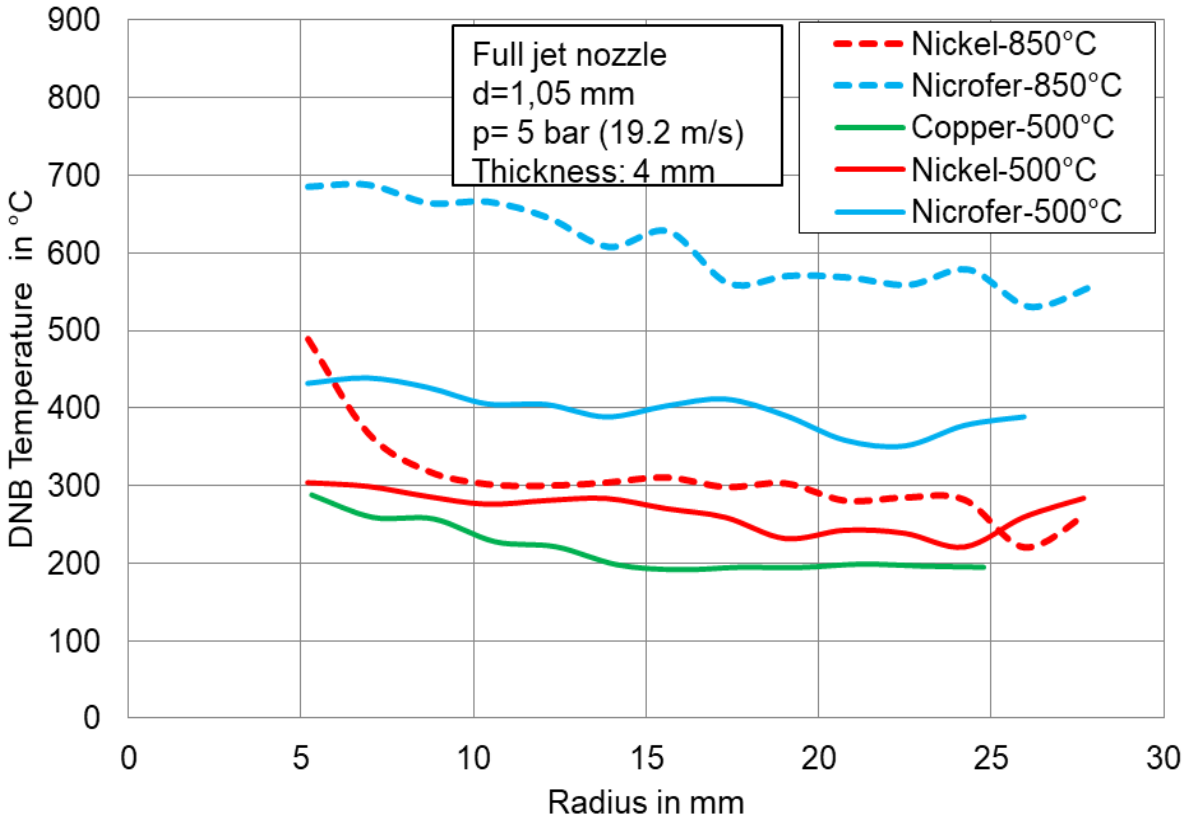

Figure 3.26: Effect of materials on DNB temperatures with full jet nozzle

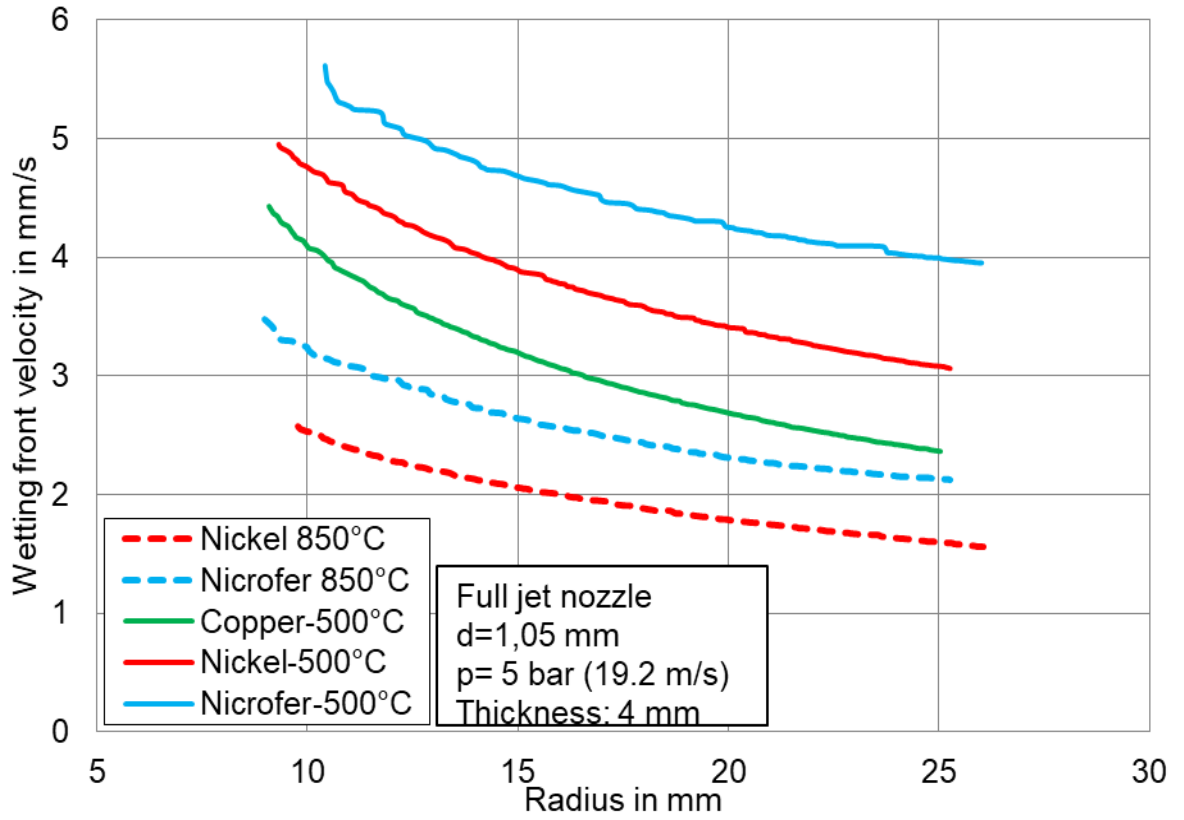

Figure 3.27: Effect of materials on wetting front velocity with full jet nozzle

3.3.3 Investigation of nozzle field

3.3.3.1 Introduction

The thermal images of the investigated inline and staggered nozzle fields are shown in **Figure 3.28**. Since both fields are comprised of the same full jet nozzles, the symmetry of the arrangements can simplify the evaluation process. The temperature history at center point C will be chosen for the comparison between inline and staggered arrangements. The heat flux up to p/2 = 17.5 mm will be analyzed, since the proposed model work only for regular wetting fronts.

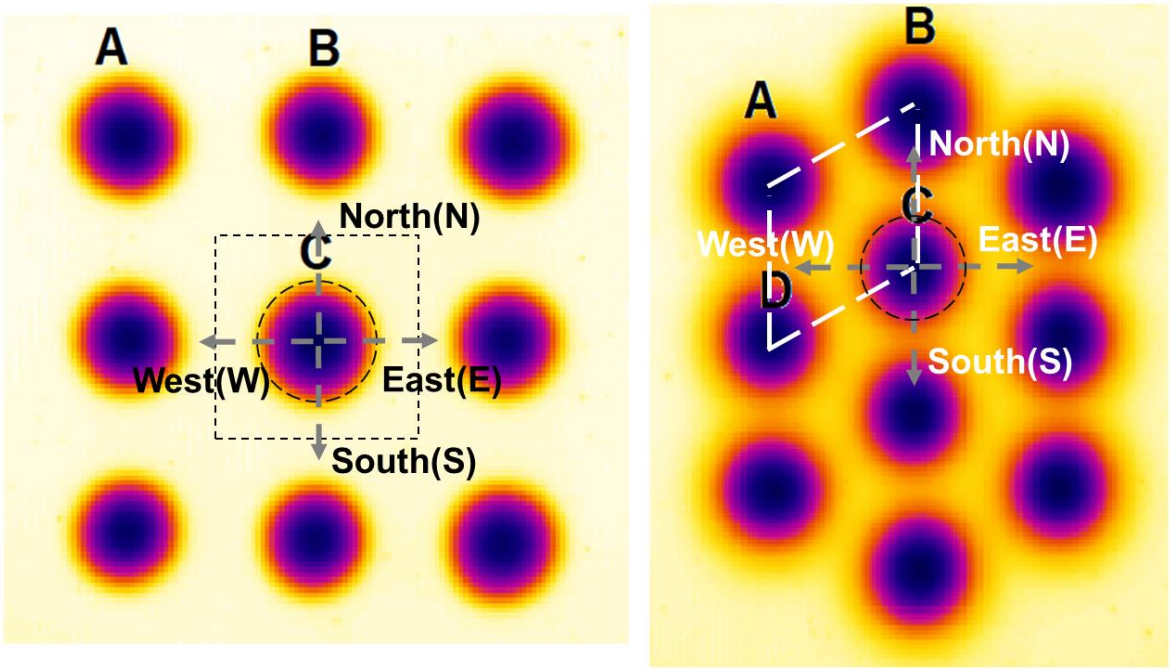

Figure 3.28: Thermal images of inline and staggered arrangements

At the starting period of the cooling with multiple jets, the cooling at stagnation points of each individual jet should be similar to that of a singular liquid jet. The jet interaction is determined by the jet-to-jet spacing in an array. San and Lai [72] reported that, for H/d = 2, the interference remained up to p/d = 8 and the maximal Nu occurred also at p/d = 8. In current research, the jet pitch (or jet-to-jet spacing p) and jet-to-plate spacing (H) remain constant, the variables which have been studied include initial temperature and the arrangement. The sample is vertically placed in current work to minimize the cross-flow effect, since a significant reduction in heat transfer rates due to the cross flows has been reported by Metzger and Korstad [73].

The analysis of the temperatures are performed in four directions at the center point C as shown in Figure 3.28. In order to further simplify the analysis route, the temperatures at four directions are compared as depicted in **Figure 3.29**. A slight deviation can be observed at four directions; hence, further analysis is done based on the average temperature values in four directions. The reason to choose center point C for analysis is attributed to the introduced side effects of points A and B which can

be observed in **Figure 3.30**. Temperature at point A in west direction drops slower for all three radii compared with that at point B and C. This is mainly due to the negligible interference of other liquid jets at point A in west direction. Hence, in order to account for the influence of jets interaction, point C is selected.

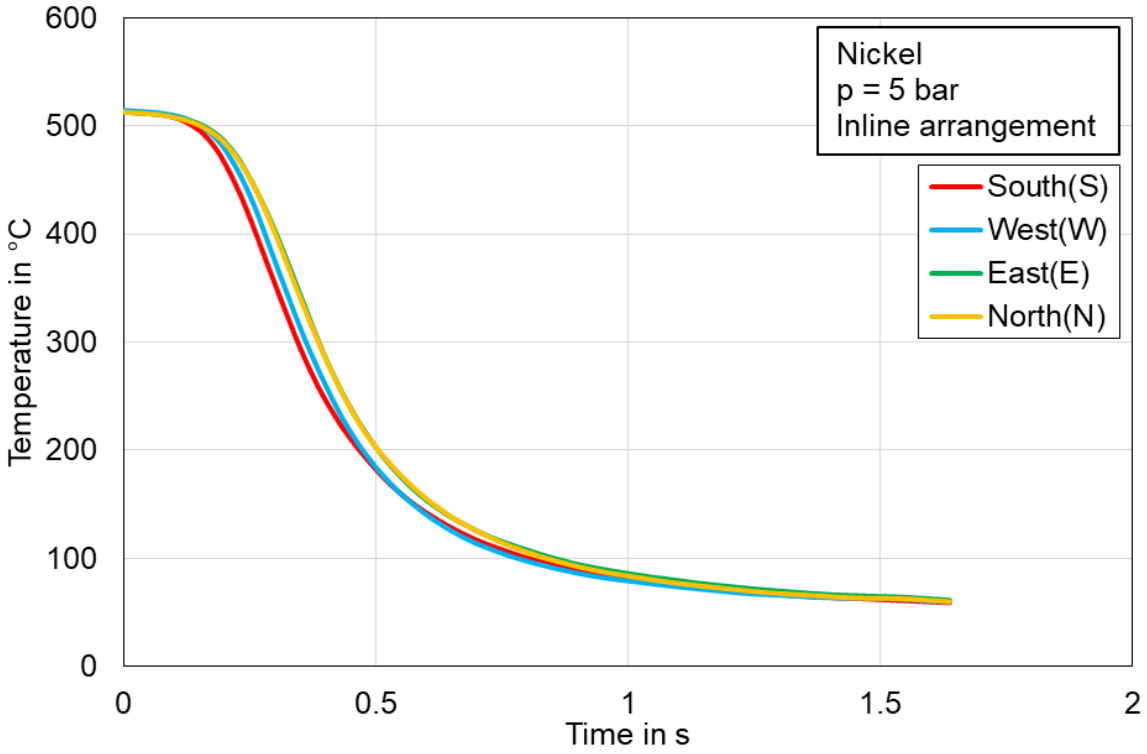

Figure 3.29: Temperature comparison at four directions for inline arrangement

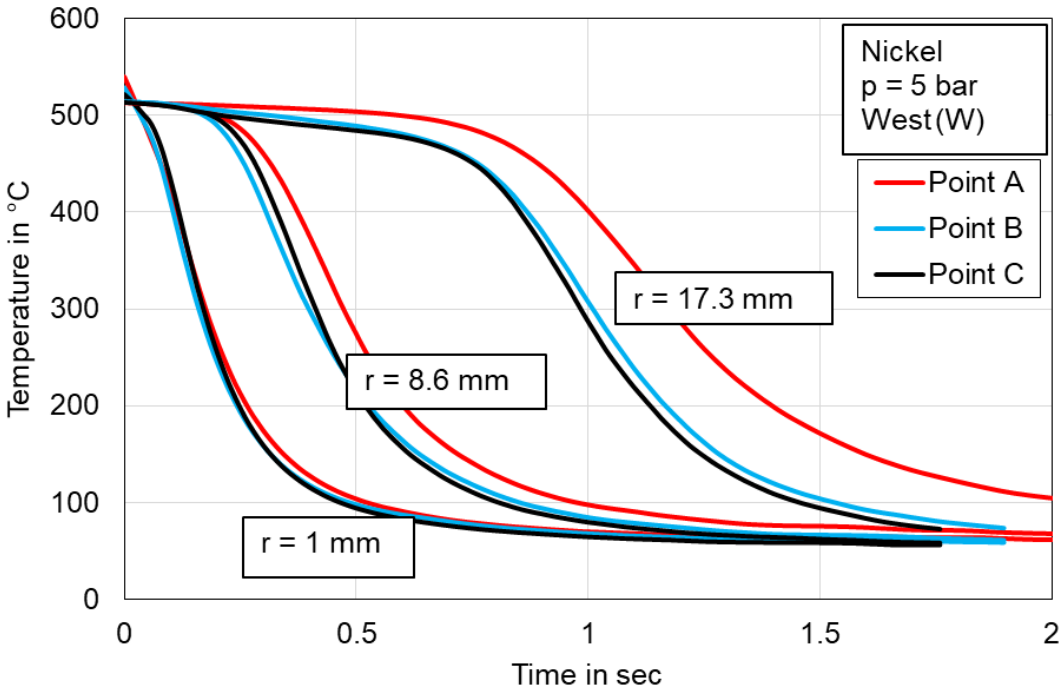

Figure 3.30: Comparison of temperatures for point A, B and C at three radii

3.3.3.2 Effect of initial temperature T_0

The metal sample was heated to three different initial temperatures; namely 500 °C, 700 °C and 850 °C. **Figure 3.31** shows the temperature distribution over the surface at t = 0.62 s for three initial temperatures. At this time point, the temperature at the stagnation point is around 100 °C for an initial temperature of 500°C, while 200 °C and 235 °C for 700°C and 850°C, respectively. And it can also be seen the temperature gradient is higher at higher initial temperatures, as shown in **Figure 3.32**. The maximum temperature gradient for T_0 = 850°C is 104 °C/mm, which is 1.5 times larger than that for T_0 = 500 °C. The sample with a higher initial temperature inherently has more energy stored which potentially increases the temperature gradient.

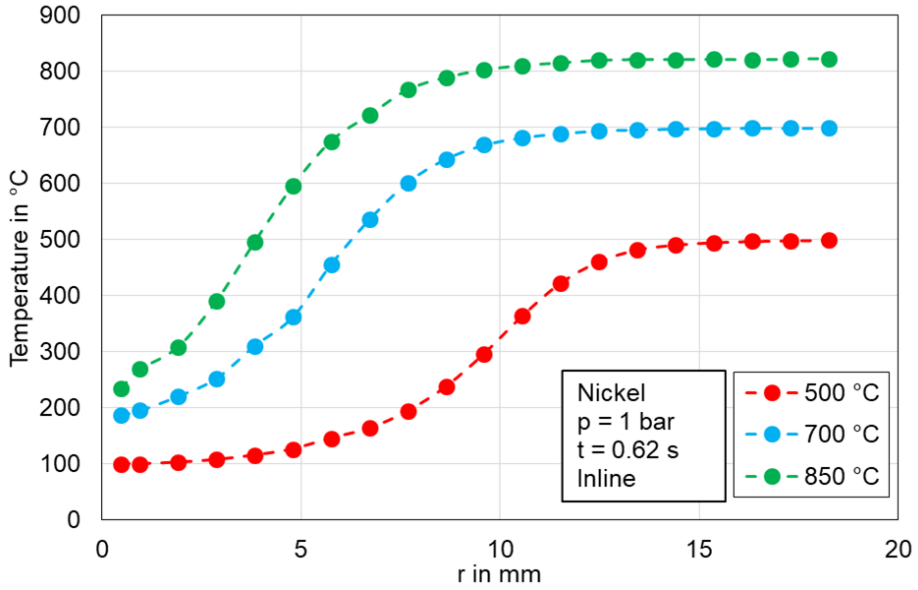

Figure 3.31: Temperature curves under three initial temperatures

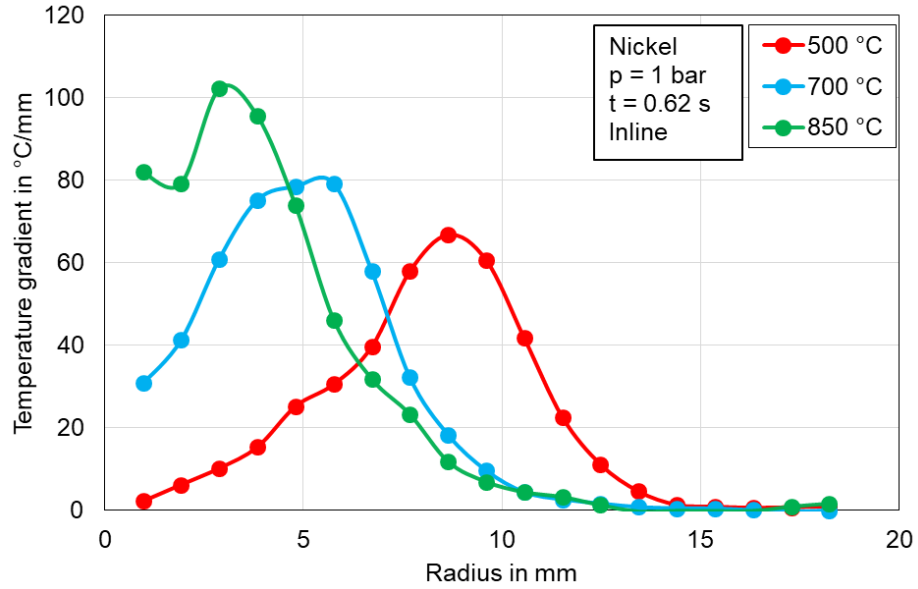

Figure 3.32: Temperature gradients under three initial temperatures

The maximum temperature gradients also occur at different radius, since the wetting front movement is also affected by the initial temperature. The rewetting temperature increases with increasing initial temperature, while variation of DNB temperatures is not significant, as shown in **Figure 3.33**; the conclusion agrees well with the results obtained by Wang et al.[11] as illustrated in black marked curves in the figure. The corresponding wetting front velocity is shown **Figure 3.34**. A higher initial temperature will inevitably impede the wetting front movement due to higher bubble nucleation frequency at the wetting front region.

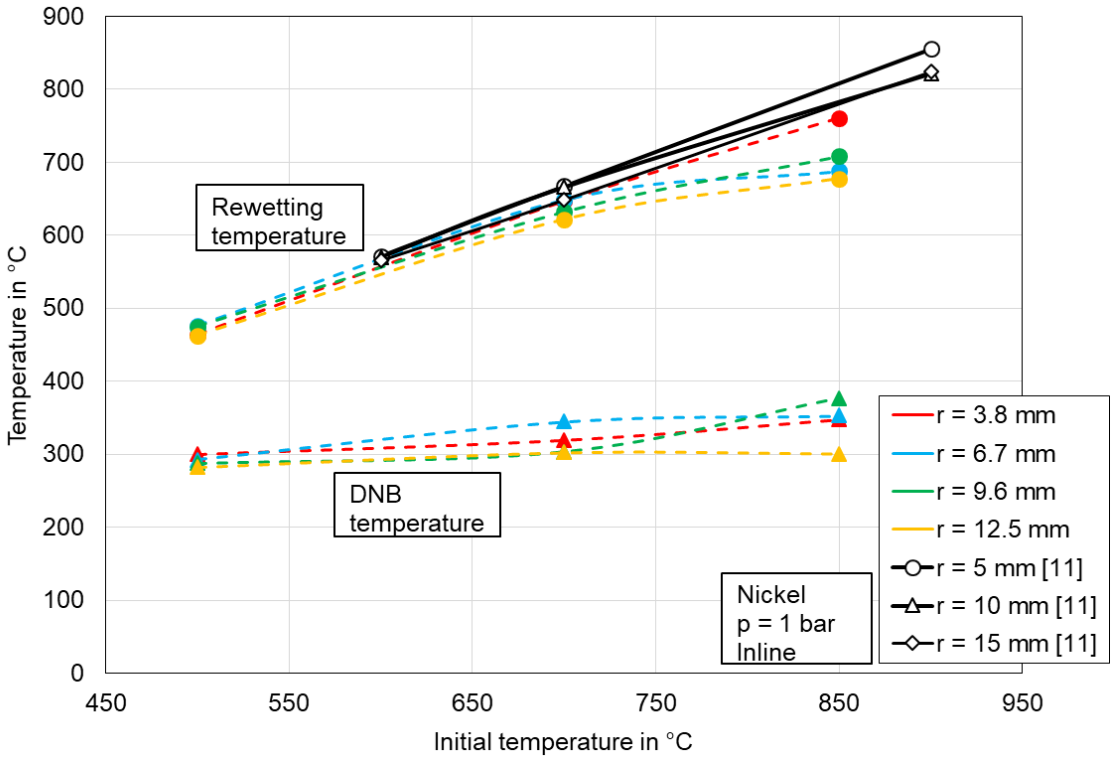

Figure 3.33: Rewetting and DNB temperatures at different initial temperatures

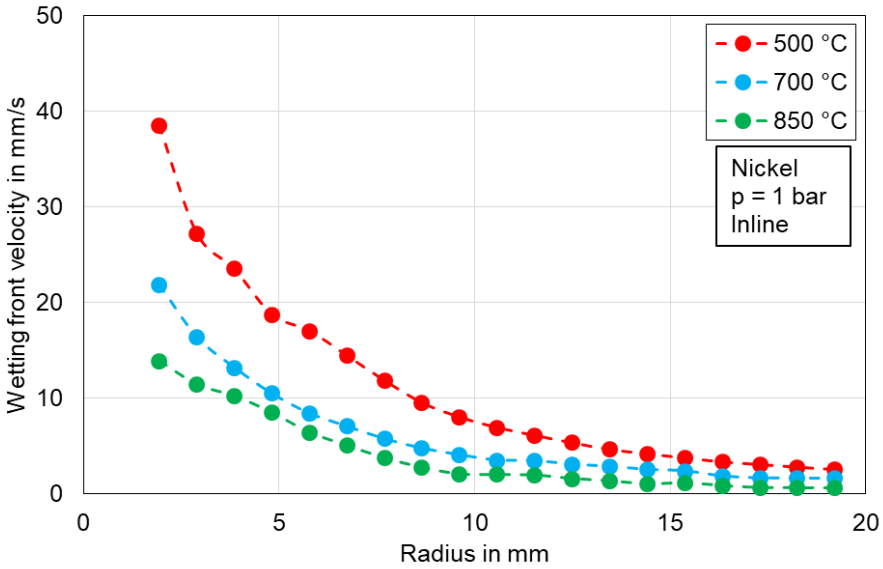

Figure 3.34: Wetting front velocity at three initial temperatures

Another comparison has been made for the wetting front propagation as shown in **Figure 3.35**. The dimensionless radius is defined as the ratio of radius to maximum analysis radius; since it is not always possible to directly compare the magnitude in different publications. Akmal et al. [74] has conducted experimental investigation of liquid jet impinging on a curved surface. They have reported that the wetting front velocity is mostly affected by the initial surface temperature, water temperature as well as the jet velocity. The current result is in good agreement when 500 °C is considered.

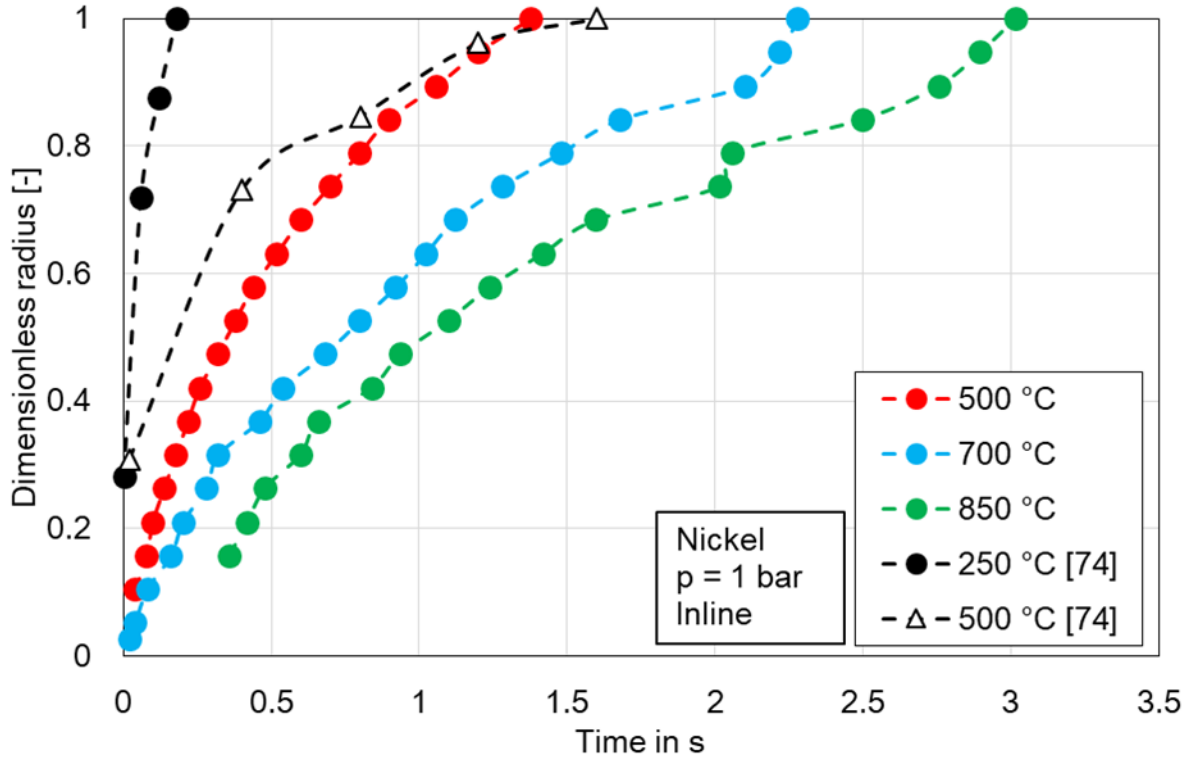

Figure 3.35: Wetting front propagation at three initial temperatures

From the aforementioned discussion, it leads to a conclusion that an increase in initial temperature of the plate promote a higher rewetting temperature and a higher heat transfer rate but a lower wetting front propagation in both nozzle configurations.

3.3.3.3 Effect of nozzle arrangement

In this section, the comparison between inline and staggered jet arrays will be discussed and explained. As mentioned, although the jet-to-jet and jet-to-plate spacing are the variables which affect the interaction of neighboring jets according to open literatures [75, 76], they maintain the same for all experiments in current research; the main point is whether different configurations will have fundamental impact on the overall cooling performance.

Figure 3.36 shows the infrared images for both configurations. The experiments were conducted with a 2 mm nickel plate at initial temperature of 500 °C. Both in the inline and staggered nozzle field, the wetting fronts of an individual jet confront with the neighboring jet after a cooling time of 1.5 seconds. There are no significant differences

in the temporal cooling behavior, so that both configurations can be considered approximately equivalent in terms of cooling technology. The graphic representation of the temperatures in the infrared images provides the possibility for a qualitative assessment of the cooling processes. The drawn conclusions result from the visual evaluation in conjunction with the cooling time. However, more detailed statements can be made based on the heat flux and the heat transfer coefficient, as will be shown later. The wetting fronts of the individual nozzles of the nozzle field propagate radially and symmetrically, which follows the cooling behavior of the single full jet nozzle. The propagation mechanism of the individual liquid jet no longer holds, once the wetting fronts of the individual nozzles start interacting with each other. There is no apparent difference between the inner (center point C) and the outer nozzles (edge and vertex point A, B and D) in both nozzle arrangements.

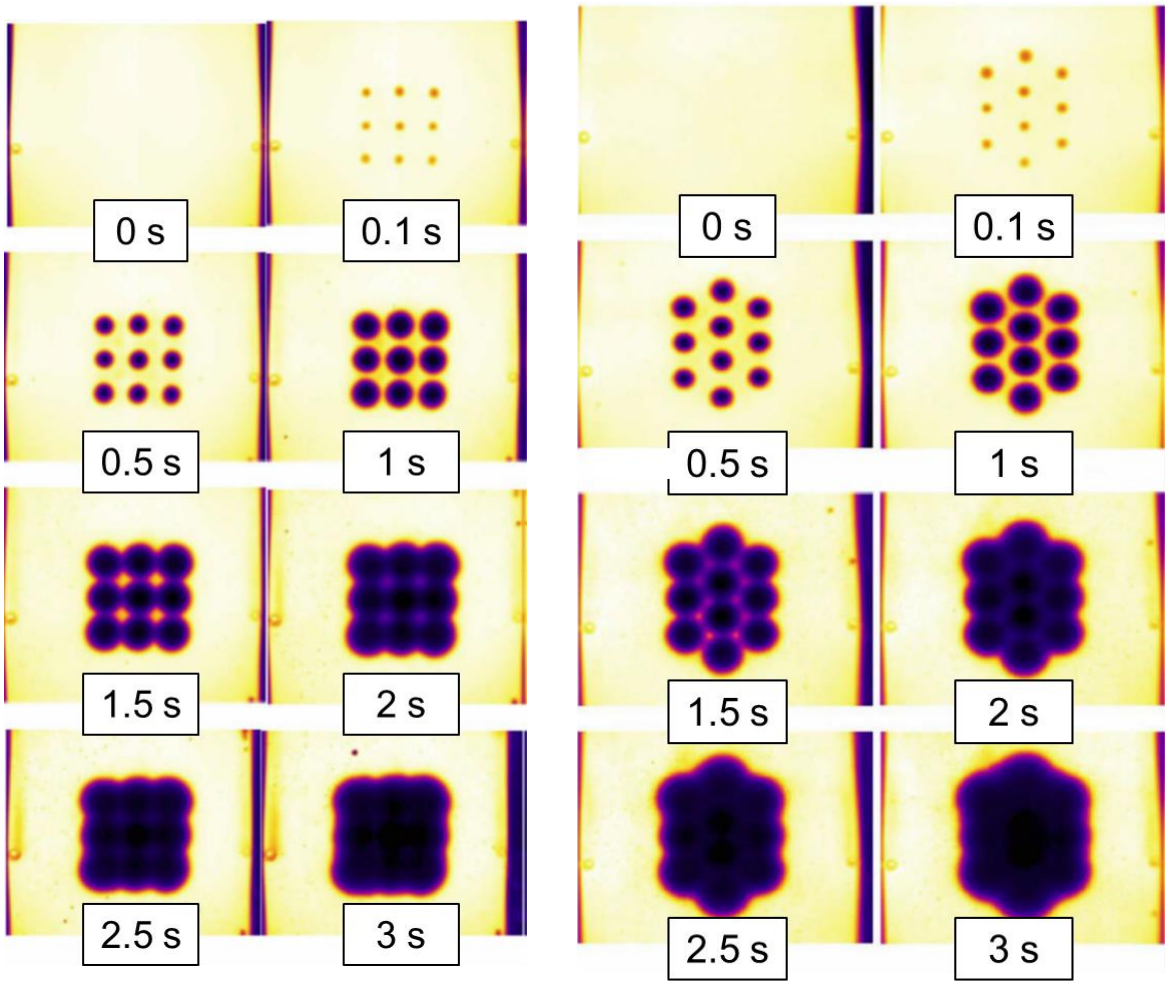

Figure 3.36: Infrared thermal images for inline(left) and staggered(right) arrangements

The infrared images and the evaluation of the temperature curves show that, until the wetting fronts meet, the individual nozzle in the nozzle field cools down according to cooling performance of a singular single nozzle. The nozzle fields considered here have a jet pitch of 35 mm. The wetting fronts theoretically meet at a distance of p/2 = 17.5 mm, which makes up the maximum radius of the whole analysis.

The heat flux and maximum heat flux distribution for both nozzle fields and a single full jet nozzle are shown in **Figure 3.37** and **Figure 3.38** separately.

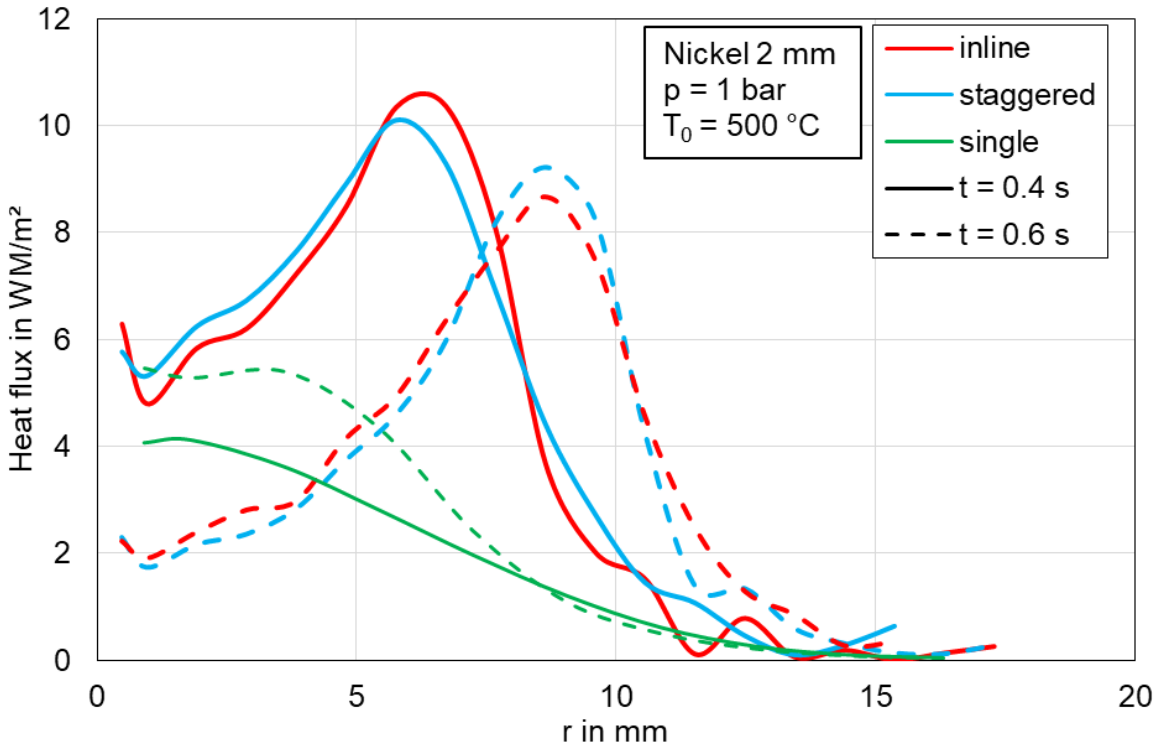

Figure 3.37: Heat flux distribution over radius for inline and staggered arrangements and a single full jet nozzle

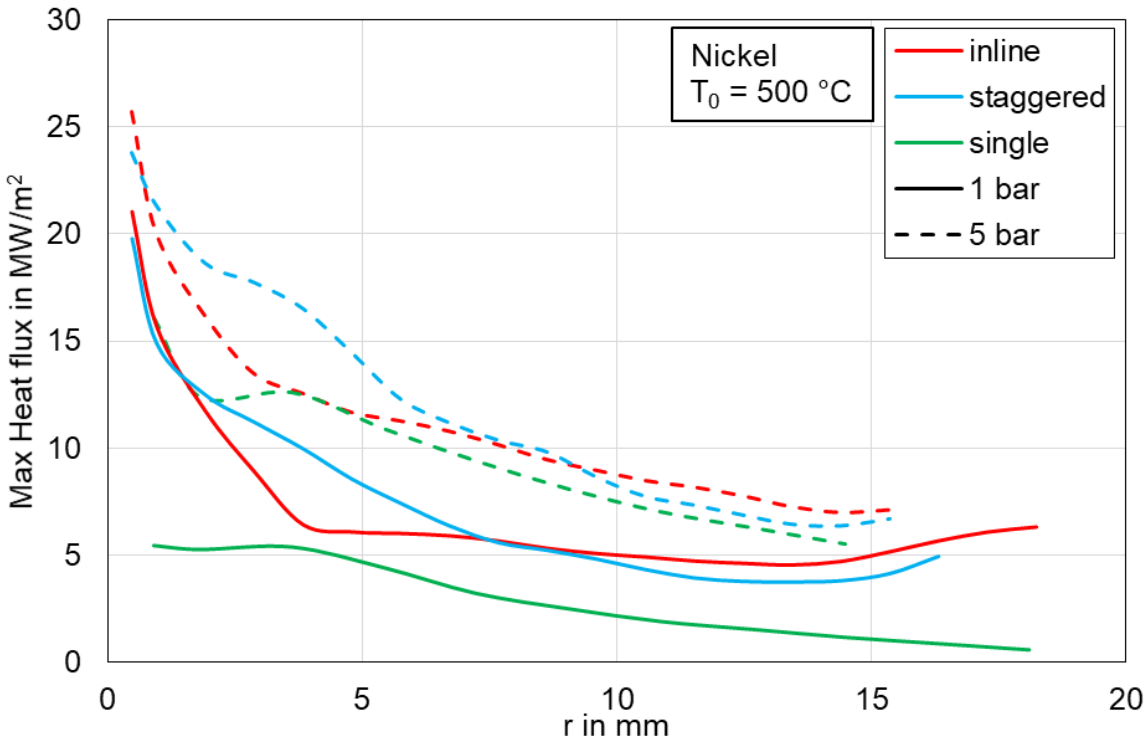

Figure 3.38: Maximum heat flux distribution for inline and staggered arrangements and a single full jet nozzle

A significant deviation between the two nozzle fields is not able to be observed, which means both configurations can be applied into the situation where a small area on a large surface needs to be cooled. However, the possibility of a better performance of either inline or staggered arrangement in other applications is by no means ruled out. A higher heat flux can be obtained for both configurations rather than the single nozzle; which means a greater and homogenous heat transfer rate is easier to be achieved, since 9 or 10 individual stagnation zones exist on the surface simultaneously.

A representation of temperature curve and rewetting and DNB temperatures give better explanation of the effect of the investigated inline and staggered configurations, as shown in **Figure 3.39** and **Figure 3.40**, respectively.

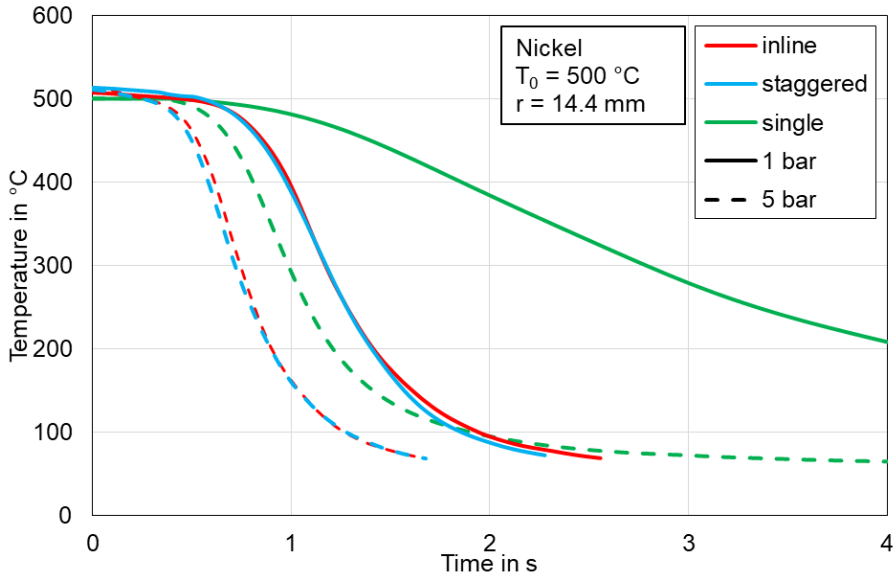

Figure 3.39: Comparison of temperature history for inline and staggered arrangements as well as a single full jet nozzle

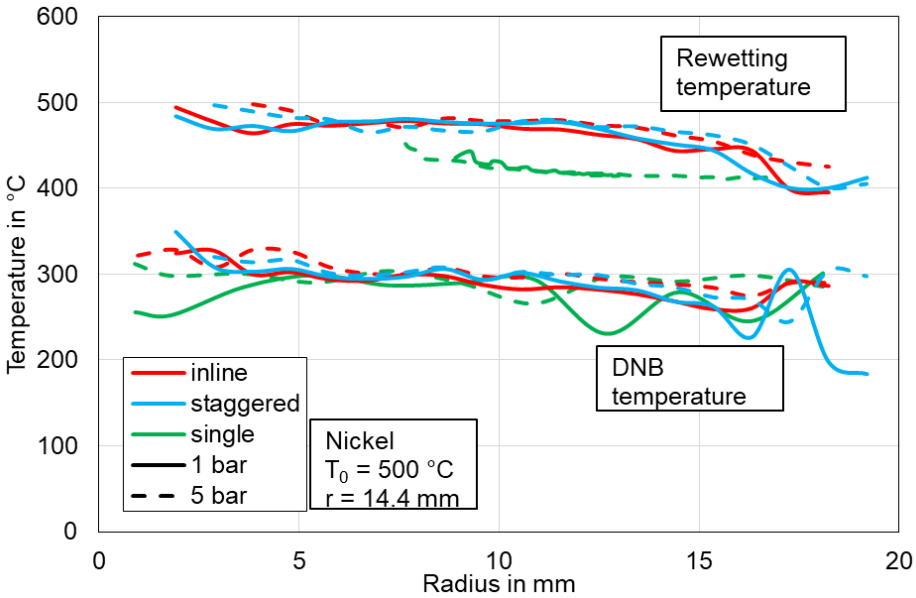

Figure 3.40: Comparison of rewetting and DNB temperatures for inline and staggered arrangements as well as a single full jet nozzle

3.3.4 Conclusion

This chapter deals with the analysis of heat transfer during cooling hot metals with a single nozzle (full jet, full cone and flat spray nozzle). As seen in many publications, the heat transfer rate of full jet nozzles is higher than flat spray nozzles followed by full cone nozzles. In the current research, it is clearly seen that the vapor film breaks down immediately when liquid jet impinges on a hot surface; however, a longer film boiling is attained as a full cone nozzle is applied. The cooling behavior of a flat spray nozzle lies between them. Generally speaking, selection of a specific cooling method is necessary and possible in a realistic applications.

The investigated parameters can be classified as either coolant- or surface-relevant. In this chapter, the studied coolant relevant parameter is mainly volume flow rate; for surface-related parameters include the sample thickness, metal type and surface roughness which is discussed thoroughly in Chapter 4. The influence of the investigated variables are summarized based on a general boiling curve which is further utilized as thermal boundary conditions in the perspective of simulations. This is shown schematically in **Figure 3.41**. It should be noticed that, the upward arrows means increase; vice versa. This representation can provide a better consideration when a liquid jet is used to cool the hot surface.

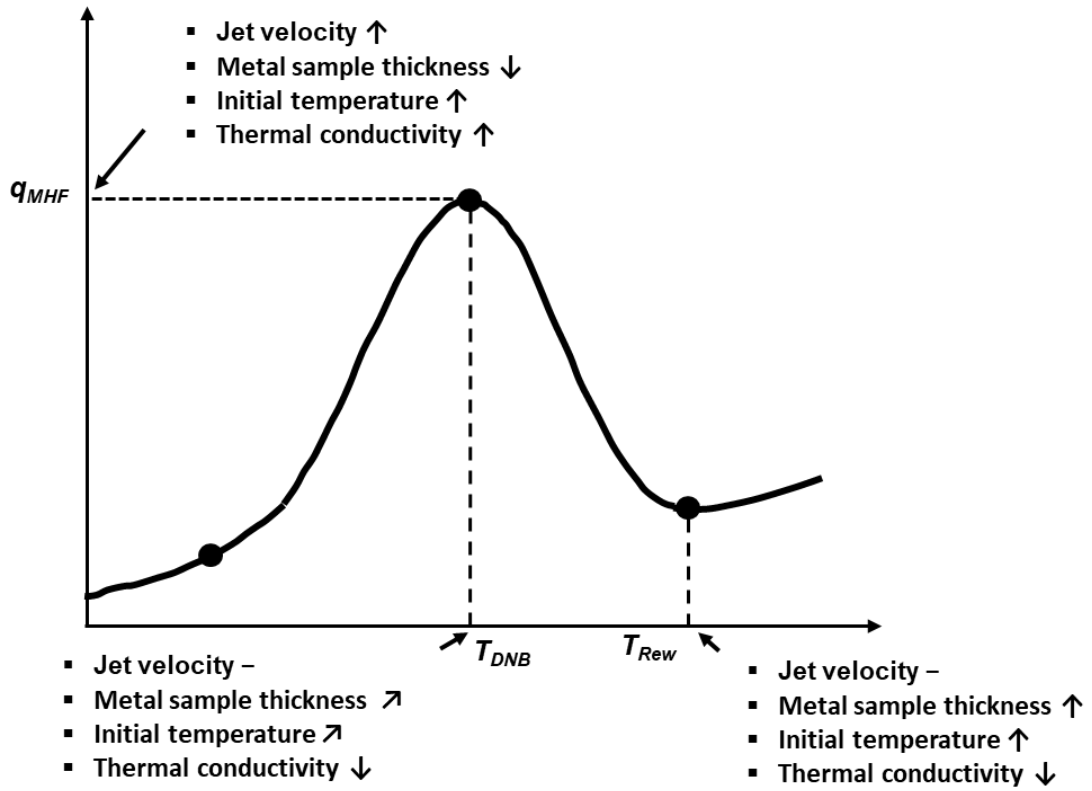

Figure 3.41: Summary of the influence of investigated parameters on schematic boiling curve

4. Investigation of Surface Roughness during Quenching Hot Metals

4.1 Overview

The results of investigation of surface roughness under different cooling strategies are discussed and summarized in this chapter. The previous studies are conducted mainly for samples with smooth surface. The real surfaces of casting products possess considerable roughness up to the millimeters which can be either unstructured or have typical grooves in the casting direction. The knowledge of the influence of the surface roughness on the cooling effect is a prerequisite for an accurate simulation of the casting process and thus for a more economical production. The cooling behavior with different surface conditions must be included in the technical parameters of the cooling process. The investigations will initially be carried out with individual nozzles, such as full cone and full jet nozzles, in order to identify the basic relations. Subsequently, a mold is investigated which can be regarded as a series of full jet nozzles. The investigations started with stationary metal samples, followed by a moving plate with certain velocity v_c.

4.2 Introduction of surface roughness

4.2.1 Literature review

The investigation of surface roughness on cooling performance has been done by many other authors and groups. To the best knowledge of the author, it was first reported by Pais et al. [77] that surface roughness has influence on air-atomized water spray cooling of copper surfaces. They proposed a one-dimensional Fourier analysis to retrieve the information of the surface morphology. Meanwhile, the ability of surface to remove heat under conditions of spray cooling using air-atomized nozzles was studied. It was reported, at very low superheats, a heat flux of 12 MW/m² was achieved. They also found out that a superior cooling performance was achieved when the surface was smooth (< 1 µm) due to the film conduction/evaporation.

Bernardin and Mudawar [78] have reported that repeated heat-quench cycles resulted in increased surface roughness and shorter overall quench periods. The surface roughness affect cooling rate by three major factors: a) raising the rewetting temperature, b) increasing the number of boiling sites on the quenched surface, and c) the impact dynamics of the spray droplets was altered.

Sinha et al.[79] studied the effect of surface roughness on the minimum film boiling temperature (in this work: rewetting temperature). A cylindrical fuel-rod simulator (FRS) was heated up in an electrical furnace with a maximum temperature capability of

1,200 °C. A profilometer was used to determine the root-mean-square (RMS) roughness levels. The unroughened rod from the manufacturer with RMS of 1.27 μm was compared with the rods polished by 80-grit sandpaper (3.81 μm) and 40-grit sandpaper (6.604 μm). The results showed that the influence of the roughness is significant. With increasing surface roughness, the minimum film boiling point is shifted from 420 °C to 520 (3.81 μm) and 560 °C (6.604 μm), respectively. Meanwhile, the maximum heat flux doubled when the surface roughness increased from 1.27 μm to 6.604 μm. The influence of roughness on fully developed film boiling was small, because the thickness of vapor layer were typically larger that the height of rough elements on the surface.

The influence of artificially structured surfaces such as cubic pin fins, pyramids, and straight fins on the heat transfer has been studied by Silk et al. [80, 81]. In addition, a plain surface is used as reference. It should be emphasized that, unlike micro coatings, the characteristic dimensions of these structures are much larger than the liquid film thickness. The coolant used was a fully fluorinated liquid, 3M™ Performance Fluid PF-5060, with a boiling point of 56 °C. The initial temperatures were between 20 and 70 °C. A copper surface of 2×2 cm^2 was cooled with a spray nozzle at a spray flux of 0,016m^3/m^2s. The distance of the nozzle to the copper surface was 17 mm. However, the investigations are interesting in that one can transfer the principle of the production of artificial surface structures to experiments with mold jets and spray nozzles in water cooling. Maximum heat flux for the four surfaces are 114, 105, 126, and 80 W/cm^2, respectively.

Sodtke and Stephan [82] used high-speed infrared camera to study the water spray cooling for both smooth and micro-structured surfaces, the latter featuring micro pyramid with various heights. The spray flux is altering by changing the nozzle-to-plate spacing. It was found out that a great improvement in cooling performance can be obtained with micro-structured surfaces, attributed to the increasing length of the three-phase contact line.

The studies on the spray cooling of the aluminum alloy AA6082 is done by Xu et al. [83]. Three samples with roughness of R_a = 0.6 / 7.6 / 40.2 μm were investigated and compared. A surface with R_a = 0.6 μm can be classified as technically smooth, with R_a =40.2 μm as very rough. It was reported, the surface roughness has a significant influence on heat flux in the nucleate boiling regime; however, its influence is small in the transition boiling regime which is shown in **Figure 4.1**. The authors thought that, the thickness of the intermittent vapor blanket in transient boiling regime is typically greater than any surface rough elements, which leads to the non-sensitivity of heat flux to the micro-surface geometry.

The influence of surface roughness in the spray cooling of a stainless steel cylinder is studied by Aamir et al. [84]. Two cylinders made of stainless steel were used, one with pyramidal pin fins and other with smooth surface as a reference, to explore heat transfer performance under different spray conditions and surface

temperatures. A spray nozzle with pressures of 4 to 13 bar and the corresponding mass flow rate of 13.5 to 23 kg/min was used. Based on the diameter of 25 mm, the average spray flux in the experiments is from 460 to 780 kg/m²s which indicates the used spray nozzle as a cooling-intensive nozzle. It was found out that, structured surface performed better at an initial temperature of 900 °C with a increment in surface heat flux by factor of 1.9, 1.56, 1.66 and 1.74 for inlet pressure of 0.4, 0.7, 1.0 and 1.3 MPa, respectively, which is illustrated **Figure 4.2**.

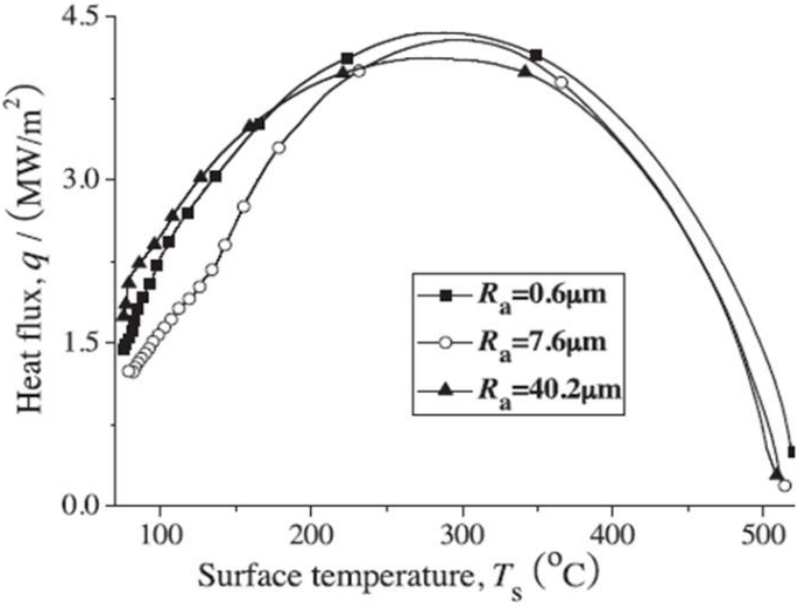

Figure 4.1: Effect of surface roughness on boiling curves (adapted from[83])

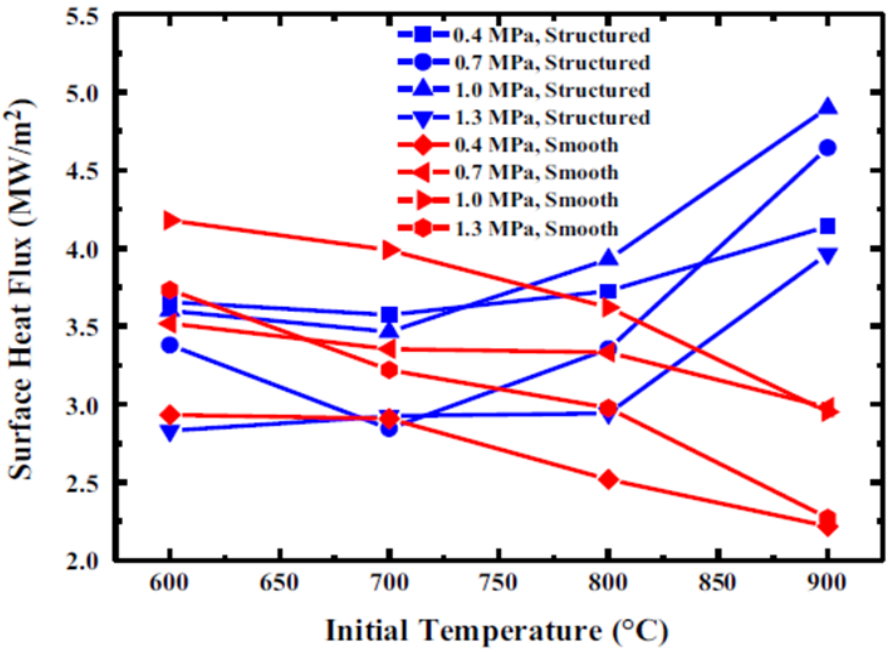

Figure 4.2: A typical boiling curve with distinct boiling regimes (adapted from [84])

According to the literatures, the influence of surface roughness on the cooling process shows the following tendencies:

- Investigations into the influence of roughness were mainly conducted for full cone nozzles.
- Small roughness does not seem to exert any significant effect in using full cone nozzles. On the other hand, investigations of real continuous casting surfaces with large roughness will be conducted in this research.
- Investigations of the influence of roughness in full jet nozzles and mold are not well categorized.
- The experiments took place without movement of the metal samples. In continuous casting, however, there is a relative movement between strand and nozzle field, resulting in a different propagation of the wetting front.

4.2.2 Characteristics of surface roughness

The surface roughness of the utilized samples was measured according to DIN EN ISO 4288 at the Institute of Production Technology and Quality Management (IFQ) at the University of Magdeburg. A stylus-type surface roughness measuring instrument was used. The arithmetic mean roughness R_a, the maximum valley depth R_v, the maximum height of the profile R_t, the average distance between the highest peak and lowest valley in each sampling length R_z and the maximum single roughness R_{max} were determined.

R_a is the arithmetic average value of filtered roughness profile determined from the deviations about the center line which is shown in **Figure 4.3**. Thus, the value is always greater than zero and only allows a statement about the absolute deviation of the height from the mean value. A statement about the distribution of the height values over the surface is not possible. According to paperback “Dubbel” [85] surfaces with an arithmetic mean roughness below 0.1 µm are classified as very smooth and those over 25 µm as very rough.

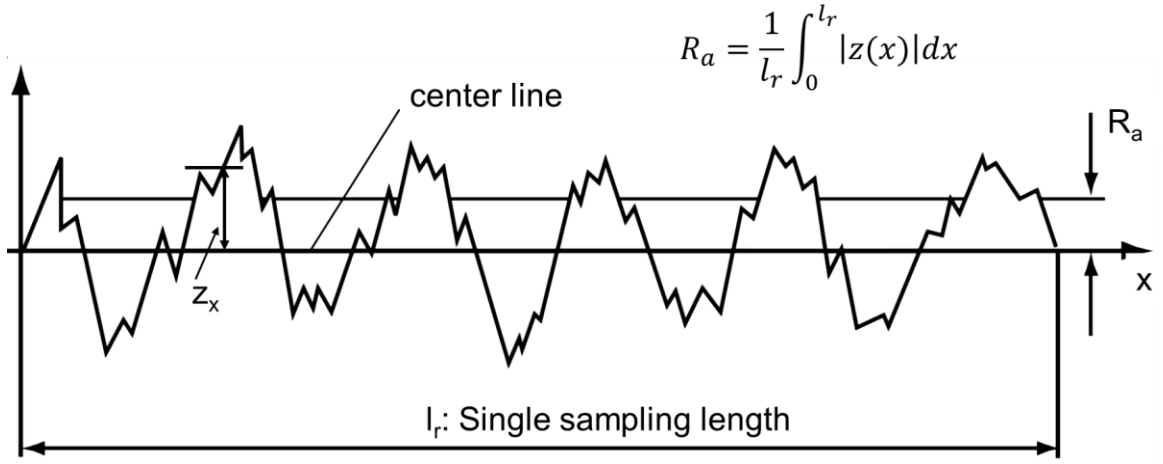

Figure 4.3: Arithmetic mean roughness R_a (adapted from [86])

In order to determine the roughness parameters, the evaluation length is divided into 5 individual sampling lengths, seen in **Figure 4.6** and also the characteristic parameters are listed in **Table 4.1**.

Table 4.1: Summary of roughness parameters

R_t – total height of the roughness profile	Difference between height of the highest peak and depth of the deepest valley within the evaluation length l_n
$R_{z,i}$ – greatest height of the roughness profile	Sum of the height of the highest profile peak and the depth of the deepest profile valley, relative to the mean line, within a sampling length $l_{r,i}$
R_z – mean roughness depth	Mean value of the five $R_{z,i}$ values from the five sampling lengths $l_{r,i}$ within the evaluation length l_n
R_{max} – maximum roughness depth	Largest of the five $R_{z,i}$ values from the five sampling lengths $l_{r,i}$ within the evaluation length l_n

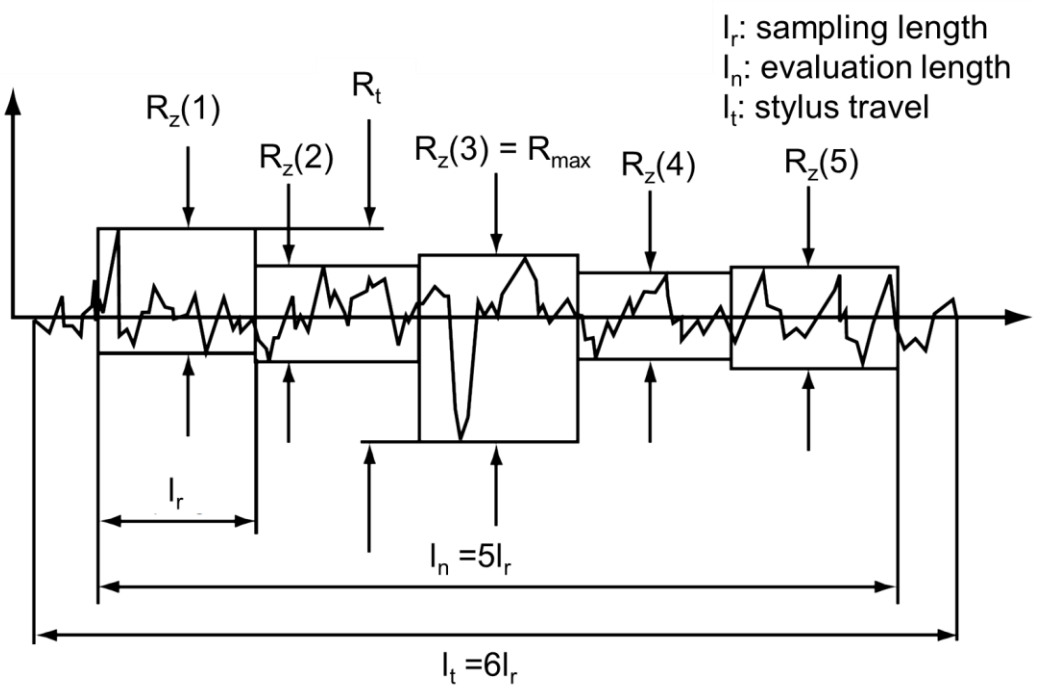

Figure 4.4: Characteristics of roughness over evaluation length(adapted from [86])

4.2.3 Investigated rough surfaces

In order to study the influence of roughness of industrial casting surfaces during cooling, different metal and alloy types have been utilized in this research. For this purpose, sample plates with dimensions of 200 mm x 230 mm and a thickness of 5 to 20 mm were cut out of industrial ingots. The principle of sample extraction from ingots of aluminum alloys is shown in **Figure 4.6**, which is quite similar for copper alloys. The surface should under no circumstances be damaged. Based on visual observation, the

casting direction can be directly recognized and the roughness in the casting direction is less than that in the transverse direction which will be documented in the following sections.

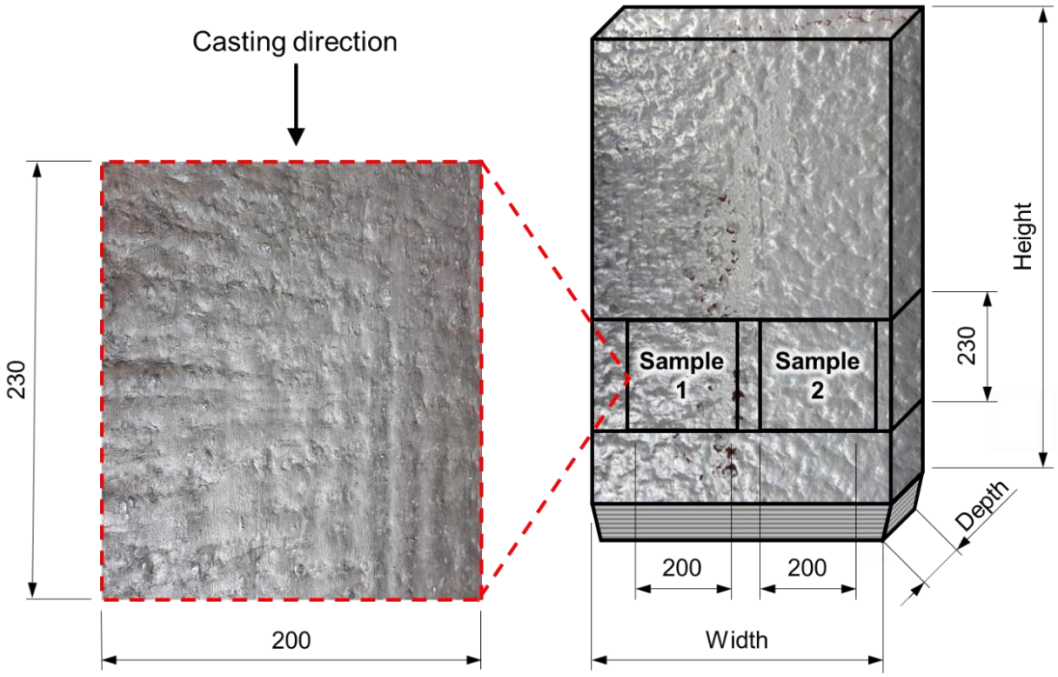

Figure 4.5: Schematics of aluminum alloy samples cut from industrial ingots

The aluminum alloys AA 6082, AA 5083 and AA 7050 as well as the copper alloys CuSn4, CuFe2P, CuNi3Si and CuCrZr were used to measure the surface roughness; however, not all the alloys have been used to investigate the heat transfer. Typical roughness parameters were determined. Additionally, roughness characteristics of smooth surfaces of aluminum and copper alloys were also determined.

On each metal sample, the roughness was usually determined on six measuring lines: three in casting direction, three perpendicular to the casting direction, as schematically shown in **Figure 4.6**. The respective measuring values for aluminum alloys and copper alloys are shown in **Figure 4.8**.

The arithmetic mean roughness R_a and also the maximum depth of the entire roughness R_{max} will be also included. The results of the measurements of all roughness characteristics are tabulated in Appendix A – Surface roughness measurement for aluminum and copper alloys with respect to the casting technology.

The roughness values R_a and R_{max} in and perpendicular to casting direction do not differ greatly for aluminum alloys; but do for copper alloys. The maximum roughness depth R_{max} is approximately 6 to 10 times higher than the arithmetic mean roughness R_a due to the definition. Taking aluminum alloys as example, a clear tendency arises when the casting method is considered. Surfaces produced by electro-magnetic-casting (EMC) shows the lowest R_a value of 2 µm. The R_a values are highest for conventional direct chill casting (DC) with 46 and 72 µm. According to Dubbel [85], surfaces with Ra>25 µm are classified as very rough in mechanical engineering.

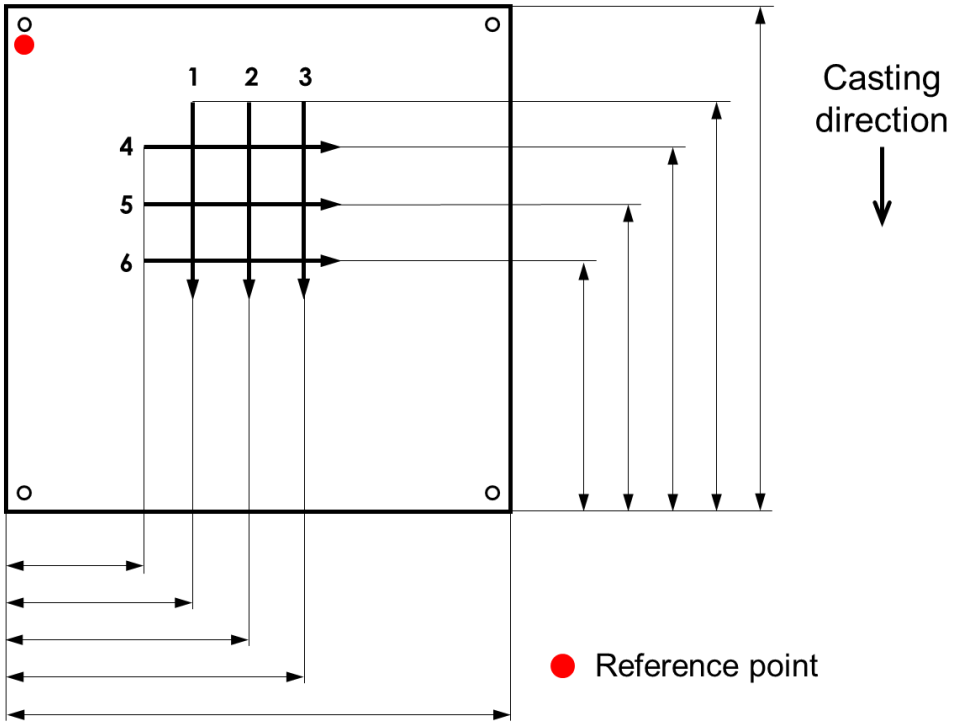

Figure 4.6: Schematics of measurement lines on the metal surface

In order to compare the cooling effect on real rough surfaces with smooth surfaces, smooth samples of copper and aluminum alloys were produced through milling in our own lab, originating from the same batch of material. The production ensures that the smooth sample has the similar specific mass in g/unit area as the rough surface. **Figure 4.8** shows the produced samples and the determined roughness parameters. Generally, depending on the alloy and surface treatment, the produced smooth surfaces for the cooling tests have R_a values between 1 and 4 µm. The arithmetic mean roughness R_a of the smooth surface of the copper alloys produced by milling ranges between 3 and 4 µm, while the aluminum alloy AA5083 from EMC continuous casting reached a value of 1 µm. The measured R_a values of 0.3 µm is found for purchased smooth samples of AA6082.

An example of the roughness profiles of copper alloys CuCrZr is shown in **Figure 4.9**. It should be noted that, the stylus travel for smooth surface is only 12 mm, while for rough surface it is 48 mm; because the sampling length for smoother surface will be selected as shorter during the measurement according to DIN EN ISO 4288. The difference between real casting surfaces and smooth surfaces produced by surface treatment can be clearly seen. The arithmetic mean roughness of the machined surfaces of the copper alloy CuCrZr is 2.5 µm which is classified as technically smooth in this research. In conclusion, all surfaces are classified as follows; this will lead to a better understanding when comparisons are made.

Ra <= 5 µm: smooth surface

Ra> 5 µm to 25 µm: rough surface

Ra> 25 µm: very rough surface

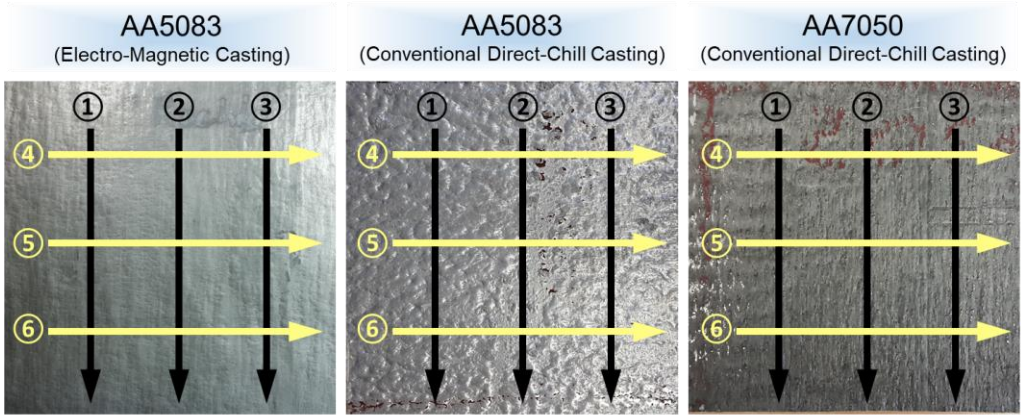

		AA5083 (EMC)	AA5083 * (DC)	AA7050 (DC)
In casting direction (Linie 1-3)	R_a [µm]	2	46	72
	$R_{z,max}$ [µm]	19	333	529
Perpendicular to casting direction (Linie 4-6)	R_a [µm]	3	44	60
	$R_{z,max}$ [µm]	21	300	582

* Experiments performed

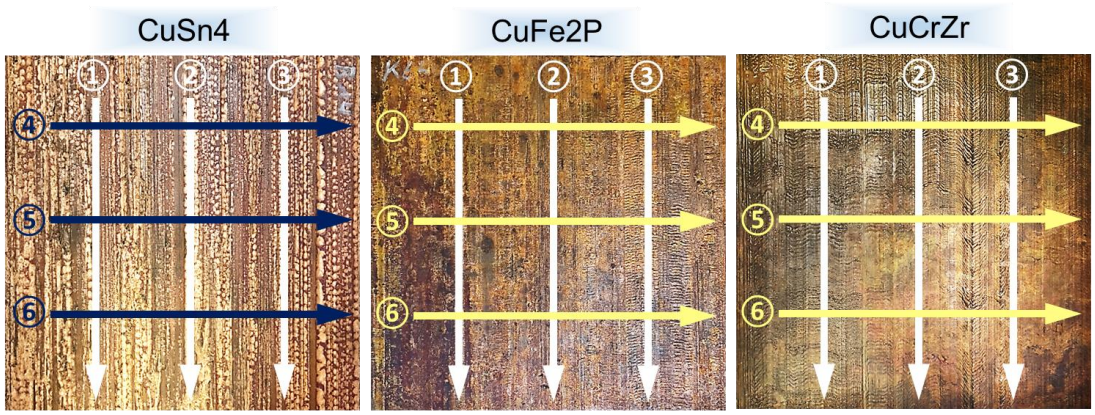

		CuSn4 *	CuFe2P	CuCrZr *
In casting direction (Linie 1-3)	R_a [µm]	15	26	43
	R_{max} [µm]	97	146	274
Perpendicular to casting direction (Linie 4-6)	R_a [µm]	95	43	34
	R_{max} [µm]	412	235	250

* Experiments performed

Figure 4.7: Investigated rough surfaces from industrial suppliers

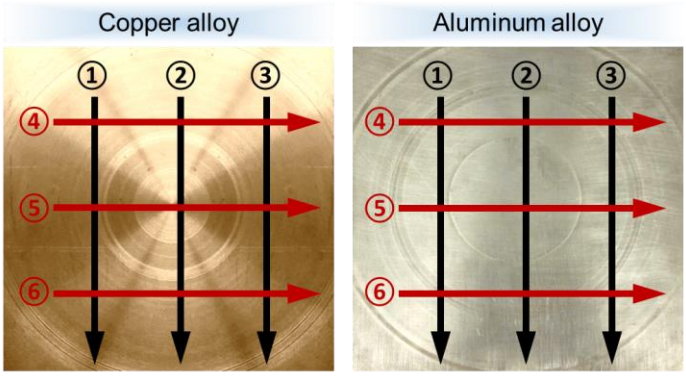

		CuSn4 (DC, through milling)	CuCrZr (DC, through milling)	AA5083 (EMC, through milling)
Mean value for 6 lines	R_a [µm]	4	3	1
	R_{max} [µm]	17	19	6

Figure 4.8: The smooth surfaces produced through milling

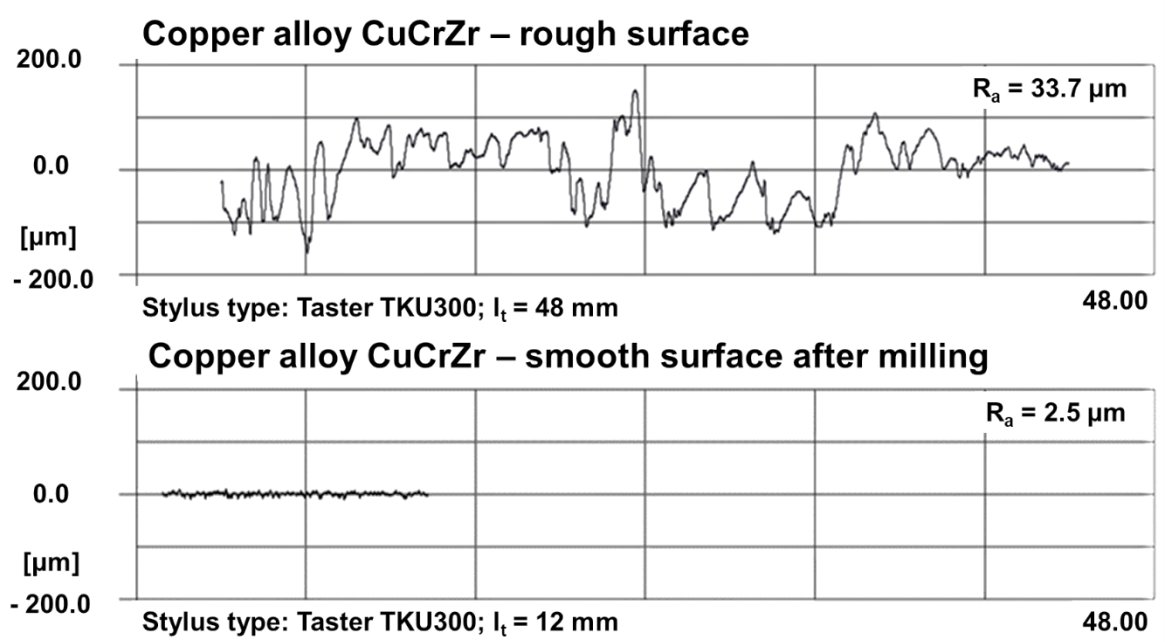

Figure 4.9: Filtered surface roughness profile for rough(original) and smooth(machined) surfaces of copper ally CuCrZr

Similar to the experimental investigation of Silk et al. [80], a surface with cubic pin fins is also produced in our lab, which is shown in **Figure 4.10**. The produced surface cubic pins have the base area of 2 mm x 2 mm and a height of 1 mm, whose center distance is 4 mm. If a center line is places on the pit of the structure, the resulted mean roughness value of R_a is 500 µm. Due to the uniformity of the structure, the maximum roughness R_{max} is identical to the values of the average roughness R_a. The plate thus produced serves as reference which has the highest roughness of a surface. A comparison with real casting surfaces should help to quantify the influence of roughness.

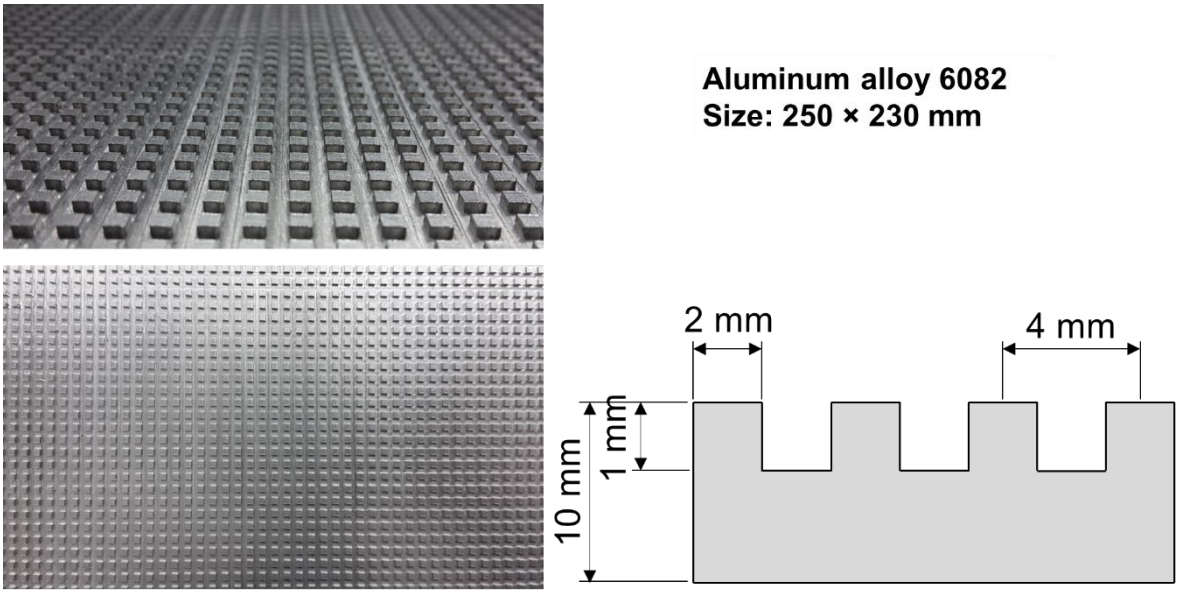

Figure 4.10: Produced artificial surfaces with cubic pin structure

A surface enlargement is first considered. Therefore, the influence of the surface enlargement should be separated from the influence of the roughness, in order to derive reliable information on the cooling process. The factor of the surface enlargement is denoted by f, which has a value of 1.5 in this case. This means that the surface of the artificial structure increases by 50 %. This should be taken into account when evaluating the experiments. For real casting surfaces, no reliable evaluation method on the factor of surface enlargement could be found.

4.3 Investigation with full cone nozzle

4.3.1 Preparation of the experiments

This subsection deals with the effect of surface roughness on the cooling behavior when a spray nozzle is utilized. In the previous descriptions, a vapor layer can easily be built up between the hot surface and impinging droplets for a spray nozzle, which is designated as film boiling region.

Three material groups are investigated: AA 6082 (cubic pin structures and purchased smooth surface); AA 5083 (industrial original surface and smooth surface after milling) and CuSn4 (industrial original surface and smooth surface after milling). They were shown in Figure 4.7, Figure 4.8 and Figure 4.10 to give a better visual impression, and the corresponding R_a values are also provided.

The used spray nozzle has a cone angle of 60°, and the volume flow rate is selected as 1.2 l/min which corresponds to a pressure of 3 bar.

4.3.2 Repeatability of the experiments with full cone nozzle

The experiments have been done to examine the repeatability of the experiments; since the amount of metal samples are limited. Some samples have to be used several times before disposed.

Figure 4.11 shows the video and infrared images for repeated cooling cycles of a smooth surface of AA 6082 after a cooling time of 9 seconds. Initially, the plate is brand new before heating in the furnace. The first cooling indicates the first subsequent cooling of this brand new sample. The second cooling denotes the second cooling cycle with same sample after a second heating without any surface treatment. The same meaning stands for the third cooling. After a cooling time of 9 seconds, no formation of wetted region can be observed in the first cooling which indicates the existence of the film boiling. At the same time, wetting and the formation of a wetted regions can be obtained in the second and third cooling cycle. Through the visual observation, the wetting front have progressed even further in the third cycle than the second. Same as the video recordings, the infrared recordings at the same cooling time also provides a qualitative analysis which demonstrates clearly that the cooling time shortens as the number of cooling cycle increases.

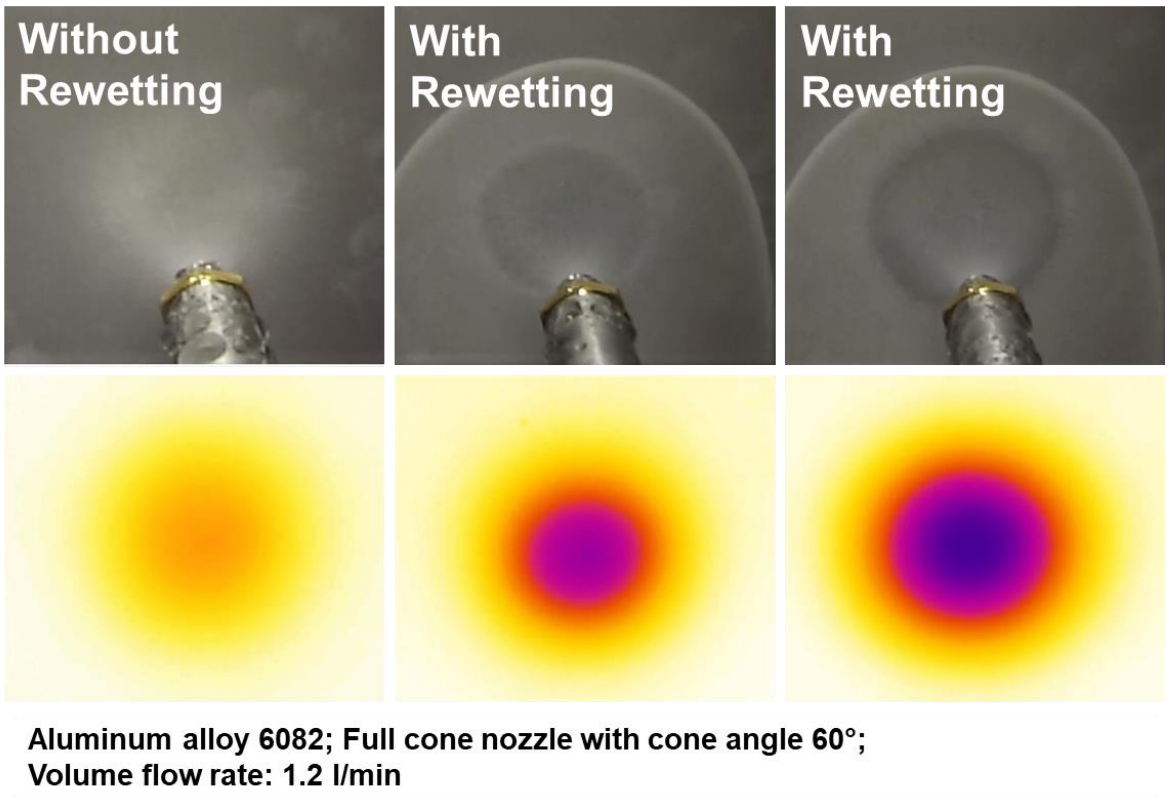

Figure 4.11: Visual representation of repeated cooling cycles with video and infrared images at a certain cooling time of 9 seconds

Additionally, the temperatures curves at two radii for repeated cooling cycles are depicted in **Figure *4.12***. It can be seen that cooling rate becomes faster with increasing the cycle numbers. The film boiling takes place for approx. 16 seconds for the first cycle, reduced to 8.5 seconds in the second, followed by around 5 seconds in the third cycle. It is hypothesized that the surface conditions have been modified during the repeated cooling cycles by salt deposition in the white bear-belly form which can be again found in the video images as shown in Figure 4.11. Cui et al. [87] have studied the effects of dissolving gas and salts on heat transfer during droplet cooling. It was

reported that the dissolved salts improve heat transfer when the surface temperature is above rewetting temperature due to the promotion of bubble formation by the salt concentrations. The similar tendency have been found in current research. A longer film boiling favors the salt deposition which will in turn leads to a faster cooling in the next repeated cycle. A direct verification of the hypothesis can be done by the surface structure examination by scanning electron microscope (SEM). Unfortunately, that was not done in the current research; however an indirect method has been used to strengthen the proposed statement.

After the third cooling, the surface on the quenching side was treated with emery paper carefully to remove the visible salt depositions. Meanwhile, the surface should be maintained as smooth as possible which avoids the influence of increased surface roughness by the manual treatment. Subsequently, another three cooling cycles were conducted which are denoted as 4^{th}, 5^{th} and 6^{th} cooling cycles. The temperature profiles were then compared with previous cooling cycles on untreated surfaces; namely; 1^{st} vs. 4^{th}, 2^{nd} vs. 5^{th} and 3^{rd} vs. 6^{th}. The comparisons are depicted in **Figure 4.13**. It can be clearly observed that the cooling behavior can be well reproduced after a cautious treatment of the deposited salts. Furthermore, experiments with distilled water were carried out under the same experimental conditions. The results are shown in **Figure 4.14**. The repetition of the experiments with the same metal sample shows no significant effect on the cooling time reduction. Through aforementioned experiments, the assumption of influence of salt deposition on cooling performance with full cone nozzle is indirectly validated.

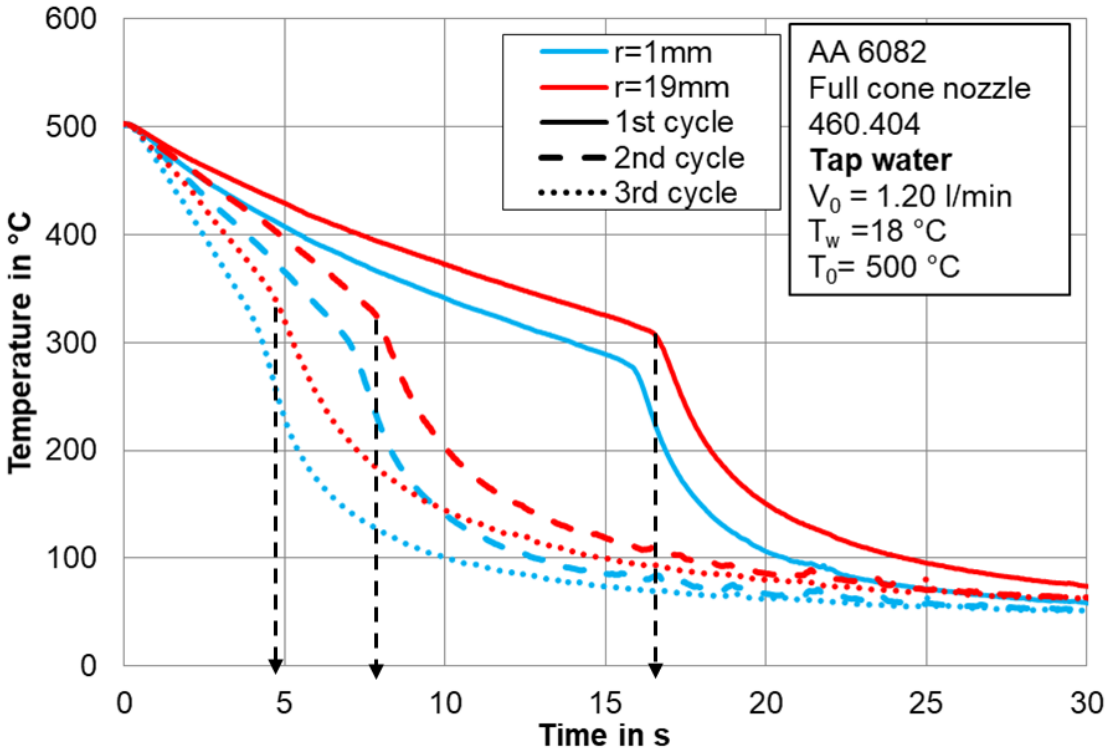

Figure 4.12: Temperature curves for repeated cooling cycles with local tap water

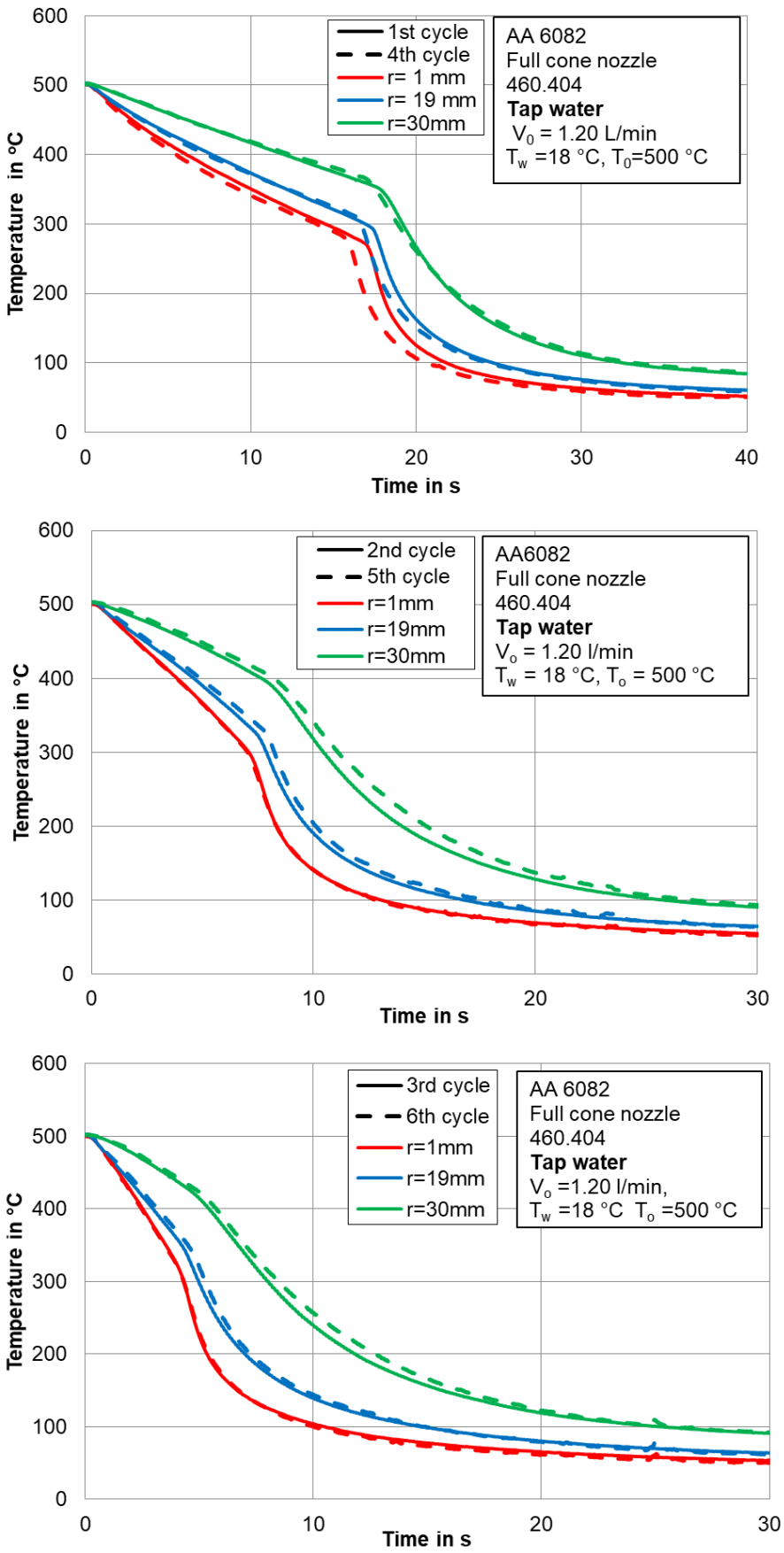

Figure 4.13: Comparisons of temperature curves before and after surface treatment with emery paper

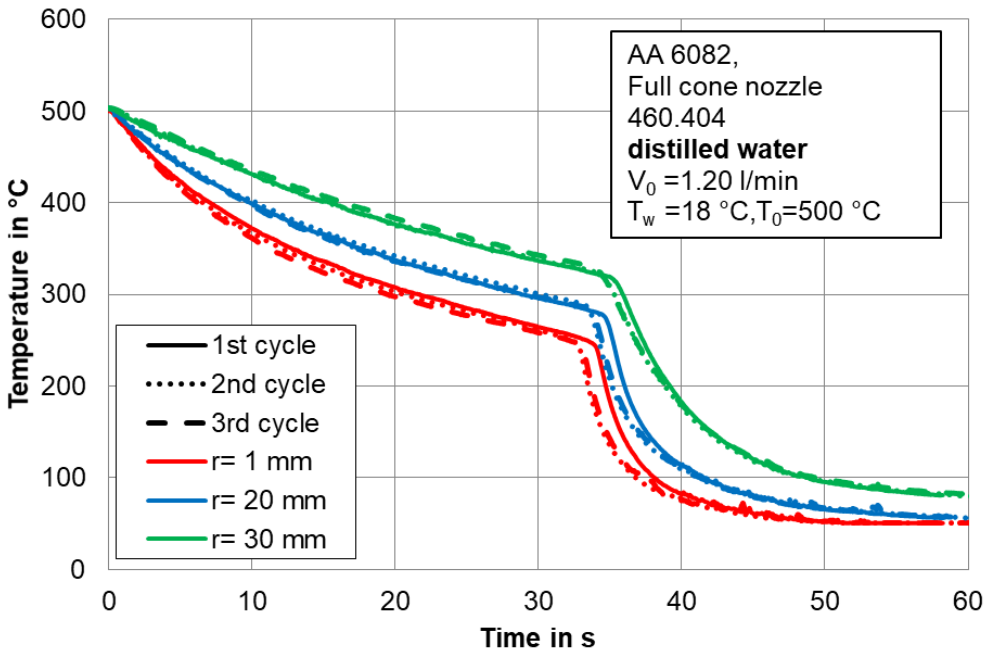

Figure 4.14: Repeated cooling cycles with distilled water

The influence of repeated cooling cycles with tap water occurs similarly in the experiments of aluminum alloy AA5083, which is shown in **Figure 4.15** for two cycles at radii r = 1/10/20 mm, respectively. Together with findings obtained for AA 6082 results in the necessity of the removal of the salt by careful surface treatment, if cross comparisons need to be made. However, this does not apply to full jet nozzles and mold as will be shown in subsequent subsections.

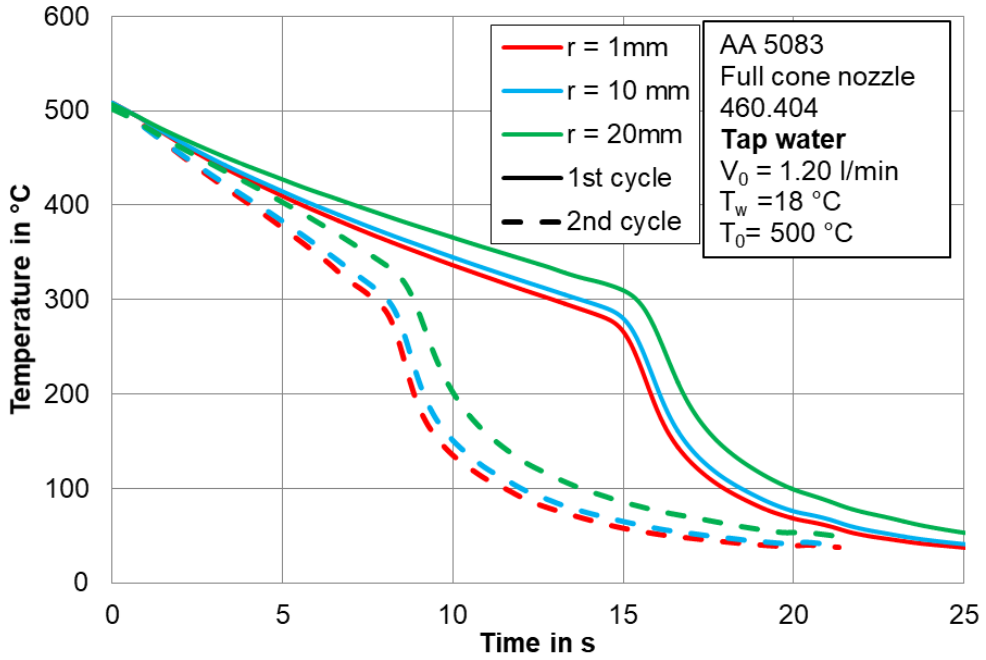

Figure 4.15: Repeated cooling cycles with local tap water for AA 5083

4.3.3 Effect of surface roughness with full cone nozzle

As shown in the previous chapter, the increasing repeated cooling cycles will enhance the cooling rate by depositing the salt on the surface which will inevitably change the surface conditions. However, all the experiments were done based on the smooth surface. In this section, a direct comparison of cooling behavior on both smooth and rough surfaces for various metal alloys is carried out.

Figure 4.16 exhibits the influence of roughness on temperature curves at different radii for aluminum alloy AA5083 with a spray nozzle. It is worth noting that the arithmetic roughness value R_a in the casting direction is given in the figure, since the temperature values are extracted in the casting direction. The temperature deviates not so much at different radii which is in accordance with the spray flux distribution as shown in Figure 3.4. On the other hand, the cooling rate increases dramatically with an increase of the arithmetic mean roughness R_a from 0.7 to 46.2 µm. Based on a cooling end temperature of 100 °C, the cooling time is reduced from approx. 20 to approx. 10 seconds. These significant reductions in cooling time are also consistent with Abdalrahman's investigations [53], but the spray flux in his experiments was 3 kg/m²s and deionized water was used which led to a longer cooling time.

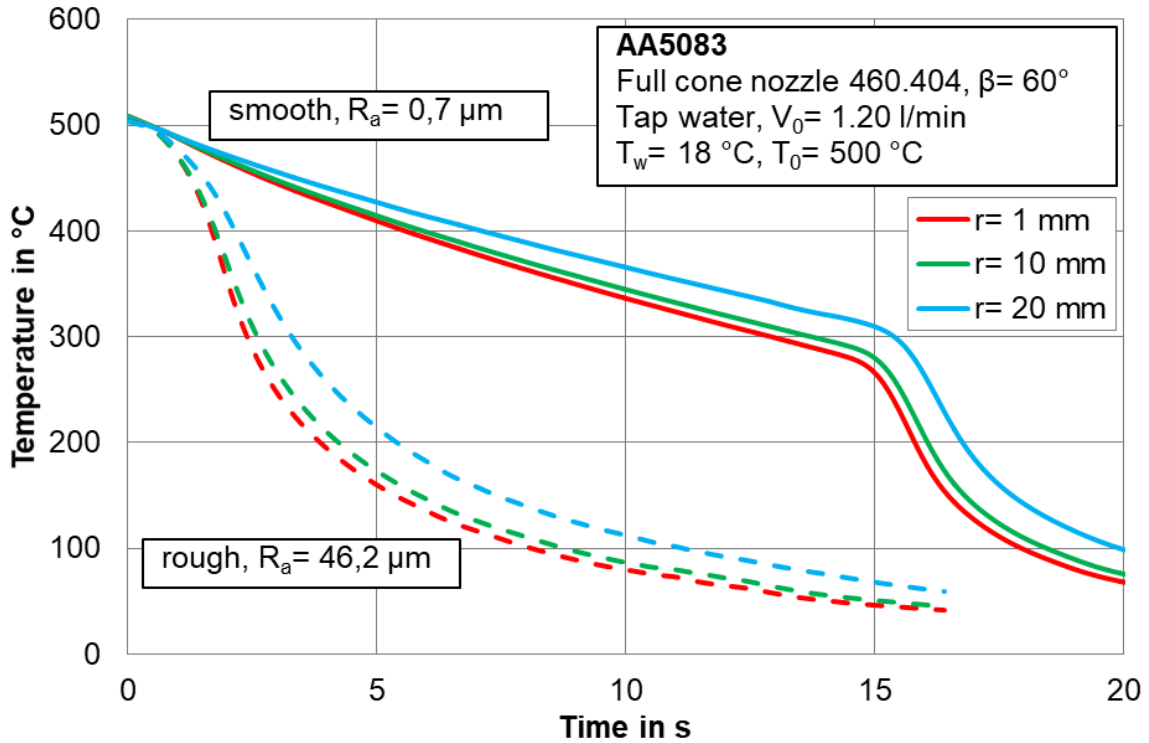

Figure 4.16: Effect of surface roughness with full cone nozzle for AA 5083

Meanwhile, it seems no apparent film boiling region can be observed for rough surface of AA 5083, which can be further evidenced in the boiling curves as shown in **Figure 4.17**. The heat flux increases dramatically when the cooling is initiated for the rough surfaces which indicates an immediate rewetting once the whole spray impacts

the hot surface, resulting a shorter transition boiling region, higher rewetting and DNB temperatures and higher heat transfer rate. One explanation could be that these rough elements acted as micro structures and enhanced the heat transfer rate from the vapor to the bulk liquid. If the transition boiling region is assumed as combination of transition and nucleate boiling, then it is also possible that the surface roughness increases nucleation site density at a given surface temperature in transition boiling which shortens its period.

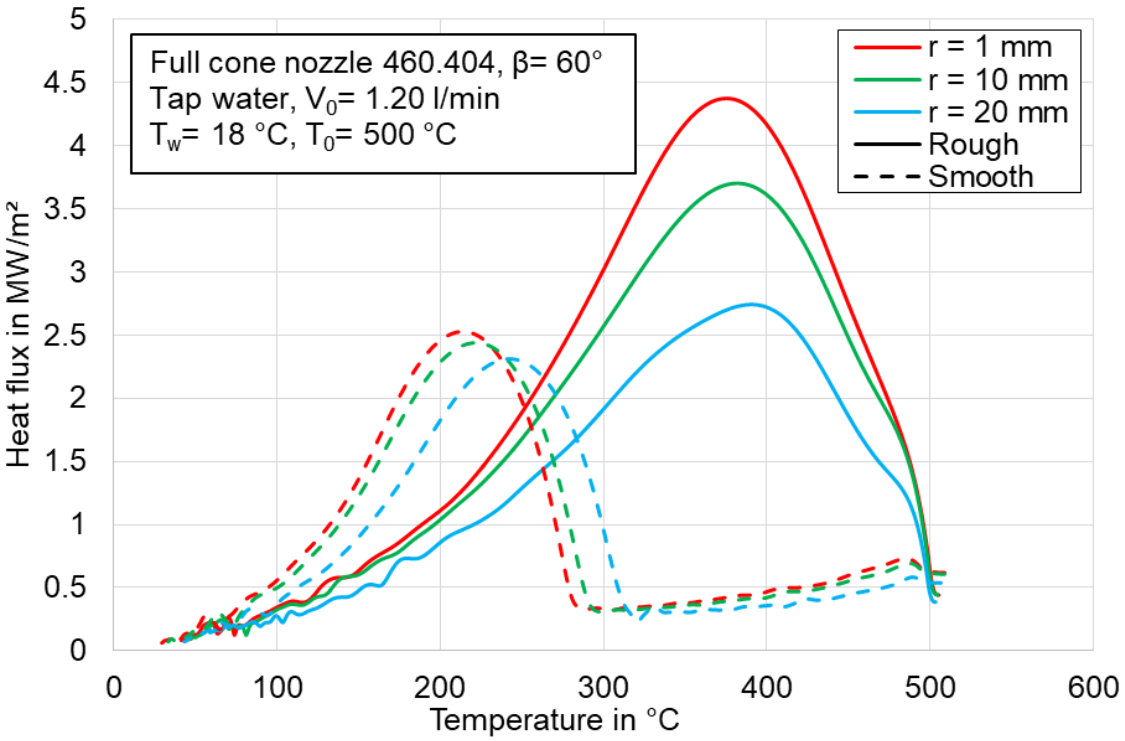

Figure 4.17: Effect of surface roughness on boiling curves with full cone nozzle for AA 5083

The maximum heat flux for rough surface is around 4.5 MW/m² at radius of 1 mm, whereas the maximum value for smooth surface is only 2.5 MW/m². This suggests clearly that increasing surface roughness helps to enhance the cooling efficiency by using a full cone nozzle.

The similar effect of surface roughness on the cooling performance can be found for CuSn4, as shown in **Figure 4.18**. The arithmetic average roughness R_a in casting direction for CuSn4 is approx. 15 µm. Generally, the rough surface is cooled faster than the smooth surface; however, the cooling time reduction is not as great as that in aluminum alloy AA 5083. One fact is that the roughness level on quenching surface is not comparative with that of AA 5083. Another fact is the severe oxidation on the quenching surface of CuSn4 which leads to inhomogeneous cooling based on the observation from video camera. Several snapshots are given in **Figure 4.19** to clarify this and also help to explain the temperature inhomogeneity for two radii.

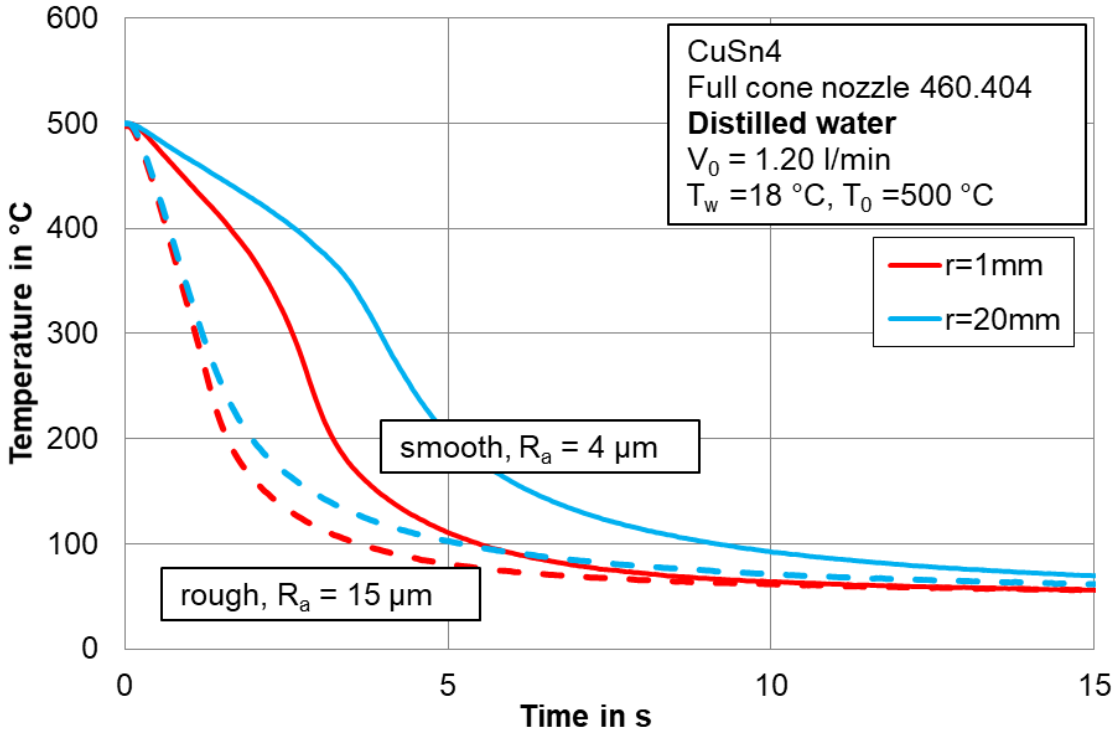

Figure 4.18: Effect of surface roughness with full cone nozzle for CuSn4

Generally, the unheated copper alloy presents a shiny bronze color; after heating in the furnace to around 500 °C, an obvious oxide layer can be found on the quenching side which can also be observed as dark grey in the snapshots. There is no wetting occurring up to three seconds; however the oxide layer is swept away by the impinging spray. The wetting initiates at around 5 seconds which is marked by the red dotted area. The irregularity is clearly shown which is not in agreement with the spray flux distribution. After 8 seconds, the whole impinged area is covered by the spray. As wetting front keeps propagating further, the produced oxide layer keeps being removed as evidenced at 21 seconds. The cooling behavior of the fluid spray on the CuSn4 surface demonstrates clearly the reason of temperature inhomogeneity, since a higher heat transfer rate can be only achieved by direct contact between liquid and hot surface. The non-uniform rewetting also results in the temperature deviation at two radii which insights that the homogeneous cooling is strongly determined by the surface conditions. It is not possible to finish the cooling process in an oxygen-free environment in current research, since the heat metal plate needs to be transferred from the furnace to the cooling chamber. However, it is encouraged to finish such experiments to avoid the influence of surface oxidation on the cooling process. One possibility is to scale down the whole testing facility and to merge the heating and cooling in one single unit through induction heating; since the cooling and heating units are separated in current research work.

The similar effect of roughness can be found for CuSn4 surface with tap water as shown in **Figure 4.20**. The other experimental conditions remain the same as for

distilled water. At the center of spray cone, the cooling time reduced from 2.8 s for smooth surface to 1.4 s for rough surface when cooling temperature of 300 °C is under consideration. However, the temperature difference between two types of surface is not as significant as in case of distilled water. The reason is that the salt concentration in the tap water also helps to enhance the heat transfer, thereafter reduces the overall cooling time. The direct comparison between tap and distilled water can be further found in **Figure 4.21**. It stresses again that salinity concentration in the water will change the cooling performance of a full cone nozzle.

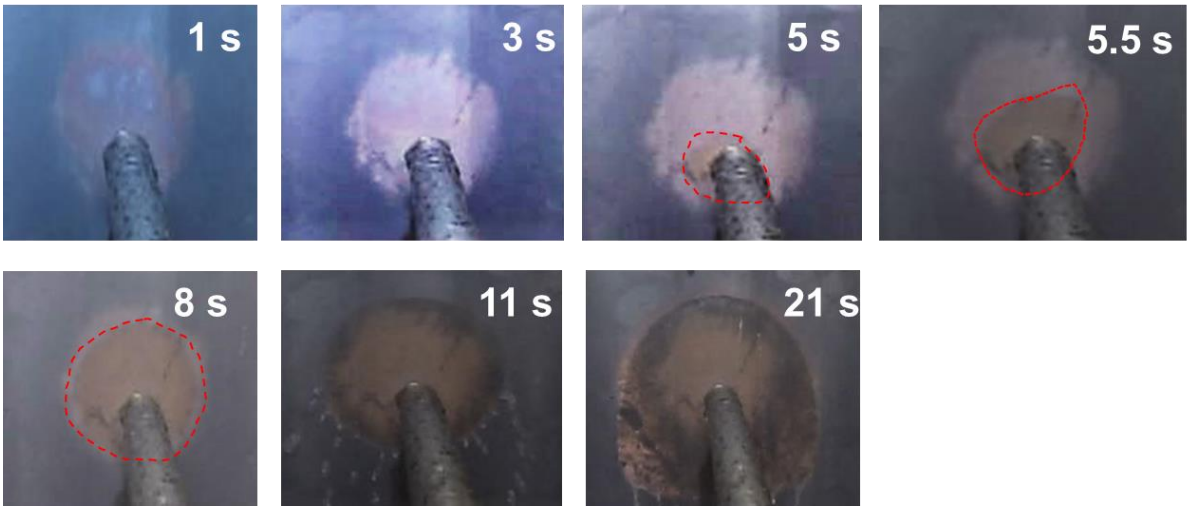

Figure 4.19: Snapshots during quenching of smooth CuSn4

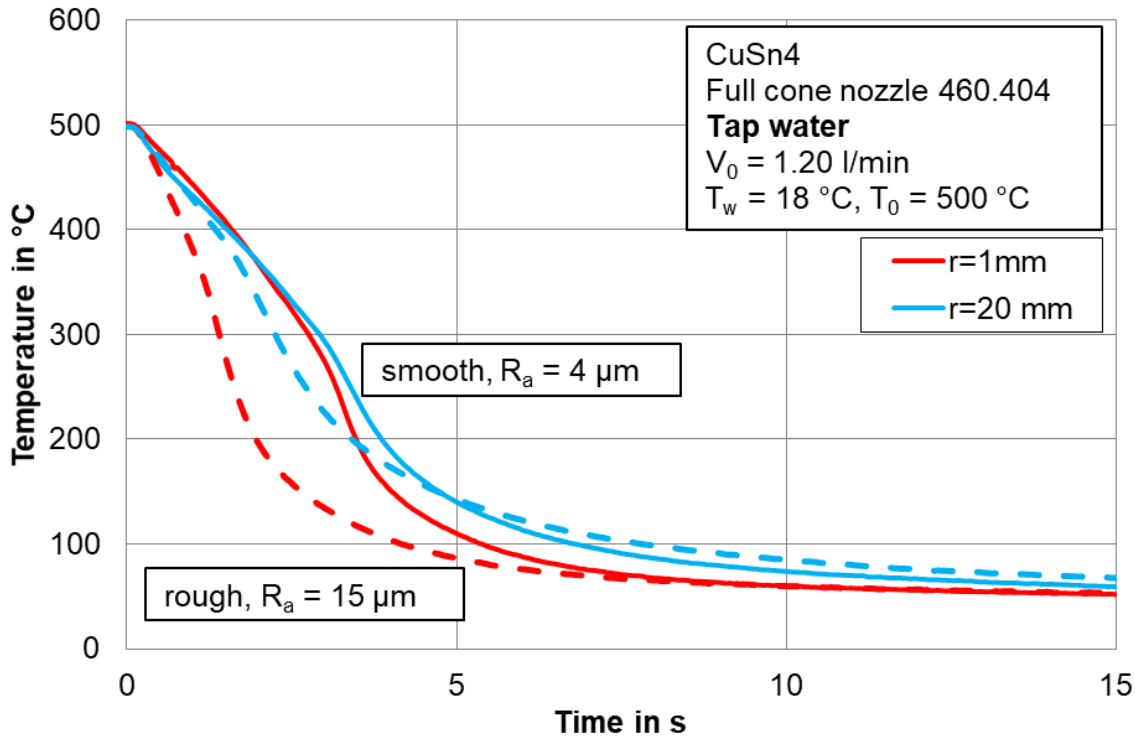

Figure 4.20: Effect of surface roughness on boiling curve with tap water for CuSn4

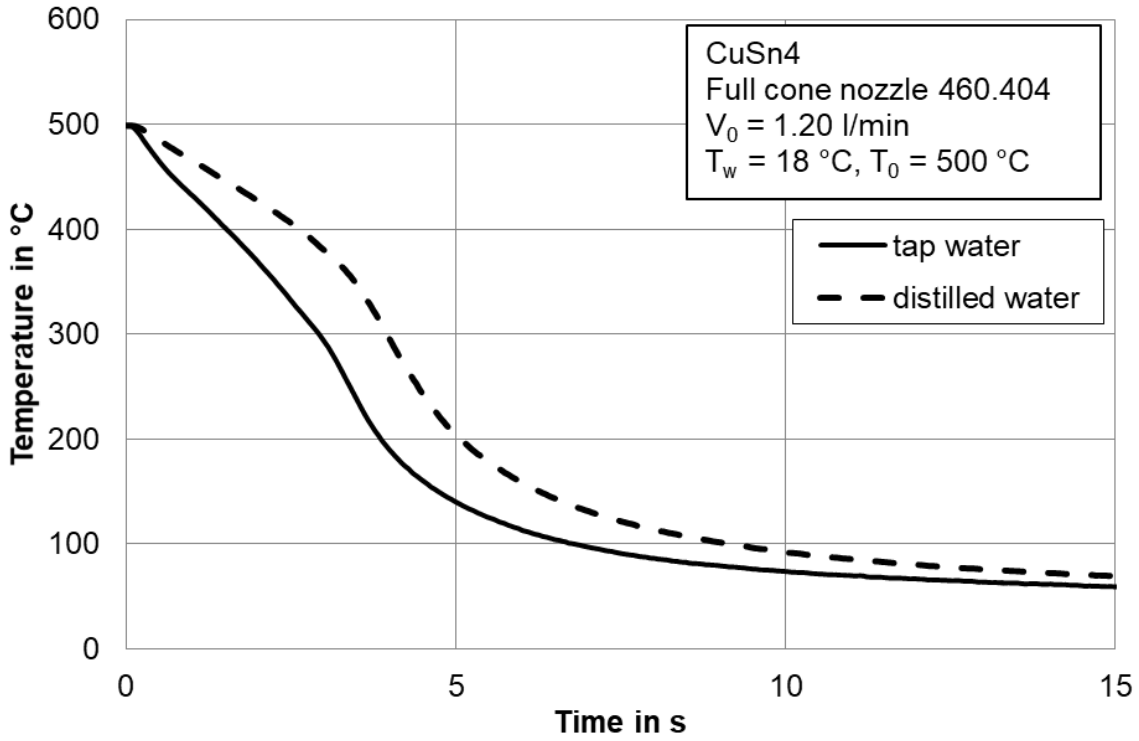

Figure 4.21: Effect of water quality with full cone nozzle

The investigation of artificial surface follows the previous studies. A sample with one-sided artificially structured surface was produced by mechanical processing from the same metal batch of the aluminum alloy AA6082 which were directly bought from the metal dealer. The technical details of the produced surfaces is depicted in Figure 4.10. It is important that both samples have similar mass to obtain comparable results. **Figure 4.22** shows both surfaces of aluminum alloy AA6082.

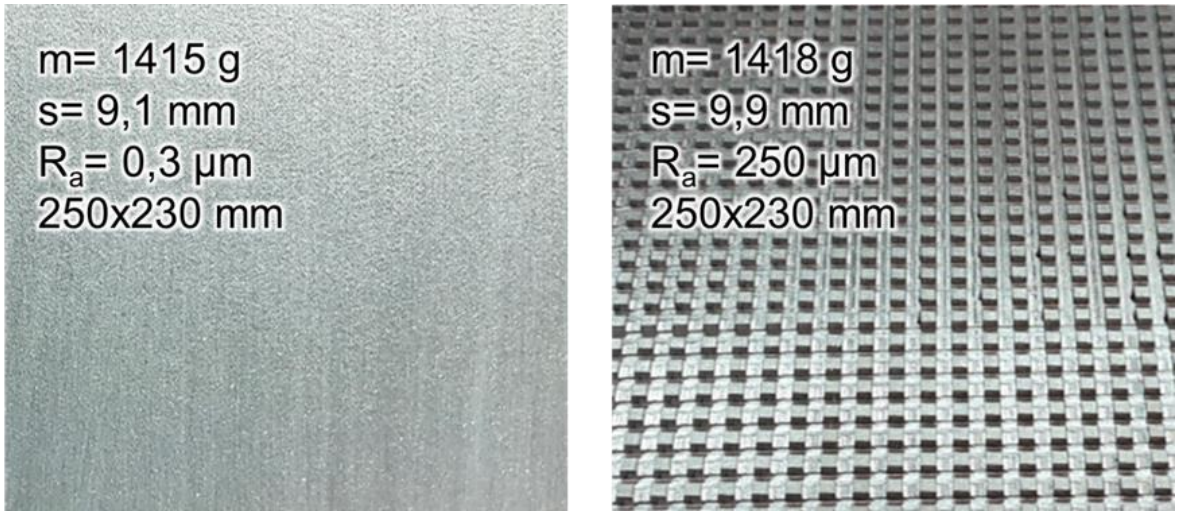

Figure 4.22: Metal samples from AA 6082 for smooth(left) and cubic pin fins(right)

The mass of both sheet samples deviates slightly from each other. The thickness difference of 0.8 mm is to compensate the mass loss in the production of structured

surface. The similar mass ensures that both metal samples have the similar stored thermal energy at the same initial temperature. The arithmetic mean roughness of the smooth sample is measured to be R_a = 0.3 µm; whereas R_a = 250 µm can be evaluated for the artificially structured surface. To measure the temperature histories, the metal samples are painted with a high-temperature thermal coating whose emissivity is determined in the calibration experiments as stated in section 2.12.

The distance from the nozzle outlet to quenching surface is 50 mm which results in an average spray flux of 7.6 kg/m²s, the detailed spray flux distribution can be found in Figure 3.4. In order to minimize the effect of salinity on the cooling performance, distilled water is used with the temperature of 18 °C.

In **Figure 4.23** cooling curves measured for both smooth and artificially structured surface are compared. The smooth surface cooling curves have solid lines while the rough surface cooling curves are in dashed lines. A significant reduction of the cooling time on a rough surface can be recognized which again indicates that the roughness of the surface promotes faster cooling. Typical cooling curves can be observed when film boiling occurs. Initially the temperature decrease approximately linearly in course of cooling until a temperature of about 280 to 300 °C is reached, and then a higher cooling gradients is expected. This transition suggests the transition from film boiling to transition boiling and is shown on the quenching side by the abrupt rewetting of the surface.

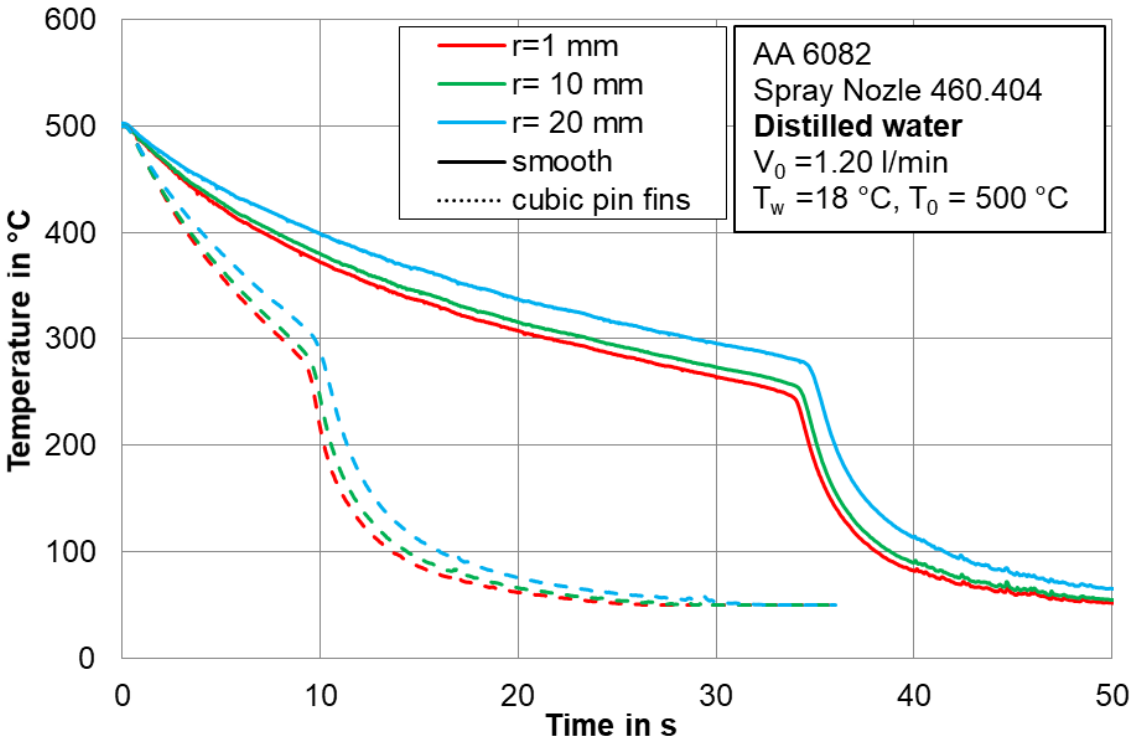

Figure 4.23: Temperature comparison in cooling between smooth and cubic pin fin

It is also worth noting that the rewetting temperatures for smooth surface are slightly lower than structured surface which can also be seen in **Figure 4.24**. The fluctuations of heat flux is caused by the numerical calculations. The rewetting

temperature is approximately 300 °C for surface with cubic pin fins; while for the smooth surface approximately 250 °C. This deviation is mainly contributed by the longer film boiling which will reduce the bulk temperature prior to initiation of rewetting. A considerable difference in the nucleation region cannot be found. Although the entire structured surface can be seen as a surface with R_a = 250 µm. The local roughness on each cubic pin is same as that of smooth surface, resulting in similar nucleation site density. The overall heat transfer efficiency is higher in case of a structured surface. The maximum heat flux increased from 1.6 MW/m² for smooth surface to 2.6 MW/m² for structured surface at the center of spray footprint. This is then mainly attributed to the enlargement of the surface area. Under the same spray impingement, the cooling area increases by 50% for investigated structure which inevitably increases the heat transfer rate. This increment can be further evidenced in the film boiling region. The average heat flux for smooth surface in film boiling region is 0.25 MW/m² and that for structured surface is 0.75 MW/m².

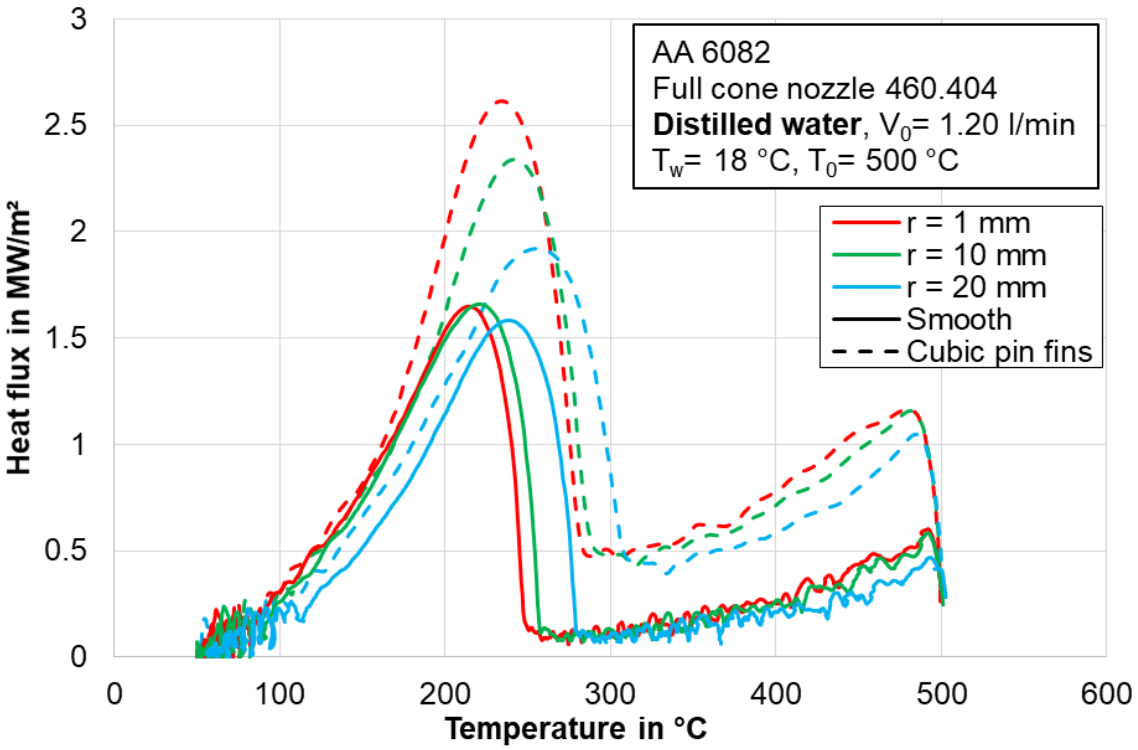

Figure 4.24: Boiling curves for both smooth and structure surfaces(cubic pin fins)

Additionally, the experiments with tap water for both surfaces were also conducted. Since water quality is of great importance during the cyclic cooling; only the first cooling cycle for both surface is compared, as shown in **Figure 4.25**. The corresponding boiling curves are given in **Figure 4.26**. The similar reduction in cooling time for cubic pin surfaces can be found. However, a closer look will reveal that salt concentration in the tap water benefit the cooling even more. Alteration from film boiling to transition boiling takes place at 5 seconds for tap water in case of structured surface, while it is nearly 10 seconds for distilled water. This deviation is contributed by the increased nucleation site density due to salt depositions. Similarly, compared with transition occurring at 17

seconds with tap water for smooth surface, it occurs at 34 seconds with distilled water for smooth surface. Considering the heat flux distribution, similar conclusions can be made. In general, the heat flux is higher for tap water. The described deviation further emphasizes the importance of water quality when a spray nozzle is used during cooling process and also insights its significance in the industrial applications.

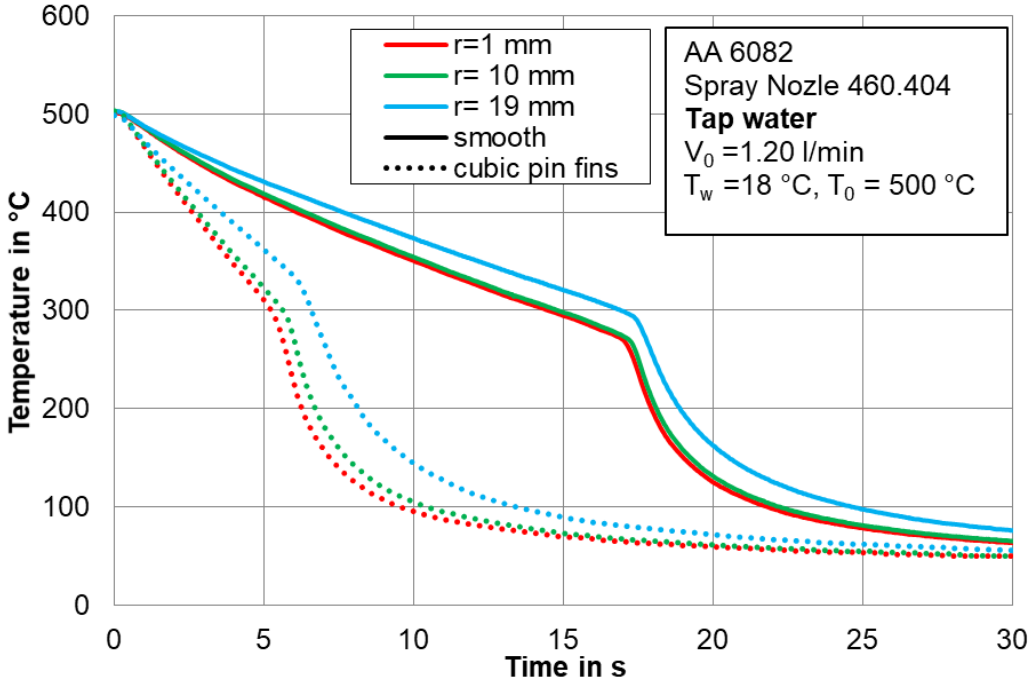

Figure 4.25: Temperatures for smooth and structured surfaces with tap water

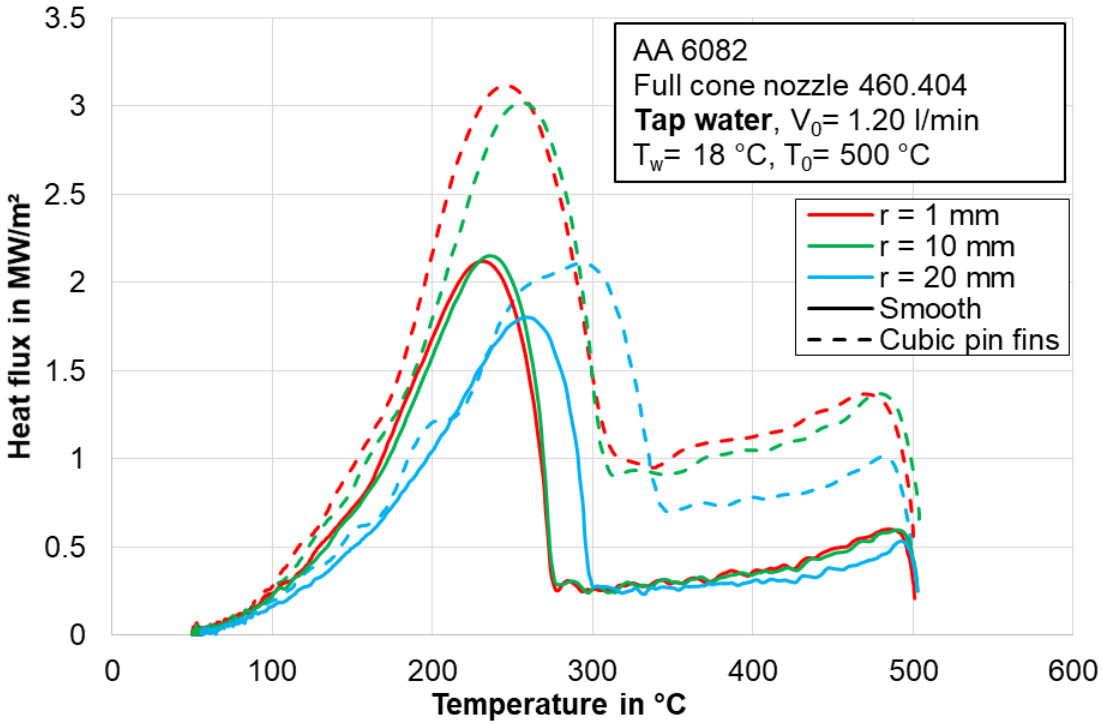

Figure 4.26: Boiling curves for smooth and structured surfaces with tap water

4.4 Investigation with full jet nozzle

4.4.1 Preparation of the experiments

The used full jet nozzle is produced by Lechler® with serial number of 544.400. It has an orifice of 1.3 mm. The jet velocity is calculated as 15 m/s when the volume flow rate is measured as 1.2 l/min and the corresponding nozzle Reynolds number is 1.94×10^4. The selected volume flow rate of 1.2 l/min allows a further comparison with the full cone nozzle. The used metal samples are given in section 4.3.1.

4.4.2 Repeatability of the experiments with full jet nozzle

As discussed in the experiments with full cone nozzle, the water quality makes a major difference during the repeated cooling cycles. Hence, it is also necessary to verify if the same phenomenon exists for full jet nozzle.

Figure 4.27 and **Figure 4.28** present the two cooling cycles for both distilled and tap water with full jet nozzles. The initial temperature of the experiment is 500 °C. All the other experimental conditions are listed in the information box. It clearly shows that repeated cooling cycles exert no fundamental influence on the cooling performance for both distilled and tap water. During the experiments, no consideration has to be taken for the selection of cooling cycles with full jet nozzle. The similar result can be found in the cooling process on AA 6082 which is shown in **Figure 4.29**.

It is also interesting to understand if the water quality has influence on cooling temperature curves when a full jet nozzle is applied. This is shown in **Figure 4.30**.

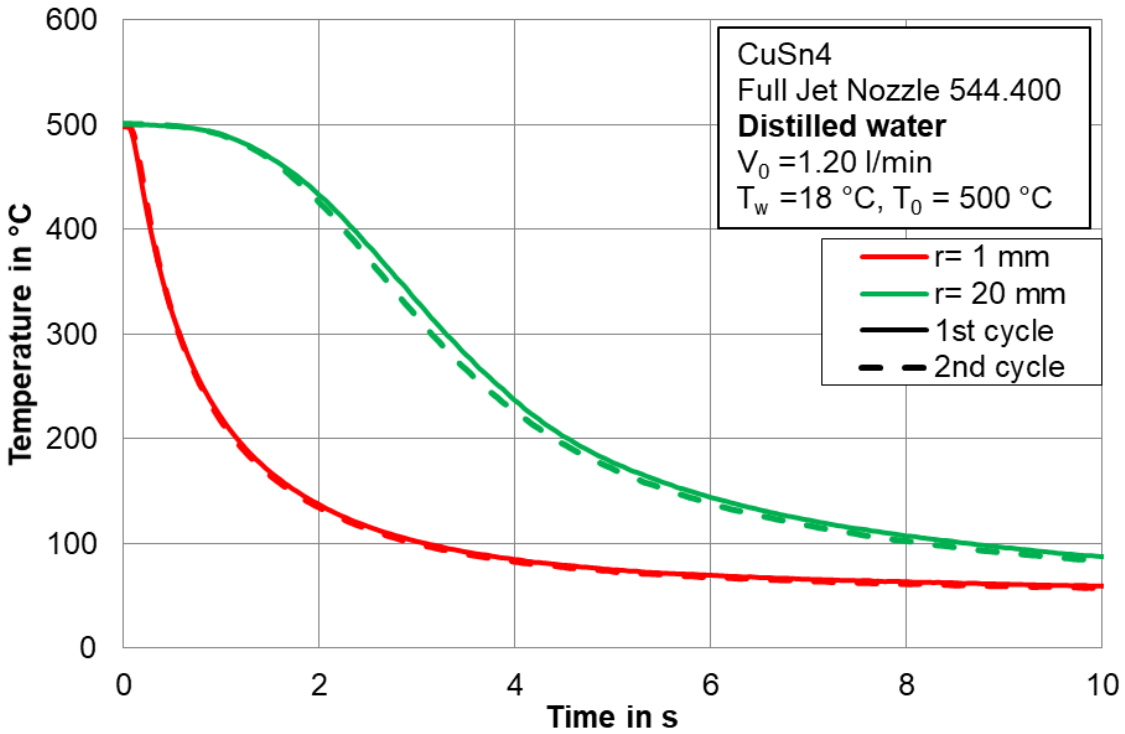

Figure 4.27: Repeated cooling cycles for full jet nozzle with distilled water on CuSn4

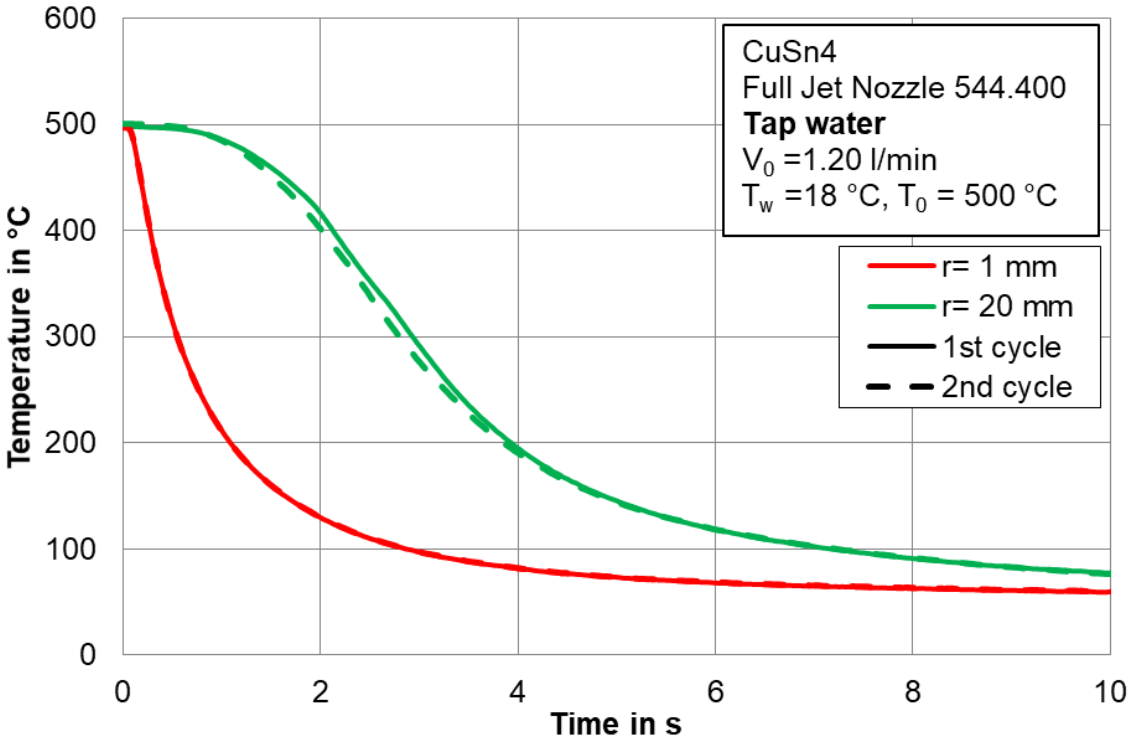

Figure 4.28: Repeated cooling cycles for full jet nozzle with tap water on CuSn4

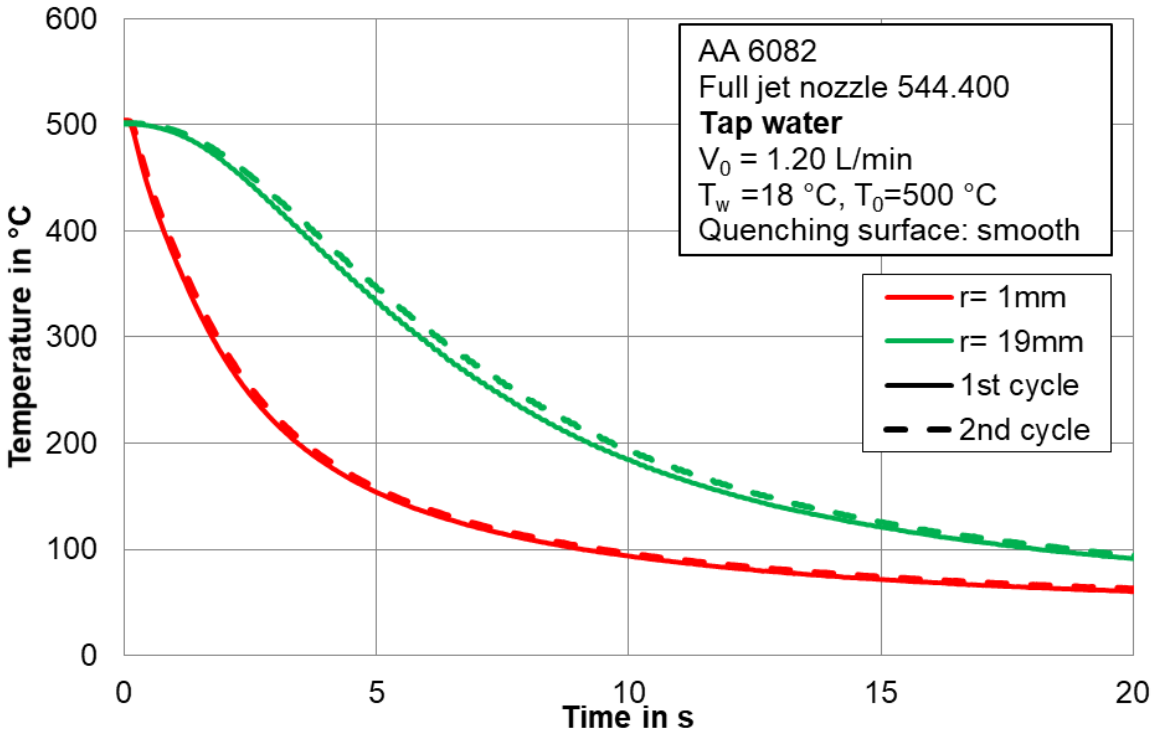

Figure 4.29: Repeated cooling cycles for full jet nozzle on AA6082

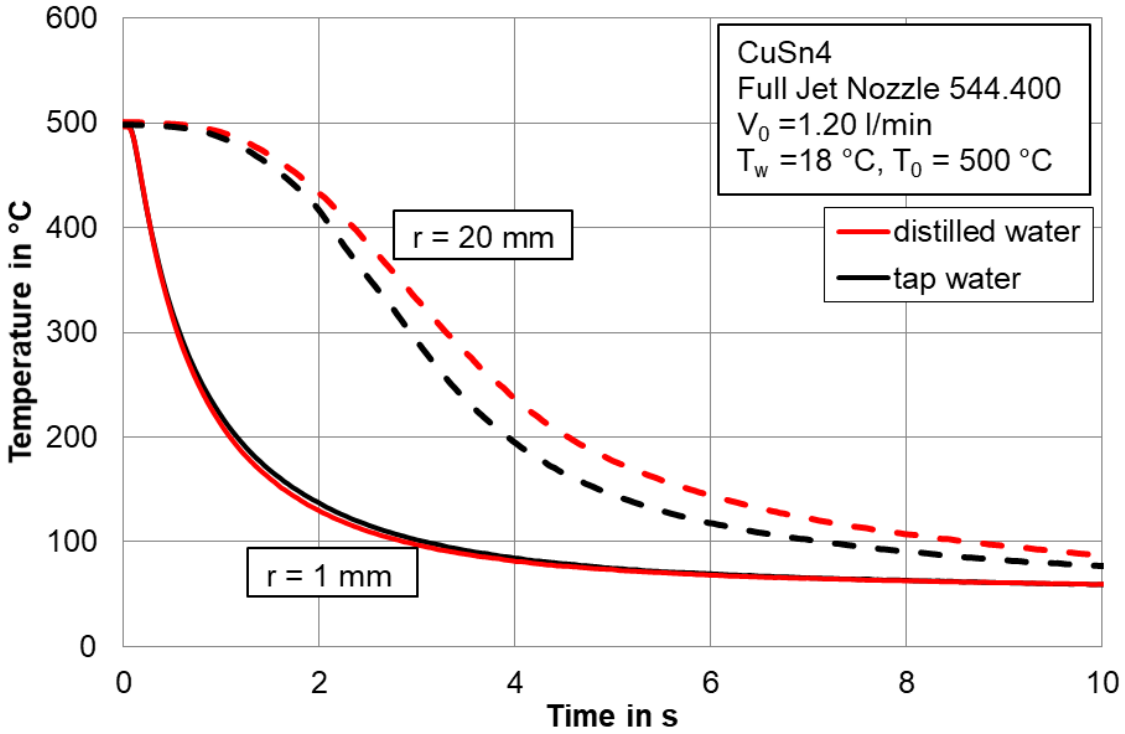

Figure 4.30: Effect of water quality on cooling curves with full jet nozzle

At the stagnation region, the cooling curves for both types of water have the same temperature profiles. However, the cooling rate is higher with tap water at a radius of 20 mm. The liquid jet strikes on the stagnation region with the highest momentum which will immediately remove the evaporated vapor. This results in a short contact time between the liquid vapor and the hot surface which is not beneficial for the salt deposition. However, as the wetting front propagates, the velocity of the wall jet reduces. The slower evaporation at the wetting front enables a longer liquid-surface contact which benefit the salt deposition and consequently enhance the cooling at downstream locations. Hence, it is also necessary to distinguish between the two types of water when comparisons need to be made. In all the following figures regarding on full jet nozzle, the water type will be mentioned in the text box.

4.4.3 Effect of surface roughness with full jet nozzle

In this section, the influence of surface roughness on cooling performance during the application of a single full jet nozzle will be presented. By far, in the open literatures, this area is not studied to the best of my knowledge.

If a full jet impacts the copper alloy CuSn4, no change in the cooling performance at the stagnation region is to be determined as a function of the arithmetic mean roughness R_a (**Figure 4.31**). At a radius of 20 mm from the stagnation point, the rougher surface of R_a = 14.7 µm is cooled even slower. This is explained by the fact that the rougher surface opposes the propagation of the wetting front, although evaporation at wetting front is more intensive for the rougher surface. The same effect

can be found for tap water as shown in **Figure 4.32**. To better clarify the differences, the wetting front propagation for both types of water is shown in **Figure 4.33**.

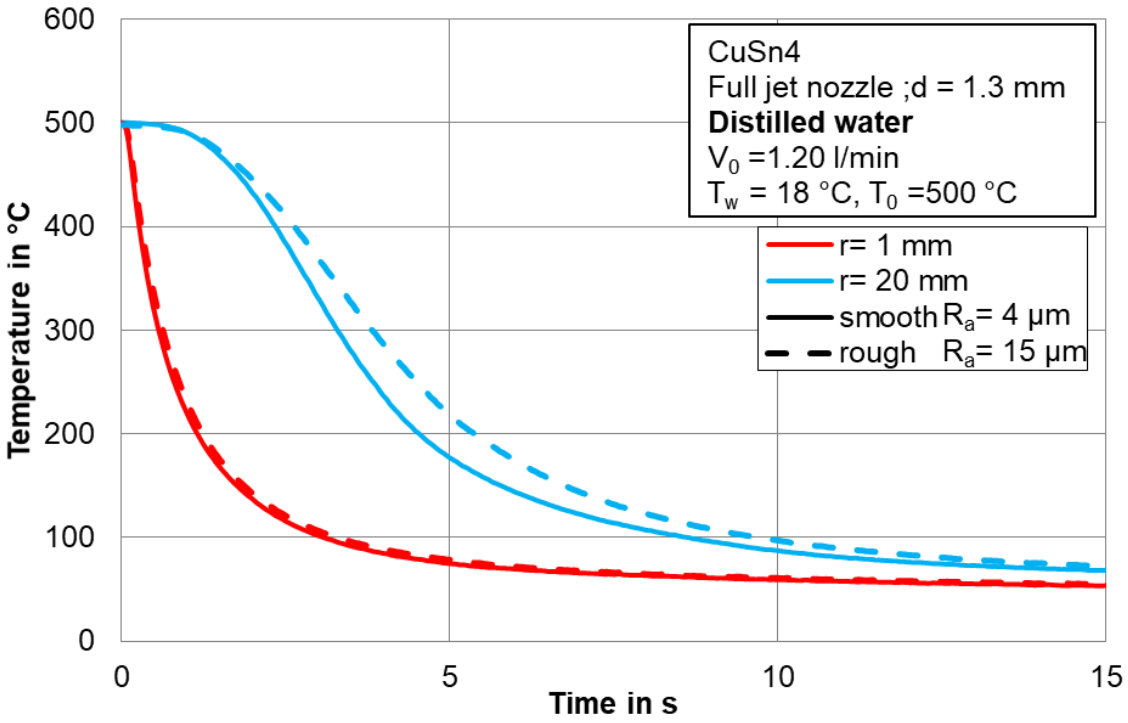

Figure 4.31: Effect of surface roughness with full jet nozzle and distilled water

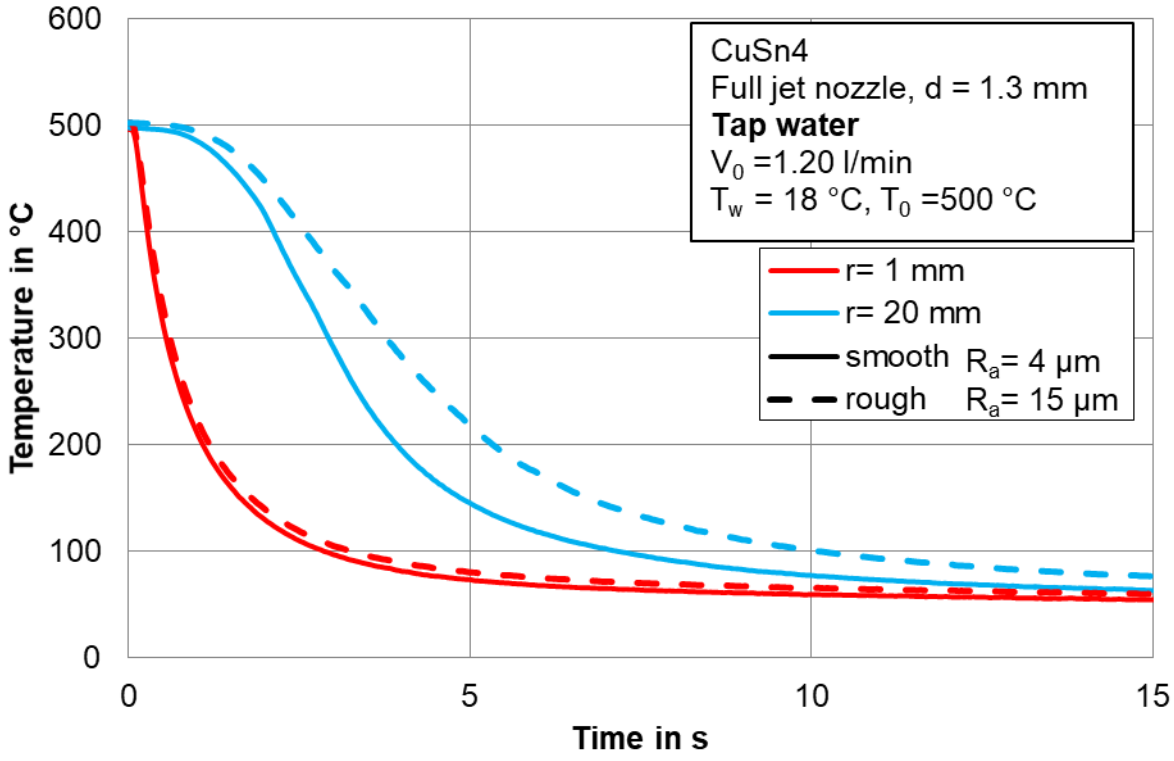

Figure 4.32: Effect of surface roughness with full jet nozzle and tap water

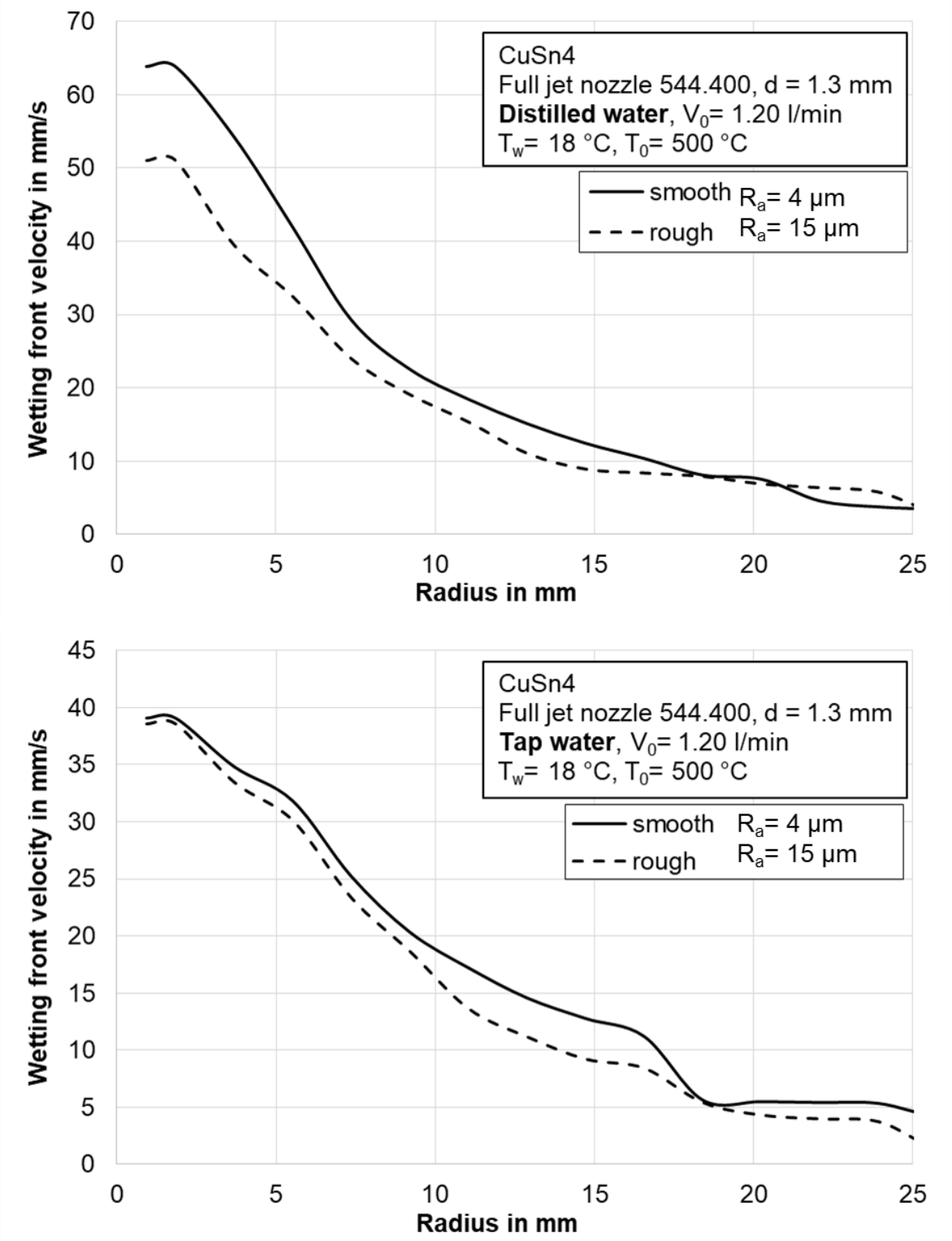

Figure 4.33: Wetting front propagation for distilled (top) and tap (bottom) water

For both types of water, the wetting front on rough surface propagates slower than on smooth surface which further indicates the opposition effect of surface roughness on wetting front propagation. And it is worth noting that the wetting front moves generally faster with distilled water than with tap water. At stagnation region, the velocity with distilled water is approx. 65 mm/s while 40 mm/s for tap water. This again supports the hypothesis that salt deposition at the wetting front due to intensive

evaporation, since the deposited salt acts as a surface rough element which will inevitably slow down the wetting front propagation.

Figure 4.34 depicts the corresponding local boiling curves for both water types. Generally, the heat flux is slightly higher for smooth surfaces. However, a difference of surface heat flux between two types of water cannot be recognized.

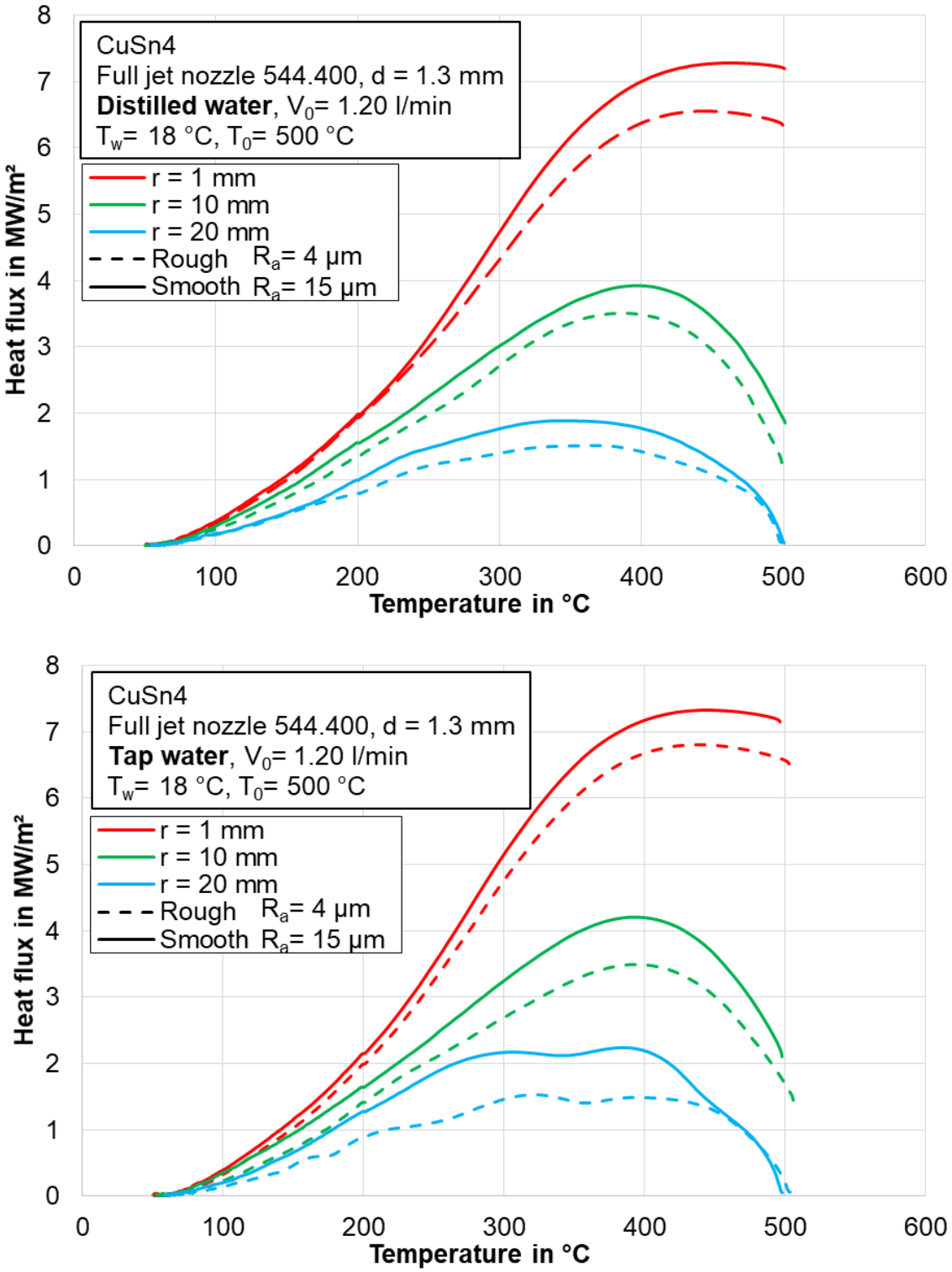

Figure 4.34: Boiling curves for distilled(top) and tap(bottom) water with full jet nozzle

Investigations on real surface AA 5083 with tap water is shown in **Figure 4.35**. The very effect of surface roughness on temperature profiles can be observed. This argues that the effect of surface conditions on wetting front propagation is not material-related.

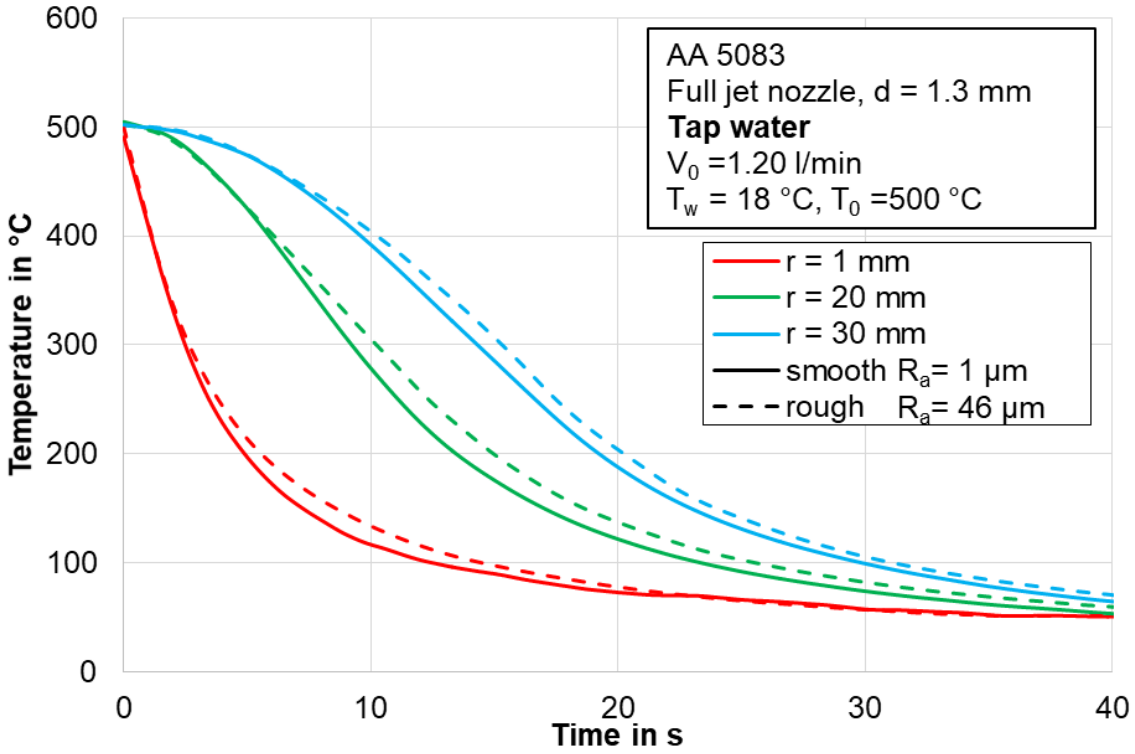

Figure 4.35: Effect of surface roughness with full jet nozzle on AA 5083

The experiments with liquid jet impinging on cubic pin fins were also conducted. Compared with smooth surface, the temperature profile and boiling curve for structured surface is depicted in **Figure 4.36** and **Figure 4.37**. In order to make a comparison with the full cone nozzle, the same volume flow of 1.2 l/min is chosen which results in a jet velocity v_j of 15 m/s. All other process parameters are identical to those of the tested full cone nozzle. In contrast to the full cone nozzle, a relatively small difference between smooth and rough surface is observed for full jet nozzle. Another characteristic is the slower cooling of structured surface which can be explained from the visual observation of the liquid flow pattern on the quenching side. The impact of the jet on the cubic pin fins leads to a stronger deflection of liquid jet, since the jet diameter of 1.3 mm is smaller than the pit distance of 4 mm. At the same time, this structure hinders the propagation of the wetting front in the radial direction. Unfortunately, due to the strong reflection of the water jets and the vapor formation, no video clips with high quality were recorded and presented. The influence of surface magnification by the cubic fin structures are offset by the described phenomena.

A direct comparison between full cone and full jet nozzle is presented in **Figure 4.38**. The cooling curves are shown at radius of 1 mm. At the same volume flow rate, full jet nozzle achieves faster cooling than with full cone nozzle. The shorter cooling time of the artificially structured surface when using a spray nozzle results from both

of the surface enlargement and roughness. In the case of the full jet nozzle, the effect of the surface enlargement due to artificial roughness is insignificant.

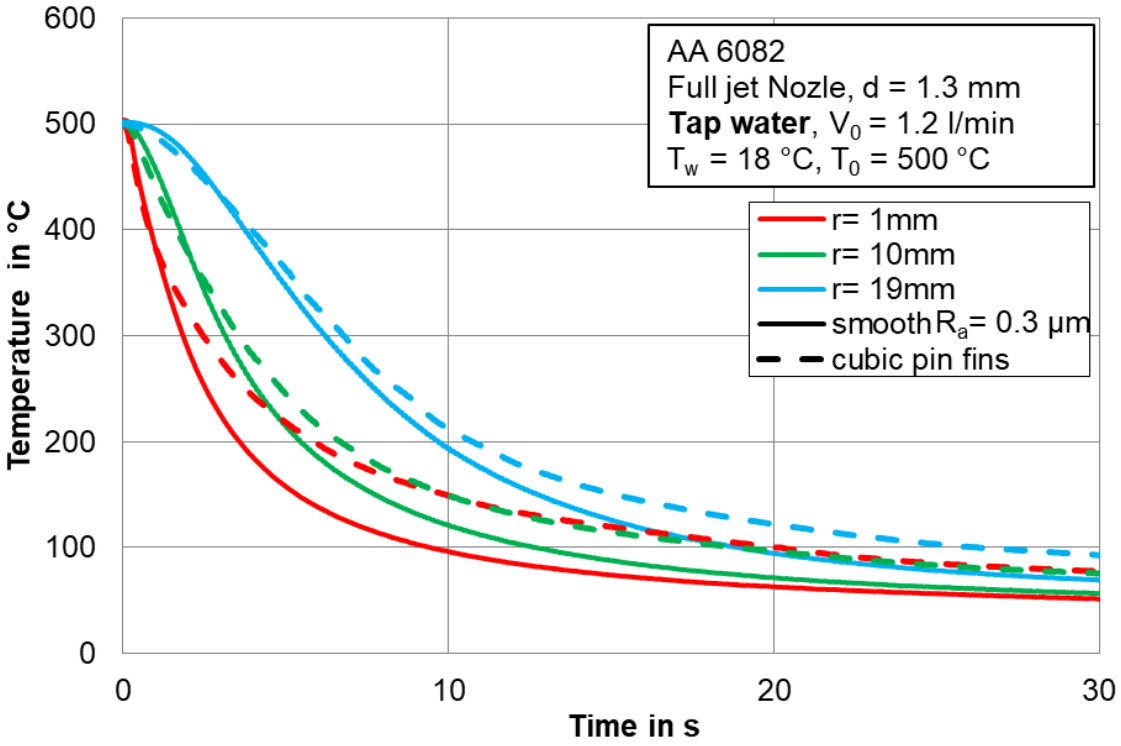

Figure 4.36: Effect of surface roughness with full jet nozzle on AA 6082

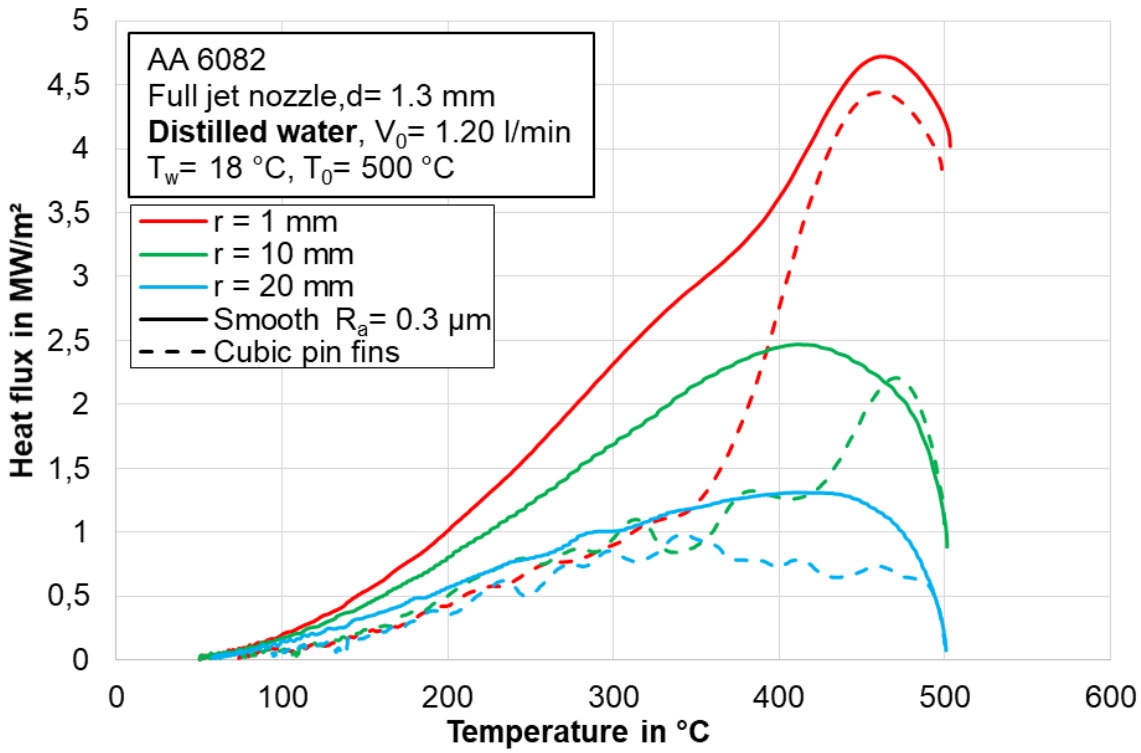

Figure 4.37: Boiling curves for smooth and structured surface with full jet nozzle

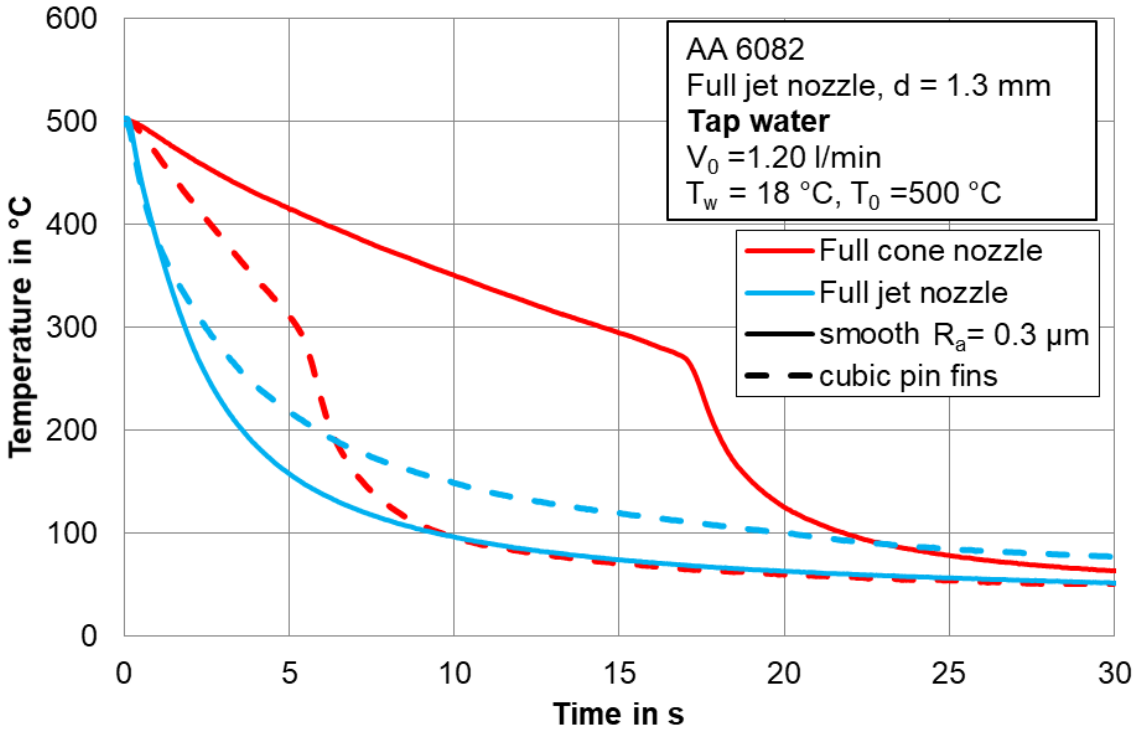

Figure 4.38: Comparison of full cone and full jet nozzle on AA 6082

4.5 Investigation with mold

4.5.1 Preparation of the experiments

In order to mimic the industrial application of direct chill (DC) casting, especially the secondary cooling regime, a house made miniature mold is used. The detailed description of the mold can be found in **section 2.6**. It has 11 orifices at its base, each of 2 mm in diameter. Hence, it can be also regarded as a row of liquid jets.

The metal samples are similar to those used in tests with full cone and full jet nozzles. Additionally, one more copper alloy CuCrZr is utilized which is supplied by "KME Germany GmbH & Co. KG".

4.5.2 Repeatability with mold

As same as full jet and full cone nozzles, the repeatability with mold is also examined. As described previously in **section 2.11.2**, only the quasi-steady state will be discussed when a mold during cooling is used. Analysis of the initial dynamic regime needs to be done in a further study. For conciseness, only the repeated cooling cycles with tap water on AA 5083 is shown in **Figure 4.39**, which clearly demonstrates that repeated cooling cycles have no influence on the cooling behaviors with mold. Since the tap water with electrical conductivity of 0.56 µS/cm is used, it also indicates that salt deposition during the mold cooling is not as significant as in full cone nozzle.

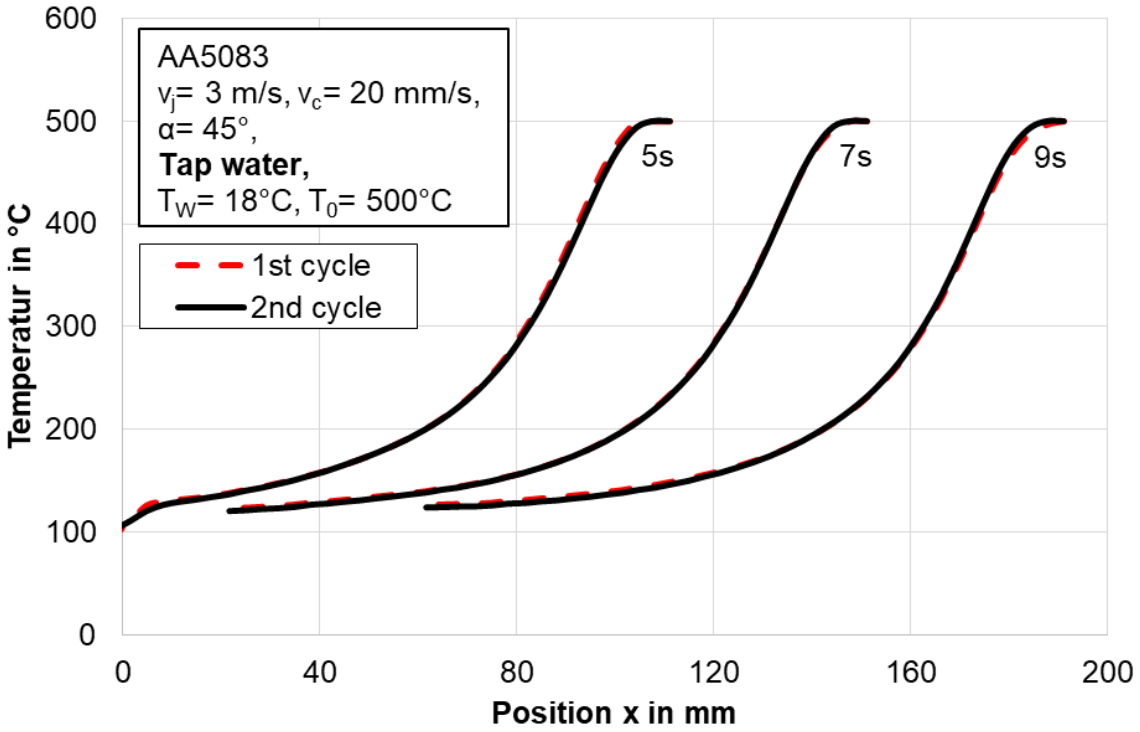

Figure 4.39: Effect of repeated cooling cycles with mold

4.5.3 Effect of surface roughness with mold

In this section, the results based on investigation of surface roughness with mold during cooling will be presented. Four types of alloys with different levels of roughness are used: three of them originate from industrial manufacturer with the origin surface conditions; the last one is the cubic pin structure which is in-house produced. All the surface conditions have been measured with a profilometer to determine their surface roughness which is summarized in Figure 4.7 and Figure 4.8.

The following figures in this section are presented in Eulerian coordinate which focuses on the quasi-steady state. **Figure 4.40** depicts the influence of surface roughness on cooling when CuSn4 is investigated. A slight difference between two surfaces can be observed, especially in the transition and nucleate cooling region, which is further illustrated as boiling curves in **Figure 4.41**. The plate moves continually downward at preset velocity v_c while the mold remains fixed. This enables the liquid jets always to impinge on the fresh untouched surfaces, which avoids the possibility of effect of deposited salt on the surface. Furthermore, high momentum of the impinging liquid jets compensates more intensive evaporation on the rough surfaces by sweeping the nucleated bubbles faster away. These two factors together make mold cooling insensitive to the surface roughness created during industrial manufacturing.

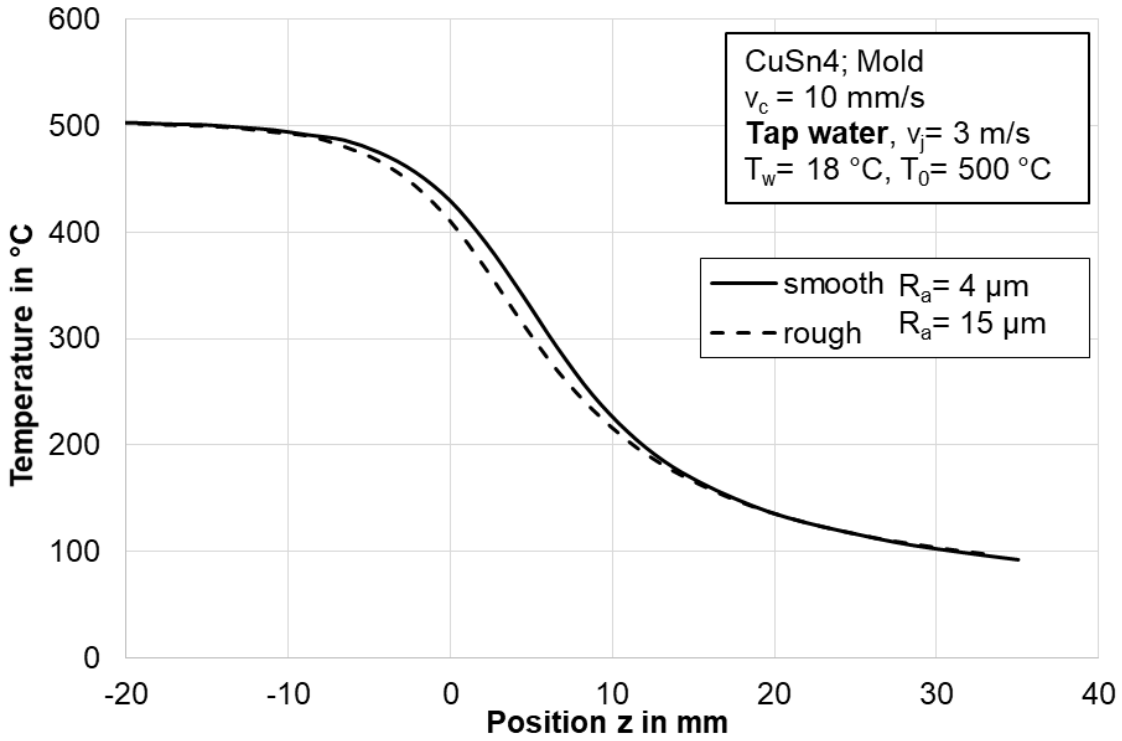

Figure 4.40: Effect of surface roughness on temperatures with mold cooling of CuSn4

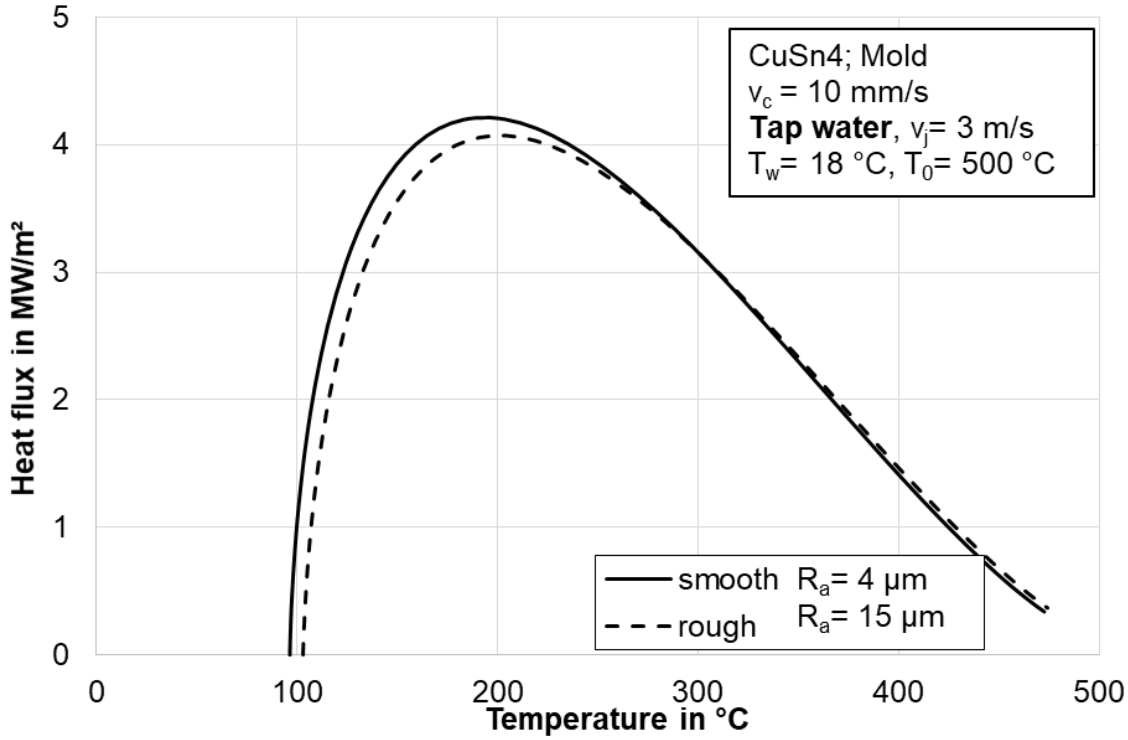

Figure 4.41: Effect of surface roughness on boiling curves with mold cooling of CuSn4

The similar effects can be found for both CuCrZr and AA 5083. They were produced under different casting technology by different manufacturers. Although the surface roughness levels depicted by the arithmetic mean roughness R_a is different, the resulted tendency remains same. The corresponding temperature profiles and boiling curves are presented in **Figure 4.42** (for CuCrZr) and **Figure 4.43** (for AA 5083).

The last investigated surface is the artificial structure of cubic pin fins. The results are shown in **Figure 4.44**. The theoretical arithmetic mean roughness R_a is 250 µm. When the cooling temperature is higher than 200 °C, the deviations are marginal; however, at temperatures below 200 °C, the roughness begins to play a major role. This can be further ascertained in the boiling curves. The maximum heat flux for structures surface is approx. 8 MW/m², while 7 MW/m² for smooth surfaces. The difference in this case is mainly contributed by the water accumulation among the fin structures. The accumulated water enables a longer contact between the hot surface and the cooling medium, namely, water, which inevitably enhances the heat transfer rate. This phenomenon insights the possibility of enhancement of cooling rate by structured surfaces when a relative movement between the cooling medium and the surface.

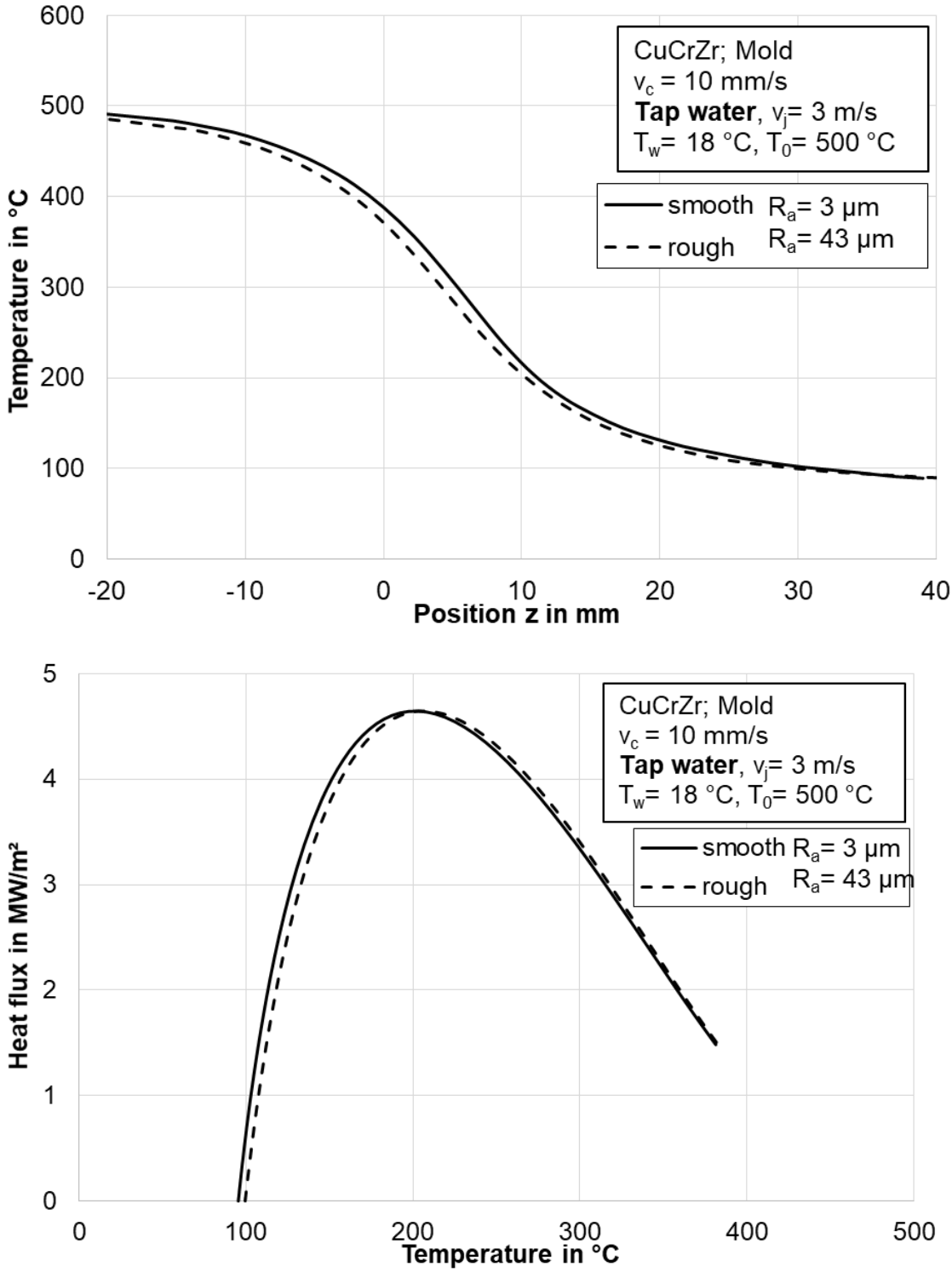

Figure 4.42: Effect of surface roughness on temperatures and boiling curves with mold cooling of CuCrZr

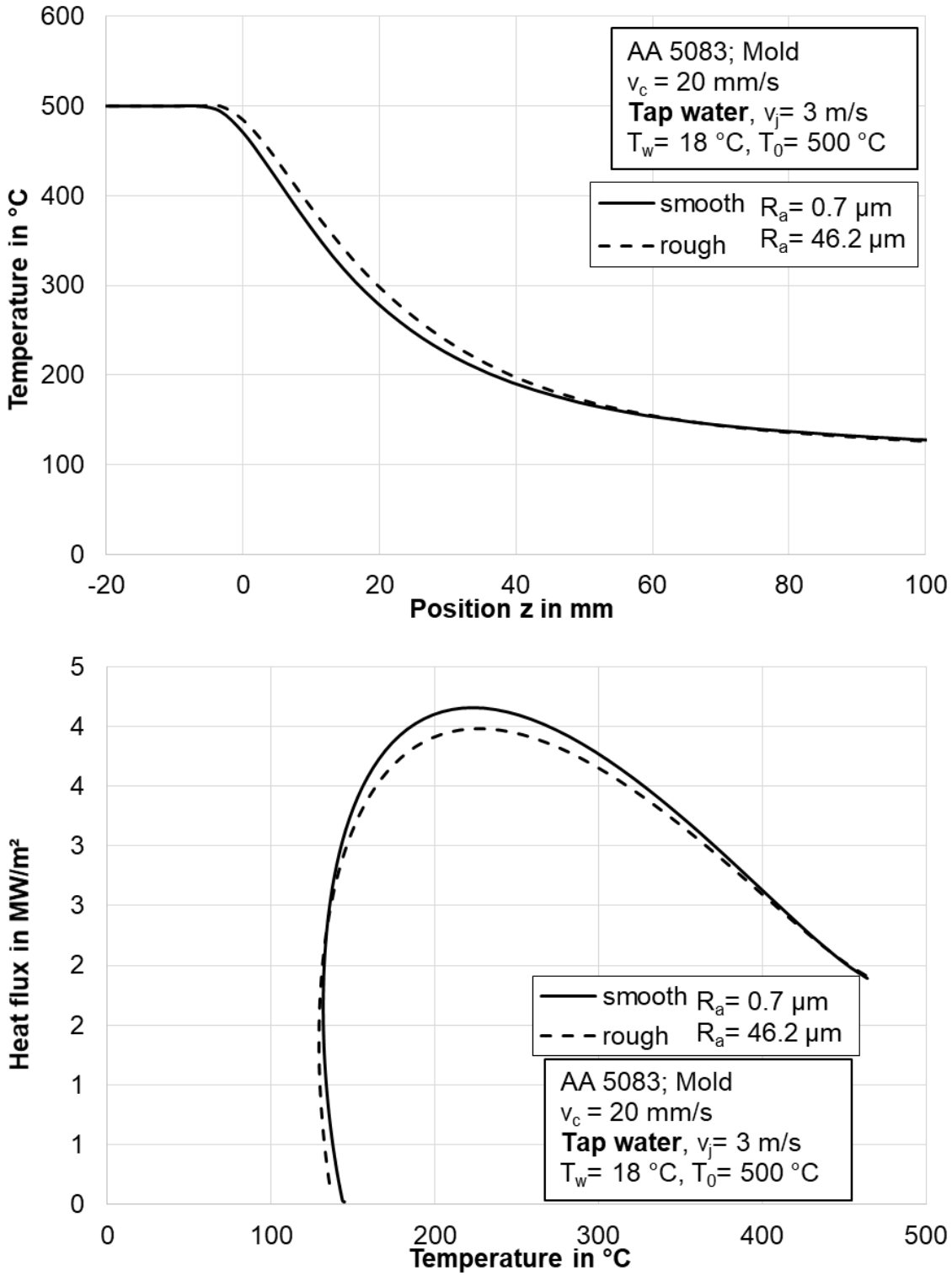

Figure 4.43: Effect of surface roughness on temperatures and boiling curves with mold cooling of AA 5083

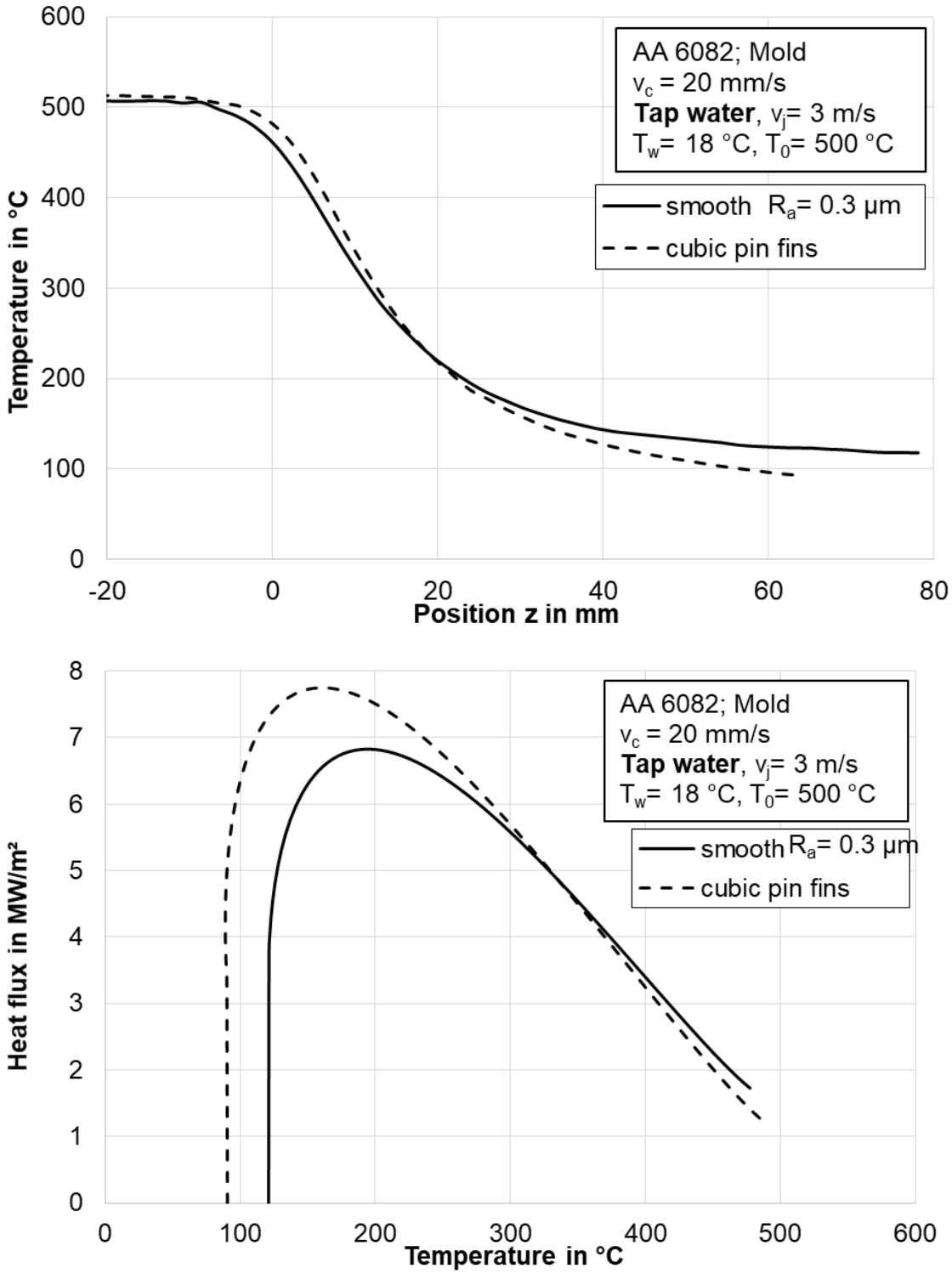

Figure 4.44: Effect of surface roughness on temperatures and boiling curves with mold cooling of AA 6082

5. Conclusion

Metal quenching by using various cooling strategies under different experimental conditions have been investigated and discussed thoroughly in this work. The temperature on the rear side is measured using infrared thermography where a precise and accurate determination of surface emissivity is required. Two high temperature thermal coatings from two manufacturers, namely, “Senotherm” and “Ulfalux”, have been utilized and their performance have been examined at various conditions. It is found out that “Senotherm” is more appropriate when the initial temperature is not higher than 500 °C; while the temperature limit is 1200 °C for “Ulfalux”. The corresponding average emissivities are 0.86 for “Senotherm” and 0.85 for “Ulfalux”, respectively. These values are measured and evaluated based on the utilization of infrared camera with serial number of FLIR® SC 3000. The measured thermal history data with high spatial and temporal resolution is further analyzed to obtain the boiling curves, distribution of rewetting and DNB temperatures as well as wetting front propagation.

The achieved results in this dissertation can be divided as the structure of text in main body and therefore are listed as follows.

- **Heat transfer analysis with single nozzles** (detailed in Chapter 3)

1. Full cone nozzle

Aluminum alloy AA 6082 with three thicknesses, e.g. 3, 5 and 10 mm, are quenched with a full cone nozzle at volume flow rate of 1.2 l/min. The initial temperature is set as 500 °C. It is found out that a larger thickness promotes a longer film boiling regime, resulting in increasing of the cooling time. The maximum heat flux increases as well with increasing thickness. This is mainly contributed by the higher stored thermal energy in the sample which can then be extracted by the impinging spray. It is also found out that the cooling with full cone nozzle is mainly influenced by the distribution of spray flux.

2. Flat spray nozzle

Both inclination angle and liquid outlet pressure are studied. It is found out that with increasing inclination angle, wetting front propagates faster. This is logical and reasonable, since a larger inclination angle enables a higher vertical momentum of the liquid flowing on the hot surface. Accompany this, a reduction of rewetting temperature at the initial impact area of the flat spray can be observed for smaller inclination angle, since the impact at that area is not so vigorous when inclination angle is small. This will inevitably prolong the evaporation process and hence film boiling region which lead to smaller rewetting temperatures. It is also found out that increasing nozzle outlet

pressure for a flat spray nozzle will also increase the wetting front velocity. However, the rewetting and DNB temperatures are not significantly influenced.

3. Full jet nozzle

In this case, jet velocity, the sample thickness and metal type are studied and discussed. Results obtained for jet velocity and sample thickness have also been compared and are in good agreement with those found in literatures. For example, a higher jet velocity and thinner plate benefit wetting front movement and heat flux enhancement. As for the effect of metal type, three materials are selected: CuSn4, nicrofer and nickel. It is found out that the effect of thermal conductivity is paramount. A material with higher thermal conductivity such as CuSn4 leads to a slower propagation of wetting front and a lower rewetting temperature. The thermal energy cannot be conducted well in material with lower thermal conductivity such as nicrofer, therefore it takes longer time for the energy to be conducted from the bulk body to the wetting front which will increase the rewetting temperature.

4. Nozzle fields

Inline and staggered arrangements are investigated and presented. Several individual jets are selected as reference points in both arrangements. For example, side, corner and center points are selected for inline configuration. The initial temperature is also studied. The obtained results are also compared with those in literature, which shows a good agreement. A higher initial temperature leads to a higher rewetting temperature but a slower wetting front propagation. It is also found out that the cooling behavior of full jet nozzle in a nozzle field is similar to that of single nozzle quenching. However, with multiple stagnation existing simultaneously on the metal surface, the overall cooling efficiency is much better and homogenous in nozzle field. In this study, there is no significant deviation between these two nozzle fields. It might be attributed by the smaller ratio of covering area by the nozzle field to the surface area. Hence, the possibility of better performance of either inline or staggered arrangements should not be ruled out.

- **Effect of surface roughness** (detailed in Chapter 4)

Hereby, the single nozzle such as full jet and full cone and a mold are utilized to quench the rough surfaces. A stylus profilometer is used to determine the characteristic values of the investigated surfaces. Part of the surfaces are originated from industrial productions; and also plate with cubic pin fins is in-house produced. It is found out that the effect of surface roughness is most paramount in application of full cone nozzles. Even with a slight increase of arithmetic mean roughness R_a, the cooling time can be reduced dramatically. However, the effect of surface roughness is not that significant in case of full jet and mold cooling. A clear conclusion can be drawn though these three series of tests: a cooling method which promotes film boiling is much more sensitive to the variation of surface conditions, since the produced rough surface elements in industry are in general larger than the film thickness in the film boiling region. This

enables intermittent direct contact between liquid and hot surface which reduces the cooling time significantly. However, this is not directly proved with experimental observations, which requires further measurements of the liquid film thickness.

Bibliography

[1] M.K. Chung, Y.W. Lee, Description and Discussion of the Current State of the Knowledge about the Leidenfrost Phenomenon, Nuclear Engineering and Technology, 14(4) (1982) 204-218.

[2] J. Filipovic, F. Incropera, R. Viskanta, Rewetting temperatures and velocity in a quenching experiment, EXPERIMENTAL HEAT TRANSFER An International Journal, 8(4) (1995) 257-270.

[3] D.E. Hall, F.P. Incropera, R. Viskanta, Jet impingement boiling from a circular free-surface jet during quenching: Part 1—single-phase jet, Journal of heat transfer, 123(5) (2001) 901-910.

[4] D.E. Hall, F.P. Incropera, R. Viskanta, Jet impingement boiling from a circular free-surface jet during quenching: Part 2—two-phase jet, Journal of heat transfer, 123(5) (2001) 911-917.

[5] Z.-H. Liu, J. Wang, Study on film boiling heat transfer for water jet impinging on high temperature flat plate, International Journal of Heat and Mass Transfer, 44(13) (2001) 2475-2481.

[6] Z. Liu, D. Fraser, I. Samarasekera, Experimental study and calculation of boiling heat transfer on steel plates during runout table operation, Canadian metallurgical quarterly, 41(1) (2002) 63-74.

[7] P. Zhang, Study of boiling heat transfer on a stationary downward facing hot steel plate cooled by a circular water jet, University of British Columbia, 2005.

[8] M. Gradeck, A. Kouachi, F. Volle, J. Borean, P. Gardin, M. Lebouche, Cooling of a hot cylinder with an impinging planar water jet, in: International Heat Transfer Conference 13, Begel House Inc., 2006.

[9] J. Wendelstorf, K.-H. Spitzer, R. Wendelstorf, Spray water cooling heat transfer at high temperatures and liquid mass fluxes, International Journal of Heat and Mass Transfer, 51(19-20) (2008) 4902-4910.

[10] K.H.M. Abdalrahman, Sabariman, E. Specht, Influence of salt mixture on the heat transfer during spray cooling of hot metals, International Journal Of Heat And Mass Transfer, 78 (2014) 76-83.

[11] B.X. Wang, D. Lin, Q. Xie, Z.D. Wang, G.D. Wang, Heat transfer characteristics during jet impingement on a high-temperature plate surface, Applied Thermal Engineering, 100 (2016) 902-910.

[12] I. Sarkar, S. Chakraborty, A. Ashok, I. Sengupta, S.K. Pal, S. Chakraborty, Comparative study on different additives with a jet array on cooling of a hot steel surface, Applied Thermal Engineering, 137 (2018) 154-163.

[13] A. Labergue, M. Gradeck, F. Lemoine, Comparative study of the cooling of a hot temperature surface using sprays and liquid jets, International Journal of Heat and Mass Transfer, 81 (2015) 889-900.

[14] M.N. Özisik, H.R.B. Orlande, Inverse Heat Transfer: Fundamentals and Applications, CRC Press, 2000.

[15] N. Schweizer, Multi-scale investigation of nucleate boiling phenomena in microgravity, PhD thesis, Technische Universität Darmstadt, 2010.

[16] A. Bejan, A.D. Kraus, Heat transfer handbook, John Wiley & Sons, 2003.

[17] J. Sengupta, B. Thomas, M. Wells, The use of water cooling during the continuous casting of steel and aluminum alloys, Metallurgical and Materials Transactions A, 36(1) (2005) 187-204.

[18] S. Matthews, B. James, Review of thermal spray coating applications in the steel industry: Part 1—Hardware in steel making to the continuous annealing process, Journal of Thermal Spray Technology, 19(6) (2010) 1267-1276.

[19] J. Brimacombe, K. Sorimachi, Crack formation in the continuous casting of steel, Metallurgical transactions B, 8(2) (1977) 489-505.

[20] J. Grandfield, P. McGlade, DC casting of aluminium: process behaviour and technology, in: MATERIALS FORUM-RUSHCUTTERS BAY-, 1996, pp. 29-51.

[21] Sabariman, Heat Transfer Analysis in Metal Quenching with Sprays and Jets, Docupoint-Verlag, 2015.

[22] K. Baumeister, F. Simon, Leidenfrost temperature—its correlation for liquid metals, cryogens, hydrocarbons, and water, Journal of Heat Transfer, 95(2) (1973) 166-173.

[23] J. Bernardin, I. Mudawar, The Leidenfrost point: experimental study and assessment of existing models, Journal of Heat Transfer, 121(4) (1999) 894-903.

[24] W. Klinzing, J. Rozzi, I. Mudawar, Film and transition boiling correlations for quenching of hot surfaces with water sprays, Journal of Heat Treating, 9(2) (1992) 91-103.

[25] I. Mudawar, W. Valentine, Determination of the local quench curve for spray-cooled metallic surfaces, Journal of Heat Treating, 7(2) (1989) 107-121.

[26] N. HATTA, J.-i. KOKADO, K. HANASAKI, Numerical analysis of cooling characteristics for water bar, Transactions of the Iron and Steel Institute of Japan, 23(7) (1983) 555-564.

[27] N. Hatta, Y. Tanaka, H. Takuda, J.-i. Kokado, A numerical study on cooling process of hot steel plates by a water curtain, Isij International, 29(8) (1989) 673-679.

[28] R. Ishida, A. Mizuta, K. Korida, S. Yasunaga, K. Takisawa, Basic characteristics of pipe nozzle cooling with retaining water on plate, ISIJ International, 29(4) (1989) 339-344.

[29] N. Karwa, P. Stephan, Experimental investigation of free-surface jet impingement quenching process, International Journal of Heat and Mass Transfer, 64 (2013) 1118-1126.

[30] Y. Lee, W.-Q. Shen, Effect of coolant vapor quality on rewetting phenomena, International journal of heat and mass transfer, 28(1) (1985) 139-146.

[31] L. Qiu, S. Dubey, F.H. Choo, F. Duan, Recent developments of jet impingement nucleate boiling, International Journal of Heat and Mass Transfer, 89 (2015) 42-58.

[32] A.K. Mozumder, M. Monde, P.L. Woodfield, M.A. Islam, Maximum heat flux in relation to quenching of a high temperature surface with liquid jet impingement, International Journal of Heat and Mass Transfer, 49(17-18) (2006) 2877-2888.

[33] M.K. Singh, D. Yadav, S. Arpit, S. Mitra, S.K. Saha, Effect of nanofluid concentration and composition on laminar jet impinged cooling of heated steel plate, Applied Thermal Engineering, 100 (2016) 237-246.

[34] J. Hammad, Y. Mitsutake, M. Monde, Movement of maximum heat flux and wetting front during quenching of hot cylindrical block, International journal of thermal sciences, 43(8) (2004) 743-752.

[35] Y.-h. Qiu, Z.-h. Liu, Nucleate boiling on the superhydrophilic surface with a small water impingement jet, International Journal of Heat and Mass Transfer, 51(7-8) (2008) 1683-1690.

[36] M. Monde, H. Kusuda, H. Uehara, Burnout heat flux in saturated forced convection boiling with two or more impinging jets, Heat Transfer Jpn.Res.9, 3 (1980) 18-31.

[37] M. Monde, T. Inoue, Critical heat flux in saturated forced convective boiling on a heated disk with multiple impinging jets, Journal of heat transfer, 113(3) (1991) 722-727.

[38] C. Agrawal, D. Gotherwal, C. Singh, C. Singh, Effect of surface thickness on the wetting front velocity during jet impingement surface cooling, Heat and Mass Transfer, 53(2) (2017) 733-741.

[39] R. Nadella, D. Eskin, Q. Du, L. Katgerman, Macrosegregation in direct-chill casting of aluminium alloys, Progress in Materials Science, 53(3) (2008) 421-480.

[40] D. Weckman, P. Niessen, A numerical simulation of the DC continuous casting process including nucleate boiling heat transfer, Metallurgical Transactions B, 13(4) (1982) 593-602.

[41] Y. Watanabe, N. Hayashi, 3-D solidification analysis of the initial state of the DC casting process, in, Minerals, Metals and Materials Society, Warrendale, PA (United States), 1996.

[42] J. Langlais, T. Bourgeois, Y. Caron, G. Beland, D. Bernard, Measuring the heat extraction capacity of DC casting cooling water, Light Metals, (1995) 979-986.

[43] S. Hamilton, Heat transfer and water quality in DC casting, 4th chemical engineering project, Oct, (1995).

[44] M. Wells, D. Li, S. Cockcroft, Influence of surface morphology, water flow rate, and sample thermal history on the boiling-water heat transfer during direct-chill casting of commercial aluminum alloys, Metallurgical and Materials Transactions B, 32(5) (2001) 929.

[45] J. Bakken, T. Bergström, Heat Transfer Measurements during DC Casting of Aluminium Part I: Measurement Technique, in: Essential Readings in Light Metals, Springer, 2016, pp. 646-652.

[46] J. Wiskel, S. Cockcroft, Heat-flow-based analysis of surface crack formation during the start-up of the direct chill casting process: Part II. experimental study of an AA5182 rolling ingot, Metallurgical and Materials Transactions B, 27(1) (1996) 129-137.

[47] E. Tarapore, Thermal modeling of DC continuous billet casting, in: JOURNAL OF METALS, MINERALS METALS MATERIALS SOC 420 COMMONWEALTH DR, WARRENDALE, PA 15086, 1988, pp. 83-84.

[48] H. Kraushaar, R. Jeschar, V. Heidt, E. Jensen, W. Schneider, Correlation of surface temperatures and heat transfer by D. C. casting of aluminium ingots, LIGHT MET(WARRENDALE PA), (1995) 1055-1059.

[49] L. Maenner, B. Magnin, Y. Caratini, A comprehensive approach to water cooling in DC casting, LIGHT METALS-WARRENDALE-, (1997) 701-708.

[50] A.K. Nallathambi, E. Specht, Estimation of heat flux in array of jets quenching using experimental and inverse finite element method, Journal of Materials Processing Technology, 209(12-13) (2009) 5325-5332.

[51] X. Ling, R.G. Keanini, H. Cherukuri, A non-iterative finite element method for inverse heat conduction problems, International Journal for Numerical Methods in Engineering, 56(9) (2003) 1315-1334.

[52] U. Alam, Experimental Study of Local Heat Transfer during Quenching of Metals by Spray and Multiple Jets, PhD thesis in Process and System Engineering Faculty, Otto-von-Guericke-Universität Magdeburg: Magdeburg, 2011.

[53] K.H.M. Abdalrahman, Influence of water quality and kind of metal in the secondary cooling zone of casting process, Universitätsbibliothek, 2012.

[54] E.D. Suyitno, V. Savran, L. Katgerman, Effects of alloy composition and casting speed on structure formation and hot tearing during direct-chill casting of Al-Cu alloys, Metallurgical and Materials Transactions A, 35(11) (2004) 3551-3561.

[55] L. Zhang, D. Eskin, A. Miroux, T. Subroto, L. Katgerman, Influence of melt feeding scheme and casting parameters during direct-chill casting on microstructure of an AA7050 billet, Metallurgical and Materials Transactions B, 43(6) (2012) 1565-1573.

[56] E.J. Caron, M.A. Wells, Effect of Advanced Cooling Front (ACF) Phenomena on Film Boiling and Transition Boiling Regimes in the Secondary Cooling Zone during the Direct-Chill Casting of Aluminium Alloys, in: Materials science forum, Trans Tech Publ, 2006, pp. 1687-1692.

[57] P. Zhao, E. Specht, X. Song, Influence of Jet Velocities and Material Properties in Quenching of Metal with Array of Jets, Advanced Materials Research, 1090 (2015).

[58] F. Puschmann, E. Specht, Transient measurement of heat transfer in metal quenching with atomized sprays, Experimental Thermal and Fluid Science, 28(6) (2004) 607-615.

[59] A. Labergue, J.-D. Pena-Carillo, M. Gradeck, F. Lemoine, Combined three-color LIF-PDA measurements and infrared thermography applied to the study of the spray impingement on a heated surface above the Leidenfrost regime, International Journal of Heat and Mass Transfer, 104 (2017) 1008-1021.

[60] S. Freund, A. Pautsch, T. Shedd, S. Kabelac, Local heat transfer coefficients in spray cooling systems measured with temperature oscillation IR thermography, International journal of heat and mass transfer, 50(9-10) (2007) 1953-1962.

[61] G.A. Kulkarni, A.K. Nallathambi, E. Specht, Eulerian steady state solution of boiling curve for impinging water jet on moving hot metal plate, Heat and Mass Transfer, (2019).

[62] M.K. Agrawal, S. Sahu, Analysis of conduction-controlled rewetting of a hot surface by variational method, Heat and Mass Transfer, 49(7) (2013) 963-971.

[63] G. Liang, I. Mudawar, Review of spray cooling–Part 1: Single-phase and nucleate boiling regimes, and critical heat flux, International Journal of Heat and Mass Transfer, 115 (2017) 1174-1205.

[64] J. Yang, M.R. Pais, L.C. Chow, Critical heat flux limits in secondary gas atomized liquid spray cooling, EXPERIMENTAL HEAT TRANSFER An International Journal, 6(1) (1993) 55-67.

[65] W. Vorster, S. Schwindt, J. Schupp, A. Korsunsky, Analysis of the spray field development on a vertical surface during water spray-quenching using a flat spray nozzle, Applied Thermal Engineering, 29(7) (2009) 1406-1416.

[66] F. Ramstorfer, J. Roland, C. Chimani, K. Mörwald, Investigation of spray cooling heat transfer for continuous slab casting, Materials and Manufacturing Processes, 26(1) (2011) 165-168.

[67] M. Visaria, I. Mudawar, A systematic approach to predicting critical heat flux for inclined sprays, Journal of Electronic Packaging, 129(4) (2007) 452-459.

[68] T. Fu, Z. Wang, X. Deng, G. Liu, G. Wang, The influence of spray inclination angle on the ultra fast cooling of steel plate in spray cooling condition, Applied Thermal Engineering, 78 (2015) 500-506.

[69] M. Molana, S. Banooni, Investigation of heat transfer processes involved liquid impingement jets: a review, Brazilian Journal of Chemical Engineering, 30(3) (2013) 413-435.

[70] R. Panda, B. Prasad, Conjugate heat transfer from a flat plate with shower head impinging jets, Frontiers in Heat and Mass Transfer (FHMT), 2(1) (2011).

[71] N. Karwa, T. Gambaryan-Roisman, P. Stephan, C. Tropea, Experimental investigation of circular free-surface jet impingement quenching: transient hydrodynamics and heat transfer, Experimental Thermal and Fluid Science, 35(7) (2011) 1435-1443.

[72] J.-Y. San, M.-D. Lai, Optimum jet-to-jet spacing of heat transfer for staggered arrays of impinging air jets, International Journal of Heat and Mass Transfer, 44(21) (2001) 3997-4007.

[73] D.E. Metzger, R.J. Korstad, Effects of crossflow on impingement heat transfer, Journal of Engineering for Power, 94(1) (1972) 35-41.

[74] M. Akmal, A. Omar, M. Hamed, Experimental investigation of propagation of wetting front on curved surfaces exposed to an impinging water jet, International Journal of Microstructure and Materials Properties, 3(4-5) (2008) 654-681.

[75] M. Goodro, J. Park, P. Ligrani, M. Fox, H.-K. Moon, Effects of hole spacing on spatially-resolved jet array impingement heat transfer, International Journal of Heat and Mass Transfer, 51(25-26) (2008) 6243-6253.

[76] Z.-X. Wen, Y.-L. He, Z. Ma, Effects of nozzle arrangement on uniformity of multiple impinging jets heat transfer in a fast cooling simulation device, Computers & Fluids, 164 (2018) 83-93.

[77] M. Pais, L. Chow, E. Mahefkey, Surface roughness and its effects on the heat transfer mechanism in spray cooling, Journal of Heat Transfer, 114(1) (1992) 211-219.

[78] J.D. Bernardin, I. Mudawar, An experimental investigation into the relationship between temperature-time history and surface roughness in the spray quenching of aluminum parts, Journal of engineering materials and technology, 118(1) (1996) 127-134.

[79] J. Sinha, Effects of surface roughness, oxidation level, and liquid subcooling on the minimum film boiling temperature, Experimental heat transfer, 16(1) (2003) 45-60.

[80] E.A. Silk, J. Kim, K. Kiger, Spray cooling of enhanced surfaces: impact of structured surface geometry and spray axis inclination, International Journal of Heat and Mass Transfer, 49(25-26) (2006) 4910-4920.

[81] E.A. Silk, J. Kim, K. Kiger, Investigation of Enhanced Surface Spray Cooling, (4711Xb) (2004) 685-690.

[82] C. Sodtke, P. Stephan, Spray cooling on micro structured surfaces, International Journal of Heat and Mass Transfer, 50(19-20) (2007) 4089-4097.

[83] R. Xu, L. Li, L. Zhang, B. Zhu, X. Liu, X. Bu, Influence of pressure and surface roughness on the heat transfer efficiency during water spray quenching of 6082 aluminum alloy, Journal of Materials Processing Technology, 214(12) (2014) 2877-2883.

[84] M. Aamir, Q. Liao, W. Hong, Z. Xun, S. Song, M. Sajid, Transient heat transfer behavior of water spray evaporative cooling on a stainless steel cylinder with structured surface for safety design application in high temperature scenario, Heat and Mass Transfer, 53(2) (2017) 363-375.

[85] H. Dubbel, DUBBEL: Taschenbuch für den Maschinenbau, Springer-Verlag, 2013.

[86] S. Jung, Oberflächenbeurteilung-Rauheitsmessung, Institut für Maschinenelemente, Universität Stuttgart, Vorlesungsskript, (2012).

[87] Q. Cui, S. Chandra, S. McCahan, The effect of dissolving gases or solids in water droplets boiling on a hot surface, Journal of heat transfer, 123(4) (2001) 719-728.

[88] P.L. Woodfield, A.K. Mozumder, M. Monde, On the size of the boiling region in jet impingement quenching, International Journal of Heat and Mass Transfer, 52(1-2) (2009) 460-465.

Appendix A – Surface roughness measurement

Table A. 1 Results of surface roughness measurement of copper alloys

Material und Casting technology		**In casting direction**				**Perpendicular to Casting direction**			
		Line 1	**Line 2**	**Line 3**	**Ø Linen 1-3**	**Line 4**	**Line 5**	**Line 6**	**Ø Linen 4-6**
Copper alloy $CuSn_4$ **Conventional Direct-Chill Casting**	**R_a [µm]**	14.7	13.6	15.8	**14.7**	90.1	89.6	105.6	**95.1**
	R_t [µm]	175.0	71.1	114.4	**120.2**	476.8	413.8	402.9	**431.2**
	R_z [µm]	85.6	51.1	80.6	**72.4**	292.9	305.0	303.6	**300.5**
	R_{max} [µm]	133.0	69.7	86.9	**96.5**	459.3	398.8	377.1	**411.7**
Material und Casting technology		**In Casting direction**				**Perpendicular to Casting direction**			
		Line 1	**Line 2**	**Line 3**	**Ø Linen 1-3**	**Line 4**	**Line 5**	**Line 6**	**Ø Linen 4-6**
Copper alloy $CuFe_2P$ **Conventional Direct-Chill Casting**	**R_a [µm]**	16.0	21.1	41.1	**26.1**	43.5	39.3	44.8	**42.5**
	R_t [µm]	112.9	146.7	198.1	**152.6**	280.7	230.3	261.2	**257.4**
	R_z [µm]	83.6	109.9	167.1	**120.2**	199.7	174.6	165.3	**179.9**
	R_{max} [µm]	110.7	134.8	193.4	**146.3**	241.5	222.2	241.9	**235.2**
Material und Casting technology		**In Casting direction**				**Perpendicular to Casting direction**			
		Line 1	**Line 2**	**Line 3**	**Ø Linen 1-3**	**Line 4**	**Line 5**	**Line 6**	**Ø Linen 4-6**
Copper alloy CuCrZr **Conventional Direct-Chill Casting**	**R_a [µm]**	50.8	35.3	44.4	**43.5**	50.8	25.9	24.5	**33.7**
	R_t [µm]	312.0	339.8	363.5	**338.4**	312.0	246.2	251.6	**269.9**
	R_z [µm]	190.1	189.6	226.2	**202.0**	190.1	143.5	148.8	**160.8**
	R_{max} [µm]	267.6	338.6	363.5	**323.2**	267.6	232.7	251.1	**250.5**

Table A. 2 Results of surface roughness measurement of aluminum alloys

Material und Casting technology		**In casting direction**				**Perpendicular to casting direction**			
		Line 1	**Line 2**	**Line 3**	**Ø L. 1-3**	**Line 4**	**Line 5**	**Line 6**	**Ø L. 4-6**
Aluminum alloy AA5083 Electro-Magnetic Casting	**R_a [µm]**	2.8	1.6	-	**2.2**	2.9	2.8	-	**2.9**
	R_t [µm]	22.8	15.8	-	**19.3**	24.1	19.9	-	**22.0**
	R_z [µm]	16.1	12.6	-	**14.4**	15.2	16.6	-	**15.9**
	R_{max} [µm]	22.8	15.3	-	**19.1**	21.8	19.7	-	**20.8**
Material und Casting technology		**In casting direction**				**Perpendicular to casting direction**			
		Line 1	**Line 2**	**Line 3**	**Ø L. 1-3**	**Line 4**	**Line 5**	**Line 6**	**Ø L. 4-6**
Aluminum alloy AA5083 Conventional Direct-Chill Casting	**R_a [µm]**	27.8	53.8	56.9	**46.2**	50.2	32.8	47.4	**43.5**
	R_t [µm]	172.5	465.9	360.2	**332.9**	404.0	306.7	316.7	**342.5**
	R_z [µm]	134.6	251.7	270.1	**218.8**	246.3	192.5	223.3	**220.7**
	R_{max} [µm]	172.5	465.9	360.2	**332.9**	351.0	286.5	263.5	**300.3**
Material und Casting technology		**In casting direction**				**Perpendicular to casting direction**			
		Line 1	**Line 2**	**Line 3**	**Ø L. 1-3**	**Line 4**	**Line 5**	**Line 6**	**Ø L. 4-6**
Aluminum alloy AA7050 Conventional Direct-Chill Casting	**R_a [µm]**	66.8	82.2	68.2	**72.4**	59.9	60.5	59.8	**60.1**
	R_t [µm]	573.3	581.4	432.3	**529.0**	627.9	560.0	612.8	**600.3**
	R_z [µm]	274.0	353.7	294.3	**307.3**	277.4	275.9	287.0	**280.1**
	R_{max} [µm]	573.3	581.4	432.3	**529.0**	574.0	560.0	612.8	**582.3**

Appendix B – Width of wetting front region in case of full jet nozzle

The propagation of size of wetting front region is important for understanding the boiling phenomenon occurring on the hot surface impinged by subcooled liquid jet, since it is a prerequisite for a thorough and accurate simulation. In this appendix, the width of wetting front region under different experimental conditions for a single full jet nozzle is given.

Determination of width of wetting front

The determination of rewetting and DNB temperatures are detailed in **section 2.11.5**. Along with the saturation temperature of liquid, in this study, water of 100 °C, it is possible to evaluate the width of the wetting front region accordingly. The propagation of rewetting, DNB and liquid saturation temperatures are shown in **Fig. B. 1**. The width of transition wetting front region is determined by the distance between rewetting and DNB temperatures, while nucleate wetting front region by the distance between DNB and liquid saturation temperature. Take an example at 1.5 second, the rewetting, DNB and saturation points are about 22 mm, 20 mm and 1 mm from the stagnation point. In the following sections, the propagation of size of wetting front region will be described based on parameters variation.

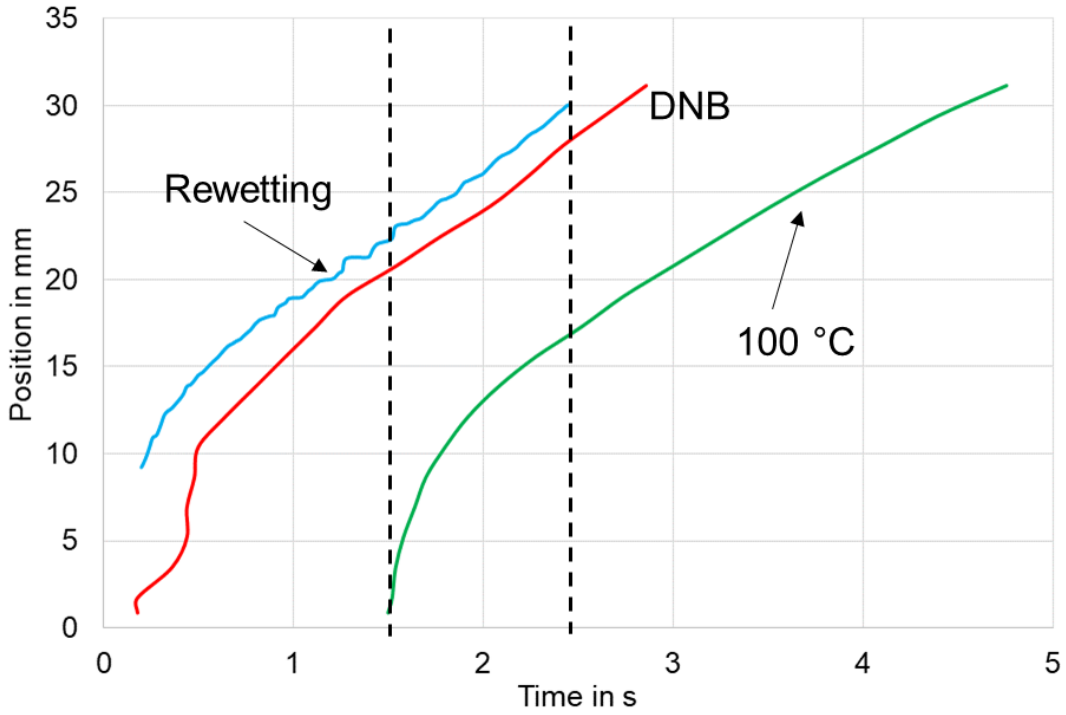

Fig. B. 1: Propagation of rewetting, DNB and liquid saturation temperatures

Effect of radial position on width of wetting front region

The width of wetting front region develops on the hot surface while the wetting front moves radially towards circumferential region. The heat flux distribution along with temperature profiles at three different times (0.8, 1.8 and 2.8 s) are depicted in **Fig. B.** 2, in order to clarify the development of size of wetting front region. Obviously, with time increasing, the heat flux distribution becomes wider. And the temperature gradient at maximum heat flux are also calculated, they are 65 °C/mm, 61°C/mm, 50°C/mm, respectively. The width of wetting front region at three times, however, increases from 17 mm through 21 mm to 24 mm, which means a steeper temperature gradient leads to a narrower wetting front region. This reverse correlation can simply explained by the fact that the area where boiling occurs occupies a smaller size on the hot surface at a larger radial temperature gradient.

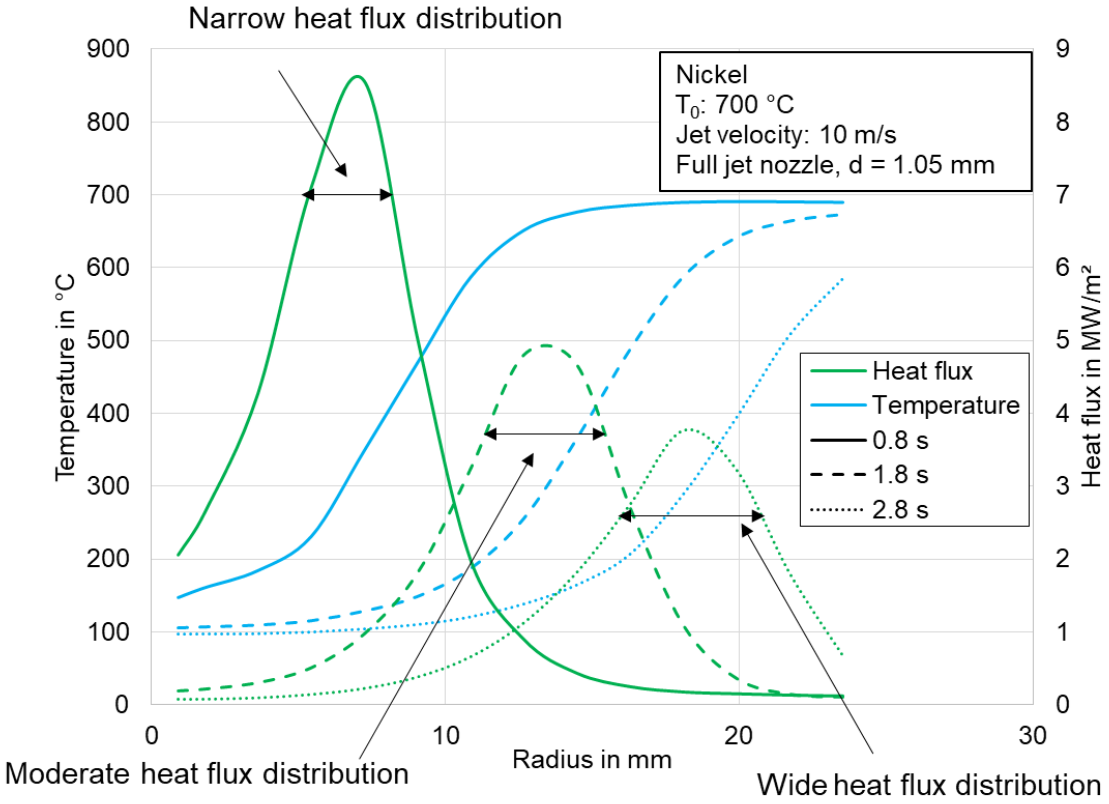

Fig. B. 2: Variation of heat flux during wetting front movement

Effect of jet velocity

The investigated liquid jet has a diameter of 1.05 mm. The jet velocity at three pressures are investigated. The corresponding jet velocities are 10, 19, 26 m/s, respectively. The development of wetting front region at these velocities are depicted in **Fig. B. 3**. Clear tendency can be observed that a higher jet velocity leads to a narrower wetting front. This is again evidenced by the fact that a higher temperature gradient at a higher jet velocity impedes the spread of the wetting front.

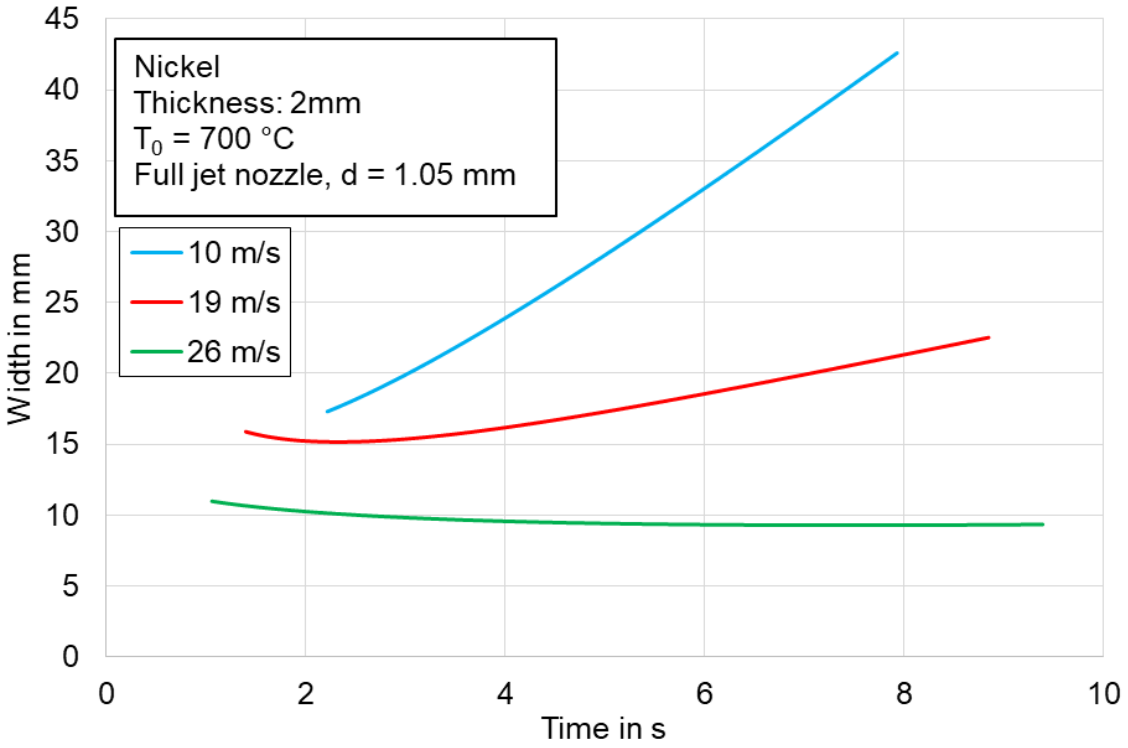

Fig. B. 3: Effect of jet velocity on width of wetting front region

Effect of Material

Three materials are investigated for the comparison: Nicrofer, Nickel and Copper B14. Their thermophysical properties are included in Table 3.4. Quite clearly, material properties have a significant influence on the wetting front size. At 10 seconds, the boiling width for nicrofer is 26 mm, while 22 mm and 18 mm for nickel and copper B14, respectively. The thermal conductivity of copper B14 is about 3 times that of nickel and 10 times that of nicrofer. It is obvious that a higher thermal conductivity leads to less intensive local cooling which evens out steep temperature gradient. Then the width of wetting front region will be smaller for the material with smaller thermal conductivity. The sequence copper B14-nickel-nicrofer is easily observed in **Fig. B. 4**.

Effect of initial body temperature

The temperature of a body determines how much thermal energy is stored in it. So a higher initial temperature of the investigated metal samples provides much more thermal energy to be extracted by the coolant. Meanwhile, a higher initial temperature also promotes more vigorous local cooling, since it can conduct more thermal energy from the dry region to the wetted region, which again creates a steeper temperature gradient. This will as described above inevitably result in narrower wetting front width as shown in **Fig. B. 5**.

Summary

As discussed in previous subsections, the dominant factor on the size of wetting front region is the local temperature gradient. Cooling strategy which favors a higher temperature gradient will lead to a narrower wetting front, which is in accordance with the finds of Woodfield et al. [88].

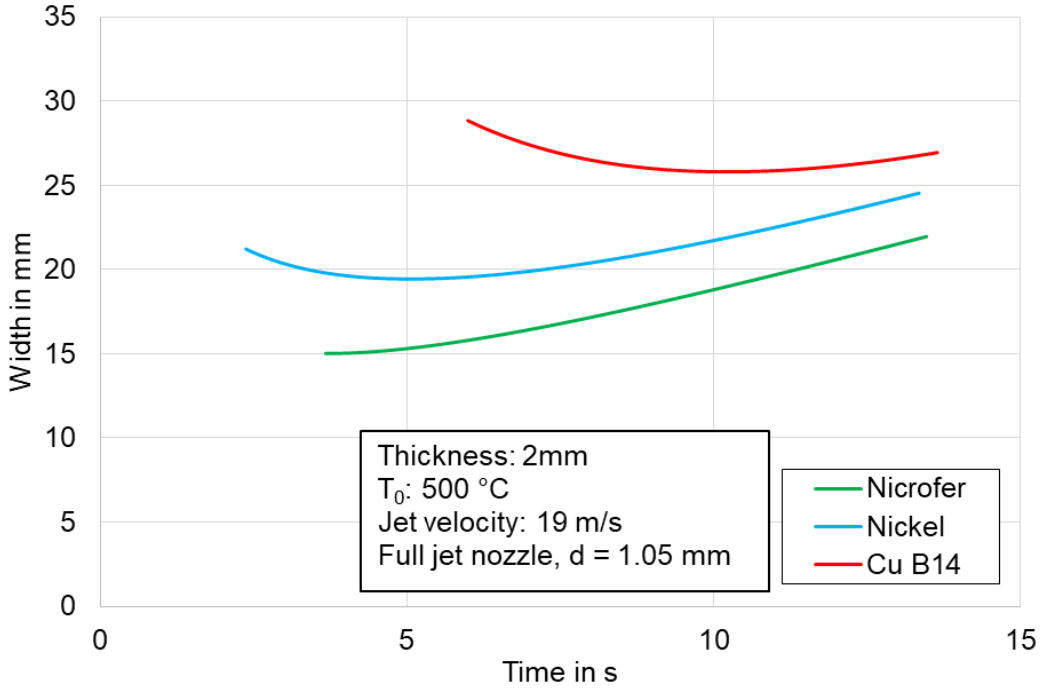

Fig. B. 4: Effect of material on width of wetting front region

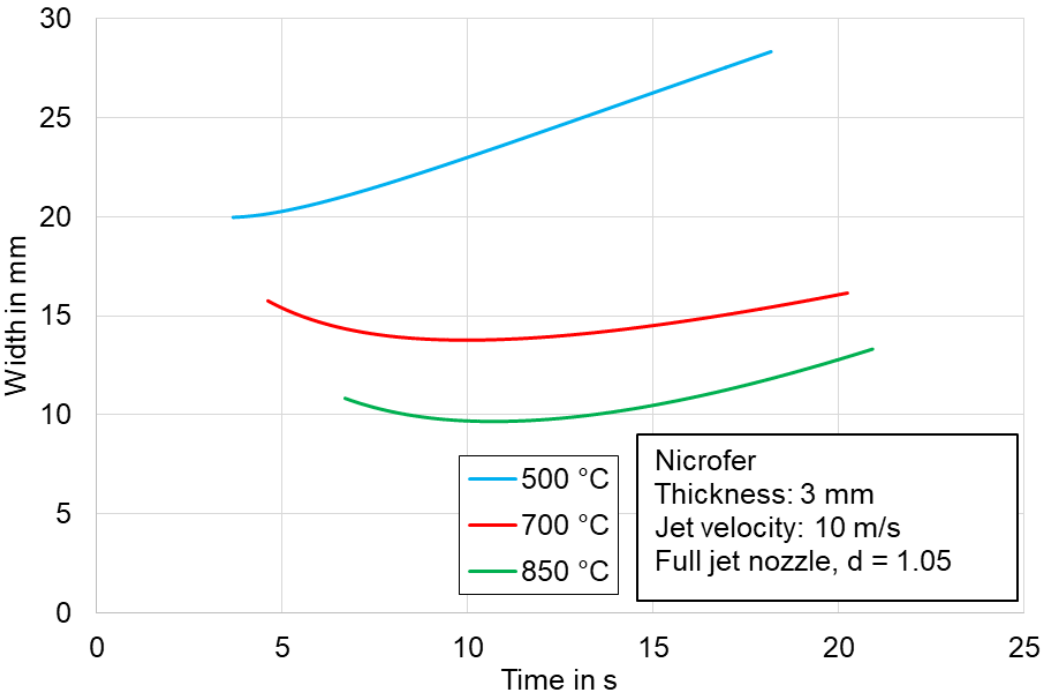

Fig. B. 5: Effect of initial temperature on width of wetting front region

List of Publications

1. Y. Fang, E. Specht, *Local heat transfer analysis during intensive cooling with water sprays and jets*, 13th international conference on Heat Transfer, Fluid Mechanics and Thermodynamics (HEFAT), pp: 401-404, Slovenia, 17-19 July (2017).
   ISBN: 978-1-77592-140-0

2. Y. Fang, Sabariman, E. Specht, *Analytical and experimental describing the heat transfer in metal quenching with water sprays and jets*, 12th international conference on Heat Transfer, Fluid Mechanics and Thermodynamics (HEFAT), pp: 689-693, Malaga, Spain, 11-13 July (2016).
   ISBN: 978-1-77592-124-0

3. Y. Fang, E. Specht*, Heat transfer analysis during jet impingement on metal plates*, International Heat Transfer Conference 16 (IHTC16), pp: 2323-2331, Beijing, China, 10-15 August (2018).

4. H. Woche, Y. Fang, E. Specht, *Wärmeübergang von Sprays und Strahlen bei der Kühlung heißer Metalle*, Prozesswärme, Jan/2018, pp: 129-136, ISSN: 2567-3742, Vulkan-Verlag.

5. H. Woche, Y. Fang, E. Specht, *Heat transfer analysis during metal cooling with sprays and jets*, Heat Processing, Jan/2018, pp: 41-47, ISSN: 1611-616X, Vulkan-Verlag.

6. E. Specht, H. Woche, Y. Fang, J. Hoffmann, Örtlicher Wärmeübergang von Spray und Strahlen bei der Intensivkühlung von Metallen, 1. Aachener Ofenbau- und Thermoprocess Kolloquium, pp: 75-85,11th-12th May, 2017, Aachen
   ISBN: 978-3-95886-165-7

7. Sabariman, Yuan Fang & Eckehard Specht, *Analytical Model for Describing Experimental Results on Parameters Influencing Heat Transfer in Film Boiling with Spray Quenching*, Heat Transfer Engineering, 40:1-2, 16-25, 2019.
   DOI: 10.1080/01457632.2017.1404551

8. Y. Fang, H. Woche, E. Specht, Influence of surface roughness on heat transfer during quenching hot metals with different nozzles, Heat and Mass Transfer (submitted)

List of Thesis Supervised

1. Chulpan Eremeeva, “Investigation of the influence of surface roughness on the cooling of cast steel plates by spray and full jet nozzles”, *Master thesis, Otto-von-Guericke-Universität Magdeburg*, 2017
2. Leontev Aleksandr, “Investigation of the influences of plate and jet velocity on cooling performance with smooth and rough plates by using mold or single full jet nozzle”, *Master thesis, Otto-von-Guericke-Universität Magdeburg*, 2018
3. Xi Chen, “Experimental investigation of the influence of metal plate thickness and material on the heat transfer with usage of solid jet nozzle”, *Master thesis, Otto-von-Guericke-Universität Magdeburg*, 2016
4. Kabbir Ali, “Investigation of the influence of surface roughness and water quality on the cooling of Aluminum alloy and copper alloy by spray and full jet nozzle”, *Master thesis, Otto-von-Guericke-Universität Magdeburg*, 2017
5. Qianlin Min, “Experimental Investigation of the Influence of the Spray Injection Angle on the Heat Transfer with Utilization of Flat Spray Nozzle”, *Master thesis, Otto-von-Guericke-Universität Magdeburg*, 2015
6. Wentao Xu, “Heat transfer analysis during cooling hot metals by applying nozzle field”, *Master thesis, Otto-von-Guericke-Universität Magdeburg*, 2018
7. Yannik Pajung, “Untersuchung des Einflusses der Oberflächenrauigkeit auf die Abkühlung bewegter Kupferplatten bei feststehenden Kokillenstrahlen”, *Master thesis, Otto-von-Guericke-Universität Magdeburg*, 2017
8. Antje David, “Untersuchung der Abkühlung bewegter Nickel- und Nicroferplatten bei feststehenden Kokillenstrahlen und Vergleich mit der Abkühlung einer einzelnen Vollstrahldüse”, *Bachelor thesis, Otto-von-Guericke-Universität Magdeburg*, 2017
9. Jan Hoffmann, “Untersuchung des Abkühlverhaltens von Sprühkopfdüsen, Vollkegel- und Flachstrahldüsen in Abhängigkeit von Kühl-wässern und definierten Betriebsparametern”, *Bachelor thesis, Otto-von-Guericke-Universität Magdeburg*, 2016
10. Christian Gröber, “Experimentelle Untersuchung eines Strahlfeldes mit versetzten Vollstrahldüsen auf den Wärmeübergang an vertikalen Blechen”, *Bachelor thesis, Otto-von-Guericke-Universität Magdeburg*, 2016
11. Max Lantzberg, “Experimentelle Untersuchung eines Strahlfeldes mit fluchtenden Vollstrahldüsen auf den Wärmeübergang an vertikalen Blechen”, *Bachelor thesis, Otto-von-Guericke-Universität Magdeburg*, 2016
12. Stephan Ryll, “ Untersuchung des Einflusses der Oberflächenrauigkeit auf die Abkühlung bewegter Aluminiumplatten bei feststehenden Kokillenstrahlen”, *Bachelor thesis, Otto-von-Guericke-Universität Magdeburg*, 2017